UNIVERSITY OF OXFORD

# EPICARDIAL SIGNALLING IN MAMMALIAN HEART REGENERATION

Megan L Masters

Thesis submitted for the degree Doctor of Philosophy (D.Phil.)

Jesus College, University of Oxford

Department of Physiology, Anatomy and Genetics

Supervisor: Professor Paul R Riley


2015

# Abstract

Whilst lower vertebrate species, such as newt and zebrafish, can regenerate their hearts following substantial injury throughout life, humans and other adult mammals undergo cardiac scarring and remodelling in response to myocardial infarction (MI), which leads to chronic heart failure. However, recent work has identified a 'regenerative window' in mammals such that the 1 day-old mouse (P1) was able to regenerate lost myocardium following MI induced by ligation of the left anterior descending coronary artery (LAD) within three weeks, but an equivalent injury sustained on or after P7 resulted in adult-like wound healing. These findings suggest that developmental cues may be instructive towards regeneration.

The epicardium, the outer mesothelial lining of the heart, is an important source of cardiovascular cells and signals that respectively contribute directly to the major lineages of the forming heart and instruct muscle growth during heart development. Under normal conditions, the epicardium is quiescent in the adult heart, but is activated upon injury and can be ectopically stimulated to contribute to neovascularisation and myocardial repair in infarcted adult mouse hearts. Furthermore, organ-wide activation of the epicardium underpins zebrafish heart regeneration, functioning, in part, to contribute a vascular niche and regulate cardiomyocyte cell-cycle re-entry and proliferation. We, therefore, hypothesised that epicardial signalling may also influence heart regeneration in neonatal mice.

The aims of this project were to 1) establish the neonatal MI injury model in-house; 2) confirm and characterise neonatal mouse heart regeneration by magnetic resonance imaging (MRI) and 3) investigate the role(s) of the epicardium and epicardial signalling in mammalian heart regeneration. In addressing these aims, novel anaesthetic and aseptic protocols were designed to refine cardiothoracic surgery in neonatal mice and establish the injury model. A protocol for MRI assessment of heart regeneration in neonatal mice was also established. Consistent with previous reports, we observed significant, although incomplete myocardial regeneration after 21 days with limited anterior wall scarring when MI was induced at P1, compared to significant collagen deposition and remodelling following MI at P7. Epicardial potential was lost coincident with closure of the 'regenerative window' and the epicardial response following injury induced at regenerative (P1) and reparative (P7) time-points was documented via retinoic acid signalling as a key developmental epicardial mitogen. This work furthers our understanding of the cell and molecular mediators of regeneration in neonatal mice, and may lead to therapeutic strategies for amplifying the regenerative response of adult mammalian hearts to injury.

# Acknowledgements

Firstly, I thank my Supervisor, Paul Riley, for allowing me to join his lab, inspiring my research interests and also for his reliable advice on comma placement and semi-colon use. Secondly, I would like to thank Paul Trethowan for finding a beautiful black Labrador to keep us company whilst we were writing. Best boyfriend ever. I'm so glad we went through this D.Phil. larky together and look forward to many more adventures, preferably far away from our desks and laptops. Cough *Rome* cough. Thanks also to Sophie and Caitlin, my lab loves and the best surf and turf chefs I know. I really don't know how I would have managed without you both. I hope we continue 'Tuesday Funday' forevermore and that you remember this poor medical student as you jet off into your city jobs and much deserved six-figure salaries. Thanks also to Dr. Damien Barnette for your sound advice, critical mind and moves like Jagger. There's nothing like a good twirl to cheer you up after another failed experiment. I would like to thank all members of the Riley group and Smart lab, new and old, for your ongoing support and input over the last three years. Joey, Nicola, Dee, Mala, Cristina, Tilly, Abby, Sonali, Jana, Philippa, Katie, Tertia – we have had some fun times and interesting lunchtime conversations! I would especially like to thank Dr Sveva Bollini and Dr Anke Smits for passing on their surgical expertise. Sveva, it was a shame your career took off so quickly (!) but your supervision in those first few months was greatly appreciated. Also, many thanks to the 'real Docter' Tom for all your help, I look forward to the day when the mentee becomes mentor! Humans can't be half as fiddly. A huge thank you to Neens as well for keeping Bruno and his girls happy, fed and watered.

There are so many people that have helped my professional growth over the last three years. Thank you to Dr Hesham Sadek and Dr Shalini Muraldihar for hosting me in Texas and providing me with the skills necessary to pursue this work. Thank you also to Dr Kathy Murphy and Dr Caroline Bergmann for your patience and advice on establishing the skills I learnt in the Wild West back in Oxford. Thank you to the funding body of the Marie Curie ITN network and all members of the CardioNet, particularly to Dr Maurice Van den Hoff and Dr Jan Ruijter for hosting me in Amsterdam and for allowing me to work with your wonderful groups at the AMC. A special thanks to Quinn and Corrie for all your help and patience during my stay and to Stuti and Andrea for just being great. Thank you to the co-ordinators of the network, Inga and Enrique and to all of the fellows. It was inspiring to know you all and I hope that our paths cross many times across the continent as we move on in our careers. Thank you also to our collaborators Professor Jurgen Schneider, Dr Mahon Maguire and Vicky at the BMRU.

I would also like to thank my friends and family. Dad, thanks for knowing exactly what I need to hear, pretty much always. Mum, I'm lucky to have a SFP and friend that has me in tears laughing when I need it most. I'm the proudest daughter and look forward to coming home when I run out of degrees to do and my perpetual student life has to end. Unless brother takes me in. Tom, as brothers go, you're okay. The fact that you found me a fun sister-in-law earns you points. Thanks for being so great at life in general and for fuelling our healthy sibling rivalry. I'll catch up with you one day - although one day soon (hopefully) my gown will be prettier than yours, which basically means I've won. Grandad, your pride and interest in my studies spurs me on, kazi kubwa sana. And to all of my family, I'm lucky to have you all.

To my friends, who are practically family, sorry for being boring/absent over the last few weeks. To the Oxford lot: Sam, Emrys, Anna, Phil, Lottie, Bobs, Ellie, you're pretty much my favourite part of Oxford. I'm glad and proud to know you all. To the girls at home, Em, Carlene, Nikki, Rhia, Anita, Sam, George, Kelly, Jenny – I'd be lost without knowing every detail of your lives on a daily basis. A special thanks to Em and Scott for making me baby Finley to play with! And thanks to Ash, just because I don't want to leave you out.

A special thank you also to Dr Carolyn Carr and Dr Gillian Gray for taking the time to examine this thesis.

I would like to dedicate this work to the memory of my wonderful Nan.

“Man will occasionally stumble across the truth, but most of the time, he will pick himself up and carry on”.

- Winston Churchill

# Table of Contents

# List of Figures:

# List of Tables

## Abbreviations:

4-HT: 4 hydroxytamoxifen

αSMA: alpha smooth muscle actin

ATRA: all-trans retinoic acid

BMCs: bone marrow-derived cells

BMP2: bone morphogenic protein 2

CAL: coronary artery ligation

CD45: lymphocyte common antigen

C/EBP: CCAAT/enhancer binding protein

CHD: coronary heart disease

CoE: coronary endothelium

CPC: cardiac progenitor cell

Cre: Cre recombinase

CYP26B1: Cytochrome P450 B1

DDR2: discoidin domain receptor-2

Dpa: days post-ablation

Dpi: days post-injury

DTA: diphtheria toxin A-chain

ECM: extracellular matrix

EGFP: enhanced green fluorescent protein

EMT: epithelial-mesenchymal transition

EPDC: epicardium-derived cell

EYFP: enhanced yellow fluorescent protein

FGF: fibroblast growth factor

FSLT1: folistatin-like 1

FSP-1: fibroblast specific protein-1

Fn: fibronectin

Hpi: hours post-injury

IVS: interventricular sulcus

LAD: left anterior descending coronary artery

LA: left atria

LV: left ventricle

mRFP: modified red fluorescent protein

MTZ: metronidazole

MI: myocardial Infarction

NSAIDS: non-steroidal anti-inflammatory drugs

P: postnatal day

PECAM: platelet endothelial cell adhesion molecule

pHH3: phospohistone H3

RA: retinoic acid

RV: right ventricle

RAR: retinoic acid receptor

RARE: retinoic acid response element

RXR: retinoid X receptor

Raldh2: retinaldehyde dehydrogenase-2

Scx: Scleraxis

Sema3D: Semaphorin 3D

Tβ4: thymosin beta-4

Tbx18: T-box protein 18

Tcf21: transcription factor 21

VEGF: vascular endothelial growth factor

Vm: vimentin

VSMCs: vascular smooth muscle cells

Wt1: wilm's tumour 1

# 1

# General Introduction

### 1.1. Myocardial infarction and heart failure

In the UK, someone is hospitalised by a heart attack every three minutes (BHF, 2014). During a heart attack, or myocardial infarction (MI), a coronary artery becomes blocked, typically due to occluded blood flow secondary to atherosclerotic plaque rupture, which cuts off blood supply to the heart muscle (myocardium) and leads to irreversible loss of heart muscle cells (cardiomyocytes). Due to numerous medical, surgical and technological advances, the number of people dying from MI is decreasing. The incidence of heart failure, conversely, is increasing (Fig. 1.1). After a heart attack, the billions of cardiomyocytes lost by ischemia are replaced by the formation of a non-contractile scar in the muscular void. Whilst immediately indispensable to prevent organ rupture, the resulting changes to ventricular geometry and dimensions cause haemodynamic uncoupling and progressive deterioration of pump function (Jugdutt, 2003, Jessup and Brozena, 2003). The heart is unable to sufficiently replace the lost muscle and the irreversibly compromised organ undergoes remodelling. Progressive heart failure ensues. The symptoms of heart failure can be life curtailing and the only cure at present remains a heart transplant. With more and more people living with the consequences of MI, a restricted number of donor hearts for transplant and a plateau of clinical interventions in the field, there is an urgent need for the development of novel therapies to restore or replace the lost tissues that result from the initial insult.

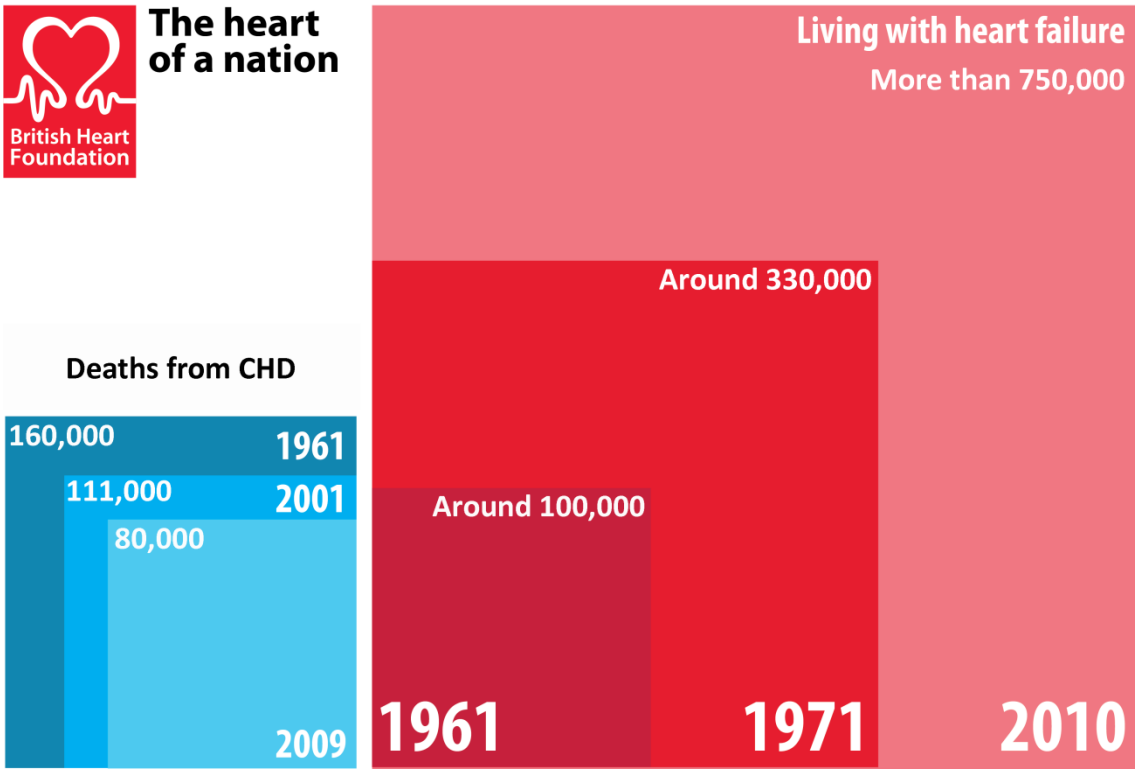


**Figure 1. 1. Incidence of coronary heart disease and heart failure in the UK**
Infographic adapted from the British heart foundation (BHF) website. The number of people dying from coronary heart disease (CHD) has decreased whilst the number of people living with heart failure has increased.

### 1.2. Regenerative lessons from evolution

Not all species are destined for heart failure following cardiac injury. Some lower vertebrate species such as newts and zebrafish are capable of regenerating their hearts following substantial injury throughout life (Poss et al., 2002, Chablais et al., 2011, Wang et al., 2011). As a result, zebrafish have emerged as an intense research focus for deciphering the critical mechanisms of heart regeneration that may have separately evolved in teleost, or have been actively selected against in mammals through the course of evolution (Poss et al., 2002). Improved understanding of these mechanisms could offer therapeutic strategies for translating regenerative capacities up the branches of the evolutionary tree to humans (Ausoni and Sartore, 2009).

## 1.3. Regenerative lessons from development

Recent studies, however, suggest that mammals may have the potential to regenerate their hearts following injury. The newborn mouse heart (one day old) was shown to regenerate lost myocardium just three weeks after amputation of 10-15% of the apex (Porrello et al., 2011) or ischaemia induced by permanent ligation of the left anterior descending coronary artery (LAD) (Porrello et al., 2013, Haubner et al., 2012). However, this capacity was lost within the first week of life, such that if the same injury was sustained on or after postnatal day (P) 7, scar formation and adult-like wound healing was observed. This phenomenon has been termed the neonatal 'regenerative window'. These first demonstrations of effective heart regeneration in a mammalian system reinforced the hypothesis that developmental mechanisms may be permissive to regeneration (Nachtrab and Poss, 2012) and identified the neonatal mouse as a powerful tool for identifying key cell and molecular players in this process. Improved understanding of the mechanisms that regulate 'closure' of the 'regenerative window' could uncover therapeutic targets for reawakening developmental mechanisms instructive towards heart regeneration in adult mammals.

## 1.4. Conserved mechanisms of heart regeneration

A key question, therefore, is: what changes in the neonatal mouse heart during the first week of life? And, also, what do the hearts of neonatal mice and zebrafish have in common that the adult mouse heart lacks? Indeed, it was the anatomical similarities between the teleost and embryonic mammalian heart before septation that first led Sadek and colleagues to investigate the regenerative capacities of neonatal mice (Porrello et al., 2011). Table 1.1 (adapted from Masters and Riley, 2014) summarises some notable similarities and disparities between zebrafish, neonatal and adult mouse hearts.

**Table 1. 1. Comparison of zebrafish, neonatal and adult mice hearts:**
adapted from Masters & Riley (2014). CM, cardiomyocyte.

| | | Zebrafish  | Neonatal (P1-P2) mouse 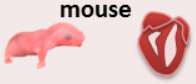 | Adult mouse  |
|---|---|---|---|---|
| Chambers | | 2 | 4 | 4 |
| Pulmonary circulation | | No | Yes | Yes |
| Heart rate (bpm) | | ≈ 130 | ≈ 400 | ≈ 600 |
| Systolic blood pressure (mmHg) | | ≈ 2.5 | ≈ 30 | ≈ 120 |
| Cardiomyocyte | Size | Small | Intermediate | Large |
| | Density | Low | Moderate | High |
| | Nuclei | Mononuclear | Mostly mononuclear | Mostly binuclear |
| Cardiac fibroblast density | | Low | High | High |
| Hypoxia resistant | | Yes | Likely | No |
| Myocardial growth | | Hyperplasia | Hyperplasia | Hypertrophy |
| Injury response | Epicardial signalling | Yes | Yes | Yes |
| | CM proliferation | Yes | Yes | Negligible |
| | Regeneration | Yes | Yes | No |

The adult zebrafish heart comprises a two chambered, single circulation, hypoxia-resistant organ (Marques et al., 2008), which operates at a pressure that is 50 times lower than that of the human circulation (Hu et al., 2001). The ventricular wall is thin and highly trabeculated, with a much smaller fibroblast population than the mammalian heart (Ausoni and Sartore, 2009). Also, zebrafish cardiomyocytes are small, mononuclear and retain the capacity to proliferate indefinitely (Poss, 2007, Wills et al., 2008).

Analogous to the zebrafish, the neonatal mouse heart contains a high proportion of proliferative mononuclear cardiomyocytes, which undergo karyokinesis (nuclear division) without cytokinesis (cell division) between P4 and P5, rendering more than 50% of cardiomyocytes binuclear by P7. This increases to more than 80% by P14, at which point, most cardiomyocytes have exited the cell cycle and heart growth continues mainly by hypertrophy (Ikenishi et al., 2012). Conversely, in adult mice, very limited turnover of cardiomyocytes is

described (Soonpaa et al., 1996, Soonpaa and Field, 1997, Senyo et al., 2013); similar to that described in humans (Bergmann et al., 2009, Mollova et al., 2013). It is also suggested that the mammalian heart retains hypoxia resistance transiently after birth as the newborn adapts from a reliance on glycolytic to oxidative metabolism (Lopaschuk and Jaswal, 2010, Puente et al., 2014) - a 'switch' that further coincides with the loss of cardiomyocyte hyperplasia. Cardiac fibroblast density was also reported to increase by almost 30% between P1 and P5 (Banerjee et al., 2007).

### 1.5. Animal models of heart regeneration

Given the similarities between the hearts of zebrafish and neonatal mice, it is possible that similar mechanisms underpin their regenerative capacities. Numerous models of heart injury have been developed to permit the study of heart regeneration in these animals. Each form of insult incurs differences in injury type, extent and the timings and duration of regeneration, as outlined in Figure 1.2.

#### 1.5.1. Resection injury

As previously mentioned, resection injury involves amputation of around 15% of the apex of the heart. This methodology was used for the initial demonstrations of heart regeneration in zebrafish (Poss et al., 2002) and neonatal mice (Porrello et al., 2011). Regeneration by this model was first described to occur in just 3 weeks in P1 mice and by 60 days in zebrafish. Fate mapping by myocardial targeted Cre recombinase (Cre) labelling showed that regeneration was largely mediated by the division of pre-existing, surviving cardiomyocytes in both species (Jopling et al., 2010, Kikuchi et al., 2010, Porrello et al., 2011). In mice, resection injury is achieved by performing thoracotomy, exposing the heart and 'shaving' the tip of the apex until the chambers are visible (Mahmoud et al., 2014). This results in the formation of a

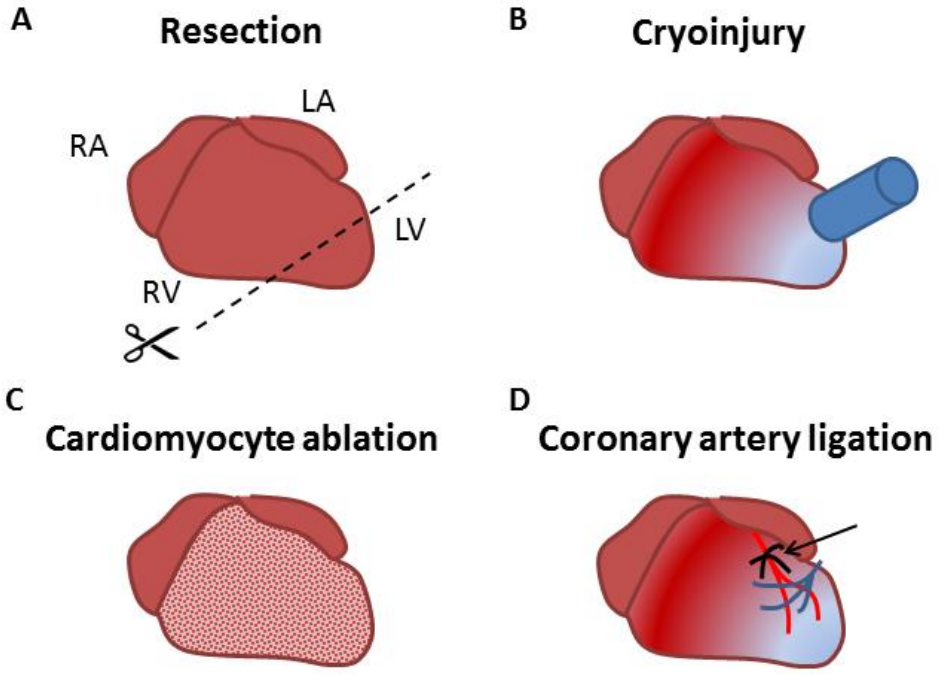


**Figure 1. 2. Injury models of heart regeneration in neonatal mice:**
(A) resection injury involves removal of around 15% of the apex. Dashed line and scissors indicate resection plane. (B) Cryoinjury involves application of a liquid nitrogen cooled probe to the left ventricle to induce ischemia-like necrotic cell death across around 20-30% of the ventricle. (C) Cardiomyocyte ablation results in the selective loss of up to 60% of the ventricular myocardium. (D) Coronary artery ligation by suture placement to occlude perfusion of the left anterior descending coronary artery (LAD, indicated by arrow) induces ischemia in around 15-20% of the left ventricle (RA: right atria; LA: left atria; RV: right ventricle; LV: left ventricle).

'blood clot' to seal the apex. Less tissue is resected in P7 pups than in P1 pups as they are prone to exsanguination. Due to the tissue removal component, this model does not induce widespread necrotic and apoptotic cell death that is caused by ischemia and, therefore, has limited clinical relevance.

### 1.5.2. Cryoinjury

An alternative surgical model is cryoinjury, which involves the application of a liquid nitrogen-cooled cryoprobe to the left ventricle. This form of injury induces 'ischaemia-like' necrotic and apoptotic cell death across ~20-30% of the ventricle. One advantage of this injury method is

relative control of injury size and reproducibility. In zebrafish, the regenerative process post-cryoinjury is described to take from 30 (Chablais et al., 2011) to more than 130 days (Gonzalez-Rosa et al., 2011, Gonzalez-Rosa and Mercader, 2012, Gonzalez-Rosa et al., 2012, Schnabel et al., 2011) during which, an initial scar is formed at the site of injury and is gradually replaced as the myocardium regenerates (Gonzalez-Rosa et al., 2011). In zebrafish, lineage analyses again identified the source of *de novo* cardiomyocytes in the regenerate as pre-existing, proliferating cardiomyocytes (Chablais et al., 2011, Gonzalez-Rosa et al., 2011, Schnabel et al., 2011).

In mice, a recent report suggests that the regenerative process following cryoinjury is significantly prolonged and injury dependent. Darehzereshki and colleagues (2015) compared the extent of regeneration following varying extents of neonatal cryoinjury. Following transmural injury (i.e. full wall thickness, spanning epicardial-endocardial borders), induced by prolonged probe application to the left ventricle, extensive scarring, wall thinning and severe ventricular dilation was observed without signs of regeneration after 120 days. In contrast, following mild, non-transmural injury (by injuring up to half of the left ventricular wall with a shorter application time) minimal scarring was observed 21 days post-injury (dpi). This group failed to observe colocalisation of the cell cycle G2 and M phase mitotic marker phospohistone H3 (pHH3) in cardiomyocytes above control levels, suggestive of limited cardiomyocyte proliferation in neonatal hearts following cryoinjury.

A significant contribution of c-kit$^{+}$ cardiac precursor cells (CPCs) to the regenerate following cryoinjury in neonatal mice has been reported (Jesty et al., 2012). In a c-kit$^{BAC}$ enhanced green fluorescent protein (EGFP) reporter line, EGFP$^{+}$ cells were localised to the 'infarct', and by day 5, more than 75% of (c-kit)EGFP$^{+}$ cells expressed the mature myocyte marker, α-Actinin. Further, these cells constituted 42% of the proliferating cardiomyocyte population within the infarct, as demonstrated by bromo-deoxyuridine (BrdU) incorporation, which is a synthetic nucleoside analogue of thymidine. The remaining EGFP$^{+}$ cells co-expressed the endothelial

marker platelet endothelial cell adhesion molecule (PECAM/CD31) whilst a small number (less than 3%) co-expressed the hematopoietic lineage marker, lymphocyte common antigen (CD45). Conversely, only a modest number of (ckit$^{+}$) EGFP$^{+}$ cells were found in time-matched infarcts of adult mice; and these were found to adopt vascular fates. However, despite significant scar regression and myocardial regeneration in neonates, a small amount of scarring was still evident after 3 months. Whilst this study does not negate cardiomyocyte proliferation as a means of regeneration, it implies a contribution of CPCs to neonatal heart regeneration - specifically to neomyogenesis at the injury core.

### 1.5.3. Cardiomyocyte ablation

A further model of myocardial injury in adult zebrafish utilised inducible Cre-loxP technology to induce acute cardiomyocyte loss. 4-hydroxytamoxifen (4-HT)-inducible Cre recombinase (CreER) driven by the myocardial *cmcl2* promoter (cmcl2:CreER) was used to drive cytotoxic diphtheria toxin-A chain (DTA) expression in cardiomyocytes, termed Z-CAT animals (Wang et al., 2011). 4-HT treatment of Z-Cat animals led to the specific ablation of up to 60% of cardiomyocytes; after which, complete myocardial regeneration was observed after 30 days. In these animals, lineage analysis showed that *de novo* cardiomyocytes derived from the proliferation of un-injured, pre-existing cardiomyocytes.

In mice, a similar model was recently used to assess the limits of embryonic mammalian heart regeneration. Nkx2.5-Cre and α-myosin heavy chain (αMHC)-Cre lines were used to selectively drive DTA and, thereby, cell death in CPCs or immature cardiomyocytes, respectively (Sturzu et al., 2015). Embryonic stem (ES) cells from Nkx2.5-Cre and αMHC-Cre blastocysts were injected into wild-type blastocysts to generate chimeric embryonic hearts with varying extents (0 – 95%) of CPC or cardiomyocyte ablation. Ablation of up to 60% of CPCs or cardiomyocytes was compatible with regeneration; beyond which embryonic growth was arrested. Regeneration

was associated with increased cardiomyocyte expression of pHH3 and the additional cell proliferation marker Ki-67, with no alteration to mean cardiomyocyte size. This was interpreted to suggest that morphological recovery of the ablated heart was largely due to increased proliferation of non-ablated CPCs or cardiomyocytes.

### 1.5.4. Coronary artery ligation

Prior to the recent developments of regenerative models of heart injury, for over a century, animal models of MI have progressed our understanding of the pathophysiological consequences of heart attacks (Chimenti et al., 2004). Traditionally, in mammals, MI has been induced by coronary artery ligation; typically by occluding perfusion of the left anterior descending coronary artery (LAD) to induce temporary or permanent occlusion of blood flow to the anterior left ventricle (with or without reperfusion, respectively). In larger mammals, this is now usually achieved by catheterisation of the LAD with temporary occlusion by intracoronary balloon inflation (Suzuki et al., 2011). Due to the amenability of mice to genetic manipulation, this model was scaled down to LAD ligation by suture placement, which can either be untied to allow reperfusion or left secured to permanently occlude blood flow. In what was described as a technical 'tour-de-force', further work by the Sadek lab saw the adaptation of the traditional LAD ligation model to the scale of the 1-2g neonatal mouse, in order to investigate the regenerative capacity of the newborn mammalian heart following ischaemia (Porrello et al., 2013). Permanent LAD ligation induced ischemia and 'scar' formation in the anterior left ventricular wall. When induced at P1, this scar was infiltrated by proliferating cardiomyocytes and regeneration of infarcted myocardium was evident after 21 days (Porrello et al., 2013). Persistent scarring was observed at the site of the ligature. Pulse-chase and lineage analysis identified pre-existing cardiomyocytes as the main source of *de novo* cardiomyocytes, with the latter labelling around ~70% of the regenerate. As the mechanism of this injury is actual ischemia, this model is considered the most clinically

relevant, and is also the most comparable to the adult injury setting and the existing data on experimentally induced MI thus far. A key limitation of this injury type, however, is variability of injury size due to variable coronary vessel topology and difficulty in visualising and targeting the same part of the LAD.

### 1.6. Mechanisms of heart regeneration

The leading hypothesis for how and why adult zebrafish and neonatal mice are capable of regeneration is that the proliferative capacity of their cardiomyocytes is sufficient to restore those lost during the initial insult (Muralidhar et al., 2013, Xin et al., 2013b). In zebrafish, cardiomyocytes are capable of proliferation throughout life: hence the ability of this species to regenerate lost heart muscle into adulthood. Conversely, the transition to become multinucleated and polyploidy of the majority of cardiomyocytes from P7 onwards in mice (Ikenishi et al., 2012, Soonpaa et al., 1996) may limit heart regeneration beyond the first postnatal week, whereby myocyte hypertrophy becomes the adopted response to injury. In humans, anecdotal evidence also implies heightened regenerative capacity in early life. Longitudinal studies of patients who underwent surgical correction of congenital coronary artery defects suggested that infants, despite having the worst preoperative heart function, held the best potential for functional recovery (Michielon et al., 2003). Moreover, analogous to the neonatal mouse, the human infant was shown to have the greatest proportion of proliferating cardiomyocytes, with reported cytokinesis rates dropping from 0.016% at birth to 0.005% by adolescence; proportionate to 3.4 fold cardiomyocyte increase in the left ventricle over the same time period (Mollova et al., 2013). These findings support a developmental loss of regenerative capacity in humans; inversely related to increased terminally differentiated cardiomyocytes with aging, elevating the translational relevance of the neonatal mouse as means to identify regenerative pathways lost in development.

Given the importance of neomyogenesis for heart regeneration; developmental cues that are permissive to cardiomyocyte proliferation and angiogenesis could hold potential for the treatment of ischaemic heart disease and heart failure.

### 1.7. Mammalian heart development

Heart development begins at around embryonic day (E)7 in mice and has been extensively studied (Rosenthal and Harvey, 2010). Figure 1.3 summarises the key stages. Myocardial cells derive from the mesoderm at the anterior portion of the primitive streak during gastrulation, from which, at around E7.5, a structure called the cardiac crescent is formed. At around E8, myocardial progenitor cells of the cardiac crescent migrate to the midline and form the linear heart tube. This linear muscular tube then extends anteriorly and posteriorly to give rise to the arterial and venous poles, respectively, and undergoes looping at around E8.5 to give rise to primitive chambers. Proper formation of the atria and ventricles occurs at around E10.5 as a result of embryonic growth driving anterior movement of the venous pole. By E15, chamber maturation, including atrioventricular septation and valve formation is largely complete, and the framework for maturation of the organ proper is established (Rosenthal and Harvey, 2010). Heart maturation is fully dependent, however, upon the emergence of a second cardiac cell population which derives from a small transient organ located at the in-flow region called the proepicardium (Manner, 1993, Manner, 1999, Carmona et al., 2010, Rosenthal and Harvey, 2010). The proepicardium appears at the inflow region of the looping myocardium at around E.9 and gives rise to cells which attach to and spread over the myocardial surface to instate a uniform epithelium by E11.5 (Rosenthal and Harvey, 2010). This outer epithelial layer is called the epicardium.

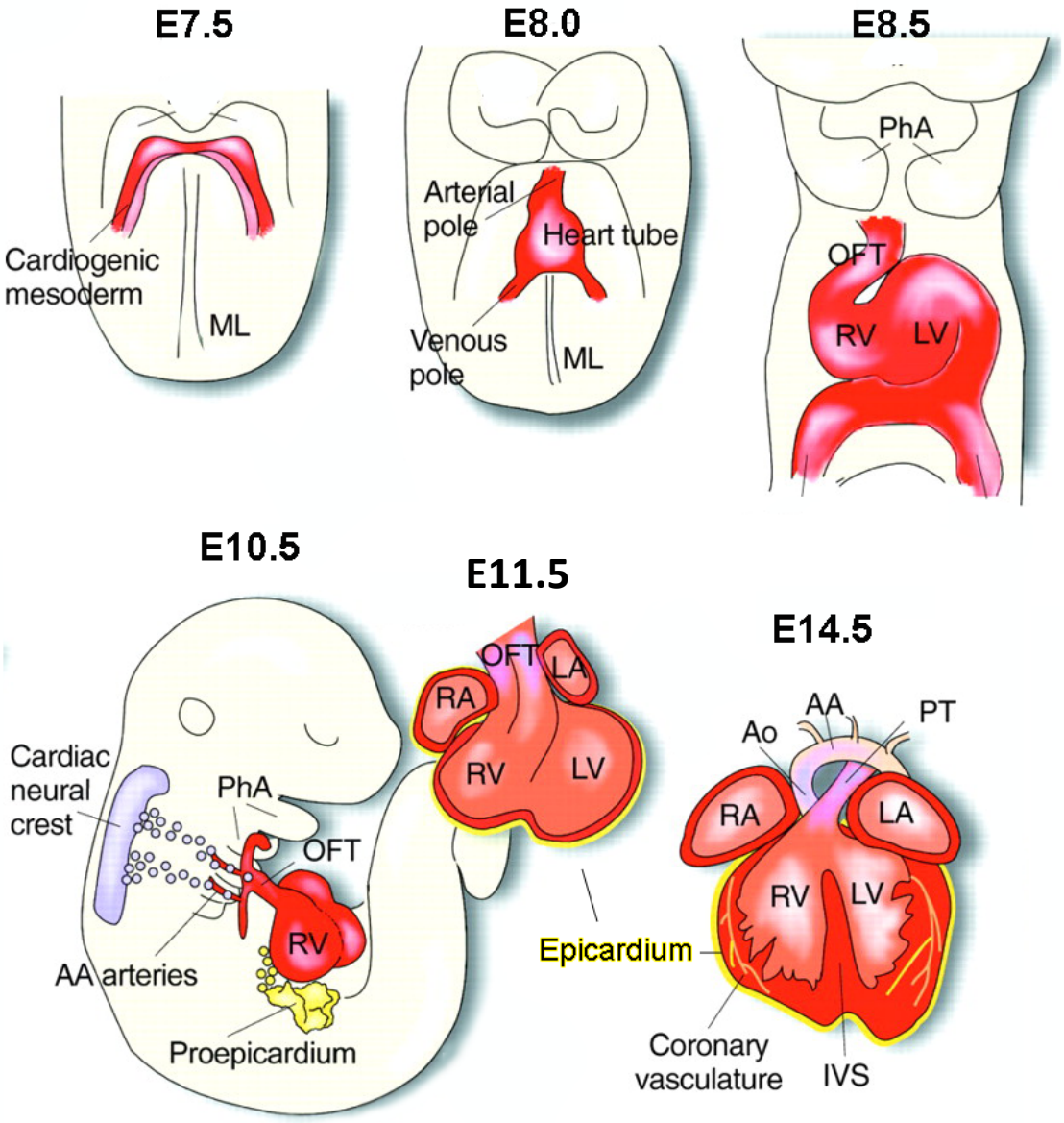


**Figure 1. 3. Schematic of mouse heart development:**
At E7.5, cardiac crescent/mesoderm is formed. At around E8, the cardiac mesoderm migrates to the midline and forms the linear heart tube with arterial and venous poles in anterior and posterior portions, respectively. At E8.5 the heart tube undergoes looping to give rise to primitive chambers. At E10.5 embryonic growth drives anterior movement of the venous pole giving rise to distinct heart chambers. At this point, the transient proepicardial organ is located at the venous pole and contributes epicardial cells which migrate and cover the myocardial surface. By E15, the epicardium is uniform across the myocardial surface and has contributed to coronary vessel growth and chamber maturation. Atrioventricular septation and valve formation is complete. Neural crest cells also contribute to heart development, particularly to formation of the great vessels. AA, aortic arch; E; embryonic day; IVS, interventricular septum; LA, left atrium; LV, left ventricle; ML, midline; OFT, outflow tract; PhA, pharyngeal arches; RA, right atrium; RV, right ventricle. Adapted from Laugwitz et al (2008).

## 1.8. The Epicardium:

For most of the last century the epicardium was largely considered a dormant epithelium, but in the last three decades, it has arisen as a critical source of cells and signals for the developing heart, including fibroblasts and coronary/vascular smooth muscle cells (VSMCs) and possibly endothelial cells and cardiomyocytes (Rosenthal and Harvey, 2010, Masters and Riley, 2014). Furthermore, whilst the epicardium adopts a state of dormancy post-development, following injury in the adult heart, the epicardium reverts to an embryonic profile and acts as a pluripotent cell source and signalling centre to modulate both heart regeneration in lower vertebrates (Lepilina et al., 2006, Kikuchi et al., 2011, Schnabel et al., 2011, Wang et al., 2011, Gonzalez-Rosa et al., 2012, Mercer et al., 2013, Wang et al., 2013, Wang et al., 2015) and heart repair in mammals (Smart et al., 2007a, Smart et al., 2007b, Smart et al., 2010, Smart et al., 2011, Zhou and Pu, 2011, van Wijk et al., 2012, Huang et al., 2012, Bilbija et al., 2012, Braitsch et al., 2013, Ruiz-Villalba et al., 2015). Thus the epicardium is implicated in both developmental and regenerative myogenesis, as well as scar formation. Improved understanding of epicardial signalling in these respective settings could permit manipulation of epicardial signals to limit fibrosis and promote neomyogenesis in the adult heart after injury (Masters and Riley, 2014).

### 1.8.1 The epicardium in heart development:

At around E9.5 in mice, the mature proepicardium migrates to the myocardial surface and encapsulates the heart. After instating a uniform epithelium (at around E11) a subset of epicardial cells undergo epithelial-to-mesenchymal transition (EMT) and populate the subepicardial space. These epicardium-derived cells (EPDCs) penetrate the myocardium to give rise to numerous cardiac cell types, and are typically detected through the expression of transcription factors Wilm's tumour 1 (Wt1), T-box protein 18 (Tbx18), transcription factor 21

(Tcf21; also known as capsulin/pod1/epicardin), as well as the retinoic acid (RA) synthesising enzyme, retinaldehyde dehydrogenase 2 (Raldh2) (Rosenthal and Harvey, 2010).

### 1.8.2. The myogenic and vasculogenic potential of epicardium-derived cells

Research into the ability of EPDCs to differentiate into cardiac cell types has gained momentum in recent years and has provided an enduring source of debate. Whilst there is consensus regarding contributions to VSMCs and interstitial and perivascular fibroblasts (Perez-Pomares and de la Pompa, 2011); the potential for EPDCs to give rise to endothelium and cardiomyocytes remains contentious. Historically, this controversy has been fuelled by inter-species differences from chick and mouse studies, but more so in recent years due to (mis-) interpretation of the EPDC fate map arising from flawed or unreliable cre-loxP-based studies.

#### 1.8.2.1. Do epicardium-derived cells give rise to coronary endothelium?

Early experiments in the chick demonstrated a direct EPDC contribution to coronary endothelium by DiI labelling experiments, quail-to-chick chimera studies and retroviral analyses (Guadix et al., 2006, Gourdie et al., 2000, Manner, 1999, Mikawa and Fischman, 1992). However, fate mapping studies utilising GATA5 (Merki et al., 2005) Tbx18 (Cai et al., 2008) and Wt1 (Zhou et al., 2008) Cre lines found little or no EPDC contribution to the endothelial lineage in mice. In contrast, Red-Horse and colleagues described a sinus venosus origin of coronary endothelium (Tian et al., 2013). Wu and co-workers further proposed an endocardial origin for coronary endothelium (Wu et al., 2012). Interestingly, sub-populations of cells within the proepicardium with endothelial potential have since been defined using Semaphorin 3D (Sema3D) and Scleraxis (Scx) as Cre-drivers in lineage trace experiments. Distinct domains of Wt1, Tbx18, Sema3D and Scx expression were observed in the proepicardium, and while Sema3D and Scx expression sometimes overlapped, both were largely distinct from the canonical markers Tbx18 and Wt1. In these studies, while $Tbx18^{+}$ and

$Wt1^+$ cells were reported to give rise to vascular smooth muscle and fibroblasts, but not coronary endothelium; Sema3D and Scx progenitors contributed to all three lineages. A modest contribution to cardiomyocytes (<0.36% by Sema3D; 6.6% by Scx) was also reported (Katz et al., 2012). Further, these populations were observed to contribute to the sinus venosus and the endocardium, offering an explanation of a potential common endothelial cell progenitor source to reconcile previous conflicting reports (Red-Horse et al., 2010, Tian et al., 2013, Wu et al., 2012).

#### 1.8.2.2. Do epicardium-derived cells give rise to cardiomyocytes?

In the chick, none of the aforementioned studies demonstrated an EPDC contribution to cardiomyocytes, although two independent explant studies revealed that stimulation by bone morphogenic protein-2 (BMP-2) could drive chick proepicardial cells towards a cardiomyocyte fate *in vitro* (van Wijk et al., 2009, Kruithof et al., 2006). In contrast, fate mapping by Wt1 (Zhou et al., 2008) and Tbx18 (Cai et al., 2008) Cre lines in mice demonstrated significant epicardial contributions to the myocardial lineage. However, these reports were disputed: Christoffels and co-workers subsequently demonstrated Tbx18 expression in the inter-ventricular septum (IVS) and left ventricular myocardium, even in epicardium-deficient embryos (Christoffels et al., 2009). Rudat and Kispert further reported that the Wt1 Cre lines used by the Pu lab (Zhou et al., 2008) were unsuitable for lineage analyses as they were 'leaky' and demonstrated inefficient recombination (Rudat and Kispert, 2012).

#### 1.8.2.3 Epicardium-derived cells are a major source of coronary smooth muscle cells

In contrast to the lack of clarity surrounding the endothelial and myocardial potential of EPDCs, studies have consistently demonstrated a significant EPDC contribution to VSMCs. In standard culture medium, VSMCs are the default EPDC fate (Dettman et al., 1998, Guadix et al., 2006). Functionally, one of the roles of these cells is to provide structural integrity to the developing coronary endothelium. Intriguingly, *in vivo* EPDCs do not automatically

differentiate into VSMCs and inhibitory mechanisms are at play to permit vascular remodelling of the primary coronary endothelial plexus.

#### 1.8.2.4. Epicardium derived cells are a major source of cardiac fibroblasts

Studies in chick and mouse have also consistently identified EPDCs as the major source of embryonic perivascular and interstitial fibroblasts (Mikawa and Fischman, 1992, Manner, 1999, Cai et al., 2008, Zhou et al., 2008, Mikawa and Gourdie, 1996). Cardiac fibroblasts are a poorly defined, heterogeneous population of inconsistent morphology that express a plethora of 'markers'; including vimentin, fibroblast specific protein-1 (FSP1), discoidin domain receptor-2 (DDR2) and α-smooth muscle actin (αSMA). Key roles of cardiac fibroblasts include extracellular matrix (ECM) maintenance and turnover and coronary vessel homeostasis. Interestingly, their emergence in the embryonic heart coincides with cardiomyocyte proliferation and myocardial expansion (Ieda et al., 2009). *In vitro*, embryonic fibroblasts exert potent proliferative signals by paracrine secretions of ECM components fibronectin and collagen (Ieda et al., 2009). This report also described a positive correlation between cardiomyocyte proliferation and fibroblast density, which was dependent upon myocardial β1-integrin expression. Interestingly, adult cardiac fibroblast cultures stimulated myocyte hypertrophy but not proliferation.

To summarise, during development, EPDCs undergo EMT and give rise to VSMCs and interstitial and perivascular fibroblasts. Contributions to endothelial and myocardial lineages during development are described but the precise extent of contribution remains debatable. There are also likely to be species differences and further validation by multiple lineage tools, DiI-labelling, clonal analyses and explant co-cultures will be required. Importantly, in all recombinase based lineage analyses, the conclusions reached depend upon the assumption that the gene driving Cre expression is specific to the cell population or tissue being mapped; as well as on the efficiency of the recombination. There is, therefore, an absolute requirement

for rigorous characterisation of the native expression pattern of the Cre driving gene, alongside validation by parallel approaches, as described. Furthermore, the heterogeneity of epicardial cell-types is becoming increasingly clear, meaning that few assumptions about the epicardium can be drawn from individual Cre-reporters.

### 1.8.3. Epicardial signalling during development

In addition to direct cellular contributions to the developing heart, the epicardium and EPDCs also provide paracrine signals which influence myocardial maturation. An epicardial-derived signalling molecule that is particularly interesting with regards to its myogenic potential is RA (Sucov et al., 1994, Niederreither et al., 1997, Chen et al., 1998, Niederreither et al., 1999, Medhora, 2000, Chen et al., 2002, Stuckmann et al., 2003, Azambuja et al., 2010, Brade et al., 2011, Braitsch et al., 2012, Xavier-Neto et al., 2015).

### 1.8.4. Retinoic acid signalling

RA is a pleiotropic signalling molecule that is central to developmental patterning programs in vertebrates (Xavier-Neto et al., 2015). It is synthesised by the conversion of retinol to retinal by retinol dehydrogenases (RoDH) and then to RA by retinaldehyde dehydrogenase (Raldh) enzymes (Fig. 1.4). The most abundant of these in mesenchymal cells is Raldh2 (Niederreither et al., 1997). RA acts by entering the nucleus, either by direct diffusion or facilitated transport by cellular retinoic acid binding proteins (CRABPs) (Tang et al., 2014); which may also sequester RA in cytosol to limit RA signalling (Elder et al., 1992). In the nucleus, RA binds to retinoic acid receptor (RAR):retinoid X receptors (RXR) heterodimers to convert them from transcriptional repressors to activators at specific DNA sequences, called RA response elements (RAREs). Consequently, genes containing these sequences are transcribed in the presence of RA. RARs and RXRs are divided into distinctive α, β and γ sub-types, which each

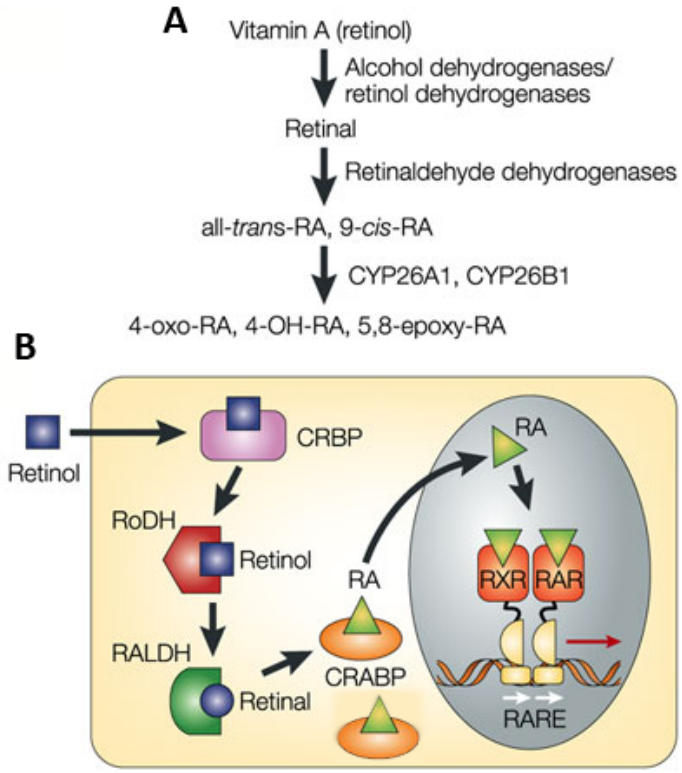


**Figure 1. 4. Retinoic acid metabolism and signalling pathway:**
(A) Retinol is converted to retinal by retinol dehydrogenases (RoDHs)/alcohol dehydrogenases. Retinal is converted to RA by retinaldehyde dehydrogenase enzymes. RA is metabolised by CYP cytochrome P450 enzymes (CYPs). (B) The cellular mechanism of retinoid action. Circulating retinol diffuses into the cell and is bound by CRBP (cellular retinol-binding protein) in the cytoplasm. Retinol dehydrogenase (RoDH) enzymes metabolize retinol to retinal and then retinal is metabolized to RA by the retinaldehyde dehydrogenases (RALDHs). RA is bound in the cytoplasm by CRABP (cellular RA-binding protein). CRABP proteins can sequester RA in the cytoplasm or transport RA to the nucleus where it binds to RA receptors (RAR): retinoid X receptor (RXR) heterodimers; which bind to a sequence of DNA known as the RA response element (RARE). This activates transcription of RA inducible genes. Adapted from (Maden, 2002)

have multiple isoforms. Some receptors are ubiquitous whilst others demonstrate tissue specificity. For instance, in the developing heart, *rarα* and *rarβ* isoforms are mostly expressed throughout the myocardium, whilst *rarγ* transcripts are specifically expressed in endocardial tissues and the developing great vessels at E12.5 (Dolle, 2009). *Rxr* genes are also ubiquitously expressed in the developing heart. Consequently, there is a level of functional redundancy between receptors, although conditional knockouts have demonstrated the absolute requirement for certain paralogs in certain cell types for normal embryogenesis (Dolle, 2009) such as *rxrα* expression in the epicardium (Merki et al., 2005), as discussed (1.8.4.1). Levels of

RA itself are majorly regulated by cytochrome P450 enzymes (typically CYP26A1/B1) which are typically expressed in RA-non-responsive cells and, themselves, contain RAREs. RA signalling is, therefore, self-regulating. This property enables the generation of RA gradients and is central to the patterning roles of RA signalling during development (Xavier-Neto et al., 2015).

#### 1.8.4.1. Retinoic acid signalling in heart development

In the developing heart, RA is a critical mitogenic and patterning factor. Mice carrying the null mutation for Raldh2 fail to undergo axial rotation and the heart comprises a single dilated chamber (Niederreither et al., 1999). Conversely, exposing embryos to a teratogenic dose of RA also leads to heart defects (D'Aniello et al., 2013) highlighting the necessity for tight regulation of RA signalling during development. Mice lacking *rxrα* die mid-gestation due to detachment of the epicardium and a hypoplastic myocardium (Sucov et al., 1994). Early evidence suggested that this phenotype was epicardium specific, as deletion of myocardial RXRα led to a normally formed heart (Chen et al., 1998) whilst 'epicardial specific' Gata5-Cre mediated RXRα deletion recapitulated the RXRα null phenotype (Merki et al., 2005). This suggested an autocrine epicardial response to RA that is necessary for heart development, irrespective of a direct myocardial RA signalling component. In this instance, fibroblast growth factor-2 (FGF2) was identified as the downstream mitogenic factor (Merki et al., 2005). However, as previously discussed, the use of Cre-lines must be interpreted with caution. Our laboratory has found that the GATA-5-Cre demonstrated non-specific recombination in numerous cardiac cell-types (Smart,N. Dube. K, Balmer. G, unpublished) and so the loss of RXRα in these mutants may not have been epicardium specific. However, an epicardium-dependent RA effect has also been demonstrated in chick heart slice cultures: RA induced cardiomyocyte proliferation in slices incorporating the epicardium, but not in those without (Stuckmann et al., 2003). Further, cultured mouse embryonic epicardial cells and stable epicardial cell lines were found to secrete factors in response to RA treatment, and this conditioned medium stimulated proliferation of cultured myocytes. However, by P4, the

potential of cultured epicardial cells to secrete factors in response to RA was lost (Chen et al., 2002).

GATA-5 Cre mediated deletion of RXRα also led to compromised coronary arteriogenesis (Merki et al., 2005). Arteriogenesis is an intricate process which involves the initial formation of endothelial plexuses, which are later remodelled by the recruitment of VSMCs and ECM components (Rosenthal and Harvey, 2010). This developmental delay maintains plasticity in the coronary network and permits vascular remodelling to accommodate increased physiological load and myocardial thickness through development. Coronary development and remodelling continues postnatally and is related to a 4-fold increase in capillary density in the first 3 weeks, coupled to a 10-fold increase in the number of VSMC coated arteries over the same time-frame (Luttun and Carmeliet, 2003). In chick proepicardial explant cultures, RA was shown to inhibit the differentiation of VSMCs by both autocrine and paracrine mechanisms (Azambuja et al., 2010). Proepicardial cultures also demonstrated inefficient RA signalling, offering an explanation as to why proepicardial cells readily differentiate into VSMCs *in vitro* - as proepicardial cultures exhibit insufficient RA signalling.

#### 1.8.4.2. Regulation of epicardial retinoic acid signalling

*Wt1* encodes a zinc-finger transcription factor expressed robustly in epicardial cells and kidney epithelium; the loss of which in the epicardium results in abnormal coronariogenesis and myocardial hypoplasia, secondary to premature differentiation of myocardial cells and reduced epicardial EMT (Moore et al., 1999). Consequently, Wt1 is widely considered the master regulator of epicardial EMT (Martinez-Estrada et al., 2010) and may mediate this effect via transcriptional regulation of *Aldh1a2 (Raldh2)* in which it has three binding motifs in the 5' prime region (Martinez-Estrada et al., 2010, Guadix et al., 2011, von Gise et al., 2011). Conditional knock-out of Wt1 in mice also reduced Raldh2 levels in the epicardium and resulted in a hypoplastic compact myocardium (Guadix et al., 2011), similar to Raldh2 mutants

and RXRα epicardial deficient mice. Huang et al (2012) also showed that CCAAT/enhancer binding protein (C/EBP) transcription factors drive both the developmental expression of epicardial Raldh2, as well as the re-expression of Raldh2 in the adult heart after injury.

### 1.8.5. The adult epicardium in cardiac homeostasis

The epicardium and its derivative cells and signals evidently play important roles in myogenesis during heart development. In the healthy adult heart, however, the epicardium becomes 'quiescent', as embryonic epicardial markers are expressed at very low levels, if at all (van Wijk et al., 2012, Zhou et al., 2011). This transition to relative dormancy is poorly characterised. In contrast, the zebrafish epicardium has been suggested to regularly contribute to adult myocardial homeostasis throughout life via an FGF dependent dialogue with cardiomyocytes (Wills et al., 2008) and may underpin perpetual myocyte turnover. This may be a significant factor for the regenerative capacity of the zebrafish heart.

### 1.8.6. The 'reactive' epicardium in fibrotic wound healing in adult mammals

In response to MI in adult mammals, the epicardium characteristically reinstates an embryonic epicardial expression profile and signals to modulate the injury response. However, reactivation of a foetal epicardial program is not associated with an appreciable myogenic response (Zhou et al., 2011, van Wijk et al., 2012, Huang et al., 2012, Mercer et al., 2013, Wang et al., 2013, Limana et al., 2010, Smart et al., 2011, Smart et al., 2012, Smart et al., 2010, Smart et al., 2007a) and may not reflect the reinstatement of an embryonic phenotype (Bollini et al., 2014). In humans, embryonic epicardial gene expression has also been reported in hypertensive and ischaemic patients in a disease specific manner (Braitsch et al., 2013). In adult hearts, EPDCs are involved in the formation of a collagenous scar (Ruiz-Villalba et al., 2015). To assess the contribution of EPDCs to fibrosis following MI and their interaction with infiltrating bone marrow cells, which also give rise to cardiac fibroblasts (Zeisberg and Kalluri, 2010), mice with *Wt1*Cre driven enhanced yellow fluorescent protein (eYFP) expression were

irradiated and transplanted with the bone marrow from mice ubiquitously expressing monomeric red fluorescent protein (mRFP). These mice then underwent LAD ligation and the relative contribution of $eYFP^+$ cells (EPDCs) and $mRFP^+$ cells (bone marrow-derived cells (BMCs)) to the infarct were assessed. By D7, densely packed populations of $eYFP^+$ and $mRFP^+$ cells were evident in the infarct core. FACS isolation of the $eYPF^+$ population demonstrated a significant increase in collagen I transcription in these cells; with negligible levels detected in the $mRFP^+$ cells. This correlated with mass extracellular deposition of collagen I, detected in parallel to elongated $eYFP^+$ EPDCs. Interestingly, the authors state that $eYFP^+$ cells appeared to be resident interstitial cells as opposed to cells derived from injury induced epicardial activation (Ruiz-Villalba et al., 2015), although it is unclear how this conclusion was reached.

### 1.8.7. Epicardium-derived cells in heart repair

As in development, the contribution of adult EPDCs to endothelial and cardiomyocyte lineages post-injury remains contentious, but highly topical given their myogenic potential. Lineage analyses by van Wijk et al (2012) revealed the formation of a Wt1 positive sub-epicardial mesenchyme, from which predominantly fibroblasts were derived, followed by a contribution of coronary endothelium and at later stages, a modest number of cardiomyocyte-like cells. Using the inducible Wt1-CreERT2 reporter, Pu and colleagues reported no epicardial contribution to cardiomyocytes or endothelial cells post-MI, but did demonstrate the secretion of pro-angiogenic factors by $Wt1^+$ EPDCs. FACS isolation and culture of this population generated conditioned medium containing relatively high concentrations of vascular endothelial growth factor (VEGF) and FGF2, which improved cardiac remodelling when administered following MI (Zhou et al., 2011).

Previous work in our lab demonstrated that 'priming' of the epicardium with the actin monomer binding protein thymosin beta-4 (Tβ4) prior to MI induction could induce a small sub-population of $Wt1^+$ EPDCs towards a myocardial fate (Smart et al., 2011). Tβ4 administration had no effect on EPDC fate when administered after MI, however, with EPDCs

almost exclusively differentiating into fibroblasts (Zhou et al., 2012, Kispert, 2012). Regardless of the debate around whether re-activated EPDCs contribute *de novo* vasculature and cardiomyocytes to the injured adult mammalian heart, the positive contribution to injured myocardium as described (Smart et al., 2011) is insufficient for effective myocardial regeneration.

### 1.8.8. Epicardial retinoic acid signalling in heart repair

Epicardial RA signalling is also implicated in wound healing post-MI in the adult mammal. Reactivation of RA signalling following adult injury is suggested by re-expression of epicardial Raldh2 (van Wijk et al., 2012). Bilbija et al (2012) aligned the upregulation of Raldh2 with a downregulation of RA degrading CYP26B1, and further utilised RARE-luciferase reporter mouse to investigate RA signalling post-MI (Bilbija et al., 2012). Fluorescent luciferase activity was detectable through the thorax, and *ex vivo* analysis identified the heart as the major source of chemiluminescent signal. Furthermore, when isolated post-MI, cardiomyocytes and fibroblasts demonstrated robust luciferase activity compared to sham treated controls. Interestingly, when all-trans RA (ATRA) was added to cardiac fibroblast cultures, proliferation was inhibited. In humans, RA levels were also increased in the hearts of patients with coronary heart disease (CHD) and RA target genes were elevated in atherosclerotic plaque biopsies (Bilbija et al., 2014).

Epicardial RA signalling may also influence the immune response to MI. Olsen and colleagues analysed enhancer regions of epicardial genes activated in response to injury and identified C/EBP binding sites in Wt1 and Raldh2 promoter regions. Inhibition of epicardial C/EBP signalling following ischaemia-reperfusion injury resulted in significantly decreased fibrosis and improved contractile function, associated with reduced neutrophil influx to the infarct zone (Huang et al., 2012). This suggests that injury-induced epicardial RA, through Raldh2, may act as a cue for immune cell infiltration and modulation of the inflammatory response.

### 1.8.9. The epicardium in zebrafish heart regeneration

Following injury in the adult zebrafish, the epicardium covering both chambers expresses embryonic markers. EPDCs then accumulate in the injury zone to modulate neomyogenesis (Lepilina et al., 2006, Kim et al., 2010, Wang et al., 2011). Early studies of resection injury in zebrafish demonstrated organ-wide epicardial *raldh2* expression as early as 24 hours post-injury (hpi) followed by *tbx18* expression by 1-2 dpi. These cells underwent organ-wide proliferation, enveloped the exposed myocardium at the resection site and invaded the injury core. As healing progressed, raldh2$^{+}$ and tbx18$^{+}$ cells became localised to the injury zone. This EPDC invasion was suggested to stimulate proliferation of resident CPCs (Lepilina et al., 2006) but subsequent lineage analyses identified pre-existing cardiomyocytes as the major source of *de novo* myocardium (Jopling et al., 2010, Kikuchi et al., 2010). In order to investigate the regenerative capacity of the epicardium itself, as well as downstream effects on myocardial regeneration, the Poss lab recently developed an inducible epicardial cell ablation system by targeting the expression of bacterial nitroreductase (NTR) to tcf21$^{+}$ cells. When treated with metronidazole (MTZ), cells expressing NTR convert this non-toxic substrate into a cytotoxin, resulting in their specific ablation. Following treatment with MTZ, around 90% of the tcf21$^{+}$ population was ablated. At 3 days post-ablation (dpa) spared epicardial cells re-entered the cell cycle and by 7 dpa, tcf21$^{+}$ cells were reinstated across the ventricles from apex to base. Fate mapping revealed that spared tcf21$^{+}$ cells were the primary source of *de novo* tcf21$^{+}$ cells. To then assess the effect of an ablated epicardium on the robust regenerative capacity of the zebrafish heart, they performed resection injury on these animals. MTZ treatment between 2 and 5 dpi reduced epicardial cell number by around 45% and reduced cardiomyocyte proliferation indices by around 33%. This was further associated with reduced muscularisation and revascularisation of the ventricle; coupled to persistence of fibrin and collagen in the resection plane.

### 1.8.10. Retinoic acid signalling in zebrafish heart regeneration

Epicardial RA has also been implicated as a myogenic cue during heart regeneration in zebrafish. Raldh2 expression was induced in the endocardium (the inner mesothelium lining the internal cardiac chambers) and epicardium in an injury specific manner (Kikuchi et al., 2011). Induced transgenic inhibition of RA receptors or expression of an RA-degrading enzyme (Cyp26a1) decreased regenerative cardiomyocyte proliferation indices by 86 and 87%, respectively, disrupting regeneration. Robust Raldh2 expression was also observed in the *Polypterus senegalus* (another ancient fish capable of regeneration) whilst only modest expression was detected in poorly regenerative adult mice post-MI. This led the authors to predict a positive correlation between the extent of injury-induced Raldh2 expression and the capacity of regeneration of respective species (Kikuchi et al., 2011)

### 1.8.11. The epicardium in mammalian heart regeneration

In zebrafish, the epicardium clearly exerts a myogenic influence on the regenerating myocardium. However, at present, relatively little is known about the role of the epicardium and its derivative signals in the neonatal mouse heart following injury. A modest increase in embryonic epicardial markers Wt1 and Raldh2 was observed 7 dpi, providing the first suggestion of epicardial activation in mammalian heart regeneration (Porrello et al., 2011); which has also since been reported by others (Rui et al., 2014). Epicardial expansion and proliferation of $Wt1^+$ cells was also observed following cryoinjury (Darehzereshki et al., 2015). To date, however, no published works have specifically addressed the role of the epicardium in heart regeneration following coronary artery ligation in neonatal mice.

## 1.9. Hypothesis

The primary aim of this thesis, therefore, was to investigate the epicardium and epicardial signalling in the postnatal switch from regenerative to reparative injury response in the

neonatal mouse following MI induced by coronary artery ligation. Given the significant involvement of epicardial RA signalling in myogenesis in the developing heart and in adult zebrafish after injury; coupled to the implied loss of epicardial RA signalling within the 'regenerative window' (Chen et al., 2002, Merki et al., 2005), we hypothesised that epicardial RA signalling influences heart regeneration following MI in newborn mice.

### 1.10. Thesis aims

To test this hypothesis, the following aims were established:

1) Learn neonatal mouse MI surgery and establish the neonatal coronary artery ligation model in Oxford.
2) Validate regeneration following coronary artery ligation in neonatal mice and characterise the regenerative process.
3) Characterise the epicardium and RA signalling through the neonatal 'regenerative window'.
4) Analyse the epicardium and epicardial signalling following injury at P1 and P7 in order to investigate the role(s) of the epicardium in regenerative and reparative wound healing.

These aims are addressed in the following chapters:

### 1.11. Chapter synopsis

**Chapter 2**

Chapter 2 outlines the general materials and methods used to perform the experiments described in chapters 3, 4 and 5. Novel materials, methods and experimental protocols, including neonatal MI surgery and magnetic resonance imaging (MRI) of neonatal mice are described separately in chapters 3 and 4, respectively.

**Chapter 3**

In order to permit assessment of the potential of epicardial RA signalling in myocardial regeneration following coronary artery ligation in the neonatal mouse, it was necessary to acquire the skills to induce this injury. To learn the surgery, I went to Hesham Sadek's lab in UTSouthwestern Medical Center, Dallas, Texas where I was trained to perform LAD ligation in neonatal mice. At the time, this procedure had not been established in any institution in the UK; nor had any neonatal mouse model of cardiac injury. Significant differences regarding the legislation of the use of animals in research between the US (Texas) and the UK meant that we encountered significant difficulty implementing the neonatal surgery protocols. Specific issues related to the use of appropriate anaesthesia and aseptic practice for *in vivo* neonatal recovery procedures. The problems encountered and efforts towards achieving the implementation of neonatal coronary artery ligation in Oxford are discussed in Chapter 3.

**Chapter 4**

Following implementation of the surgery in-house, the next step was model validation: to assess the regenerative capacity of the neonatal mouse heart in our hands. The absolute requirement for this was underscored by the publication of a study, which (coincident with our successful implementation of the surgical protocol) called into question the robustness of neonatal mouse heart regeneration. One group failed to observe complete regeneration in 100% of the 400 hearts on which they performed resection injury (Andersen et al., 2014). Although this is a completely different type of injury to LAD ligation, it highlighted the necessity of rigorous and reproducible model validation. There is also considerable disparity between the reported extents of regeneration post-ischemia induced by LAD ligation (Sen and Sadek, 2015), as discussed further in chapter 4. In order to definitively validate and characterise the model, we adapted adult mouse MRI to non-invasively acquire high resolution, functional and anatomical information in longitudinal studies of repair and regeneration, in the same neonatal mice over time. To this end, we collaborated with

Professor Jurgen Schneider and colleagues at the Biomedical Magnetic Resonance Unit (BMRU) in Oxford. These experiments are described in Chapter 4.

**Chapter 5:**

Following establishment and validation of the neonatal coronary artery ligation model; we then sought to use this model to investigate our hypothesis: that epicardial signalling is involved in modulating myocardial regeneration following cardiac injury in the neonatal mouse. These experiments are described in Chapter 5.

**Chapter 6:**

Finally, in chapter 6, the wider contributions of this project, as well as the limitations and future directions of this work are discussed. Prepared manuscripts, collaborative publications and conference abstracts are included in the appendices.

# 2

# General Materials & Methods

## 2.1. Mice

All mice were housed in either the Biomedical Services building (BMS) or at the biomedical magnetic resonance imaging unit (BMRU)/FGF, within the University of Oxford. Mouse strains used for this thesis were either outbred ICR/CD1 or RARE-LacZ strains. The latter is previously described (Rossant et al., 1991). Briefly, this strain contains three copies of the 34-bp oligonucleotide encoding the retinoic acid response element (RARE) present in the retinoic acid receptor-β (RAR β) upstream of a mouse hsp68lacZ construct, on the outbred ICR/CD1 background.

## 2.2. Tissue collection

Mice were euthanized by a Sch1 method appropriate to their age: hindbrain destruction for neonates or cervical dislocation for adult mice. Where genotyping was necessary, ear or tail biopsies were collected in 1.7mL Eppendorf tubes for DNA isolation. Hearts were excised and were prepared for different experimental end-points. For staining protocols, hearts were washed in ice-cold PBS prior to fixation in 4% PFA overnight at 4°C. For heart-lysate preparations (i.e. RNA extraction) atria were separated from ventricles and only the ventricles were homogenised. In injured hearts, the ventricular portion beneath the suture site (i.e. the infarcted portion) was used for molecular analyses. Dissected tissues were snap frozen over dry ice and 70% ethanol, and stored at -80°C for long-term storage; or were processed immediately.

## 2.3 Molecular techniques

### 2.3.1. DNA Extraction

Ear or tail biopsies were placed in 500µl tail lysis buffer (Table 2.4) and were incubated overnight at 55°C in a water bath. DNA was precipitated by addition of equal volumes of isopropanol with 30 minutes agitation at room temperature. Samples were then centrifuged

at 13,000 rpm for 15 minutes at 4°C. Supernatant was then discarded and samples were washed twice with 200µl of 70% ethanol. Following washes, ethanol was aspirated and samples were re-suspended in 200µl TE buffer (Table 2.4). Prior to use, samples were incubated at 37°C for 30 minutes and vortexed.

### 2.3.2. Polymerase chain reaction (PCR)

Genotyping PCRs were carried out using PCR beads (GD Healthcare) in a 96 well Veriti™ thermal cycler (Applied Biosystems). 0.05pmol/ml of forward and reverse primers was added to 5µl of total DNA in TE buffer to a total volume of 25µl. Primer sequences and thermal cycler program are shown in Table 2.1.

**Table 2. 1. Primer sequences and thermal cycles for genotyping**

| Gene | Forward | Reverse | Thermocycler program | | |
|---|---|---|---|---|---|
| RARE-LacZ | CGTGGCCTGATTCATTCC | ATCCTCTGCATGGTCAGGTC | **TaqGenome2:** | | |
| | | | **Temperature** | **Time** | **Cycles** |
| | | | 94°C | 2:00 | X1 |
| | | | 94°C | 00:30 | X35 |
| | | | 58°C | 00:30 | |
| | | | 72°C | 00:45 | |
| | | | 4°C | Until use | |

### 2.3.3. Agarose gel electrophoresis

DNA samples were separated on agarose gels to discriminate transgenic animals from wild-type littermates. 1.5% weight by volume agarose gels were made by dissolving 1.5g agarose (Sigma Aldrich, UK) in 100ml of TBE buffer (Table 2.4) and boiling in a microwave. 5µl of Gel-Red (VWR) was added to the molten solution before pouring the gel. Plastic combs were used to create an appropriate number of wells per sample-set. Orange DNA Loading Dye (Life

Technologies) was added to samples prior to transferring to wells. A current of 120 V was passed through the gel for around 45 minutes (or until the bands were sufficiently resolved). Gels were visualised using a UV box.

### 2.3.4. RNA Extraction

RNA extraction was performed using the miRNeasy kit (Qiagen, UK) according to manufacturer's instructions. Hearts were extracted and ventricles were dissected from atria. Previous observations of differential atrioventricular molecular expression profiles (Smits A, Dube K, Balmer G, unpublished) restricted molecular analyses to ventricular portions. Tissues were placed in 1.7ml eppendorfs (labelled using an ethanol resistant marker) and were either snap frozen by placement over 70% ethanol on dry-ice for storage; or placed in 700µl QIAzol solution for immediate homogenisation. Ventricles were homogenised using a tissue grinder followed by aspiration with a sterile 21G needle and RNase free 1mL syringe (BD Biosciences). Briefly, post-homogenisation, 140µl chloroform was added to the samples, which were vigorously shaken and allowed to stand for 2 minutes at room temperature. Samples were then centrifuged at 12,000 x g for 15 minutes at 4°C. The upper aqueous phase was extracted and transferred to a fresh reaction tube containing 525µl 100% ethanol and was thoroughly mixed. This solution was then transferred to a mini spin column which was centrifuged at 10,000 rpm for 15 seconds at room temperature. Flow-through was discarded. The column was then washed by addition of 700µl RWT followed by 15 seconds centrifugation (10,000 rpm, flow-through discarded); followed by addition of 500µl RPE, with 15 seconds centrifugation (10,000 rpm, flow-through discarded). RNA was then eluted from the column in 31µl RNase free water. RNA quality and quantity was measured using a Nanodrop2000 (ThermoScientific, UK).

### 2.3.5. cDNA synthesis

Complementary, i.e. double-stranded, DNA was synthesised from the mRNA template by reverse transcription. Reactions were prepared in 200µl reaction tubes (ThermoFisher Scientific). 1ug of RNA was added to each reaction tube (according to the measured quantity of RNA) and was made up to a total volume of 8.5µl with DEPC water. A masterMix containing 0.5µl of random primers (20µg/ml; Promega); 1µl dNTPs (from 10mM GE Healthcare); 2µl $MgCl_2$ (25mM, Thermo Scientific); 2µl Dithiothreitol (DTT; 0.1M, Life Technologies); 1µl RNasin® plus RNase inhibitor (Promega); 4µl 5X FS Buffer (Life Technologies) and 1µl of SuperScript® III Reverse Transcriptase (Life Technologies) was made for the number of samples (n) + 1. 11.5µl of this mix was added to each RNA sample. For each reaction set, a separate mix lacking the SuperScript®III Reverse Transcriptase enzyme was included as a negative control sample for downstream experiments. The reaction tubes were then placed in a 96-well Veriti™ thermal cycler (Applied BioSystems) and cycled at 25°C for 10 minutes; 42°C for 50 minutes and 70°C for 15 minutes, before cooling to 4°C. Samples were diluted to 4ng/µl in DEPC water and stored at 4°C short-term or -20°C long-term.

### 2.3.6. quantitative real-time PCR (qRT-PCR)

qRT-PCR was used for relative quantification of genes of interest. Reactions were performed in 0.1ml Fast 96-well plates on a ViiA™ 7 Real-Time PCR System. 4ng (1µl) cDNA was added per well; to which, 6.25µl SYBR® Green (Fast-mix; Life Technologies); 3.25µl DEPC $H_2O$; and 0.25µl of each primer was added, to a total volume of 11µl. All samples were run in triplicate. The thermal cycles were 95°C for 15 minutes; 40 cycles of 95°C for 15 seconds and 60°C for one minute. A melt-curve to detect non-specific amplification products was run where un-tested primers were included in the experiment. Cycle Threshold (Ct) values were determined using the ViiA™ 7 Software and values were exported to Microsoft Excel for manual analysis. Primer sequences are listed in Table 2.2. Relative quantification of gene expression was determined

using the comparative cycle threshold method ($2^{-\Delta\Delta CT}$) (Livak and Schmittgen, 2001). ΔCt values were calculated by normalisation of Ct values of genes of interest to either GAPDH or an average of the Ct values for the 18S and GAPDH. ΔΔCt values were calculated by calibrating values to calibration samples i.e. adult heart samples for post-natal time-course studies and time-matched intact controls for post-infarction studies.

**Table 2. 2. Primer sequences:**

| Gene | Forward | Reverse |
|---|---|---|
| **Wt1** | TTCAAGGACTGCGAGAGAAG | GGGAAAACTTTCGCTGACAA |
| **TbX18** | ACGAAATAGGCACCGAGATG | TTGTCCACCGGCACAATATC |
| **Tcf21** | CGACAAGTACGAGAACGGTTAC | TGTAGTTCCACACAAGCGGTT |
| **Raldh2** | TGCCACCCGCGACAA | TTGTTGTGAGGCAAGAGTGG |
| **RARα** | CTGGACTGCTCAGTGCCATCT | TGCAGCATGTCCACCTTGTC |
| **RARβ** | GGGTAAATACACCACGAATTCCA | TGTCCCAGAGGCCCAAGTC |
| **RXRα** | ATGGACACCAAACATTTCCTGC | CCAGTGGAGAGCCGATTCC |
| **RXRβ** | CCACCTCTTACCCCTTCAGC | TGGAAGAACTGATGACTGGGA |
| **CYP26B1** | TGCCACCCGCGACAA | GGAACCCTGTAGCAACCAGTGA |
| **CRABPII** | GCGAGCAGAGGCTTCTGAAG | CATTGTCAGGATCAGCTCTCCAT |
| **Fibronectin** | GCAGTGACCACCATTCCTG | GGTACGCAGTGAGCTGAACAC |
| **ProCol3A1** | GTGTGCAATATGATCCAACTAAGTC TC | CCCACAAAAATAACACTGCAAACA |
| **FSP-1** | TCCACAAAATACTCAGGCAAAGAG | GCAGCTCCCTGGTCAGTA |
| **18S** | CATTCGAACGTCTGCCCTAT | GTTTCTCAGGCTCCCTCTCC |
| **GAPDH** | AGGTCGGTGTGAACGGATTTG | TGTAGACCATGTAGTTGAGGTCA |

## 2.4. Staining methods

### 2.4.1. Whole-mount X-Gal staining

Whole hearts were collected into ice-cold PBS plus 2mM $MgCl_2$ in individual wells of a 24 well-plate and were fixed for 2 hours in X-Gal fixative (see table 2.4) at room temperature. Hearts were then washed 3 x 5 minutes in PBS + 2mM $MgCl_2$ at room temperature before being placed in 1.5ml 5-bromo-4-chloro-3-indolyl-β-D-galactosidase (X-Gal) staining solution (Table 2.4) overnight at room temperature. Post-staining, hearts were post-fixed in 4% PFA for 2 hours at room temperature before being washed (3 times for 5 minutes) and stored in PBS at 4°C. Hearts were then imaged using a Zeiss dissecting microscope with Zen imaging software.

### 2.4.2. Whole-mount immunostaining

Postnatal hearts were dissected into ice-cold PBS and fixed in 4% PFA overnight at 4°C. Following 3 PBS washes, hearts were washed twice in 0.3% Triton-X in PBS and incubated in blocking solution (1% BSA, 0.3% TritonX-100 in PBS) for two hours and then incubated for 48 hours in primary antibody (Table 2.3) in blocking solution. Hearts were then washed 5 times in 0.3% Triton-X100 in PBS at room temperature for 1 hour per wash before being incubated overnight in Alexafluor® secondary antibody overnight at 4°C. The following day, hearts were again washed 5 times in 0.3% Triton-X100 in PBS at room temperature and were subsequently post-fixed for 30 minutes in 4% PFA.

Hearts were mounted for confocal microscopy by dissecting along the coronal axis and placing on Superfrost$^{+}$ slides (Fisherbrand, UK). Each slide was fitted with 4-7 layers of electrical tape, into which wells were cut with a scalpel blade, deep enough to cover the tissue with a 22x50mm coverslip and mounting media (1:1 PBS, glycerol with 1:500 DAPI). Slides were sealed with clear nail varnish.

### 2.4.3. Wax embedding

Whole hearts were collected, washed in ice-cold PBS and fixed in 4% PFA overnight at 4°C. Hearts were then dehydrated through ethanol series (50%; 70%; 80%; 90%; 96%; 100%; 100%; at least 2 hours per solution) and were placed in butanol overnight. Samples were then washed in 50:50 butanol and paraffin wax (Histoplast, Fisher) at 56°C for one hour; after which they were washed through 100% paraffin (56°C) twice (1 hour each time) before tissue orientation and embedding (in histoplast). Sections were cut at 8µm on a microtome and mounted on Superfrost slides. Slides were left to dry overnight on a heated rack (40°C) before use.

For all staining procedures, sections were deparaffinised by washing through Histoclear (Fisher Scientific (twice for 5 minutes) and were rehydrated through ethanol series (as for dehydration, in reverse order).

### 2.4.4. Haematoxylin and Eosin staining

This protocol was performed at room temperature. Post rehydration, slides were washed once in PBS before being immersed in Haematoxylin (Sigma Aldrich, UK) for 5 minutes. The slides were then cleared under running tap water for 5 minutes (or until the water ran clear). Following immersion in distilled water, slides were immersed in Eosin staining solution (Sigma, UK) for approximately 1 minute and then rinsed in distilled water. The slides were then quickly dehydrated (as for rehydration, in reverse order) and mounted using DPX mounting media (Sigma, UK).

### 2.4.5. Masson's Trichrome staining

This protocol was performed at room temperature according to manufacturer's instructions (Sigma Aldrich, UK; HT-15). Briefly, post-rehydration, slides were washed once in PBS before being immersed in Bouin's fixative solution overnight. Slides were then immersed in the following solutions: Haematoxylin (5 minutes then wash under running tap water followed by distilled water); Beibrich Scarlet-Acid Fushchin (5 minutes then wash with distilled water); Working-Phosphotungstic/Phosphomolybdic acid solution (5 minutes); Analine Blue solution (5 minutes); 1% Acetic Acid solution (30 seconds). Slides were then rinsed in distilled water and quickly dehydrated (through ethanol series into histoclear) and were mounted using DPX mounting media.

### 2.4.6. Immunostaining

#### 2.4.6.1. IHC-P

This protocol was optimised for β-galactisidase immunostaining using the antibody listed in Table 2.3. Post-rehydration, slides were placed in 3% $H_20_2$ for 30 minutes. Slides were then

washed in PBS before boiling for 5 minutes in low pH citrate based antigen unmasking solution (VectorLabs, UK: HH-30) in a pressure cooker. Tissue sections were then permeabilised with 0.3% Triton X100 at room temperature for 15 minutes, and were blocked with TNB solution (Table 2.4) for 30 minutes. Primary antibodies were diluted in TNB and applied to tissue sections according to dilutions described in Table 2.3 and were left to incubate overnight at room temperature. The next day, slides were washed in TNT (Table 2.4) 3 times prior to incubation with biotinylated secondary antibody (for TSA amplification of rabbit antibodies in CY3 channel; 1:200 in TNB) with Alexafluor488 (1:500 in TNB) for 2 hours at room temperature. Herein, slides were protected from the light. Amplification slides were then incubated with Streptavidin-HRP (1:200 in TNB) for 3 minutes at room temperature; were washed 3 times in TNT; and were incubated with Fluorophore tyramide (Perkin Elmer) (1:200 in Amplification diluent) for 5 minutes at room temperature. Non-amplified slides were incubated for 2 hours in appropriate Alexafluor secondary antibody. All slides were then washed 3 times for 5 minutes in TNT and were mounted in 1:1 PBS:Glycerol containing 1:500 Topro nuclear stain (emission wavelength ~642; Invitrogen). Sections were then imaged using either epifluorescence or confocal microscopy.

**Table 2. 3. Antibodies:**

| Antibody | Supplier | Catalogue # | Species | Concentration |
|---|---|---|---|---|
| **β-galactosidase** | MP Biomedicals | 8559762 | Rabbit | 1:500 |
| **Wt1** | Abcam | ab89901 | Rabbit | 1:500 |
| **Raldh2** | Abcam | ab75674 | Rabbit | 1:500 |
| **TnI** | Millipore | MAb1691 | Mouse | 1:200 |
| **aSMA** | Sigma | A2547 | Mouse | 1:1000 |
| **Vimentin** | Abcam | ab45939 | Rabbit | 1:1000 |
| **Fibronectin** | Abcam | ab2413 | Rabbit | 1:200 |
| **DDR2** | Abcam | ab126773 | Rabbit | 1:200 |
| **Biotynylated goat α rabbit** | Dako/Aligent Tech. | E043201-8 | Goat | 1:200 |
| **Streptavidin HRP** | Perkin Elmer | NEL702001KT | N/A | 1:200 |
| **Alexafluor®goat anti mouse 594** | Invitrogen | A-11001 | Goat | 1:500 |

### 2.4.6.2. Quantification methods

#### 2.4.6.2.1. Measuring infarct size

Infarcts were quantified using Amira Software at the Amsterdamsch Medical Centruum in the Netherlands under the guidance of Dr Maurice Van Den Hoff and Dr Jan Ruijter or using ImageJ software in-house. Total myocardial area and TnI negative/infarct areas were marked between 2-10 sections from apex to suture site per heart. The ratio of infarcted left ventricular myocardium was calculated relative to total left ventricle area in hearts injured on P1 or P7, four days post-MI. Injury zone was calculated similarly but included epicardial and endocardial borders either side of the infarct core and was presented as a percentage of total myocardial area.

#### 2.4.6.2.2. Counting β-gal positive cells

Total nuclei counts were performed over 8-10 sections per heart and the total number of nuclei within positive regions of β-gal signal were calculated within the infarct and adjacent epi/endocardial borders (i.e. injury zone) and intact myocardium (i.e. remote zone). The percentage of β-gal positive cells relative to the total nuclei count were calculated, as were the percentage distribution of the total β-gal positive cells across injury and remote zones, in hearts injured at P1 or P7, 4 days post-MI.

#### 2.4.6.2.3. Counting β-gal$^+$/αSMA$^+$ vessels

Total vessel counts were performed over 3-10 sections per heart and total the number of vessels with any overlapping regions of β-gal$^+$/αSMA$^+$ signal were calculated within the infarct and adjacent epi/endocardial borders (i.e. injury zone) and intact myocardium (i.e. remote zone). The percentage of β-gal$^+$/αSMA$^+$ vessels relative to the total vessels were calculated, as were the percentage distribution of β-gal$^+$/αSMA$^+$ vessels across injury and remote zones, in hearts injured at P1 or P7, 4 days post-MI.

### 2.5. Flow assisted cell sorting (FACS)

See appendix III.

### 2.6. Neonatal left anterior descending coronary artery ligation surgery

Described in depth in Chapter 3.

### 2.7. Neonatal MRI

Described in chapter 4.

### 2.8. Data analysis

Data are presented as mean±SEM (unless otherwise stated). Multiple group comparison was performed by one-way ANOVA with Tukey's multiple group comparisons using GraphPad

Prism 5 (GraphPad Software, Inc.). Comparisons between two groups were performed using the unpaired Student's t test where normality of data was assumed or Mann Whitney where it was not. $P<0.05$ were considered statistically significant.

**Table 2. 4. Solutions:**

| Solution | Recipe |
|---|---|
| **'Tail' lysis buffer** | 100mM Tris pH8.5; 5mM EDTA; 0.2% SDS; 200mM NaCl with 0.05mg/ml Proteinase K |
| **TE buffer** | 10mM Tris ph8.0; 1mM EDTA |
| **TBE buffer** | 40mM Tris pH8.0; 20mM Boric acid; 1mM EDTA |
| **Protein lysis buffer** | 150mM NaCl; 50mM Tris HCl pH 8; 1% NP-40 substitute; 1mM EDTA with proteinase/phosphatase inhibitor cocktail (1:1000) (New England Biolabs) |
| **X-Gal fixative** | 2.7ml of 37% Formaldehyde; 0.8ml of 25% Glutaraldehyde; 0.2ml of 2% NP40 substitute; up to 100ml (96.3ml) with PBS + 2mM $MgCl_2$). |
| **X-Gal staining solution** | 5mM $K_3Fe(CN)_6$; 5mM $K_4Fe(CN)_6$ (0.823g and 1.056g, respectively in 500ml $H_20$) + 1.25mg/ml X-Gal substrate in DMSO. Add fresh to 50ml staining solution. |
| **Antigen unmasking solution** | (VectorLabs) 1:100 in distilled water |
| **TNB** | 0.1M Tric-HCl, Ph7.5; 0.15M NaCl; 0.05% Tween; 0.5% BSA blocking powder |
| **TNT** | 0.1M Tric-HCl, Ph7.5; 0.15M NaCl; 0.05% Tween |
| **Blocking solution** | 1% BSA in 0.3% TritonX-100 in PBS |

**Table 2. 5. Kits and reagents:**

| Reagent/Kit | Supplier | Catalogue # |
|---|---|---|
| **Gel Red Nuclear Stain** | VWR | 730-2958 |
| **Orange DNA Loading dye (6X)** | ThermoFisher Scientific | R0631 |
| **miRNeasy Kit** | Qiagen | 217004 |
| **SYBR Green** | Applied Biosystems | 4385612 |
| **X-Gal** | Invitrogen | 15521-018 |
| **Haematoxylin** | Sigma Aldrich | MHS32 |
| **Eosin** | Sigma Aldrich | HT1109132 |
| **Masson's Trichrome stain kit** | Sigma Aldrich | HT15 |
| **Antigen unmasking solution** | Vector Laboratories | HH3300 |
| **TSA Amplification kit** | Perkin Elmer | NEL702001 |
| **Topro nuclear stain** | Life Technologies | T3605 |

# 3

# Model Development

## Establishment of neonatal coronary artery ligation surgery

In order to investigate epicardial potential in neonatal mouse heart regeneration, it was necessary to learn and establish the surgical method. Prior to the beginning of my project, however, this procedure had not been established in any institution in the UK. Indeed, the protocol to describe the methodology was not published until February 2014. In the absence of a formal report on cardiothoracic procedures in neonates, we were restricted by a clause in our project licence that prohibited the use hypothermia beyond post-natal day 5 (P5). Hypothermia is indispensable for cardiothoracic procedures in neonates as it induces reversible circulorespiratory arrest, which is well tolerated and facilitates heart access without the need for intubation. Therefore, it was necessary to adapt the standard anaesthetic protocol and amend the existing project licence. Secondary to this, it was necessary to develop an aseptic protocol to bring surgical standards in line with EU requirements. The established neonatal LAD ligation procedure was, therefore, modified to incorporate novel anaesthetic and aseptic protocols. This chapter chronologically documents efforts towards acquiring Home Office approval and the establishment of the neonatal left anterior descending (LAD) coronary artery ligation injury model in Oxford. Procedural modifications were made with the guidance of University Veterinary staff: Dr Kathy Murphy and Dr Caroline Bergmann; and in collaboration with Mr Rick Carver, the Home Office Inspector for the University of Oxford.

## 3.1. Surgical materials and methods

### 3.1.1. General equipment

Wet ice

Ice pack (flat surface)

Tissue paper

Autoclave

Autoclave bags

Petri dish

Heat lamp (cat#88254; Medisana)

Tape

Cotton buds

Warming chamber

### 3.1.2. Anaesthetics:

Isoflurane

Oxygen

Vaporisation unit and tubing

Induction chamber

Marcain (AstraZeneca) Polyamp steripac 0.25%

Saline 0.9%

### 3.1.3. Sterile/sterilising equipment:

Glass bead Sterilizer

Sterillium surgical hand sterilant (cat#CLE1580; SparksLabStore (SLS))

Sterile Gloves (cat#112-1339; VWR)

Sterile drape (n of animals + 1)

Access to an autoclave

### 3.1.4. Surgical instruments:

Surgical scissors (cat#14060-10; Fine Instruments)

Curved forceps (cat#15915-G; Fine Instruments)

Sharp forceps (cat#11063-07; Fine Instruments)

Short blunt forceps (cat#11063-07; Fine Instruments)

Sprung needle holder (cat#500223-G; World Precision Instruments)

7-0 prolene taper-point sutures (cat#W8702; Ethicon)

Microscissors (cat#15000-08)

Sugi sponge points (cat#31603; Kettenback GmbH & Co. KG)

Elastic band

## 3.2. Surgical training:

In August 2013, I visited Dr Hesham Sadek's lab at the University of Texas South-western Medical Centre to be trained in the neonatal coronary artery ligation surgery. Training was performed on 20 mice across 4 litters of C57bl6 or CD1 mice under the guidance and supervision of Dr Shalini Muraldihar. The age range of the mice was P1 – P7 spanning 'regenerative' and 'reparative' time-points, respectively. As taught, the procedure involved placement of the animals on wet ice until akinesia and apnoea were observed. Coronary artery ligation surgery was then performed as follows:

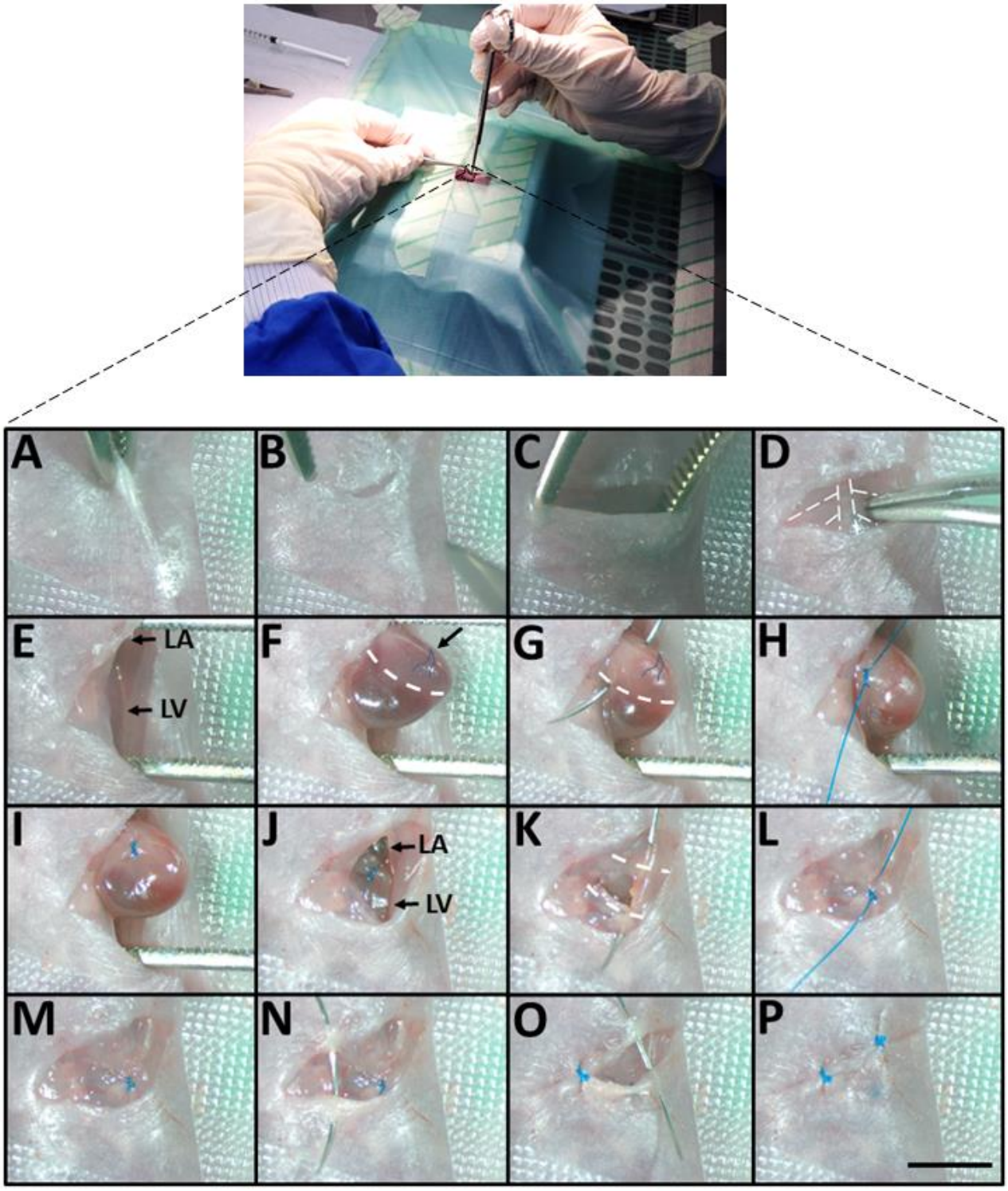


**Figure 3. 1. Neonatal coronary artery ligation surgery:**
(A) a skin incision was made using surgical scissors (A, B) and was expanded by blunt skin dissection with curved forceps (C). Thoracotomy was performed by penetrating 4$^{th}$ intercostal space with sharp forceps (D) and was then expanded using blunt forceps to visualise the heart (E). Pressure was applied to the left thorax and abdomen to expose the heart (F) Blue line indicates position of the left coronary vein dashed white line indicates the septum as landmarks. A 7.0 prolene suture was passed through the left ventricle from the lateral border of the left atria to the septum, above the left coronary vein (G-I). Blunt forceps were removed and normal organ orientation was restored (J). Thoracotomy was closed by diagonal placement of a 7-0 prolene suture (K-M) and the wound was closed by two discontinuous sutures (7.0 prolene) (N-P). Scale = 500µm. LA, left atria; LV, left ventricle.

The mouse was secured onto the surgical area, comprising an ice-pack covered with absorbent tissue and a sterile drape (Fig. 3.1). The left forelimb was taped down first to position the lungs in as lateral position as possible within the left thorax. This prevented damage to the lungs during thoracotomy and subsequent coronary artery ligation. A small skin incision was made with surgical scissors and the wound was widened by blunt dissection of the skin from underlying tissues (Fig. 3.1 A-C). Using sharp forceps, the 3$^{rd}$ intercostal space (between the 3$^{rd}$ – 4$^{th}$ ribs, Figures 3.1 and 3.2) was punctured and the thoracotomy was broadened using blunt forceps (Fig. 3.1. D-E). Pressure was then applied to the abdomen and right thorax to expose the heart (Fig. 3.1.F). Using a taper-point 7-0 prolene suture, the needle was passed through the left ventricle from the lateral border of the left atria to the septum, above the left coronary vein (Fig. 3.1. G). A surgeons knot was tied and secured to place the ligature and occlude blood flow through the LAD (Fig. 3.1. H-I). Blunt forceps were removed to allow organ repositioning (Fig. 3.2. J). The thoracotomy was then closed by placement of a 7-0 prolene suture through the 2$^{nd}$ and 4$^{th}$ intercostal muscles (i.e. above and below the thoracotomy site) in a diagonal orientation (lateral to midline from 2$^{nd}$ to 4$^{th}$ (Figure 3.1. K-M). This is a critical step. If the thoracotomy is not properly sealed, this will be evident immediately on return of respiration and will manifest as an air bubble beneath the skin at the thoracotomy site. If this is observed, normal respiration will not return due to loss of pressure in the thorax and the animal should be humanely killed by a Schedule 1 method. Two discontinuous sutures were then used to close the wound (Figure 3.1. N-P). The standard protocol is to close the wound with skin glue (Mahmoud et al., 2014) but in my experience the dam would groom the post-operative pups and remove the skin glue leading to wound dishedence. This was reduced with suture placement. The animal was then warmed and recovered in front of the heat lamp. Physical stimulation is critical for this process and was either provided directly by the experimenter or by housing the recovering pup with other littermates. Once spontaneous

respiration was regular, light pressure was applied to the tail to stimulate spinal reflexes which aided resuscitation.

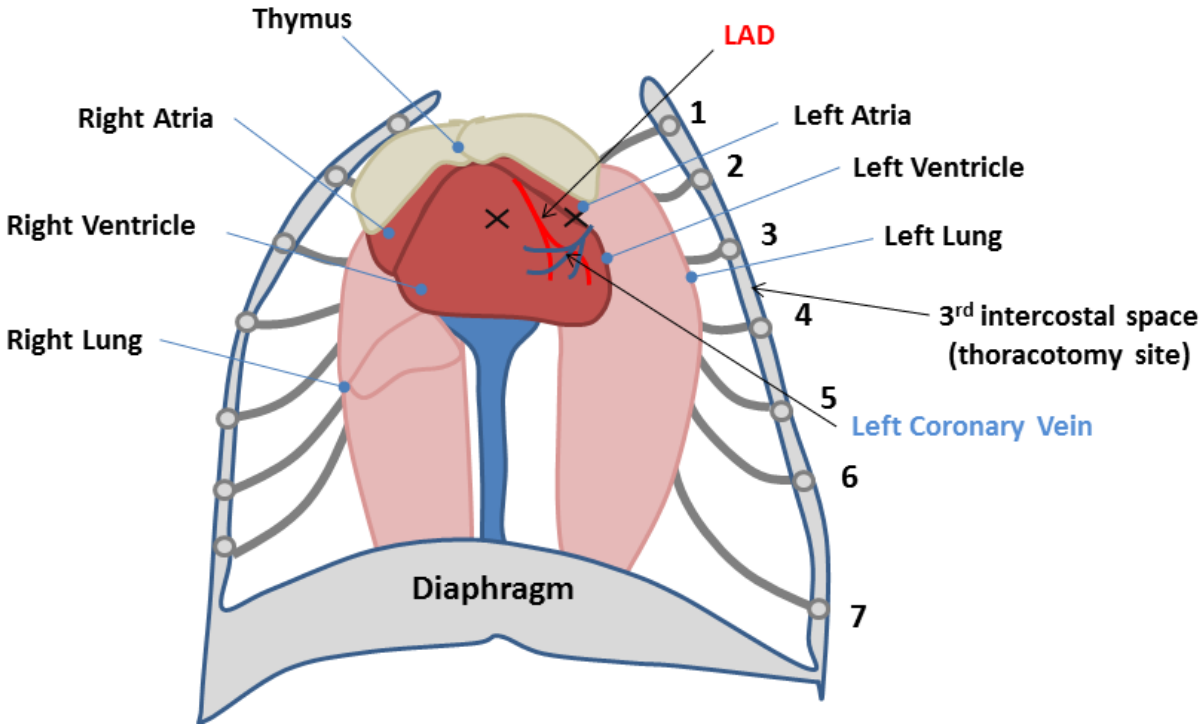


**Figure 3. 2. Diagram of thorax and key surgical landmarks:**
Thoracotomy is performed between 3rd and 4th ribs (numbered) and crosses on left ventricle indicate entry and exit point of the suture to occlude blood flow through the left anterior descending coronary artery (LAD). Approximate positions of the left coronary vein (blue) and LAD (red) are indicated.

### 3.3. Anaesthetic protocol development and project licence amendment

#### 3.3.1. The requirement for Home Office project licence amendment

The surgery, as developed by the Sadek lab, relied solely upon hypothermia as means of anaesthesia for the duration of the procedure across all neonatal ages (up to P13). However, the Home Office Inspector at the time implemented restrictions on the use of hypothermia beyond P5. Thereafter, we were instructed to use volatile agents for anaesthesia; which proved impossible. Open-chest surgery requires mechanical ventilation by tracheal intubation, which is extremely challenging in mice younger than P14. In order to be able to incorporate the critical P7 time-point, therefore, we had to significantly modify the anaesthetic protocol. It was agreed that we could attempt to modify the anaesthetic protocol under the current project licence with the supervision of University veterinary staff, in neonates up to P5. If successful in these mice, we could then extend these parameters to later neonatal stages and submit a new license protocol for amendment to extend the use of hypothermia beyond P5.

#### 3.3.2. Anaesthesia in neonatal mice

Despite widespread use of neonatal mice in research, spanning stroke (Tsuji et al., 2013) to adoptive transfer (Pievani et al., 2015) there is a lack of consensus regarding appropriate means of anaesthesia for survival procedures. Indeed, it remains contentious whether or not neonates have the capacity of nociception (pain reception or processing) at all (Marchant, 2014). The publication describing the cardiac injury models of Sadek and colleagues (2014) highlights one side of this debate by declaring anaesthetics both ineffective and redundant (Mahmoud et al., 2014). In contrast, the effectiveness of anaesthetics in neonates, particularly inhalant anaesthetics such as isoflurane, is widely demonstrated and recommended for a majority of experiments involving neonatal rodents (Fish et al., 1997); particularly for neurosurgical and non-invasive imaging procedures. As with adult surgeries, isoflurane (and other volatile agents) are advantageous as they allow the experimenter to easily monitor and manipulate anaesthetic

depth. This is a major caveat of hypothermia 'anaesthesia' as anaesthetic depth is very difficult to regulate. This is further confounded by the rapid loss of resilience to hypothermia in neonatal rodents with age (Mahmoud et al., 2014). Despite these drawbacks, hypothermia is indispensable for neonatal cardiothoracic surgeries as it induces circulatory and respiratory arrest which minimises bleeding and, importantly, maximises heart visibility and accessibility. This is unattainable by inhalant anaesthesia alone, as this method relies upon either spontaneous or mechanical respiration: neither of which is practicable for open-chest surgery in P1 mice. Mechanical ventilation by tracheal intubation is not practicable until P10 at the earliest (Lin et al., 2014), and even then is restricted by the materials available. In the absence of mechanical ventilation, the drop in thoracic pressure induced by thoracotomy invariably leads to terminal pneumothorax. Consequently, whilst inhalant anaesthetics may be the most appropriate agents for non-cardiothoracic procedures in neonates, from which the imposed restrictions were likely derived (See Boston University's Guidelines for anaesthesia for neonatal mice and rats: http://www.bu.edu/orccommittees/iacuc/policies-and-guidelines/anesthesia-of-the-neonatal-mice-and-rats/) they are unsuitable, in isolation, as an anaesthetic method for neonatal thoracotomy procedures.

### 3.3.3. Do neonatal mice feel pain?

It is widely accepted that neonatal mice do not feel pain before the second postnatal week as the cortical networks required for the transmission and perception of pain are underdeveloped at early neonatal stages in rodents (Marchant, 2014, Fitzgerald and Beggs, 2001). In my experience, however, placement of a conscious animal on ice as a means to induce a state of anaesthesia is sub-optimal; especially at later neonatal time-points. By P4, movement is coordinated enough for the animal to attempt to remove itself from the ice, which implies a meaningful response to a noxious stimulus. Further, audible and ultrasonic vocalisations (made audible by a bat detector) were detectable and more frequent than under normal conditions.

Regardless of the contentious existence of nociceptive capacity in neonates, in order to establish this procedure in Oxford, we were required by law to develop an appropriate anaesthetic method to minimise any and all potential suffering, and to demonstrate the safe and effective use of hypothermia for anaesthesia to facilitate neonatal coronary artery ligation surgery.

### 3.4. Identification of potential causes of pain during neonatal coronary artery ligation

In collaboration with Named Veterinary Surgeon (NVS) **Dr Kathy Murphy (under whose supervision the following experiments took place)** the potential causes of pain within the procedure were identified as:

1. Discomfort upon placement on ice and hypothermia induction
2. Acute pain from the thoracotomy
3. Reperfusion pain upon warming

For the purposes of anaesthetic refinement, it was decided that these were the potentially noxious events that needed to be addressed.

### 3.5. Combining inhalant and local anaesthesia with hypothermia for LAD ligation surgery

Given the widespread use of isoflurane in neonatal and adult rodent procedures, we decided to combine isoflurane with hypothermia. We reasoned that isoflurane anaesthesia should be used prior to the induction of hypothermia to eliminate discomfort upon placement on ice. A secondary benefit of this would be that circulorespiratory arrest would minimise clearance of isoflurane; the residual presence of which would convey anaesthesia upon reperfusion post-operatively, thus also addressing point 3, above. In case residual isoflurane levels were insufficient to convey appropriate anaesthesia, isoflurane supplementation could be further employed at a low concentration once respiration was resumed post-operatively (too high a concentration of isoflurane could be detrimental as it can act as a respiratory depressant at high

concentrations). However, neither isoflurane or hypothermia have any acute or long-term analgesic effect; although, as nervous transmission is lost at bodily temperatures below 9°C, the experience of pain is assumed to be lost whilst the animal is hypothermic (Antognini, 1993, Greene, 2002). As the muscular damage induced by thoracotomy can be substantial (and, therefore, potentially painful) we sought to incorporate an appropriate analgesic agent to address point 2. Agents such as non-steroidal anti-inflammatory drugs (NSAIDs) or corticosteroids were avoided so as to not affect the immune response during heart regeneration (Xin et al., 2013b). We were consequently advised to use an amide-type drug: bupivacaine (marketed as Marcain/e) which is a potent and long lasting local anaesthetic that can be applied directly to the site of injury/ (potential) pain. Marcain does not have the respiratory depressant effects of standard opioids such as buprenorphine, and was thus deemed more appropriate to be used in combination with isoflurane. Our experimental design, therefore, was to incorporate each of these anaesthetic measures into the standard protocol sequentially; assessing procedural duration, time taken to recover regular respiration; and mortality. Subjective observations of spontaneous movement (during hypothermia induction) and audible/ultrasonic vocalisations were also made. Procedural duration was a key consideration, not only to optimise individual surgeries, but to benefit the entire litter: since all pups are removed and returned to the dam simultaneously to minimise maternal distress, the duration of each surgery is cumulative to the total duration of separation. Increased separation time increased the likelihood of maternal neglect/cannibalism (Mahmoud et al., 2014). It was, therefore, crucial for animal welfare that procedural length was not extended through incorporating additional anaesthetic measures.

To begin, the whole procedure was performed according to the original protocol utilising only hypothermia as means of anaesthesia (n=6). The average duration of these experiments was 14.5 minutes from hypothermia induction to the return of regular spontaneous respiration. On average, 6.75 minutes was taken to recover spontaneous respiration upon post-operative warming. These early experiments yielded a survival rate of 79.5% (Fig. 4.3). Secondly, to incorporate isoflurane induction into this protocol, animals (n=5, P1) were placed into an induction chamber with 4% isoflurane in Oxygen (1l/min) until the righting reflex was lost (~1.5 minutes). Animals were then placed on ice until apnoea was observed, which took on average 3.5 minutes. Individual procedures by this method lasted ~13 minutes with the return of spontaneous respiration taking ~3.5 minutes. 100% of animals survived this procedure. To counter potential pain due to thoracotomy, in the next experiments (n=5, P1) we incorporated bupivacaine application (1mg/kg) to the site of thoracotomy post-closure, to avoid any direct cardiotoxic effects. The average procedure time for these animals was 13.75 minutes with respiratory recovery taking ~3.5 minutes. 100% of these animals survived the procedure. Finally, to counter any potential reperfusion pain unaddressed by residual isoflurane from anaesthesia induction; we supplemented the last cohort of animals (n=20 (10 at P2; 10 at P3)) with 0.5% isoflurane in Oxygen (0.5 l/min) via nose cone once respiration returned. The average duration of these procedures was 13 minutes with the return of regular respiration occurring in ~4 minutes. The survival rate with this protocol was 88%.

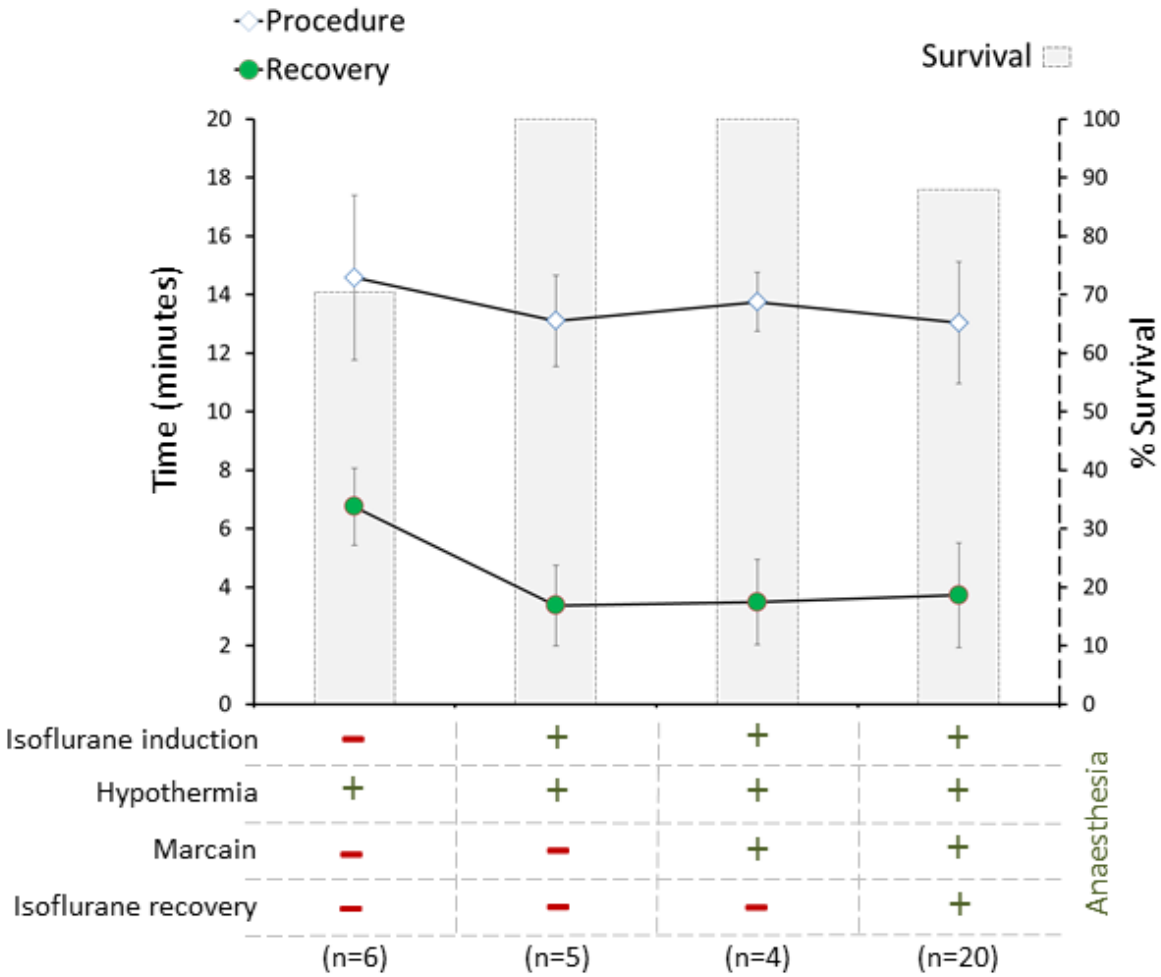


**Figure 3. 3. Effect of altered anaesthetic protocol on procedural duration, recovery and survival in coronary artery ligation procedure in neonatal mice:**
Procedural duration and time taken to recover (left y axis) is plotted alongside % survival (right y axis/histogram) when additional anaesthetic methods (x-axis) are incorporated into the anaesthetic protocol in combination with hypothermia. n = number of animals per group.

### 3.6. Licence Amendment:

These experiments demonstrated that isoflurane and bupivacaine can be used in conjunction with hypothermia for neonatal coronary artery ligation with no detriment to procedural duration; time taken to recover; or survival (beyond expected limits) (Figure 3.3). This information was collated into a report and submitted to the HO for licence amendment (Table 3.1).

**Table 3. 1. Refinement summary and proposed protocol submitted to the Home Office for amendment of 30/2987 19b11: neonatal coronary artery ligation (without reperfusion):**

| **Total surgeries:** | **20** | | |
|---|---|---|---|
| **Procedural Recovery:** | 85% | | |
| **Cannibalisation** | 0% | | |
| **Modified anaesthetic protocol Dosages and timings** | | | |
| **Issue/requirement** | **Anaesthetic method** | **Dose/concentration/method** | **Duration** |
| **Distress on hypothermia induction** | Isoflurane induction | (4% in $O_2$ (1 l/min) | ~ 01:30 |
| **Circulorespiratory arrest** | Hypothermia induction | Placement on ice | ~ 03:00 |
| **Muscular pain (thoracotomy)** | Local Anaesthetic | 0.1mg/kg | n/a |
| **Reperfusion pain** | Isoflurane on reperfusion | 0.5% in O2 (0./5 l/min) | variable |
| **Timings to be reassessed for surgeries >P5** | | | |

For P7 animals, the timings for anaesthesia were adjusted accordingly, as described in Table 3.2. P7 neonates are less resistant to hypothermia than their counterparts and thus the induction of apnoea must be closely monitored to minimise the duration of hypothermia. Figure 3.4 summarises the adaptations made to the original protocol.

**Table 3. 2. Approximate duration of induction anaesthesia for P1 and P7 mice:**

| **Age** | **Isoflurane induction (Approx. seconds)** | **Hypothermia induction (Approx. seconds)** |
|---|---|---|
| **P1** | 90 | 180 |
| **P7** | 90 | 120-180 |

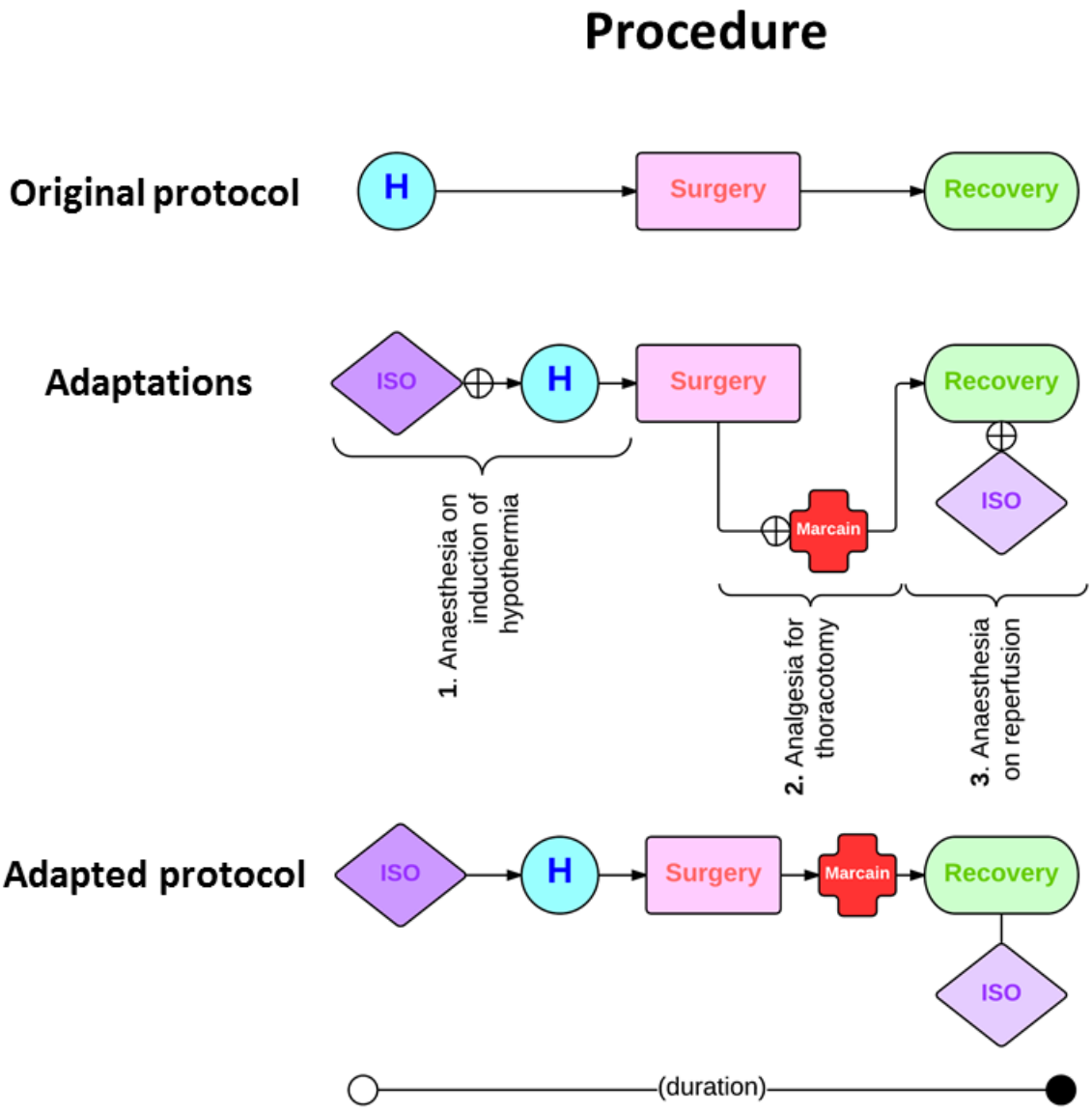


**Figure 3. 4. Development of modified anaesthetic protocol for surgical models of heart regeneration in the newborn mouse:**
The original coronary artery ligation procedure was modified to incorporate perceived refinements to address potential animal welfare concerns regarding pain/distress upon hypothermia (1.); surgical trauma (2.) and reperfusion pain (3.) Circular addition sign marks incorporation of an anaesthetic method. H = Hypothermia; ISO = isoflurane (dark purple = higher dose i.e. 5% in Oxygen; lighter purple = low dose i.e. 0.5% in Oxygen); Marcain = bupivacaine. The duration of the adapted protocol does not differ from the duration of the original protocol.

### 3.7. Aseptic technique development

Secondary to developing an anaesthetic protocol to facilitate the use of hypothermia beyond the age of P5 and establish neonatal cardiac injury models in the UK; we developed a methodology in line with best aseptic practise. Aseptic technique is a mandate of the UK Home Office for all *in vivo* recovery procedures and is implemented to minimise surgical site infections; to optimise animal welfare and experimental outcome. Despite this, aseptic technique is frequently overlooked; possibly because little exists in the way of literature to guide operators (Pritchett-Corning et al., 2011) and general training and available resources (Wolfensohn and Lloyd, 2003, LASA, 2010) describe general aseptic principals but are lacking in procedure specific guidelines.

#### 3.7.1. Causes of asepsis

These considerations were discussed with NVS Dr Caroline Bergmann who supervised and advised on implementation of aseptic technique in performing neonatal LAD ligation surgery. As in all procedures, possible contaminants fall within the following categories:

- Instruments and equipment
- The atmosphere (i.e. the procedure room and traffic in and out during surgeries)
- The surgeon
- The animal's skin

Measures were taken to control for these possible sources of contaminants in neonatal thoracotomy procedures without compromising procedural duration or, to a significant extent, financial expense.

#### 3.7.2. Instrument preparation

Prior to the start of the surgery, all tools and surgical swabs were wrapped in tissue paper; placed in an autoclave bag and autoclaved. The tools required for initial skin incision and tissue

dissection ('preparatory instruments') were prepared separately. These tools were used whilst the surgeon was undergoing sterilisation and so were kept separate from the other 'sterile' tools.

### 3.7.3. Minimising atmospheric contaminants:

The surgical area was thoroughly cleaned and, wherever possible, the operating area was set-up in a laminar flow hood. The surgical field was constructed of a flat-surface ice-pack covered with absorbent tissue and covered by a sterile drape. Although this drape did not remain sterile, it provided a clean surface on which to operate. Once the animal was secured to the operating area, the animal was draped so that only the surgical site was exposed. This set-up maintained a sterile field.

### 3.7.4. A sterile surgeon:

The surgeon scrubbed and was wearing appropriate PPE according to standard operating procedures (Wolfensohn and Lloyd, 2003). Before commencing the first procedure, two pairs of sterile gloves were worn. At the point of first incision following manipulation and positioning of the animal, the surgeon then removed the outer layer of gloves and was sterile. Alternatively, to reduce costs Sterillium (Bode Chemic, Hamburg, Germany) a propanol based surgical sterilant, was used to sterilise the gloved hands of the surgeon for all subsequent animals during batch surgery. Sterillium requires around 90 seconds to convey surgical levels of sterility. To avoid extending the length of the procedure, surgery continued with skin incision and blunt dissection of tissues with preparatory instruments (those kept separate from the rest of the tools) and progressed to thoracotomy, by which point the sterillium had taken effect.

### 3.7.5. Sterilising the skin of the animal:

Hibiscrub is a commonly used skin sterilant, but requires 60 seconds to take effect. Application would normally be performed at least 60 seconds in advance of the first incision with the

animal secured within the surgical area. Due to the time-sensitivity of the surgery, with individual surgeries typically lasting between 7.5 - 8.5 minutes, it was not possible to allow a 60 second delay between hypothermia induction and surgery. We, therefore, applied hibiscrub to the surgical area in a unidirectional motion whilst the animal was still on the ice. The average duration of hypothermia induction for P1-P7 animals was between 90 – 180 seconds with akinesia manifesting between 30 – 60 seconds. Hibiscrub was thus applied at ~60 seconds into hypothermia induction. Care was taken not to re-contaminate the surgical site post-application and whilst moving the animal from the ice to the operating area. Once secured in the operating area, the animal was covered with a sterile drape so that only the surgical site was exposed.

### 3.7.6. Subsequent surgeries:

Once individual surgeries were complete, the animals were recovered away from the sterile field and returned to a warmed chamber with their littermates. During batch surgeries, a litter can be considered microbiologically identical and thus the same set of instruments was used for subsequent surgeries. (Wolfensohn and Lloyd, 2003). Similarly, suture material was also re-used for an entire litter, which significantly reduced experimental costs. Instruments, however, were cleaned between surgeries and a bead steriliser was used to sterilize instrument tips and minimise biological transfer. In order to minimise the total duration of separation from litter and dam, the instruments were cleaned whilst the next animal was being anaesthetised. These measures maintained a sterile environment throughout the procedure to control for all key contaminants, as described in Figure 3.5.

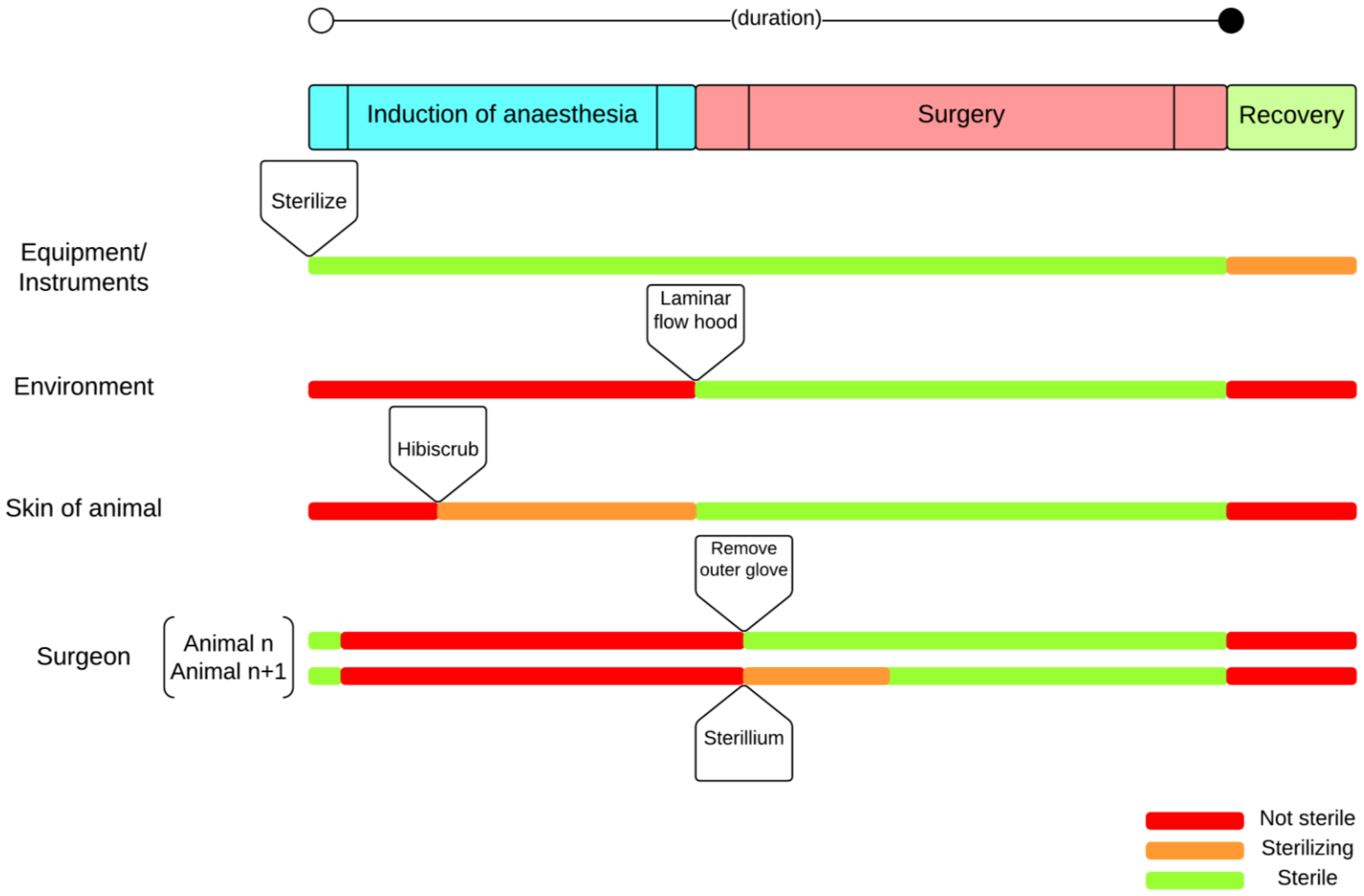


**Figure 3. 5. Aseptic measures were incorporated into the procedure without increasing experiment duration:**
Aseptic measures (arrow heads) were incorporated into the procedure to control for potential contaminants. Sterility of potential contaminant through the procedure is indicated in green (sterile); orange (sterilizing) or red (not sterile).

### 3.8. The complete modified protocol for CAL surgery:

Following incorporation of the described **anaesthetic** and *aseptic* methodologies, the complete protocol that was developed to implement neonatal LAD ligation surgery in Oxford, is as follows:

- All pups were removed from the nest and placed in a warmed chamber for the duration of the procedure.
- Droppings from the dam were collected simultaneously and were placed in the petri dish with warm water to soak.
- *All instruments were wrapped in tissue and autoclaved in three separate packages:*
  - *Preparatory instruments (surgical scissors, 2 x curved forceps)*
  - *Surgical instruments (remaining instruments)*
  - *Swabs (sugi sponge points) and cotton buds and tissues*
- *The surgeon donned two pairs of sterile gloves.*
- **The animal was anaesthetised (4% isoflurane; 1 l/minute) by placement in an induction chamber until righting reflex was lost:**
- **Hypothermia was induced: the animal was wrapped in tissue paper and buried in ice.**
- *After 30s hibiscrub was applied to the left chest in a unidirectional motion using a sterilized cotton bud. Care was taken not to re-cover or contaminate the skin surface thereafter.*
- Once akinesia and apnoea were observed, the animal was transferred to the surgical area.
- The animal was secured to the operating surface. The left arm was taped down first to orientate the left lungs in as lateral position as possible.

- *A sterile drape with a small window to allow access to the surgical site was placed over the animal and operating area.*
- *For the first animal of a batch procedure, the surgeon then removed the outer layer of gloves. For subsequent surgeries, the surgeon then applied sterillium to their gloved hands.*
- A skin incision was made using surgical scissors and the wound was widened by blunt dissection with blunt curved forceps *(i.e. the preparatory instruments).*
- Using sharp forceps, a thoracotomy was performed at the 3$^{rd}$ intercostal space.
- Thoracotomy was widened using short blunt forceps. The retraction of the forceps was adjusted accordingly by placement of the elastic band/rubber tubing at a more proximal or distal location on the forceps.
- Pressure was applied to the thorax and diaphragm to expose the heart.
- Ligation of the LAD was performed using a 7.0 prolene suture. Suture placement was from the lateral portion of the left atria to the septum above the left coronary artery.
- Thoracotomy was closed using a 7.0 prolene suture through 2$^{nd}$ and 4$^{th}$ intercostal muscles in a diagonal orientation (lateral to midline).
- **Bupivacaine (Marcain) (0.1mg/kg) was applied to surface of the ribs at the site of the closed thoracotomy (approx. 1-2 drops from an insulin syringe if 0.25% steripac capsule is diluted 1:50 in 0.9% saline).**
- The wound was closed using a 7-0 prolene suture. As few stitches as necessary were used.
- The mouse was then warmed under an infrared lamp.
- **When spontaneous respiration returned, 0.5% isoflurane in oxygen (0.5 l/min) was administered until respiration was regular, via nose cone.**
- The mouse was then returned to the warmed chamber with other littermates.

- For performing batch surgery on a whole litter, the next animal was anaesthetised at this point.
- *Whilst the next animal was anaesthetised, the instruments were cleaned and tips sterilized using a glass bead sterilizer.*
- Before returning the post-operative litter to the dam, the collected faeces were homogenized in warmed water which was used to wash the animals to mask surgical smells.

### 3.9. Discussion

The original protocol for neonatal coronary artery ligation surgery developed by Sadek and colleagues in Texas (Mahmoud et al., 2014) described a technique based on the premise that neonatal mice feel no pain due to their incapacity for nociception. Whilst this remains controversial (Marchant, 2014) subjective observations suggest otherwise and, regardless, legislative bodies in the UK require that necessary steps are taken in all animal experiments to limit *potential* suffering. To this end, under the guidance of University veterinary staff, a novel anaesthetic protocol was developed to address all potentially noxious stimuli, including hypothermia induction; traumatic injury by thoracotomy and reperfusion pain. Particular care was taken to incorporate these measures without increasing procedural duration which could negatively impact animal welfare. To this end, isoflurane and bupivacaine (Marcain) were used in conjunction with hypothermia without negatively impacting on experiment length or survival. Furthermore, when isoflurane induction was employed prior to hypothermia induction on ice, and in subsequent experiments in which bupivacaine and additional isoflurane were administered; coordinated/spontaneous movement and audible/ultrasonic vocalisations were no longer evident. Although subjective, these responses are suggestive of purposeful responses to a negative stimulus and their absence could be considered a refinement to animal welfare in this procedure (Masters et al (*under revisions*: appendix I).

Although some fluctuations in survival rates were observed (Figure 3.3), these were within normal limits. Following supplementation of hypothermia with additional anaesthetic measures, survival appeared to increase (Figure 3.3). It is more likely, however, that the greatest mortality occurred in the initial 'hypothermia only' experiments due to relative surgical inexperience at this point, although on balance, considerably lower mortality rates were recorded compared to those described by Mahmoud et al (2014) in implementing the original protocol. P1 procedural survival ranged from 70 – 90% but was exacerbated by maternal neglect/cannibalism, which reduced overall survival rates to 60 – 70%. Survival rates for animals operated on at P7 were not stated but described as being lower than for those animals injured at P1 (Mahmoud et al., 2014). In our hands, over the duration of the project, survival was been between 85 – 100% for all litters used at both P1 and P7. Post-procedure, we also observed considerably less cannibalisation/neglect by dams than the levels previously described. I believe that this was largely due to replacing the ethanol wash and placement in original bedding prior to returning the pups to the dam (described by Mahmoud et al (2014) at step 13 in troubleshooting) with wiping the pups in warmed liquidised faeces from the dam prior to returning. This appeared to encourage maternal grooming and may have masked smells of the procedure.

Contrary to the published troubleshooting guidelines for step 13: return of post-operative pups to dam (Mahmoud et al., 2014) we did not observe any preferential cannibalisation/neglect of injured mice compared to sham injured controls. This is an important point as it permits the combination of treatment groups within the same litter, which can markedly reduce the number of animals required for individual experiments, as well as reducing variability of genetic backgrounds/developmental stages. It is absolutely vital, however, that post-operative pups are not returned to a litter containing healthy, un-injured pups. This significantly increased the likelihood of cannibalisation of the post-operative pups.

Finally, we further refined the procedure by incorporating an inexpensive and time-efficient aseptic technique, which enabled a single operator to perform the entire procedure independently; again without increasing length of the overall procedure. Given the particularly challenging nature of this type of surgery for aseptic technique, the described protocol was prepared for publication as a case study to guide implementation of aseptic technique in high-throughput, time-sensitive surgical procedures (Masters & Bergmann, Appendix II).

### 3.10 Conclusions

This chapter documents the successful development of novel anaesthetic and aseptic protocols for neonatal coronary artery ligation surgery in neonatal mice which enabled the first implementation, to the best of our knowledge, in the UK. This work may have wider applications for the refinement of procedures requiring thoracotomy in neonatal mice (Masters et al (*in review*; Appendix I) and for time-sensitive, high-throughput surgeries for which aseptic technique is challenging (Masters & Bergmann, submitted *JAALAS*; Appendix II). Since implementing this protocol in Oxford, numerous colleagues have been trained in the surgery and we have been able to offer consultation on the establishment of the procedure in other institutions in

the UK.

# 4

# Model Validation

## Longitudinal assessment of heart regeneration in neonatal mice by MRI

Following adaptation of the methodology for neonatal LAD ligation, it was necessary to validate the model and assess the regenerative capacity of the newborn mouse heart in our hands. The need for this was underscored by the publication of a study which, coincident with the granting of our licence amendment to practise neonatal cardiac injury, called into question the robustness of neonatal mouse heart regeneration. Andersen and colleagues failed to observe complete regeneration in 100% of the 400 hearts on which they performed resection injury (Andersen et al., 2014). Although this is a completely different type of injury to LAD ligation, it highlighted the necessity of model validation. There is also considerable disparity between the reported extents of regeneration post-ischemia induced by LAD ligation (Sen and Sadek, 2015). In agreement with the Sadek lab, less than two weeks after the initial demonstrations of regeneration following MI by LAD ligation, an independent study also reported complete regeneration without anterior wall scarring by the same method (Haubner et al., 2012). Remarkably, in their hands, almost complete regeneration was observed after just 7 days. However, a more recent study compared the extent of regeneration following resection injury and LAD ligation and reported complete regeneration following resection but limited regeneration following MI (Konfino et al., 2015). The reported extents of regeneration in various disease models by different groups are summarised in Table 4.1.

**Table 4. 1. Summary of reports of heart regeneration in neonatal mice:**

| Report | Injury type | Regeneration | Duration of regeneration |
|---|---|---|---|
| **(Porrello et al., 2011)** | Resection | Complete | 21 days |
| **(Jesty et al., 2012)** | Cryoinjury | Almost complete | >90 days |
| **(Haubner et al., 2012)** | MI | Complete | 7 days |
| **(Porrello et al., 2013)** | MI | Complete | 21 days |
| **(Mahmoud et al., 2013)** | MI | Complete | 21 days |
| **(Andersen et al., 2014)** | Resection | Negligible | N/A |
| **(Aurora et al., 2014)** | MI | Complete | 21 days |
| **(Konfino et al., 2015)** | Resection | Complete | 21 days |
| | MI | Incomplete | 28 days |
| **(Bryant et al., 2015)** | Resection (small ~10%) | Almost complete | 21 days |
| | Resection (large ~20%) | Incomplete | 28 days |

These varying reports of the regenerative capacity of the neonatal mouse heart not only necessitate assessment and characterisation of the LAD ligation model as produced in our hands, they also suggest a need to improve the methodology to assess regeneration. For instance, histological analysis only provides a single snap-shot of a single heart at one time-point; therefore, in the context of regeneration, analysis by this method assumes that the initial injury was equivalent across surgical replicates and that it was successfully induced in the first instance. Consequently, histology is sub-optimal and requires large animal numbers. Instead, what is required is non-invasive assessment of initial injury and longitudinal assessment of regeneration. Some groups have used short axis, two-dimensional echocardiography (2D-Echo) for initial and end-point analyses (Konfino et al., 2015, Porrello et al., 2011). The advantages of this method are that it is widely available and reasonably fast; however, 2D-Echo is suboptimal for assessing regeneration as it offers limited tissue resolution

and only permits heart visualisation and functional assessment in a single plane at once. In the context of assessing regeneration, this could be problematic as it would be extremely difficult to relocate the exact plane that was previously imaged and could lead to misinterpretation of the extent of regeneration. In addition, the heart can adhere to the thoracotomy site within the chest wall post-operatively, which may result in abnormal ventricular motion that does not necessarily reflect infarction injury. The gold standard imaging technique requires non-invasive, three-dimensional (3D), high resolution and reproducible functional imaging of the whole heart, in the same animal, over time. This can be achieved by magnetic resonance imaging (MRI).

### 4.1. Magnetic resonance imaging

MRI exploits the principles of proton nuclear magnetic resonance (NMR) to generate high resolution images of internal structures. This relies on the fact that nuclei with an odd number of protons and neutrons have 'spin' associated with a magnetic moment that can be measured. In MRI, hydrogen nuclei, which are present throughout the body (mainly in water and fat) and have single proton nuclei, are detected by exposing them to a strong static magnetic field. The interaction of these nuclei with the external magnetic field is similar to that of bar magnets: i.e. they align, producing a macroscopic magnetisation vector. In this alignment, they precess or 'spin' about the direction of the applied magnetic field, defined as the z-axis. In order to generate NMR signal, it is necessary to shift the net alignment of these 'bar magnets' into the x-y plane. To achieve this, energy is put into the system in the form of a radiofrequency oscillating magnetic field, which is equal to the precessional frequency (or Larmor frequency) of the nuclei. This oscillating magnetic field rotates the net alignment of the 'bar magnets' into the x-y plane, where they continue to precess around the z axis, until they return back to equilibrium (termed T1 relaxation). These oscillations in the x-y plane induce an NMR signal in the MR probe. To determine the position of protons in space, linear magnetic

field gradients are applied across the sample to generate different precessional frequencies and 'phase angles' of spin systems across the sample. The spatial dependence of the NMR signal from these vectors (i.e. frequency and phase encoding) can be resolved by means of Fourier transform. As proton densities and/or relaxation constants (T1) differ between tissue types, as well as in diseased or infarcted tissues, MRI can distinguish internal organs and certain types of pathologies with high resolution. Contrast between different tissue types can be enhanced using contrast agents, such as compounds that contain gadolinium.

### 4.1.1. MRI of murine infarcts

In the clinic and in research, MRI is widely used to acquire high resolution images and functional and anatomical data, repeatedly from the same patient or animal model. Indeed, it is also routinely used in adult mice to assess cardiac function following experimentally induced MI. Comparative study of cardiac MRI and 2D-Echo in rats showed that, whilst there were correlations between functional data acquired from the two methods, repeated measurements on the same animals over several days were much more consistent by MRI; to the extent that 5 times more animals would be required to achieve statistical significance between groups if using 2D-Echo (Stuckey et al., 2008). No previous study, however, has demonstrated the use of MRI for assessing MI in the hearts of neonatal mice. One study demonstrated the utility of MRI for acquiring detailed, time-resolved visualisation of the P3 mouse heart to assess cardiac morphology and function without recovery (Wiesmann et al., 2000) (invasive ECG probe placement meant that the animals had to be euthanized post-scanning); so the tolerance of neonatal mice to repeated scans also remained untested. To date, no study has imaged a P1 mouse heart by MRI, nor repeatedly imaged the same neonate within the pre-weaning period. This could be partly due to issues with scan duration and the risk of maternal neglect and cannibalisation following extended periods of separation.

#### 4.1.1.1. Late gadolinium enhancement MRI

Significant advances have been made in fast, high-resolution MRI as applied to rodent hearts post-MI using late gadolinium enhancement (LGE) MRI, which is routinely used clinically for assessing myocardial viability following a heart attack (Bohl et al., 2009, Wech et al., 2011, Yang et al., 2004). LGE MRI relies on the accumulation of gadolinium, a lanthanide element, at ischemic sites due to the expansion of extracellular space and compromised perfusion in these areas. Gadolinium has powerful paramagnetic properties that facilitate T1 relaxation of hydrogen nuclei, which is exploited in MRI to visualise compromised tissues relative to healthy myocardium. The shortening of T1 relaxation in tissues in which gadolinium contrast agents accumulate can be utilised using T1-sensitive pulse-sequence (i.e. T1 weighting). As a result, ischaemic tissues generate a brighter signal than healthy tissues in T1 weighted images, facilitating direct visualisation of infarcts (Bohl et al., 2009).

#### 4.1.1.2. Multiframe (cine) MRI

Another common method for assessing MI utilises indirect measurements of wall-motion captured over contiguous ventricular slices by multiframe (cine) MRI (Schneider et al., 2006). This method routinely required long scan-times which would be incompatible with time-sensitive procedures. However, the recent development of an accelerated cine-MRI protocol has been applied for imaging infarcts in adult mice and reduced scan times by under-sampling data acquisition 3-fold, without compromising spatial or temporal resolution (Wech et al., 2011); a reconstruction process called 'compressed sensing'.

As we have optimised neonatal mice handling regimes to minimise maternal neglect and cannibalisation following prolonged periods of separation, we collaborated with Professor Jurgen Schneider at the Biomedical Resonance Imaging Unit in Oxford, in order to optimise an MRI set-up and animal handling protocol to perform MRI for longitudinal assessment of heart regeneration following MI in neonatal mice. Both LGE-MRI and cine-MRI were assessed for

infarct visualisation. Compressed sensing and retrospective gating (Heijman et al., 2007) were employed in unison for the first time to enable fast scan data acquisition and negate the requirement of subcutaneous ECG electrode placement, which is unworkable for recovery procedures in neonatal mice.

### 4.2. Study design

Initially, we aimed to assess base-line heart function and scanned the mice at P1 immediately prior to surgery. The mice were scanned under isoflurane anaesthesia, with hypothermia induced post-scanning and surgery performed immediately thereafter. To assess initial injury, potential regeneration and functional recovery, the mice were scanned 4, 7, 14 and 21 days post-operatively (D4, D7, 14 and D21, respectively). As a previous report described regeneration following LAD ligation by D7 (Haubner et al., 2012) we performed the earliest post-operative scan at D4 in order to allow sufficient post-operative recovery time and to confirm initial injury. Heart function in mice post-MI was compared to that of sham- operated controls in order to assess normal heart function and relative injury assessment over time. The sham procedure involved thoracotomy surgery and heart visualisation but no suture placement or ligature. Intact animals were deemed unsuitable controls in this setting as they could not be simultaneously reared by the same dam, and would, therefore, be less developmentally equivalent to injured animals. To permit comparison of the deterioration of heart function versus any observed improvement in 'regenerative' P1 hearts post-MI, we assessed time-matched infarcts induced in the surgically equivalent, 'reparative' injury setting of the P7 heart. Hearts were collected for histological assessment at each time-point post-scanning. The study design is summarised in Figure 4.1. CD1 mice were used in this study as this strain produces large litters and the females were previously reported to be better at nursing post-operative pups (Mahmoud et al., 2014).

All imaging was conducted using a 9.4 T horizontal bore scanner with Direct Drive2 console and 60 mm i.d., 1 T/m, shielded gradient set (Agilent Technologies). An i.d. quadrature driven birdcage resonator of age-appropriate specifications (Rapid Biomedical) was used for signal transmission/reception (as described in section 4.4). Following scouting and shimming, retrospectively gated, 2D gradient echo multi-slice cine images of various orientation (as described in sections 4.5 and 4.8) were acquired (2x compressed sensing acceleration).

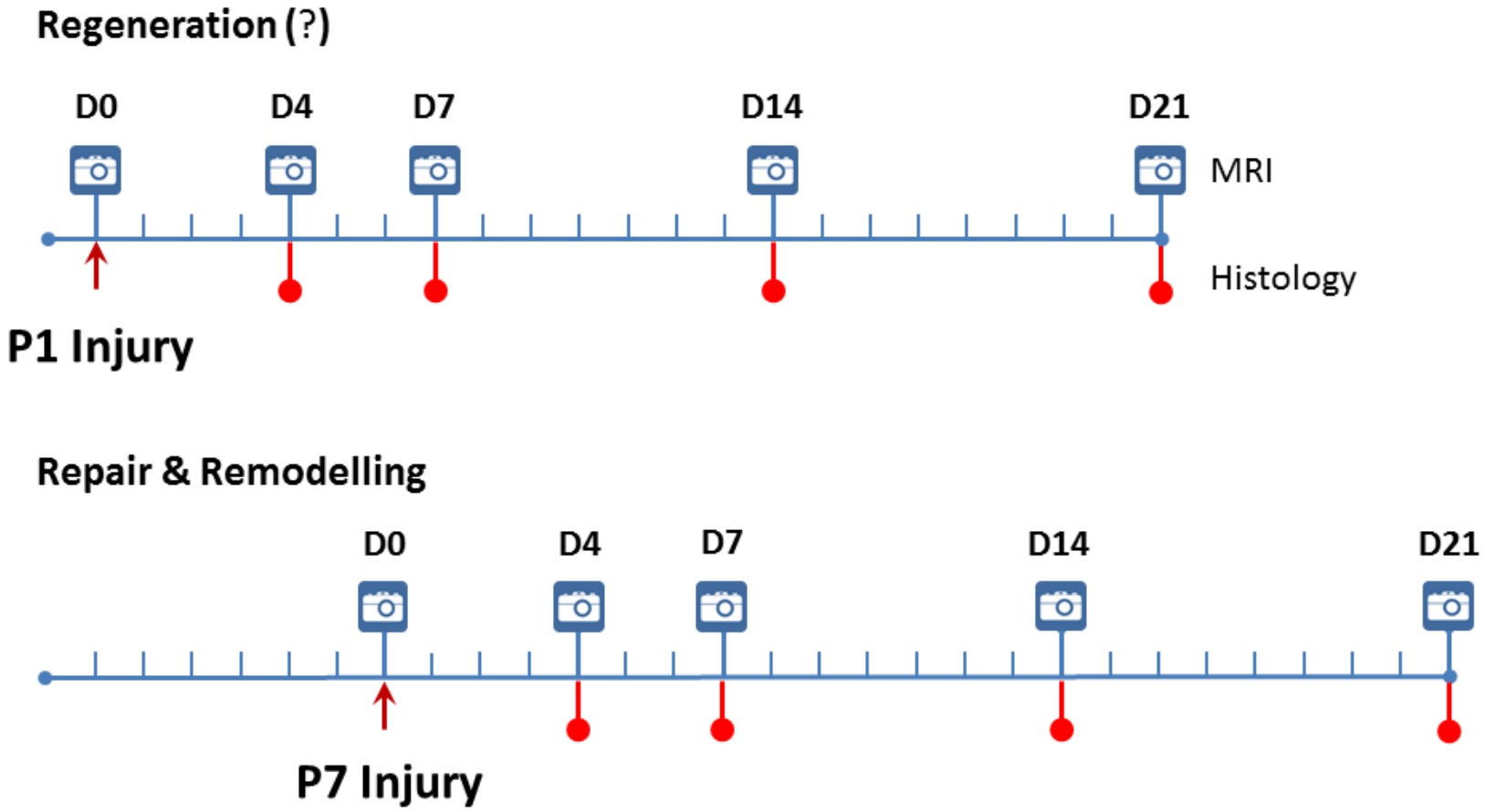


**Figure 4. 1. Schematic of neonatal MRI heart regeneration study:**
postnatal-day (P) 1 and P7 animals were scanned on P1 or P7, or day (D) 0, prior to induction of myocardial infarction by ligation of the left anterior descending coronary artery, in order to assess heart regeneration and heart repair (fibrosis and remodelling) that has been described in hearts injured at these time-points. MRI scans (camera cartoons) were performed 4, 7, 14 and 21 days post-injury (D4, D7, D14 and D21, respectively) and tissue was collected at each time-point for histological assessment (red dots). MRI = magnetic resonance imaging.

### 4.3. Injury reproducibility

To assess surgical reproducibility of infarcts in P1 and P7 hearts, the percentage of infarcted tissue (of left ventricle myocardium area) was quantified across multiple hearts injured on P1 or P7 at D4 by histology using ImageJ software (Figure 4.2). The average percentage of infarcted LV in hearts injured on P1 was 13.8±0.87 (n=7) compared to 19.5±0.92 in hearts injured on P7 (n=3) (*p<0.05; Mann-Whitney test) demonstrating reproducible induction of injury at respective time-points. Increased infarct size four days post-MI at P7 is consistent with a differential injury response in these animals. In order to assess initial injury and regeneration non-invasively in the same animal over time without tissue destruction, protocol optimisation for longitudinal cardiac MRI in neonatal mice was performed.

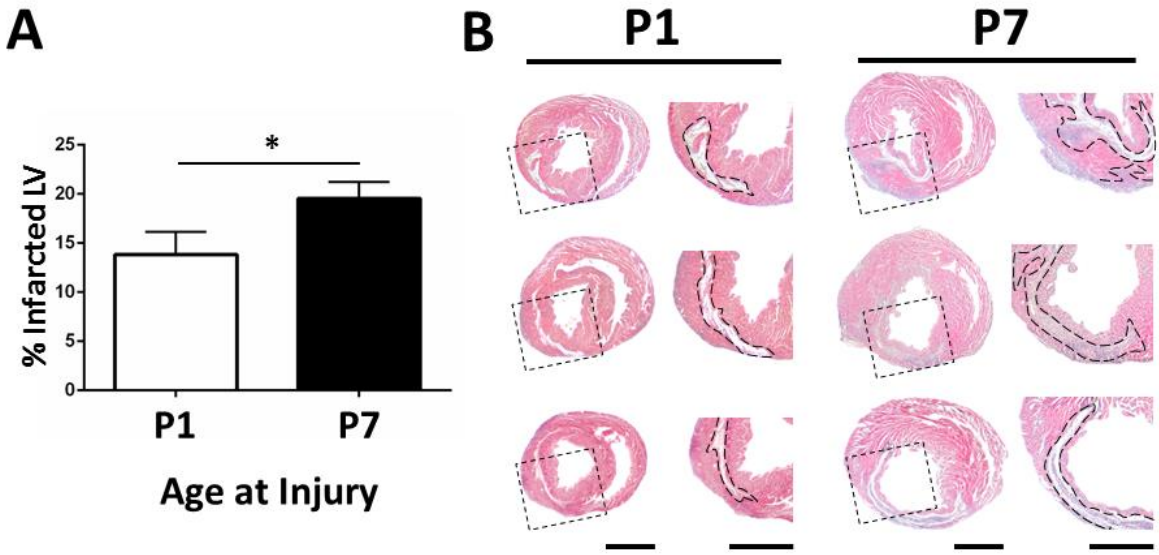


**Figure 4. 2 Infarct reproducibility four days post-MI:**
The proportion of infarcted left ventricle (LV) was quantified as a percentage of total LV myocardial area over multiple sections from hearts injured on postnatal-day (P) 1 (n=7) or P7 (n=3), 4 days post-myocardial infarction (MI). (B) H&E staining of representative sections from mid-infarct region following from P1 and P7 hearts four days post-injury. Boxed regions indicate zoomed images shown adjacent. Dashed region in zoomed images indicates infarct borders. Scale = 1mm. *p<0.05, Mann-Whitney test. Note infarct variability is consistent between groups.

### 4.4. A modified set-up for neonatal mice MRI:

To facilitate the intended MR studies, the Schneider lab developed a modified cradle optimised for placement of neonatal mice in the magnet. This modified cradle comprised a pressure pad (for respiratory monitoring); an anaesthetic line (to deliver isoflurane in oxygen via nose-cone) and a heated blanket, to maintain body temperature during scans (Figure 4.2). As animals would increase in size through the course of the study, different cradle dimensions, coil diameters and scan parameters were used as appropriate to different sizes, as summarised in Table 4.2.

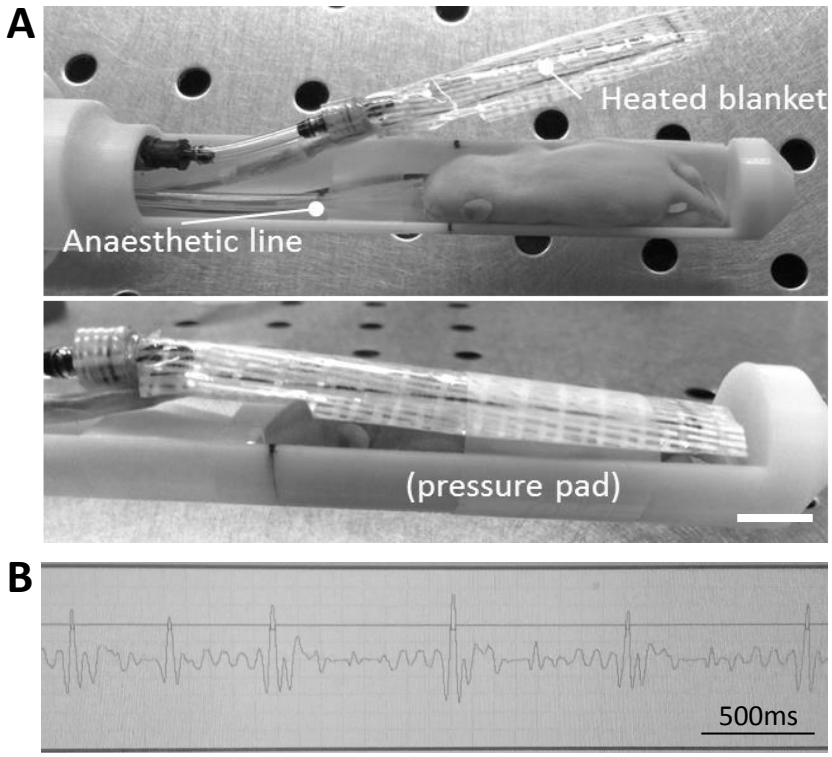


**Figure 4. 3. Modified cradle for MRI scanning of neonatal mice:**
(A) a pressure pad was positioned underneath the diaphragm of the mouse for physiological monitoring and an anaesthetic line with nose-cone delivered isoflurane in oxygen. A heated blanket covered the animal and was secured by tape during scans to maintain physiological temperature. The mouse shown is 7 days old and secured in a 20mm cradle. Scale = 1 cm. (B) an example respiratory trace used for physiological monitoring during scans.

**Table 4. 2. Cradle size, coil diameter and scan parameters for MRI:**

| Age | Weight | Coil diameter | Cradle circumference | Field of view | Slice thickness |
|---|---|---|---|---|---|
| P1-P8 | ~1.5 – 5.5g | 20mm | 18.5mm | 15 $mm^2$ | 0.5mm |
| P9 – P22 | ~8.5 – 16g | 28mm | 24 mm | 20 $mm^2$ | 0.7mm |
| P23 – P28 | 16 – 25g | 33 mm | 27 mm | 20 $mm^2$ | 0.7mm |

### 4.5. MRI of neonatal mice with recovery:

In order to establish the feasibility of MRI as a means of assessing cardiac function in neonatal mice, we performed scanning on a small cohort of neonatal animals (n=5) at P1 with recovery. As the long-term aim of this study would involve scanning and performing surgery on whole litters at P1, which would prolong the usual period of separation of litter and dam (i.e. 3 hours maximum); we removed neonates individually from the nest (instead of removing all pups at the time of the first procedure, as is standard protocol). We reasoned that this may maintain maternal behaviours over the course of the day and discourage neglect and cannibalism upon returning the post-scan pups. Individual removal of pups from the nest has been suggested to increase maternal stress (Mahmoud et al., 2014), so the behaviour of the dam was closely monitored. Animals were anaesthetised by 4% isoflurane in oxygen (2 l/min), were weighed and secured in the MRI cradle. Once a regular respiratory trace was observed (e.g. Fig. 4.3B) isoflurane levels were reduced to ~1.5-2% in oxygen (2 l/min) and animals were positioned in the magnet.

To assess heart, and particularly left ventricle (LV) function, 4-chamber (long axis coronal section); 2-chamber (sagittal section of the LV and LA) and mid-ventricular short axis cine scans were acquired (Figure 4.4). Each cine acquisition lasted ~2 minutes and was designed to

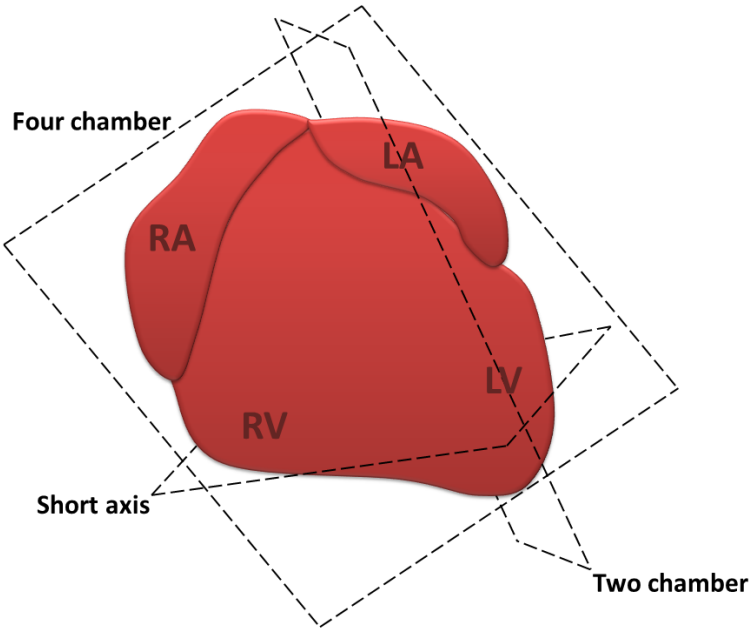


**Figure 4. 4. Scan positions for 3D MRI acquisition:**
coronal 4-chamber; mid-ventricular transverse short-axis; and sagittal 2-chamber images were acquired by MRI. RA: right atria; RV: right ventricle LA: left atria; LV: left ventricle.

minimise scan duration. The pups were maintained at 36°C for the duration of scanning. Pups were very sensitive to temperature: above 36°C, respiratory depression and terminal hyperthermia were observed. Post-scanning, animals were recovered in a warmed chamber (32°C). Once all animals had been scanned, the pups were washed in warmed faecal solution and returned to the dam. The average duration of these preliminary P1 scans was 40 minutes. During scans, we observed no obvious signs of maternal stress. The dam maintained maternal behaviour towards the remaining pups in the nest (nursing and grooming) and, otherwise, demonstrated typical foraging and self-grooming behaviour. Following return of the P1 pups post-scanning, the animals were left undisturbed until the next day. 24 hours later, all animals were present and demonstrated normal suckling behaviours. Animals were subsequently euthanized. These first experiments demonstrated the first successful use of MRI in P1 mice, in which cardiac cycle from end diastole to systole was resolved (Fig. 4.5) and functional parameters derived (Table 4.3).

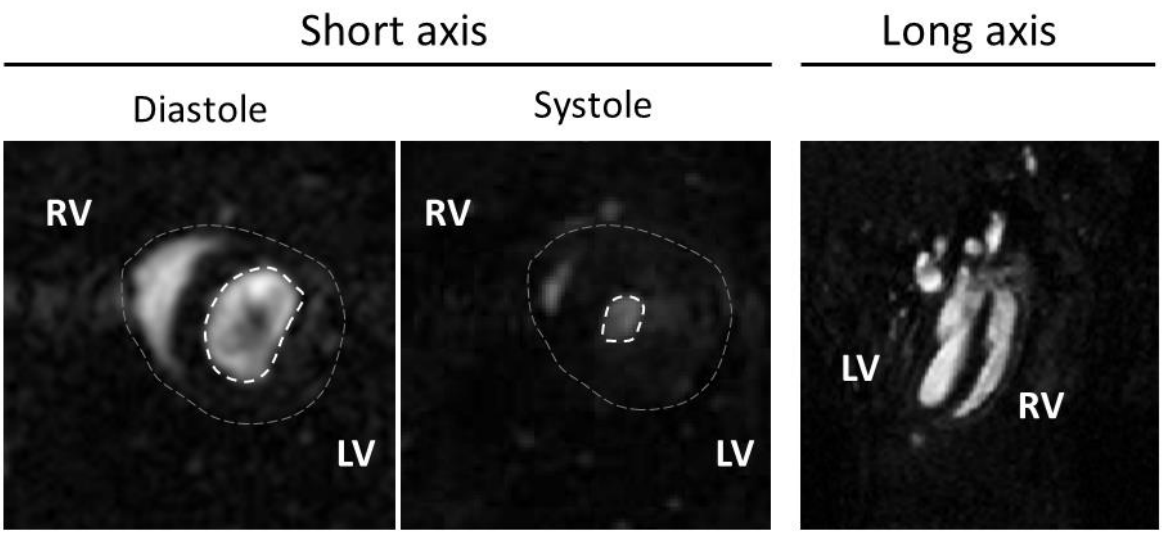


**Figure 4. 5. Frames from a representative retrospectively gated cine image of a P1 mouse:** Frames from mid-ventricular cine slices of P1 hearts in short and long axis conformations in end diastole and end systole. Dotted white line demarcates luminal circumference and dashed grey line indicates outer myocardial borders. LV = left ventricle; RV = right ventricle.

**Table 4. 3. Functional parameters derived from manual segmentation of the reconstructed cine MRI of P1 mice:**
All values quoted ± StDev. LV, left ventricular; EDV, end diastolic volume; ESV, end systolic volume; EF, ejection fraction; SV, stroke volume.

| Number of Mice | 5 |
|---|---|
| **Body Mass (g)** | 1.82±0.22 |
| **LV Mass (mg)** | 7.33±0.78 |
| **LV EDV (µl)** | 3.33±0.32 |
| **LV ESV (µl)** | 1.56±0.30 |
| **LV EF (%)** | 53±9 |
| **LV SV (µl)** | 1.77±0.38 |

**4.6. Repeated imaging of neonatal mice within the pre-weaning period:**

In order to establish the feasibility of a longitudinal MRI study which would involve repeated imaging of individual neonatal mice within the pre-weaning period, we performed scanning on a small cohort of neonatal animals (n=3) at P1 and then again at P4. Once a regular respiratory trace was observed (e.g. Fig. 4.3) isoflurane levels were reduced to ~1.5-2% in oxygen (2 l/min) and animals were positioned in the magnet. The animals were then checked

daily and re-marked for identification until P4, at which point, all pups were checked for signs of poor health (including dehydration or growth retardation) prior to scanning. All mice appeared normal and body mass had increased in-line with normal development (Table 4.3). The average duration of these scans was 29 minutes. All scans were performed without incident and the pups appeared healthy throughout the study. Animals were subsequently euthanized by an appropriate schedule 1 method. These experiments showed that repeated imaging in pre-weaning neonates was well tolerated.

**Table 4. 4. Animal weights and scan durations during initial longitudinal neonatal MRI scans:** blue values indicate normal weights (Jackson Laboratories).

| Mouse ID | Weight (g) | | Scan duration (minutes) | |
|---|---|---|---|---|
| | **P1** **(1-2g)** | **P4** **(2-3g)** | **P1** | **P4** |
| 1 | 1.6 | 2.4 | 47 | 37 |
| 2 | 1.7 | 2.3 | 46 | 24 |
| 3 | 1.8 | 2.6 | 29 | 28 |

### 4.7. Combining MRI scanning and neonatal cardiothoracic surgery:

To establish the feasibility of performing LAD ligation surgery in conjunction with MRI scanning, we operated immediately after performing baseline MRI scans on a litter of 8 animals. Animals were individually removed from the dam; weighed, anaesthetised (4% isoflurane in Oxygen (2 l/min)) and placed in the imaging cradle. The average weight of animals was 1.5g. Once a regular respiratory rate was detected, the cradle was placed inside the magnet and the established scanning protocol was repeated. The average scan duration was 21 minutes; after which animals were placed immediately on ice (still anaesthetised) for approximately 3 minutes and the surgery was performed. The average duration of surgery (from hypothermia induction to respiratory recovery) was 10.5 minutes. Between procedures, animals were kept in a warm environment (~32°C) with other post-operative littermates. Six animals underwent MI injury and two underwent the sham procedure. Two animals died under anaesthesia (1 sham and 1 MI). Once all animals had undergone scanning, the 6 remaining pups were washed in warmed faecal solution and returned to the dam. The total duration of separation from the removal of the first pup from the nest was 2 hours and 47 minutes. The cage was then left undisturbed for 24 hours. The following day, five animals were remaining, with one animal from the MI group presumed cannibalised. The remaining 5 animals demonstrated behaviours typical of their age (suckling and uncoordinated movements). This loss of animals was not beyond normal limits. These experiments demonstrated the feasibility of performing MRI scanning and neonatal LAD ligation consecutively.

### 4.8. Imaging and quantifying neonatal mouse infarcts

#### 4.8.1. Late gadolinium enhancement magnetic resonance imaging

To observe and measure infarcts in neonatal mice, we first attempted LGE MRI as this can achieve fast, direct measurement of infarcts in adult mice without relying on indirect

anatomical measurements (Bohl et al., 2009). The most efficient administration route for gadolinium contrast compounds in adult mice is intravenously (i.v.), but this is not feasible in neonates. We, therefore, established an intraperitoneal (i.p.) delivery route via catheter placement, prior to positioning in the scanner (Fig. 4.6) through which contrast agent could be delivered once the animal was positioned in the magnet and organ orientation had been established. This further minimised the delay between administration and scanning, and was achieved by skin puncture following anaesthesia, using an insulin syringe through which a mouse tail vein catheter (28cm, 23ga: Braintree Scientific) was inserted (Figure 4.5). This was connected to an automated perfusion system (Harlan, UK) to deliver the agent once the animal was placed in the magnet. Surgical tape was used to secure the catheter in place to enable manipulation of the animal post-catheter placement.

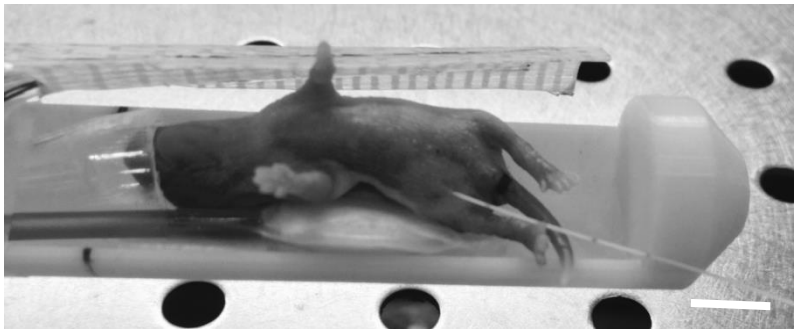

**Figure 4. 6. intra-peritoneal catheter placement for contrast agent delivery during MRI:**
A 28cm, 23ga tail-vein catheter (Braintree Scientific) was inserted into the peritoneum of neonatal mice following skin puncture prior to securing the animal in the cradle to enable contrast agent delivery once animal and organ positioning was established. Scale = 1 cm.

As LGE MRI had not been previously described in neonatal mice, the optimum kinetics and timing of administration of gadolinium needed to be established. To address this, we acquired continuous, hour-long myocardial T1 mid-ventricular slice measurements from an animal that sustained MI at P1. These scans were performed as previously described, seven days after MI surgery (D7). Baseline scans were performed before 0.5µmol/g gadolinium administration (in 50µl saline) and then repeatedly post-administration over the course of an hour. The mouse was euthanized following scans in order to perform comparative histological analyses (Figure 4.7).

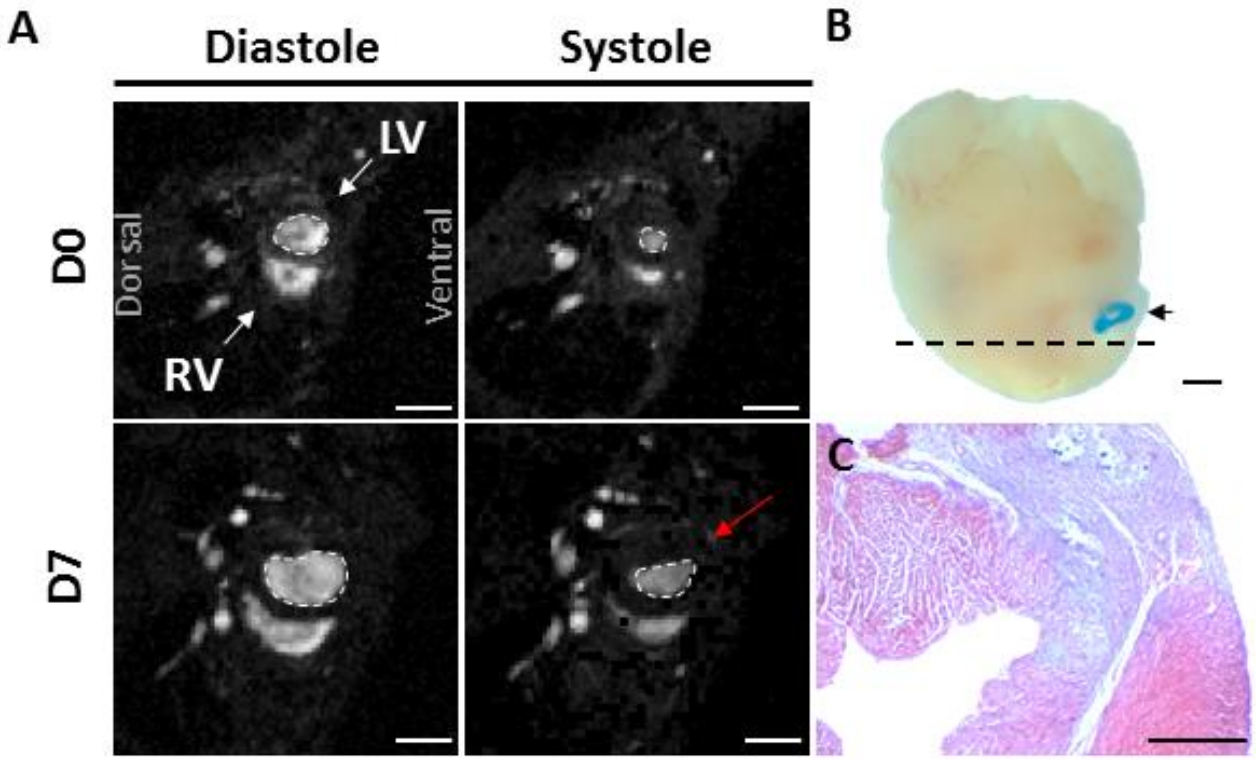


**Figure 4. 7. Infarct visualisation by wall motion and histology:**
A) Representative frames of mid-ventricular short axis cine slices of a heart in end diastole and end systole before (D0) and 7 days post-MI (D7). Note the reduced contraction of anterior left ventricle (LV) on D7 in systole (red arrow) which may represent akinetic wall motion and infarction injury in this mouse. Dashed line outlines luminal borders of the LV. B) Whole heart *ex vivo*. Arrowhead indicates suture level and dashed line indicates plane of transverse sectioning in (C) Masson's trichrome staining of the anterior LV wall. Note significant collagen deposition (blue staining) and similar morphology to that seen by MRI (red arrow). Scale = (A) 1mm; (B and C) 500µm.

In this animal, whether or not gadolinium delivery or uptake was successful was inconclusive. However, akinetic wall movement was clear by MRI at D7 (Fig.4.7 A (red arrow)) and subsequent histology confirmed collagen deposition in the anterior LV wall (Figure 4.7B), highlighting the feasibility of MRI as a means to visualise infarction injury by wall motion measurements. Consequently, subsequent experiments sought to enable infarct detection and quantification from wall motion by cine-MRI. This had the advantage of not requiring administration of contrast agent. To achieve this, in subsequent experiments, we performed contiguous cine scans to cover the entire ventricles from apex to base (Fig. 4.8). From this, we would attempt to discern the extent of injury by contractile function, which has been widely used to accurately detect and quantify infarcts in adult mice (Schneider et al., 2006, Stuckey et al., 2008, Wech et al., 2011).

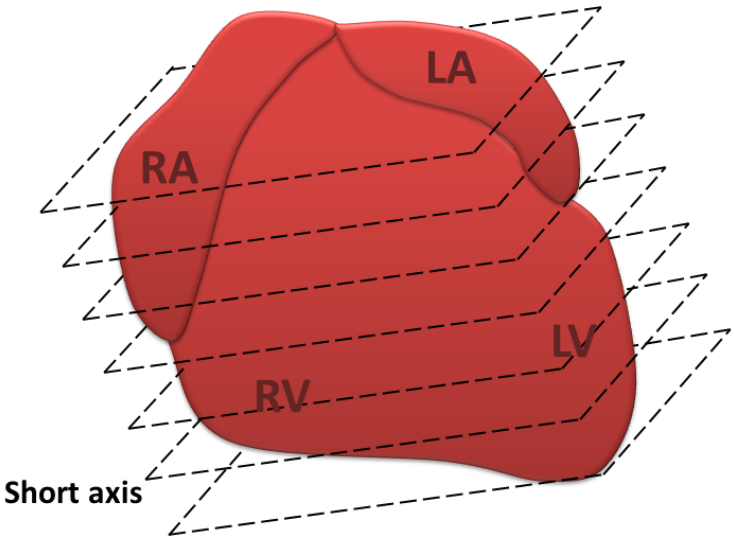


**Figure 4. 8. Scan positions for 3D MRI cine acquisition:**
Multiple short-axis slices which covered the entire left ventricle (LV) were acquired by MRI. RA, right atria; RV, right ventricle; LA, left atria; LV, left ventricle. Dashed lines indicate short axis cine imaging planes.

### 4.8.2. Cine MRI:

To assess cine-MRI and wall motion measurements to detect infarcts in neonatal mice, we operated on five mice (four MI; one sham) and acquired stacks of short axis slices across the total volume of the ventricles from apex to base at D4. In covering the whole ventricle with a 0.5mm slice thickness, we averaged 8 slices per heart, which increased average scan times to 35 minutes. On the day of the surgery (D0), the total duration of separation from removal of the first pup to return of the post-operative litter was 5 hours. This appeared to be well tolerated and by P5 (or D4, when subsequent scans were performed) all animals appeared to be healthy, with no indications of malnutrition or growth retardation in pups that were separated from the dam the longest. Following scans on D4, all animals were euthanized in order to correlate infarct size by MRI and histology. Histological assessment of the hearts at D4 (Fig. 4.9) confirmed infarcts (mean infarct size = 15.1%±0.73 of the LV); however, issues with data acquisition have delayed reconstruction and analysis of the MR data.

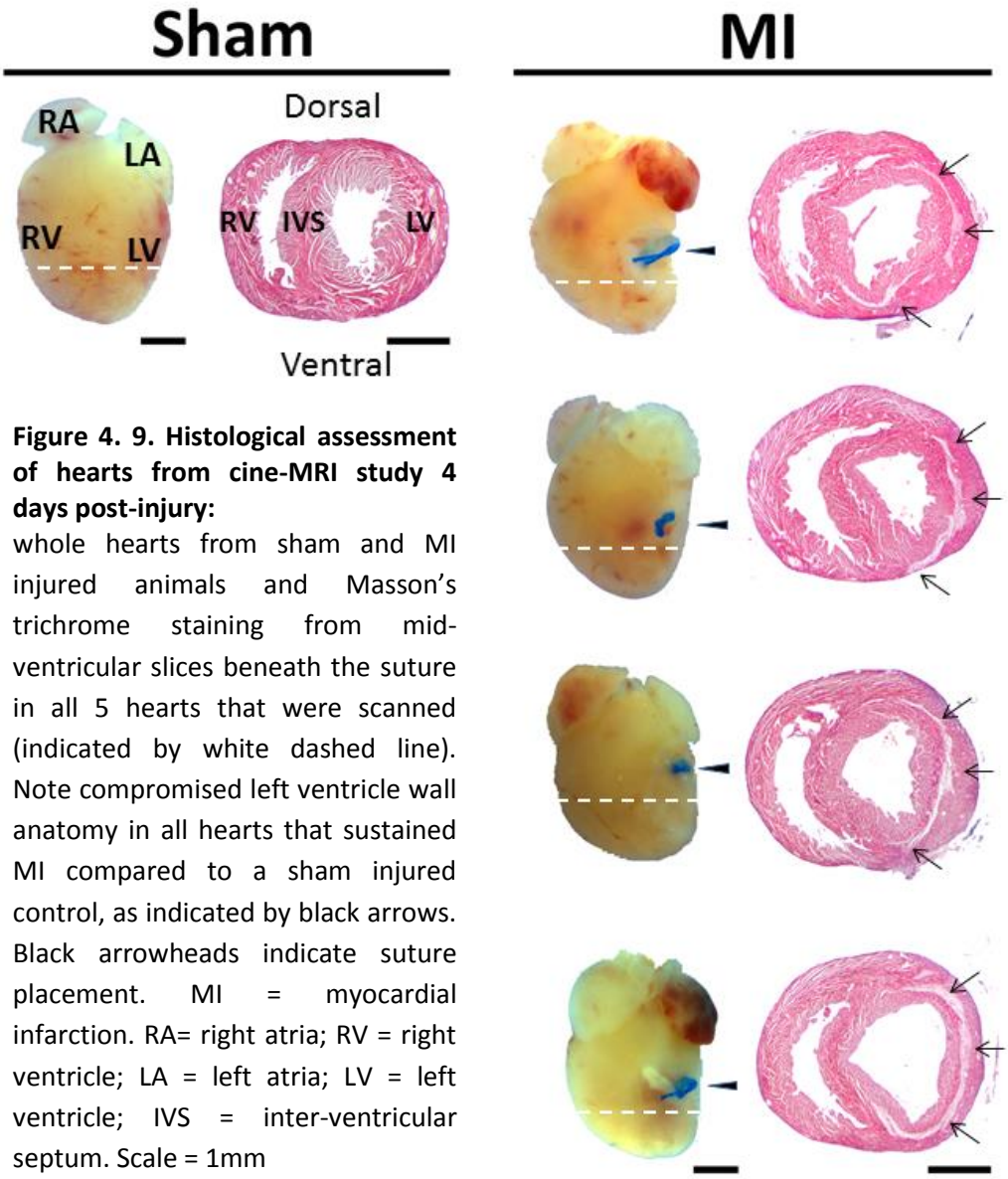


**Figure 4. 9. Histological assessment of hearts from cine-MRI study 4 days post-injury:**
whole hearts from sham and MI injured animals and Masson's trichrome staining from mid-ventricular slices beneath the suture in all 5 hearts that were scanned (indicated by white dashed line). Note compromised left ventricle wall anatomy in all hearts that sustained MI compared to a sham injured control, as indicated by black arrows. Black arrowheads indicate suture placement. MI = myocardial infarction. RA= right atria; RV = right ventricle; LA = left atria; LV = left ventricle; IVS = inter-ventricular septum. Scale = 1mm

We subsequently repeated this experiment and included D7 scans in order to permit assessment of post-MI hearts at this time-point (n=6; 2 sham, 4 MI). Unfortunately, due to problems with tissue processing (most probably due to improper tissue fixation) histological analysis was not performed on these hearts. Infarcts, however, were indicated by reduced LV wall contractility from cine MRI frames; particularly at D7, at which point akinetic wall motion was detected at end systole compared to sham operated controls (Fig. 4.10 (red arrows)). Further data processing, including segmentation of MR data and quantification of infarct size by MR for all hearts, is ongoing.

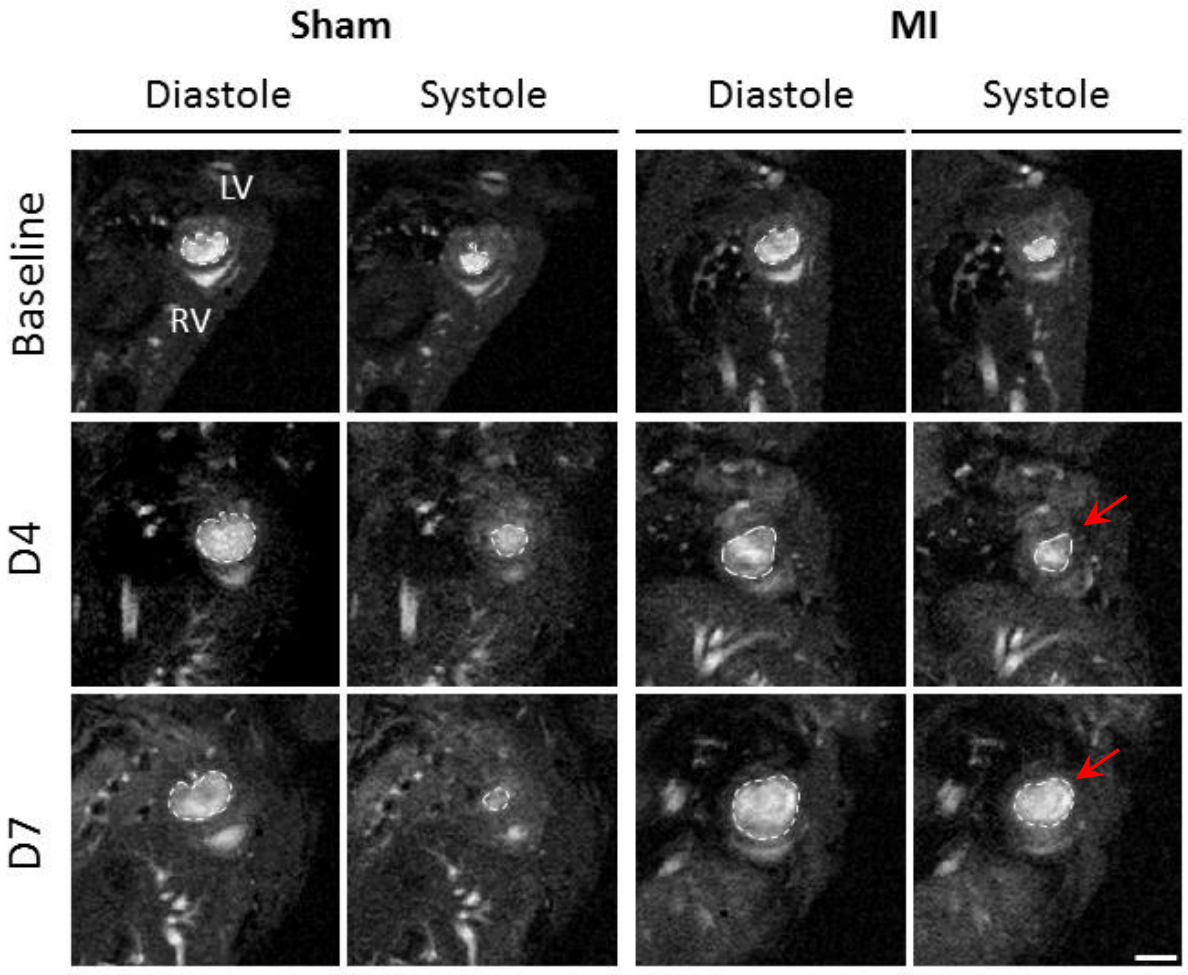


**Figure 4. 10. Longitudinal MRI assessment of neonatal hearts following LAD ligation surgery at P1:**
Representative frames of mid-ventricular cine slices of hearts from individual neonatal mice that underwent myocardial infarction (MI) (n=4) or sham (n=2) injury on P1, prior to injury (D0) and 4 and 7 days post-injury (D4 and D7). Note the wider luminal circumference at end systole of the heart that sustained MI, at D4 and D7 (indicated by red arrows) which may indicate compromised contractility and infarction injury in this heart. White dashed line indicates luminal circumference of the left ventricle (LV). RV = right ventricle.

### 4.9. Longitudinal assessment of neonatal mouse infarcts by MRI:

Having observed infarcts in neonatal mice by both histology and MRI at D4 and D7 (albeit not in the same animals) we reasoned that the established cine-MRI protocol could be used for non-invasive longitudinal assessment of heart regeneration in neonatal mice. We, therefore, performed MI surgery on litters at P1 and P7 and performed scans at D4, D7, D14 and D21 (as well as baseline scans at D0) in order to assess regeneration versus remodelling in these respective model systems (as per the original study plan: described in Figure 4.1).

### 4.9.1. Heart regeneration with limited fibrosis following LAD ligation injury at P1

To assess 'regeneration' following infarction injury by LAD ligation in P1 hearts, we scanned 6 post-operative animals on D4, D7, D14 and D21 from a single litter. On D0, all mice were scanned for baseline heart function (as described) prior to induction of MI (n=4) or sham injury (n=2). Tissue was collected from two animals (1 sham and 1 MI) for histological assessment on D14 (as this time-point was not assessed in previous experiments) and the remaining (4) animals (3 MI and 1 sham) were euthanized for tissue collection on D21.

Histological assessment by Masson's trichrome staining of hearts at D21 demonstrated minimal collagen deposition (0.84%±0.28 of the LV) and otherwise healthy myocardium at epicardial and endocardial borders (Fig. 4.11). In comparison to D4 and D7 time-points, at which significant wall thinning and contractile dysfunction were evident from histology (Fig. 4.9; 4.12) and MRI (Figure 4.10), it appeared that by D21, significant regeneration had occurred in these hearts, confirming observations of previous histological assessment on long axis sections (Fig. 4.11 A and E). Even by D14, minimal collagen deposition was observed and myocardial thickness appeared uncompromised, suggesting that significant regeneration may occur before D14, although initial injury will need to be confirmed by analysis of the MR data acquired at D4 and D7 and more hearts will need to be assessed at this time-point before any conclusions can be drawn.

The extent of initial injury, as well as the extent of functional recovery of these hearts, remains to be determined further analysis of the acquired scan data. These findings are consistent with earlier histological examinations of hearts three weeks following LAD ligation (Fig. 4.11A, E), as well as reports of significant regeneration in these animals following equivalent injuries by other groups (Porrello et al., 2013, Haubner et al., 2012). Figure 4.12 shows a time-course of the histological assessment by Masson's trichrome performed in these experiments.

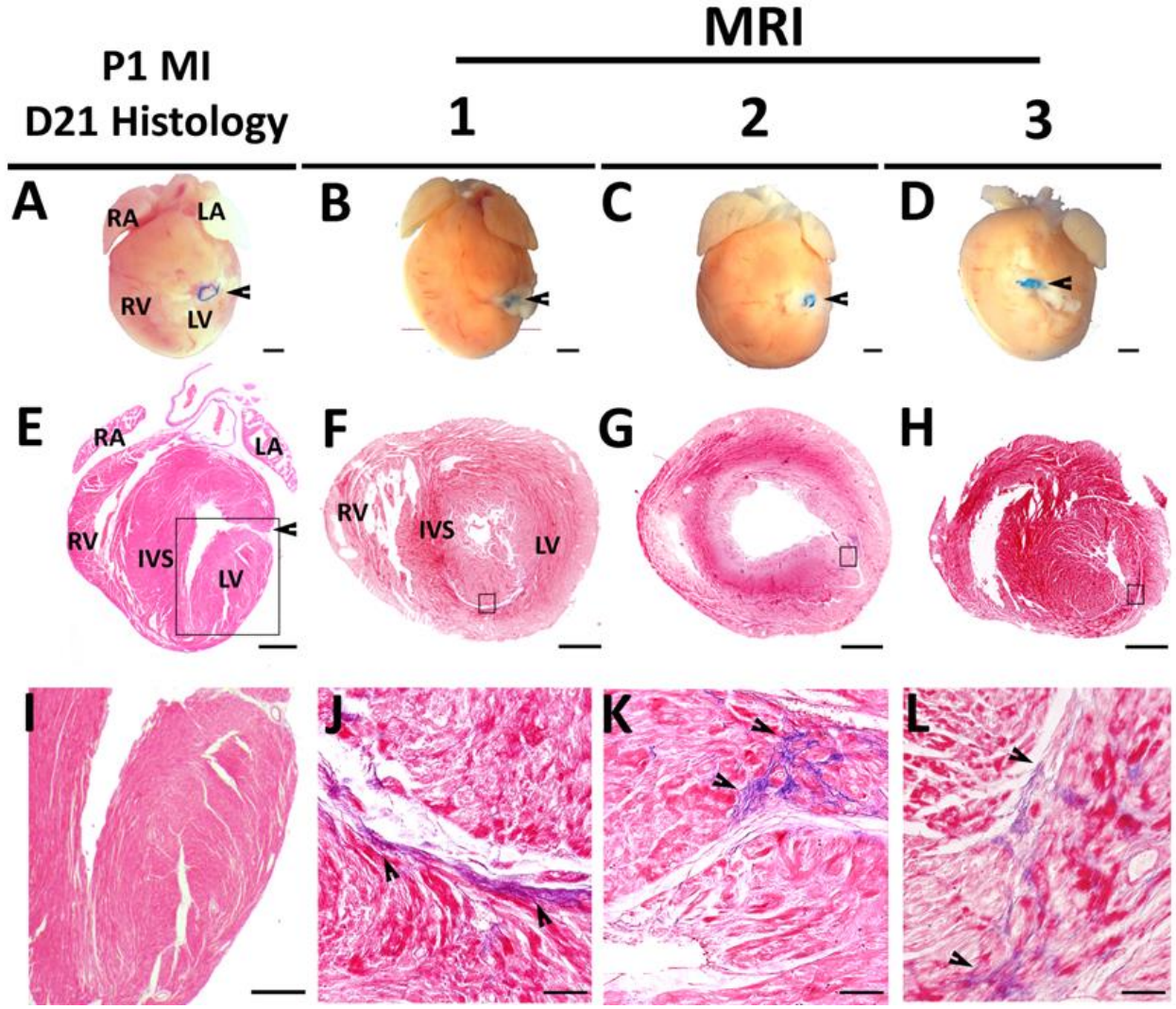


**Figure 4. 11. Heart regeneration 21 days following myocardial infarction injury at P1:**
Whole hearts (A-D) and Masson's trichrome staining of long axis (E) and short axis sections from hearts (F-H) that were injured on postnatal day (P)1 and longitudinally assessed by magnetic resonance imaging (MRI) (Except A, which shows an example of histological assessment of P1 MI at 21 days prior to MRI protocol optimisation). Arrowheads in A-D indicate suture placement. Boxed regions in E-H indicate zoomed regions shown in I-L below. Note small regions of collagen deposition (blue) indicated by arrowheads. LV = left ventricle; LA = left atria; RV = right ventricle; RA = right atria; IVS = interventricular septum. Scale: A-I = 500µm; J-L = 50µm.

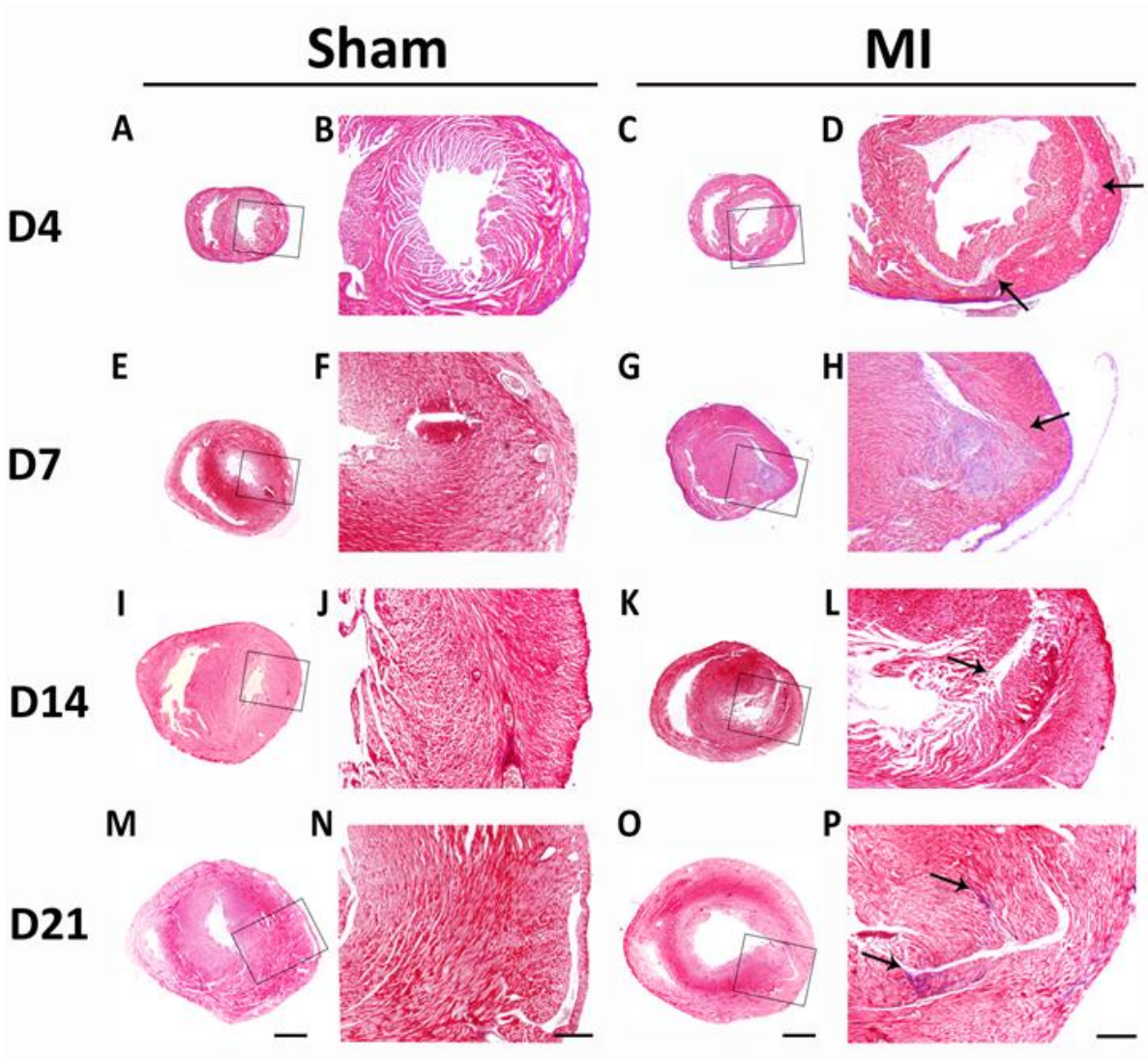


**Figure 4. 12. Histological assessment of regeneration following myocardial infarction in one-day-old mouse hearts:**

Representative Masson's trichrome staining of lower mid-ventricle sections (beneath suture level or equivalent) from representative hearts that underwent sham (left two columns) or myocardial infarction (MI) injury (right two columns) on P1; 4 (A-D), 7 (E-H), 14 (I-L) and 21 (M –P) days post-injury (D4, D7, D14 and D21 respectively). Boxed regions indicate zoomed regions shown in adjacent sections. Note the collagen deposition (blue) in hearts at D4 and D7 which is reduced in hearts at D14 and D21. Arrowheads indicate regions of collagen deposition/injury. Scale: columns A and C = 250 µm; columns B and D = 100 µm. Representative of n=1-4 per group.

Importantly, all mice that sustained MI appeared healthy at all time-points and there was no difference in overall growth and body weights between sham and MI treatment groups for the duration of the study (Figure 4.13). This is in contrast to a previous report that described stunted growth in animals after MI, compared to sham injured littermates, which was attributed to cardiac insufficiency (Konfino et al., 2015).

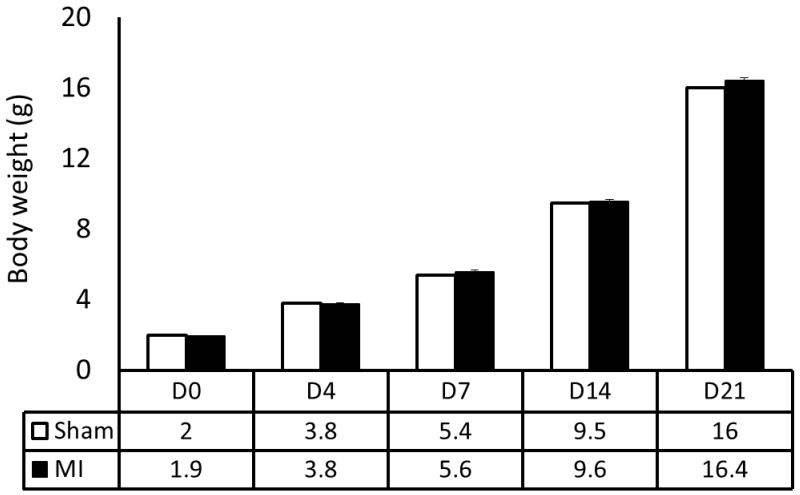


| | D0 | D4 | D7 | D14 | D21 |
|---|---|---|---|---|---|
| Sham | 2 | 3.8 | 5.4 | 9.5 | 16 |
| MI | 1.9 | 3.8 | 5.6 | 9.6 | 16.4 |

**Figure 4. 13. Normal growth of mice during the P1 MRI study:**
Body weights were compared between sham and MI groups. Mean weights are shown beneath the histogram at respective time-points; n=2 sham, 4 MI at D0, D4, D7, D14; n=1 sham, 3 MI at D21.

### 4.9.2. Heart remodelling and fibrosis following LAD ligation injury at P7

To determine the response of P7 mice to MI, we longitudinally assessed heart morphology and function by MRI at D4, D7, D14 and D21 following LAD ligation surgery (or sham procedure) in 8 mice (n=3 sham; n=5 MI). On D0, all mice were scanned for baseline heart function (as described) prior to induction of MI. Tissue was collected following scans on D7 (1 MI and 1 Sham); D14 (1 MI and 1 sham) and D21 (3 MIs and 1 sham) for histological assessment. Collagen deposition, anterior wall thinning and ventricular remodelling was evident in these hearts following Masson's trichrome staining from D7 onwards (Fig. 4.14; 4.15); consistent with previous histological assessments (Fig 4.15A) and the reports of others (Haubner et al., 2012, Porrello et al., 2013). At D21, the extent of injury was variable between the three hearts assessed (15±7.2% of the LV) (Fig. 4.15): two hearts demonstrated typical thinning of the anterior LV and one demonstrated collagen deposition and severe wall thinning in both the anterior and posterior LV, almost certainly due to erroneous suture placement (too high up the LAD). Analysis of the MRI data is ongoing. Despite observations of marked LV wall thinning and collagen deposition in mice that underwent MI on P7, all animals appeared healthy and there was no difference in the growth curves of mice that sustained MI or sham injuries (Figure 4.16). This suggests that previous observations of stunted growth in neonates post-MI (Konfino et al., 2015) are probably not due to cardiac insufficiency.

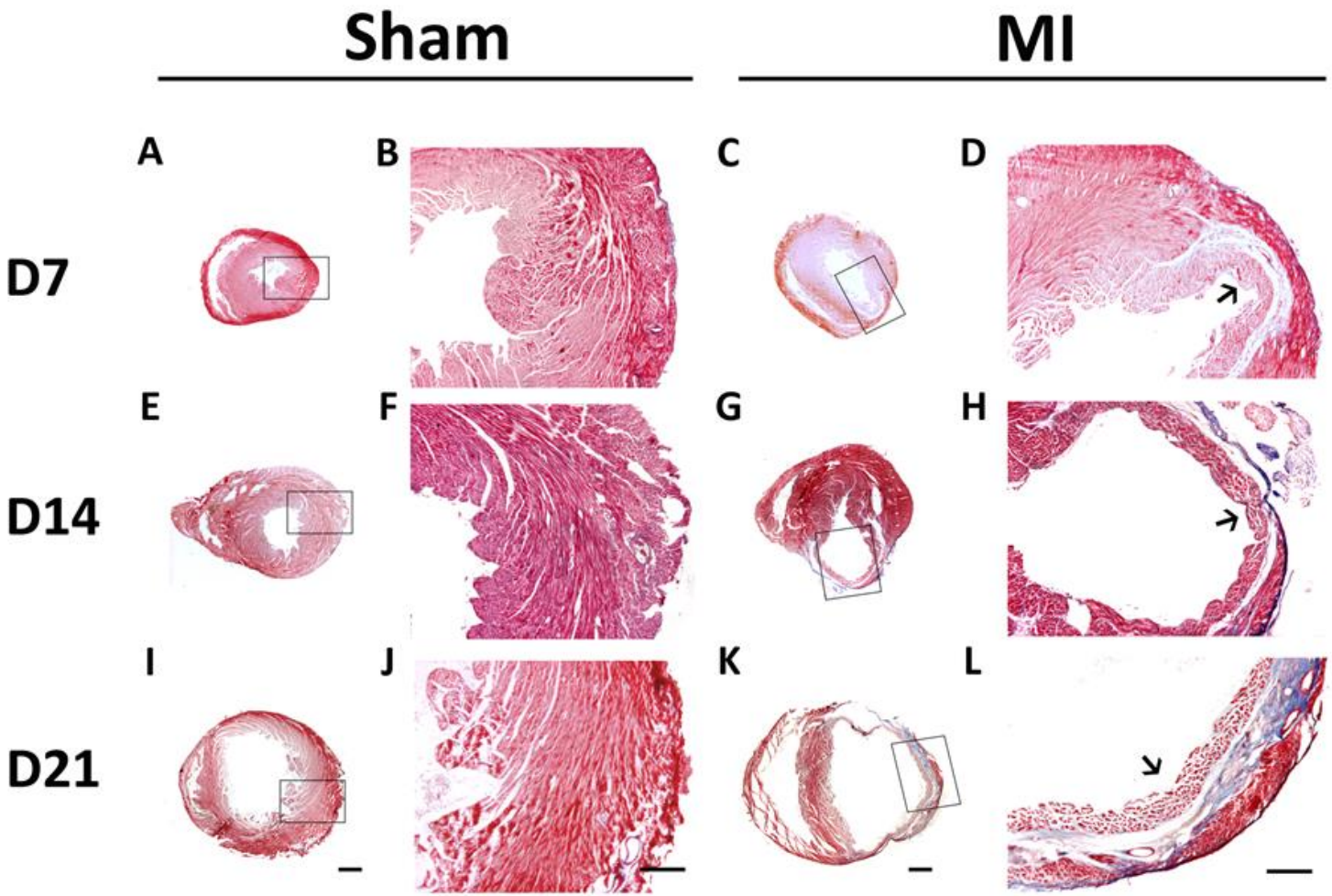


**Figure 4. 14. A time-course of histological assessment of heart repair following myocardial infarction at P7:**
Masson's trichrome staining of lower mid-ventricle sections (beneath suture level or equivalent) from representative hearts that underwent Sham (left columns) or MI injury (right columns) on postnatal day (P) 7 at 7 (A-D), 14 (E-H) and 21 (I-L) days post-injury (D7, D14 and D21 respectively). Boxed regions indicate zoomed region shown in adjacent sections. Note wall-thinning and obvious collagen deposition (blue) in hearts by D7 which increases at D14 and D21. Scale = 100µm columns A and C; 250 µm columns B and D.

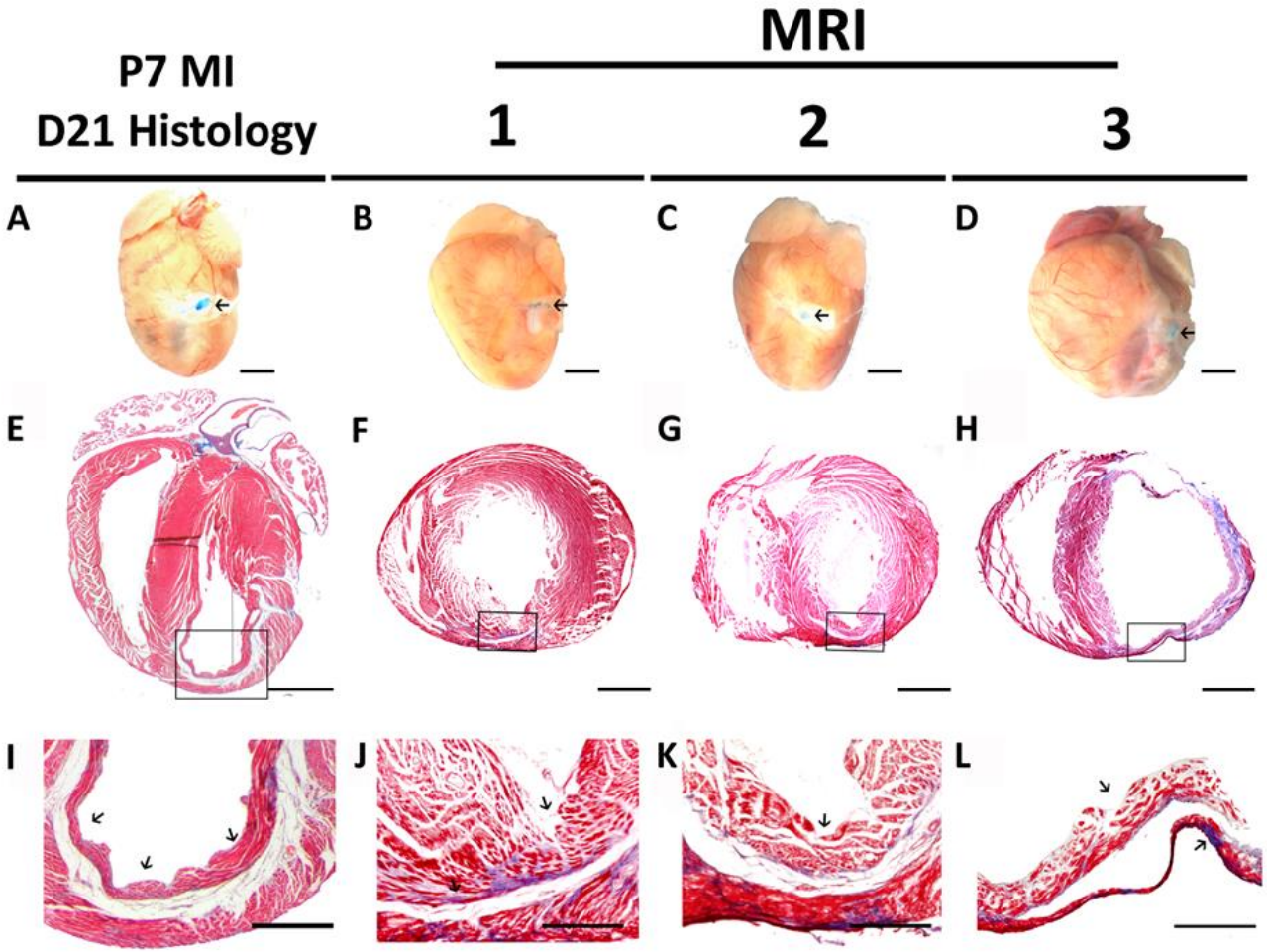


**Figure 4. 15. Significant fibrosis and remodelling following myocardial infarction injury at P7:**
Whole hearts (A-D) and representative Masson's trichrome staining of long axis (E) and short axis, mid-infarct sections (F-H) from hearts that were injure on postnatal day (P) 7 and longitudinally assessed by magnetic resonance imaging (MRI) (except A, which shows an example of histological assessment of P7 MI at 21 days, prior to MRI protocol optimisation). Arrows in A-D indicate suture placement. Boxed regions in E-H indicate zoomed in regions of collagen deposition (blue) shown in I-L below. Note LV wall thinning and collagen deposition (blue) in all hearts (indicated by arrows) at all time-points post-MI. Scale: A-H = 500µm; I = 100 µm; J-L =50µm.

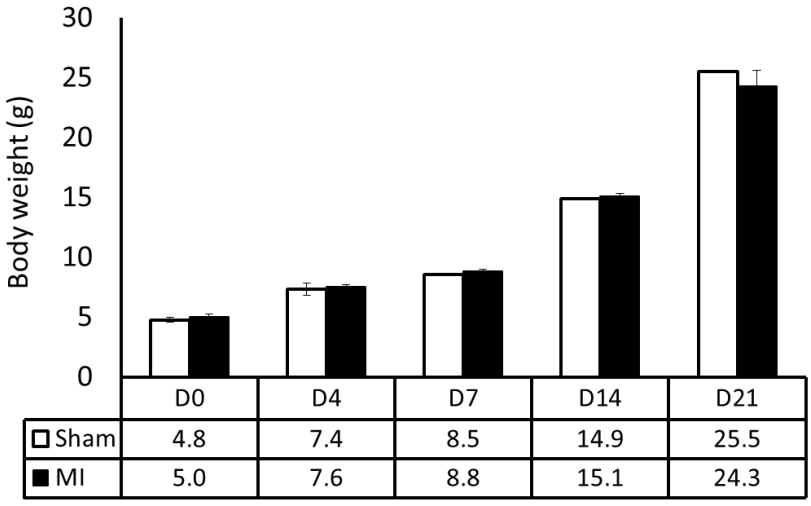


**Figure 4. 16. Normal growth of mice during the P7 MRI study:**
Body weights were compared between sham and MI groups. Mean weights are shown beneath the histogram at respective time-points; n=3 sham, 5 MI at D0 and D4; n=2 sham, 4 MI at D7 and D14; n=1 sham, 3 MI at D21.

### 4.10. Discussion:

These experiments describe the establishment of a protocol for longitudinal assessment of cardiac injury and function in neonatal mice. Through establishing this protocol, we report the first demonstrations of successful cardiac MRI of P1 mice with recovery. The neonatal mice recovered rapidly following imaging and an optimised animal handling protocol was established to allow repeated imaging of the same neonates within the pre-weening period. Cine images of P1 hearts of live animals were successfully reconstructed with full ventricular coverage (~6-7 slices). Image contrast and resolution were sufficient for manual segmentation and derivation of functional parameters (Figure 4.5; Table 4.3). Further, MRI was incorporated into the surgical protocol for inducing MI by LAD ligation, demonstrating that long-term pre-operative anaesthesia is compatible with post-operative recovery following cardiothoracic surgery in neonates. This chapter, therefore, describes how significant technical challenges were overcome to permit longitudinal MRI to assess the disputed phenomenon of heart regeneration in individual neonatal mice over time.

Limited attempts to assess infarcts in neonatal mice by LGE-MRI were initially made. This was because LGE MRI is often considered a more elegant and direct measurement of infarct size than indirect measurements of wall motion. However, LGE MRI does require administration of the contrast agent and may be less clear in neonatal infarcts as, in contrast to the typically transmural infarcts induced by LAD ligation in adult mice, they are typically non-transmural, leaving epicardial and endocardial borders intact. Consequently, tissue perfusion at the infarct borders may be increased in these hearts, which could increase wash-out of the contrast agent. However, few conclusions can be drawn from the limited attempts to perform LGE MRI described. It is possible that either contrast agent delivery or uptake was unreliable. Further work into the utility of LGE MRI for assessing neonatal infarcts is warranted.

The regenerative capacity of neonatal mice has been repeatedly called into question by other groups who aimed to reproduce the findings of the Sadek lab (Andersen et al., 2014, Andersen et al., 2015, Bryant et al., 2015, Konfino et al., 2015). Following LAD ligation in neonatal mice, Konfino and colleagues observed persistent scarring and compromised cardiac function as assessed by 2D-Echo 28 days following injury. In our hands, histological analysis of hearts at respective scanning time-points demonstrated that, after 21 days, P1 hearts demonstrate minimal collagen deposition and no obvious LV wall thinning (Fig. 4.10 and 4.11) whilst P7 hearts undergo significant scarring and remodelling in response to injury (Fig. 4.14 and 4.15). This led us to conclude that P1 hearts do have heightened regenerative capacity, although, due to the presence of some collagen deposition at D21 (0.84%±0.28 of the LV) this regeneration is incomplete. Unfortunately, due to numerous issues, there have been significant delays in MRI data reconstruction and analysis, which has limited functional assessment of the extent of regeneration following injury; as well as assessment of initial infarct size from which the described regeneration may have occurred. However, by histological analyses, at least, our findings support those of Sadek and colleagues (Mahmoud et al., 2014, Porrello et al., 2013). This is an important observation, particularly in light of the

modifications made to the anaesthetic protocol for neonatal MI surgery, as these were suggested to be why the Leor group (who also induced anaesthesia prior to hypothermia induction by isoflurane delivery in 100% oxygen (Konfino et al., 2015)) failed to observe significant regeneration following LAD ligation in neonatal mice (Sen and Sadek, 2015). In contrast, we observed histological regeneration following MI at P1, whilst incorporating a refined anaesthetic protocol to minimise potential pain or suffering. Whether or not the small collagen deposits observed in hearts 21 days after LAD ligation surgery at P1 (Fig. 4.11) translate to compromised cardiac function, as well as the extent of initial injury in these animals, remains to be determined from the acquired MRI data.

The report of Konfino and colleagues also noted severe growth retardation in animals that sustained MI compared to sham operated controls, which they described as an indicator of cardiac insufficiency. In all experiments that we have performed, sham and MI groups were indistinguishable from post-operative recovery to experimental end-point, as demonstrated in the work presented in this chapter (Fig. 4.13 and 4.16). This suggests that the injury induced by the Leor group may be more severe and consequently, regeneration may be impaired. Indeed, differences in technical protocols and injury and/or myocardial quantification methods may offer an explanation of conflicting reports of regeneration (or lack, thereof). In a comprehensive study involving more than 400 mice, Andersen and colleagues were unable to observe regeneration following resection of ~10% of the apex (using a protocol that they deemed equivalent to that of the Sadek group). Instead, they observed a persistent ~14% reduction in the ventricular mass of resected hearts versus shams; as well as significant scarring in all mice studied, which included C57Bl6 and ICR/CD1 strains. In performing "a systematic analysis of neonatal mouse heart regeneration after apical resection" Bryant and colleagues (2015) found that the extent of regeneration was inversely related to the extent of resection injury. The authors also suggested that the surgical technique of Andersen and co-workers (which involved surgical retraction of the apex prior to resection - essentially

'pinching' the heart to expose it) induced significant injury alone. It seems, therefore, that there is a need for standardisation of technical approaches to these models. Injury variability is a caveat of all cardiac injury models and of LAD ligation procedures in particular. Thus the development of accurate, non-invasive infarct detection methods is paramount to the field.

### 4.11. Conclusions

This chapter describes the first successful MRI of a P1 mouse; the first demonstrations of repeated imaging within the pre-weaning period and the establishment of an optimised animal handling protocol for longitudinal, non-invasive assessment of infarction injury in neonatal mice by MRI over time. Further, histological analyses of injured P1 hearts demonstrated minimal collagen deposition and relatively normal cardiac architecture when compared to the severe remodelling observed in time-matched infarcts of P7 hearts. This suggests that P1 hearts do indeed have heightened regenerative potential following LAD ligation and MI, although incomplete, even with a modified anaesthetic protocol. The improved understanding of the mechanisms underlying this regenerative potential may identify means to reinstate or amplify an equivalent response in adult mammalian hearts following injury.

# 5

# The epicardium in heart regeneration in the neonatal mouse

During development, the epicardium provides retinoic acid (RA) inducible paracrine signals to nurture growth of the developing heart from mid-gestation, and epicardium-derived cells (EPDCs) act as progenitors of numerous cardiac cell types; predominantly vascular smooth muscle cells (VSMCs) and fibroblasts, but possibly also coronary endothelium (CoE) and cardiomyocytes (Masters and Riley, 2014). Abrogation of epicardial formation and signalling during embryogenesis has highlighted the importance of this heterogeneous cell population for myocardial maturation and vasculogenesis (Manner, 1993, Merki et al., 2005, Martinez-Estrada et al., 2010, Brade et al., 2011, Guadix et al., 2011, Acharya et al., 2012, Braitsch et al., 2012, Wu et al., 2013). In particular, epicardial RA signalling was shown to induce cardiomyocyte proliferation via paracrine secretions (Chen et al., 2002, Stuckmann et al., 2003, Merki et al., 2005) and to regulate coronary vessel formation (Merki et al., 2005); possibly by inhibition of VSMC differentiation to permit late remodelling and normal coronariogenesis (Azambuja et al., 2010). Post-development, the epicardium becomes quiescent and epicardial markers are detected at low levels, if at all (van Wijk et al., 2012). This transition from active progenitor source to dormant epithelium, however, is poorly characterised.

In response to injury, the epicardium reinstates an embryonic gene program and proliferates at the site of injury to contribute EPDCs and signals for both regenerative and reparative wound healing (Lepilina et al., 2006, Schnabel et al., 2011, Wang et al., 2013, Wang et al., 2015) (Smart et al., 2011, Smart et al., 2007b, Zhou et al., 2011, van Wijk et al., 2012), respectively. Epicardial RA signalling has been implicated in both heart regeneration and repair, with Raldh2 expression post-injury correlating between the extent of injury-induced expression and the capacity of regeneration across several species: i.e. modest expression in poorly regenerative adult mice following MI and robust expression following various cardiac insults in robustly regenerative zebrafish and *Polypterus senegalus* (another ancient teleost fish capable of regeneration) (Kikuchi et al., 2011). RA inhibition post-resection in zebrafish,

also inhibited cardiomyocyte proliferation and, thereby, heart regeneration (Kikuchi et al., 2011). Little is known about the epicardium and epicardial signalling in heart regeneration in neonatal mice, although upregulation of embryonic markers was reported 7 days post-resection injury and cryoinjury by independent groups (Porrello et al., 2011, Rui et al., 2014, Darehzereshki et al., 2015).

Given the roles of the epicardium in heart development, repair and regeneration, and in particular, the myogenic potential of this dynamic cell population, this chapter aimed to assess the potential of the epicardium and its derivative signals in heart regeneration following MI in the neonatal mouse. As the postnatal epicardium and derivative signals are poorly described, a basic characterisation was performed in order assess epicardial potential in the 'regenerative window'; as well as to form a basis for investigating the epicardial response to injury in the regenerative P1 heart. Numerous molecular analyses were employed to characterise the epicardium, in these respective settings, in order to test the hypotheses:

1. Epicardial potential is lost coincident with the loss of regenerative potential in neonatal mice.
2. The loss of epicardial potential in neonatal hearts limits their capacity for regeneration.

**5.1. Epicardial potential is lost coincident with the loss of regenerative potential**

Previous work in our lab demonstrated decreased Wt1 expression in the first week after birth using fluorescence assisted cell sorting (FACS) to quantify $Wt1^{+}$ ($GFP^{+}$) cells from whole heart lysates from $Wt1^{GFPCre/+}$ mice at P1, P4 and P7 (Fig. 5.1), compared to wild-type littermate controls at each time-point (Bollini.S., *unpublished*). As Wt1 is a major regulator of epicardial EMT (Martinez-Estrada et al., 2010), this preliminary data implied a loss of epicardial potential,

coincident with the loss of regenerative potential in neonatal mice (Porrello et al., 2011, Porrello et al., 2013, Haubner et al., 2012)..

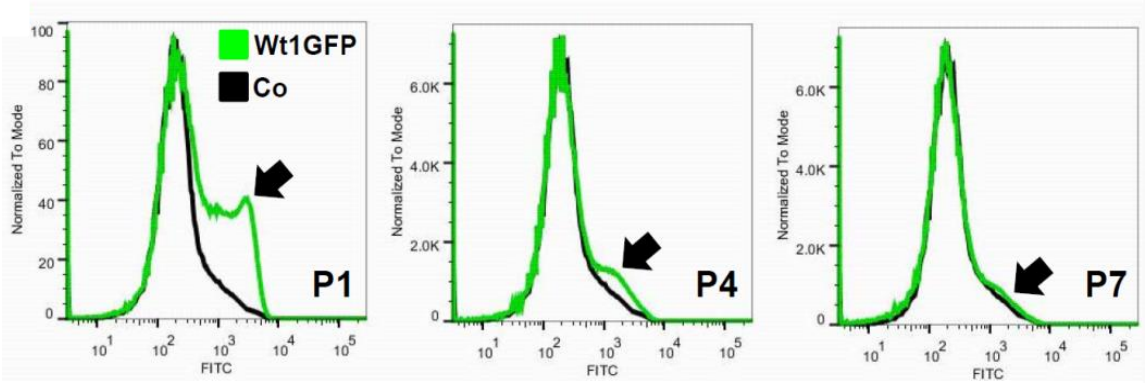


**Figure 5. 1. Decreased Wt1 expression within the first postnatal week:**
Flow-assisted cell sorting (FACS) of $Wt1^{+}/GFP^{+}$ cells (Wt1GFP) from whole heart lysates of *Wt1GFPCre/+* mice at postnatal-day 1 (P1), P4 and P7; compared to wild-type littermate control hearts (Co). Note the decrease in $FITC^{+}$ signal with increased age (black arrows) indicative of reduced numbers of $Wt1^{+}/GFP^{+}$ cells. (Bollini.S. *unpublished*).

### 5.1.1. Decreased epicardial gene expression during the first week after birth

To further assess epicardial potential in the first postnatal week, transcript levels of embryonic epicardial genes were measured in ventricular lysates of wild-type CD1 mice at P1, P4 and P7 and compared to adult expression levels to assess epicardial potential during the 'regenerative window'. The expression of canonical epicardial markers: *Wt1*; *tbx18*; *tcf21*; and *aldh1a2* (*raldh2)* were assessed by qRT-PCR at P1, P4 and P7 (n=4 per time-point) and were compared to adult levels (6 weeks, n=4). All data was normalised to the house-keeping gene *GAPDH*. Statistical analyses were performed using a one-way ANOVA* with Tukey's multiple group comparisons# using GraphPad Prism software. Expression levels of *Wt1, Tbx18* and *Raldh2* were significantly decreased between P1 and P7 (Figure 5.2). Interestingly, a transient peak in *raldh2* expression was observed at P4, at which point expression levels were 20 fold higher than adult levels at ($^{****}$P<0.0001) and almost two-fold higher than P1 levels ($^{\#}$p<0.05). Levels of *tbx18* and *tcf21* followed a similar trend, although neither was significantly greater at P4 than P1. By P7, expression of *raldh2*, *wt1*, *tbx18* and *tcf21* was no longer significantly different

from adult levels. These experiments support a transition to epicardial dormancy at the level of gene expression within the first postnatal week, coincident with the loss of regenerative potential.

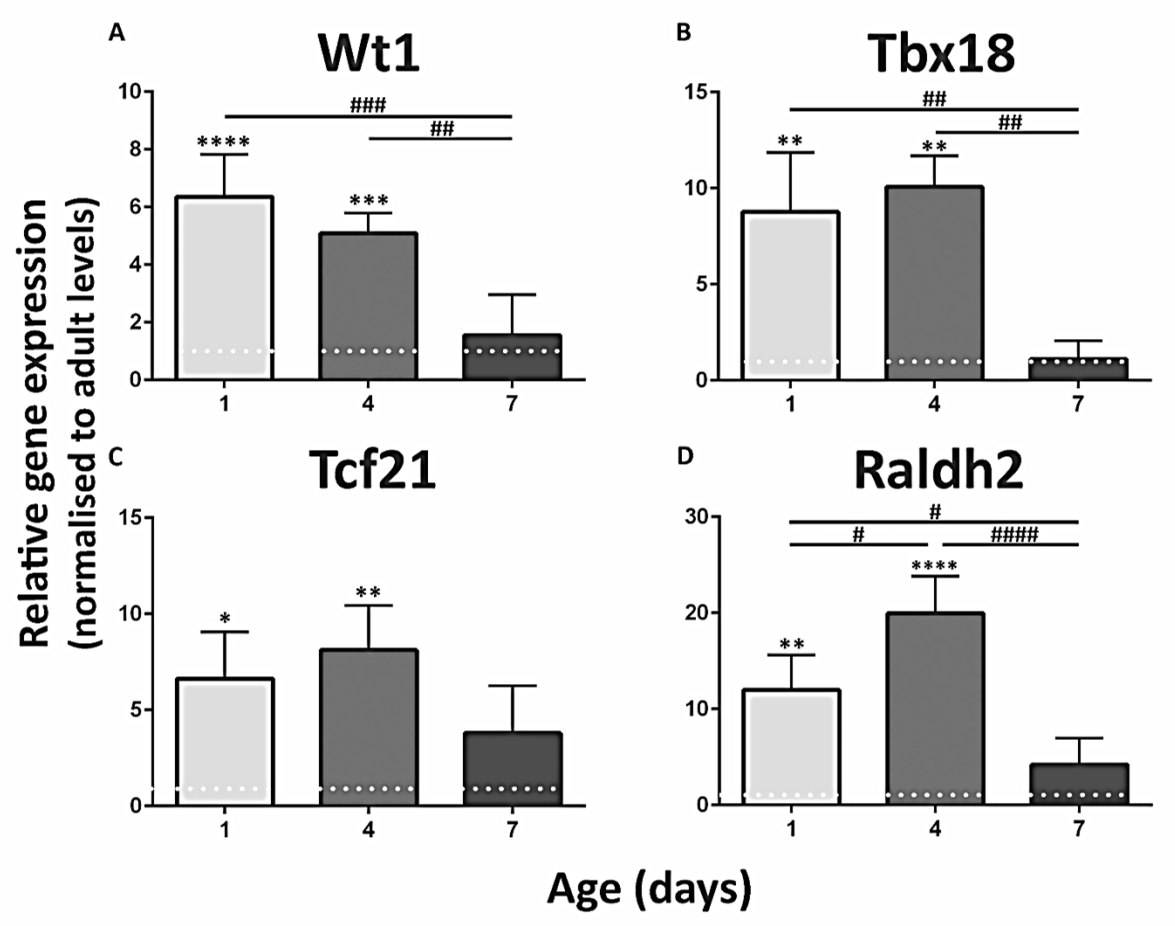


**Figure 5. 2. Decreased epicardial gene expression in the first postnatal week:**
histograms show messenger levels of epicardial genes (A) *wt1*; (B) *tbx18*; (C) *tcf21* and (D) *raldh2* from whole ventricle lysates of CD1 hearts at postnatal day (P) 1, P4 and P7 (n=4 per group) normalised to adult levels (6 weeks; n=4). Data was normalised to *GAPDH* expression and analysed by $\Delta\Delta^{CT}$ method. Data presented as mean±SEM $*^{/\#}p<0.05$; $**^{/\#\#}p<0.01$; $***^{/\#\#\#}p<0.001$; $****^{/\#\#\#\#}p<0.0001$ (one-way ANOVA*; Tukey post-hoc multiple group comparisons$^{\#}$). White dotted line indicates adult expression levels.

### 5.1.2. Altered expression pattern of epicardial markers in the first postnatal week

To assess the distribution of epicardial protein expression in P1 and P7 hearts, immunohistochemistry was performed (Fig. 5.3). Confocal imaging of the surface of whole-mount Wt1 stained hearts from CD1 mice at P1 and P7 demonstrated less dense Wt1 positive cells on the anterior LV apical surface by P7 (Fig. 5.3A). Surface images are maximum intensity

projections of 10 z-stack images per heart, acquired at equivalent laser powers, in equivalent anterior LV regions; generated using ImageJ software. Short axis section staining of hearts of CD1 mice at P1 and P7 demonstrated less dense Wt1 expression in the epicardium covering the LV and RV by P7 (Fig. 5.3B), as well as fewer $Wt1^+$ EPDCs, which were evident in P1 hearts but largely absent in P7 hearts. Raldh2 expression was uniformly detected in the epicardium covering the RV and LV in P1 hearts and in interstitial myocardial cells (Fig. 5.3. C). By P7, epicardial Raldh2 expression was patchy and a few remaining interstitial $Raldh2^+$ EPDCs constituted the majority of the $Raldh2^+$ population in these hearts. Considerable myocardial compaction was evident by P7. These protein data are consistent with decreased *Wt1* and *raldh2* gene expression by P7, coincident with the loss of regenerative potential.

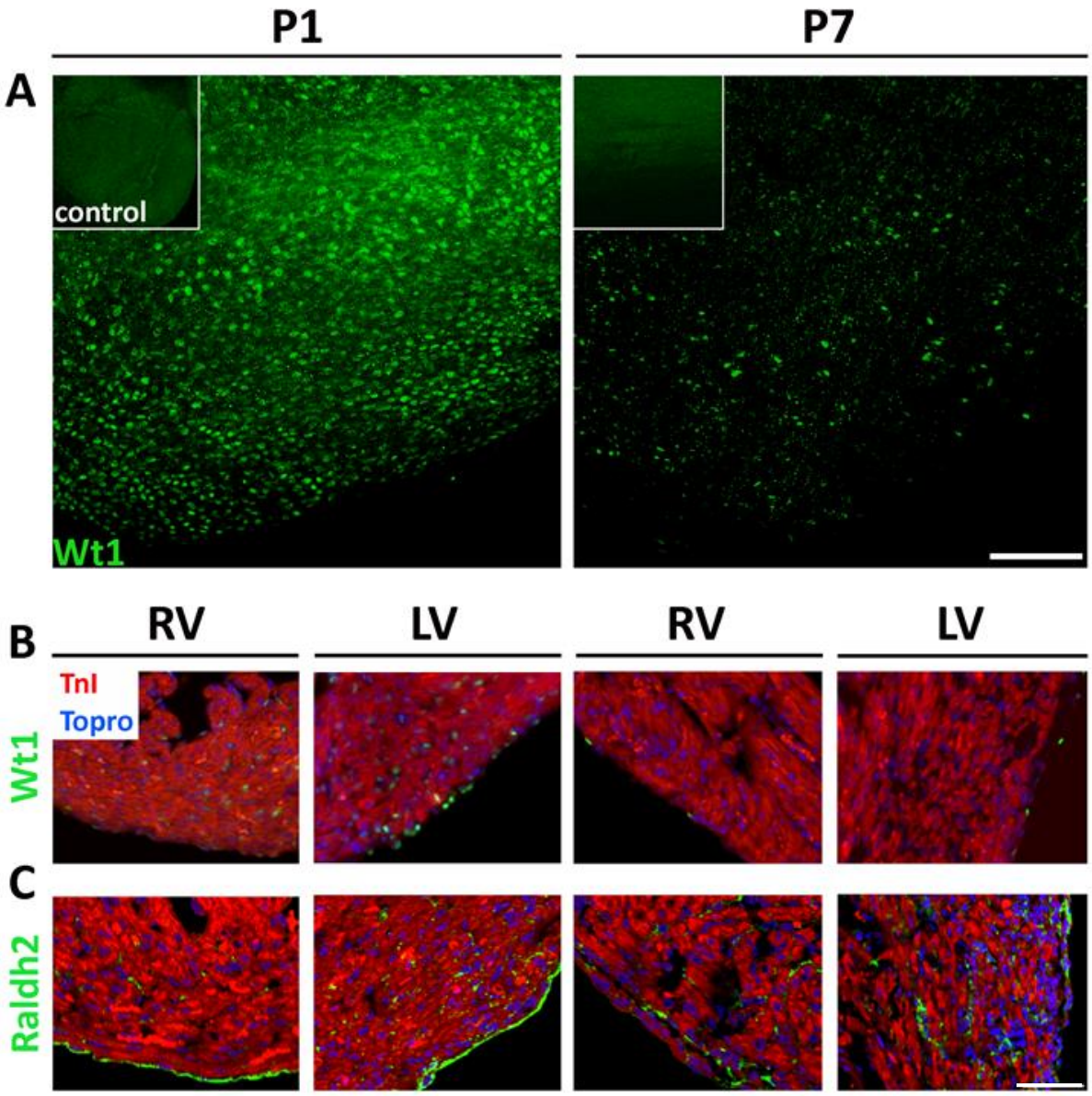


**Figure 5. 3. Altered epicardial protein expression patterns in P1 and P7 hearts:**
(A) Representative confocal imaging of 10 projected z-stack images of the surface of whole-mount Wt1 stained hearts from CD1 mice at postnatal-day (P) 1 and P7 (n=3 per group). Boxed inlets show unstained control hearts. Scale =50µm. (B) Representative Wt1 immunostainings of mid-ventricular short axis sections with troponin I (TnI) in red and Topro nuclear stain (blue). (C) Raldh2 immunostainings of mid-ventricular short axis sections with troponin I (TnI) in red and Topro nuclear stain (blue) in the same heart as in B. Note less dense green ($Wt1^{+}$) cells in the epicardium and in epicardial derived cells in the myocardium in P7 hearts. Also note the more uniform green ($Raldh2^{+}$) signal in the epicardium covering the right ventricle and left ventricle of P1 hearts, compared to patchy epicardial staining in P7 hearts. Representative of n=3 hearts per time-point. Scale = 50µm.

### 5.1.3. Decreased epicardial retinoic acid signalling in the first postnatal week

To assess the functional consequences of decreased RA synthesis in neonatal hearts as indicated by reduced Raldh2 expression (Figures 5.2, 5.3), we investigated RA signalling in the first postnatal week using the RARE-LacZ reporter mouse (Rossant et al., 1991). The LacZ reporter is expressed in cells in which RA responsive genes are transcribed and can be detected *in situ* by enzymatic X-galactosidase (X-gal) staining or by immunodetection of the β-galactosidase (β-gal) enzyme. Whole-mount X-gal staining of RARE-LacZ ($LacZ^+$) hearts at P1, P4 and P7 (n=5-8 per group) demonstrated, overall, prominent X-gal reactivity (blue staining) at P1 and P4; which was almost absent in $LacZ^+$ hearts by P7 (Figure 5.4). The staining extent and pattern was variable between hearts of the same age. $LacZ^-$ hearts of wild-type littermate controls were stained alongside, to control for endogenous mammalian galactosidase activity; which were negative.

### 5.1.4. Fluorescence-activated cell sorting for quantification and genetic profiling of retinoic acid responsive cell types

In order to quantify reporter expression and perform genetic profiling of RA responsive populations at P1 and P7 (as well as on RA responsive populations from hearts injured at P1 and P7), considerable efforts were made to isolate these cells by FACS. These experiments utilised a FACS-gal analysis system, in which galactosidase activity of the LacZ construct cleaves a fluorogenic substrate, fluorescein di-V-galactosidase (FDG), which releases a fluorescent signal, fluorescein isothiocyanate (FITC). Unfortunately, despite numerous trouble-shooting efforts, I was unable to optimise this protocol and distinguish a $FITC^+$ signal from background fluorescence – even in hearts that ubiquitously expressed the ROSA26LacZ reporter. These experiments are described in appendix III.

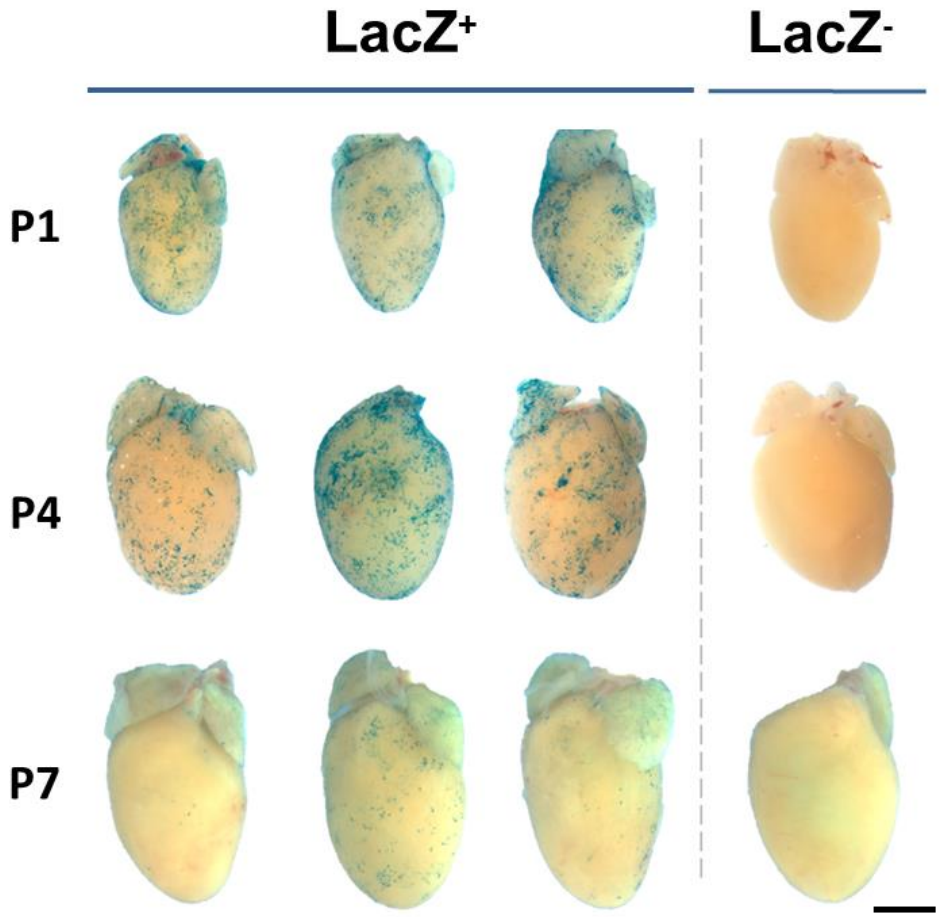


**Figure 5. 4. Reduced X-galactosidase activity in RARE-LacZ mice in the postnatal week:** representative X-gal staining of hearts from RARE-LacZ ($LacZ^+$) or wild-type littermate control ($LacZ^-$) mice on postnatal-day (P) 1, P4 and P7. Scale = 1mm, representative of n=5-8 per time-point. Note decreased X-gal reactivity (blue staining) in P7 hearts.

### 5.1.5. Decreased retinoic acid receptor expression and increased retinoic acid metabolism in the first postnatal week

In order to gain mechanistic insight into the loss of RA signalling in the first postnatal week, whole-ventricle mRNA levels of RA signalling components were assessed by qRT-PCR. Transcript levels of RA receptors *rarα* and *rarβ*; retinoid X receptors *rxrα* and *rxrβ*; as well as levels of the metabolising enzyme *cyp26b1* and the RA sequestering/ nuclear transport facilitating cellular RA binding protein, *crabp2,* were assessed in ventricular lysates from P1, P4 and P7 hearts (n=4 per time-point). Expression levels were compared to those of adult hearts (6 weeks, n=4). All data was normalised to the house-keeping gene, *GAPDH* (Fig. 5.5).

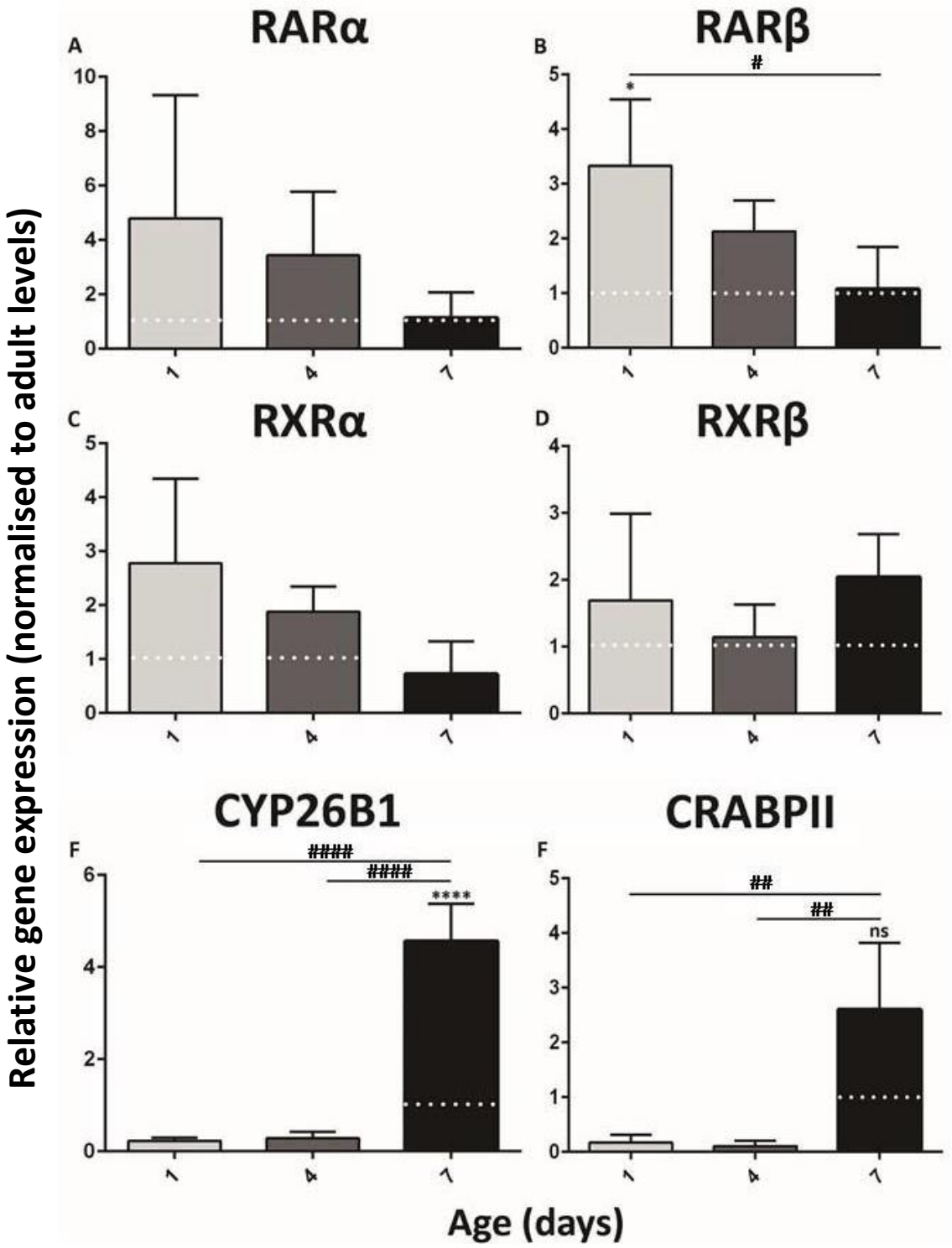


**Figure 5. 5. Decreased retinoic acid signalling in the first postnatal week:**
histograms show messenger levels of retinoic acid receptors (RAR) (A)*rarα* and (B) *rar*β; retinoid X receptors (RXR (C) *rxr*α and (D) *rxr*β; (E) cellular retinoic acid binding protein II (*crabpII*) and (F) cytochrome P45026B1 (*cyp26b1*) from whole ventricle lysates of CD1 hearts at postnatal day (P) 1, P4 and P7 (n=4 per group) normalised to adult levels (dotted white line; 6 weeks; n=3). Data was normalised to GAPDH expression and analysed by $\Delta\Delta^{CT}$ method. Data presented as mean±SEM $*^{/\#}p<0.05$; $**^{/\#\#}p<0.01$; $***^{/\#\#\#}p<0.001$; $****^{/\#\#\#\#}p<0.0001$ (one-way ANOVA*; Tukey post-hoc multiple group comparisons$^{\#}$).

No significant change in *rarα*, *and rxrα* and *rxrβ* expression levels were detected between P1 and P7 (Figure 5.5 A-C) although there were trends of reduced expression across the time-course. The lack of significance likely reflects the ubiquitous myocardial expression of these receptors (Dolle, 2009). *Rarβ* levels were, however, significantly downregulated between P1 and P7 ($^{\#}p<0.05$) and between P1 and adult hearts (Figure 5.5B; *p<0.05. R*arβ* isoforms are also expressed throughout the myocardium, but *Rarβ* was found to be more active in cardiomyocytes in the adult mouse heart post-MI than in other cell types (Bilbija et al., 2012). This reduction may, therefore, reflect a loss of cardiomyocyte responsiveness to RA signalling in the first postnatal week. Conversely, a peak in expression of *Cyp26b1* was observed at P7 that was significantly greater than expression levels at P1 and P4 ($^{\#\#\#\#}p<0.0001$) and to adult levels (****p<0.0001). Similarly, *crabp2* levels at P7 were statistically greater than P1 and P4 levels ($^{\#\#}p<0.01$), but not from adult levels. These data suggest that decreased RA signalling by P7 may be related to decreased RAR complexes available to bind RA; as well as increased RA degradation via the upregulation of *cyp26b1* expression. Crabp2 is suggested to have dual roles in nuclear transport of RA (to facilitate RA signalling) and also to sequester RA in cytosol, to limit RA inducible gene expression. Given the apparent loss in RA signalling via reduced RARE-LacZ reporter expression by P7, increased *crabp2* expression may reflect increased sequestration of RA by crabp2 to limit RA signalling in these hearts.

### 5.1.6. Retinoic acid responsive cells in P1 hearts

In order to identify RA responsive cells in P1 and P7 hearts, β-gal immunodetection was performed on short axis sections from P1 and P7 LacZ$^{+}$ mice (Fig. 5.6). Serial section staining of β-gal and Raldh2 with troponin (TnI) demonstrated contiguous regions β-gal$^{+}$ and Raldh2$^{+}$ signal in the epicardium (Fig. 5.6B) suggestive of autocrine epicardial RA signalling. Co-localisation studies were not performed in this instance (and others) due to antibody incompatibility (i.e. antibodies raised in the same species). Both proteins were also observed in an interstitial myocardial staining pattern, consistent with EPDCs; although β-gal$^{+}$ signal was more pronounced than Raldh2$^{+}$ staining in these hearts (Fig. 5.6A-B), suggestive of a greater RA responsive population than RA producing population, which may reflect paracrine epicardial/EPDC RA signalling. β-gal also co-localised with alpha smooth muscle actin (αSMA) expression in vessels. RA signalling in VSMCs has been suggested to limit their differentiation and maintain plasticity of the developing coronary vasculature (Azambuja et al., 2010). Reporter expression in these cells may reflect this function. β-gal also co-localised with TnI expression in striations of cardiomyocytes in P1 hearts (Fig. 5.6C). Although RA induced cardiomyocyte proliferation is described, *in vitro/ex vivo* studies suggested that this was mediated indirectly via secretions from the epicardium, including the release of trophic factors such as IGF1 and FGF2, but not RA itself (Chen et al., 2002, Merki et al., 2005, Stuckmann et al., 2003, Brade et al., 2011). Reporter expression may, therefore, be due to RA induced transcription of genes independent of this pathway.

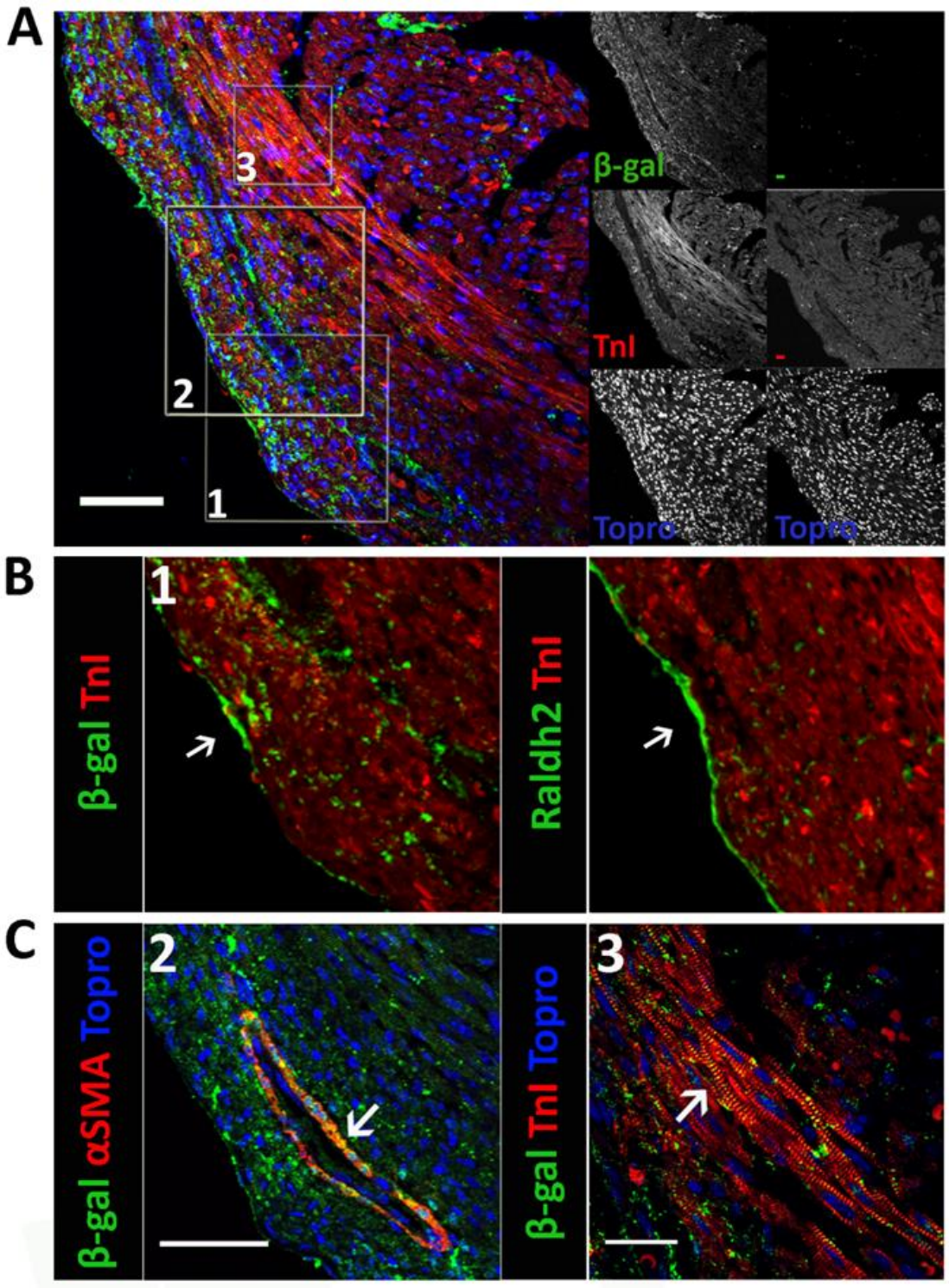


**Figure 5. 6. Retinoic acid responsive cell types in a one day-old mouse heart:**
β-galactosidase (β-gal) immunostainings of anterior left ventricles in short axis, mid-ventricle sections of hearts of P1 RARE-LacZ mice (representative of n=3 hearts). (A) Merged image of β-gal (green), TnI (red) and Topro nuclear stain (blue) of grey scale images shown to the right; alongside secondary antibody only stained (-) control images. Scale = 50µm. Numbered boxes indicate regions shown in (B) serial sections of β-gal and Raldh2 positive staining with TnI (troponin I) (arrowheads indicate regions of overlap); and (C) colocalisation of β-gal with αSMA (2, scale = 50µm) and TnI (3, scale = 20 µm); in vessels and cardiomyocytes, respectively. Arrowheads indicate regions of colocalisation (yellow).

### 5.1.7. Retinoic acid responsive cells in P7 hearts

In P7 hearts, β-gal expression was largely absent in the epicardium and restricted to interstitial cells lining the myocardium and vessels (Fig. 5.7). Serial sections stained with Raldh2, β-gal and TnI (Fig. 5.7G) demonstrated a similar interstitial staining pattern that was absent in perivascular cells, suggestive of paracrine signalling of nearby Raldh2$^{+}$ EPDCs. Notably, robust β-gal$^{+}$ signal was detected in subepicardial perivascular cells surrounding a large αSMA$^{-}$ vessel in the RV underlying a cluster of Raldh2$^{+}$ epicardial cells, presumably a vein (Fig 5.7.G). Some co-localisation of β-gal with αSMA was detected in vessels in P7 hearts (Fig. 5.7E) although to a lesser extent than in P1 hearts, but no overlap with TnI staining was observed in these hearts. Of note, many of the TnI$^{+}$ cardiomyocytes were binucleated in this heart (Fig. 5.7D).

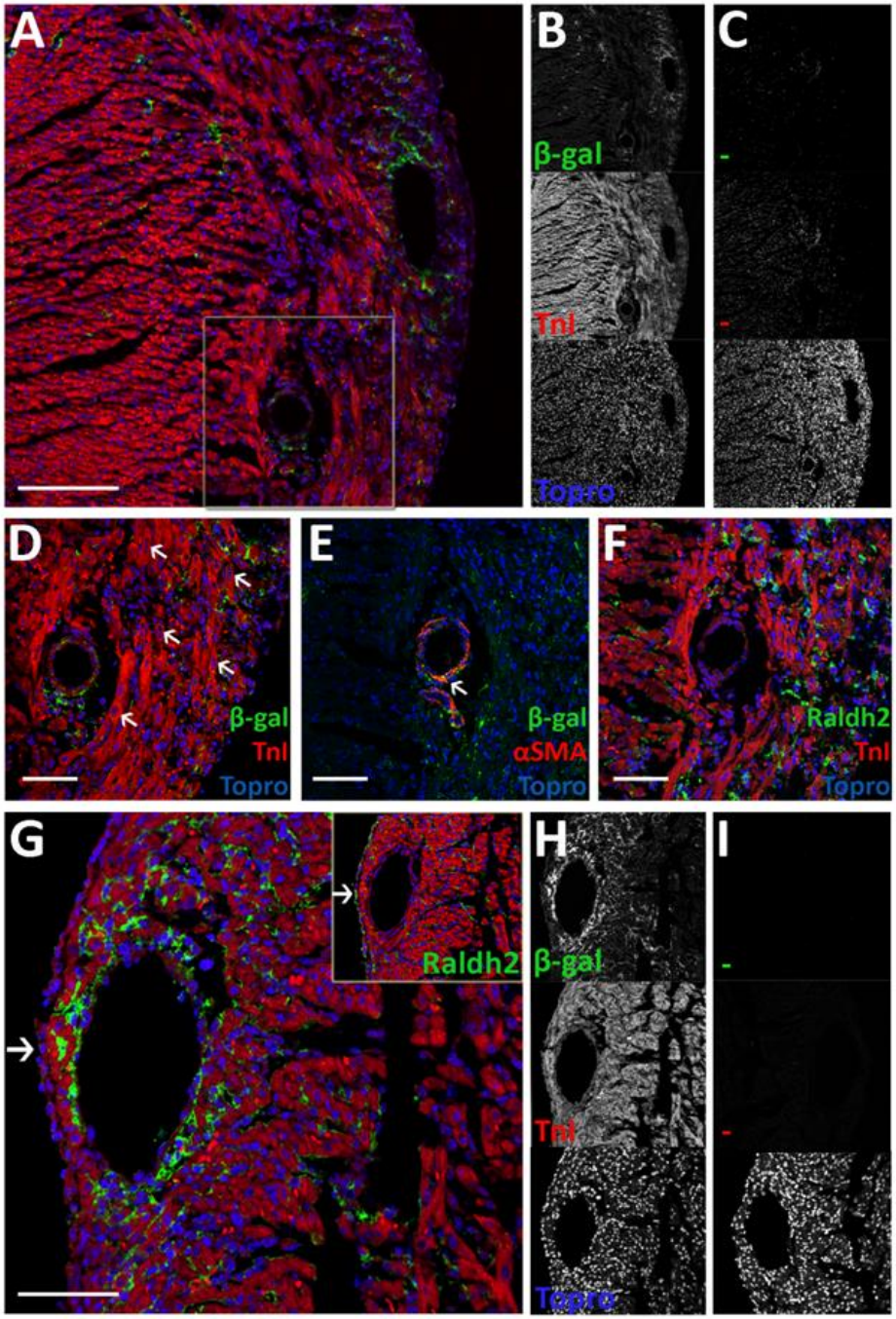


**Figure 5. 7. Retinoic acid responsive cells in 7 day-old mouse hearts:**
β-galactosidase (β-gal) immunostainings of short axis mid-ventricular sections of hearts of P7 RARE-LacZ mice (representative of n=3 hearts). (A) Merged image of β-gal (green), TnI (red) and Topro nuclear stain (blue) of grey scale mid-anterior left ventricle images shown in B. Boxed region shows zoomed region in D, E and F. (C) secondary antibody-only stained controls (-) of similar regions. (D) Zoomed image of boxed region in A. Arrows indicate binuclear myocytes. (E) Serial section of D showing colocalisation (arrowhead) of β-gal with αSMA in coronary vascular smooth muscle cells. (F) Serial section of D showing Raldh2 expression (green). (G) β-gal staining in right ventricle surrounding a superficial vessel. Boxed region shows comparative Raldh2 signal (green) in a serial section: note region of epicardial Raldh2 signal overlaying β-gal positive cells (arrowhead). (H) Grey-scale images of merged image in G and (I) secondary antibody stained controls (-) of similar region. Scale = (A) 100µm; (D,E,F,G) 50µm.

## 5.2. The role of the epicardium in neonatal heart injury

Taken together, these findings suggest that the transition from an active embryonic epicardium to a dormant epithelium in the healthy adult heart, occurs within the first postnatal week in mice; coincident with their loss of regenerative potential. To assess whether or not the more foetal-like epicardial profile of P1 hearts contributes to their regenerative capacity, the following experiments aimed to characterise the epicardial response following MI, in P1 versus P7 hearts.

### 5.2.1. Time-course of epicardial protein expression post-MI in P1 and P7 hearts

To compare the epicardial response to injury in P1 and P7 hearts, immunodetection of canonical epicardial markers Wt1 and Raldh2 were assessed on mid-infarct short axis sections. These mice underwent LAD ligation on P1 or P7 and were assessed 4, 7, 14 and 21 days post-injury (D4, D7, D14 and D21, respectively, (Fig. 5.8)). Wt1 and raldh2 were co-stained with TnI in order to discriminate healthy myocardium from the infarct. Sections were selected at mid-infarct level (below the ligature and above the apex) without incorporating injury from the suture site; around which there was persistent scarring due to permanent ligature placement (even in hearts injured at P1). This ensured assessment of ischemic injury (as opposed to that caused by the suture itself). In hearts that sustained MI at P1, few $Wt1^+$ cells were observed at D4 (Fig 5.8A), with expression most pronounced at D7 (Fig 5.8B); at which point epicardial expansion was evident at the site of injury. At D14, Wt1 was detected to a lesser extent in the epicardium overlying the injury zone (Fig. 5.8.C) and on D21, Wt1 expression was no longer detected (Fig 5.8D). In time-matched infarcts of P7 hearts, significant expansion of $Wt1^+$ cells was evident on D4 (Fig 5.8E), which was also observed in hearts on D7 (Fig 5.8F). On D14, Wt1 expression was detected but expansion appeared to have receded (Fig 5.8G), with no expression detected by D21 (Fig 5.8H). Thus Wt1 expression in these hearts was most

pronounced at D7 post-MI at P1, and at D4 and D7 post-MI at P7, suggestive of a greater epicardial response following MI at P7.

In serial sections, raldh2 staining demonstrated marked expression within the infarct core by D4 following MI at P1 (Fig 5.8I), with some staining also detected in the epicardium. At D7, Raldh2 was more localised to the epicardium (Fig 5.8J) which was reduced at D14 (Fig 5.8K) and absent by D21 (Fig 5.8L). In time-matched P7 infarcts, Raldh2 was strongly expressed in the epicardium and subepicardial myocardium in an interstitial staining pattern (Fig 5.8M), but demonstrated considerably less signal within the infarct core than P1–injured hearts. At D7, P7 injured hearts demonstrated Raldh2$^{+}$ signal in the epicardium (Fig 5.8N), similar to P1 injured hearts. On D14, small regions of Raldh2$^{+}$ signal were detected overlying the significantly thinned anterior LV wall (Fig 5.8O), which persisted until D21 (Fig 5.8P). To summarise, in P1-injured hearts, Raldh2 was expressed strongly within the infarct core at D4, but became more limited to the epicardium thereafter and was absent by D21. In P7-injured hearts, Raldh2 was mainly expressed in the epicardium at D4 and D7, with patchy epicardial expression persisting to D21.

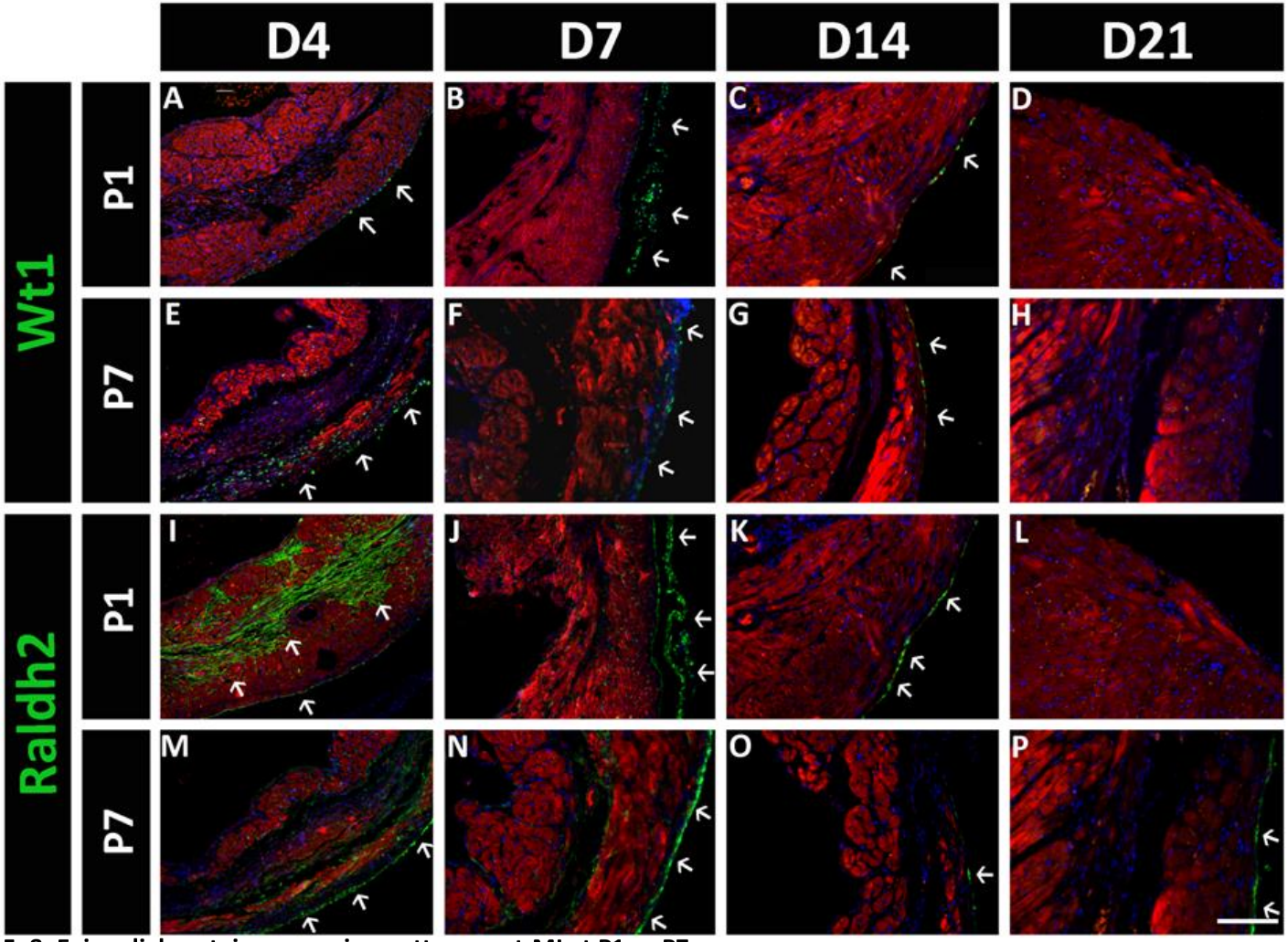


**Figure 5. 8. Epicardial protein expression pattern post-MI at P1 or P7:**
Wt1 (A-H) and raldh2 (I-P) expression were detected following myocardial infarction at P1 (A-D; I-L) or P7 (E-H; M-P) hearts on 4 days (D4) post MI (A,E,I,M; representative of n=4 at P1, n=2 at P7); D7 (B,F,J,N, representative of n=3 at P1, n=2 at P7); D14 (C,G,K,O; representative of n=1 per time-point) and D21 (D,H,L,P; representative of n=3 per time-point). Arrows indicate positive staining regions. Viable myocardium is labelled with troponin I (red) and nuclei are labelled with Topro nuclear stain (blue). Troponin negative regions indicate regions of infarct. Scale = 50µm.

In infarcted adult hearts, Raldh2 expression was found to derive mainly from fibroblasts (Bilbija et al., 2012). To assess the source of Raldh2 in infarcts of P1 hearts, serial section staining of Raldh2 and DDR2 was performed (Fig. 5.9). DDR2 is a collagen receptor expressed in fibroblasts (Camelliti et al., 2005). Again, co-localisation staining was prevented by antibody incompatibility. The expression patterns of Raldh2 and DDR2 were similar (Fig 5.8C,D) indicating potential overlap and suggesting that $DDR2^{+}$ cells (fibroblasts) may also be a source of Raldh2 in the P1 heart after injury.

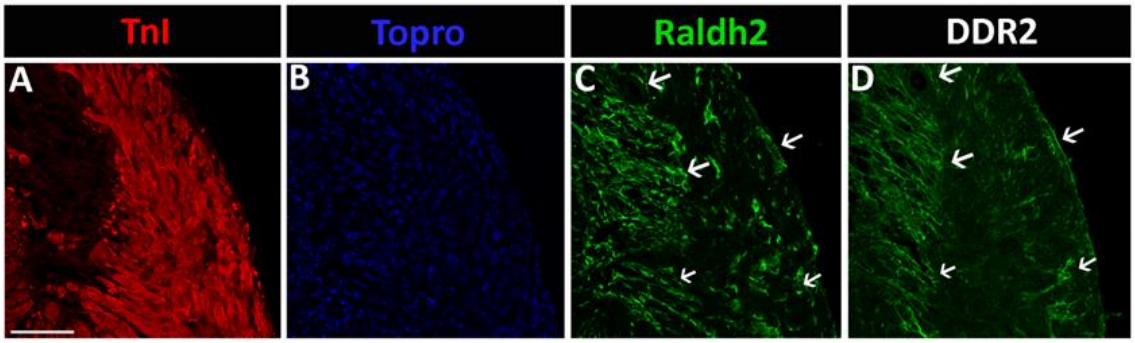


**Figure 5. 9. Fibroblasts are a source of Raldh2 expression in P1 hearts post-MI:**
Serial section immunostaining of raldh2 and DDR2 with troponin I (TnI) and Topro nuclear stain (blue) in infarcted P1 hearts on D4 (representative of n=4 hearts). Arrows indicate similar expression patterns of raldh2 and DDR2 in the epicardium and infarct core (i.e. the TnI negative region in A. Scale = 50µm.

### 5.2.2. Differential epicardial gene expression following MI at P1 and P7

Due to the observed differential expression patterns of Wt1 and Raldh2 protein at D4 post-MI at P1 or P7 (Fig.5.8), qRT-PCR was employed to investigate epicardial gene expression profiles at this time-point (Fig. 5.10). In particular, we looked at whether injury at P1 or P7 affected normal epicardial gene expression levels at D4 (P5) compared to time-matched, uninjured controls (i.e. P5 and P11). Levels of embryonic epicardial genes: *Wt1*; *Tbx18*; *tcf21*; and *raldh2* were measured in apical ventricular lysates (of the tissue beneath the suture) of wild-type CD1 mice that sustained MI at P1 (n=6) or P7 (n=4); and were normalised to expression levels in equivalent apical portions of time-matched uninjured hearts (i.e. P5 and P11, respectively; n=4 per group). Intact hearts were used as opposed to sham operated mice for controls based on initial experiments, which demonstrated that 'sham' injury (suture placement without securing the ligature) was sufficient to induce a significant epicardial response alone, which masked any significant effect of MI injury (Appendix IV). Expression data was normalised to an averaged value of the house-keeping genes 18S and GAPDH. For statistical analyses, two-group comparisons were performed by student's unpaired t-test using GraphPad Prism software. Interestingly, relative to intact controls, expression levels *Wt1, Tbx18* and *tcf21* were significantly reduced following MI at P1 whilst following P7 injury, upregulation was observed (*$p<0.05$, **$p<0.01$, respectively; Fig 5.10 A-C);. *Raldh2* expression followed the same trend but did not reach statistical significance. This may reflect a differential epicardial response at D4 in P1 and P7 hearts post-MI.

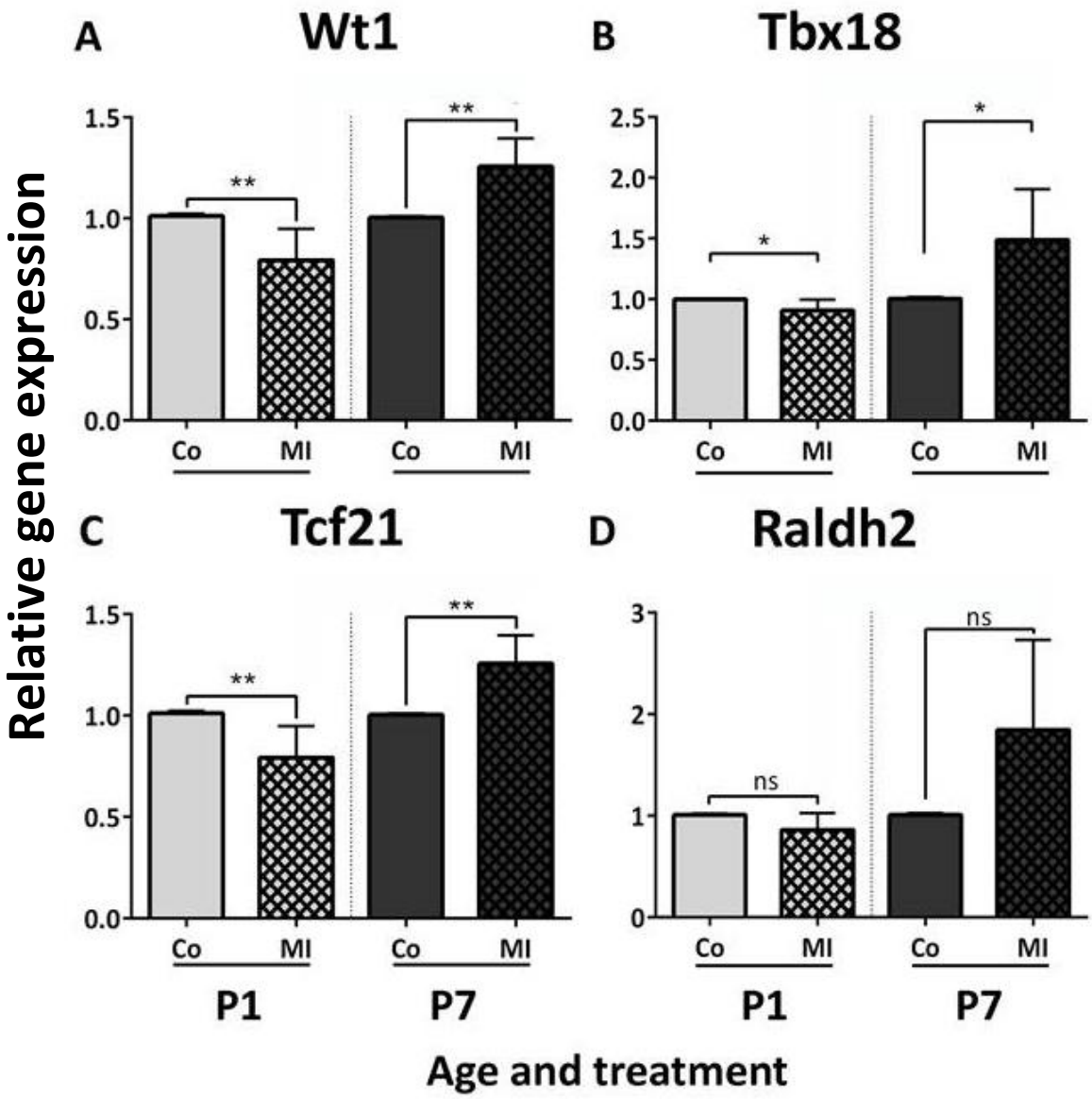


**Figure 5. 10. Epicardial gene expression post-MI at P1 or P7:**
(A)*Wt1;* (B)*Tbx18;* (C)*tcf21* and (D) *raldh2* expression levels were compared in hearts of neonatal mice following myocardial infarction (MI) injury sustained at P1 or P7 by qRT-PCR (n=6 hearts per group), relative to time-matched, intact control (Co) hearts (P5 and P11, n=4 hearts per group). Statistical analyses were performed to assess expression levels between control and injury groups (*p<0.05, *p<0.0001)) using a student's un-paired t-test.

### 5.2.3. Increased fibrosis following MI at P7

In adult hearts, increased epicardial gene expression has been associated with fibrotic scar formation (Ruiz-Villalba et al., 2015). To investigate the relative fibrotic response of P1 and P7 hearts to injury, , expression levels of fibroblast-specific protein-1 (*Fsp-1*); the gene encoding pro-alpha-1 chains of type III collagen (*Col3a1*), and the collagen binding ECM glycoprotein, fibronectin 1 (*Fn1*) were assessed at D4 post-MI at P1 or P7 (Fig.5.11); as before (Section 5.2.2). Relative gene expression revealed significantly increased expression of *Fsp1, Col3a1 and Fn1* in P7 hearts at D4, relative to intact P11 hearts (****p<0.0001; fig. 5.11A-C). In time-matched P1 infarcted hearts, there was a significant increase in *Fsp-1* relative to uninjured controls (*p=0.03) suggesting increased fibroblast marker expression in the P1 heart post-MI. However, unlike P7 hearts, no upregulation of *Col3a1* or *Fn1* was observed, suggesting that fibroblast activation in P1 hearts post-MI may not be associated with collagen or ECM deposition above basal levels, and possibly that activated fibroblasts in P1 hearts post-injury are different or behave differently to those of injured P7 hearts.

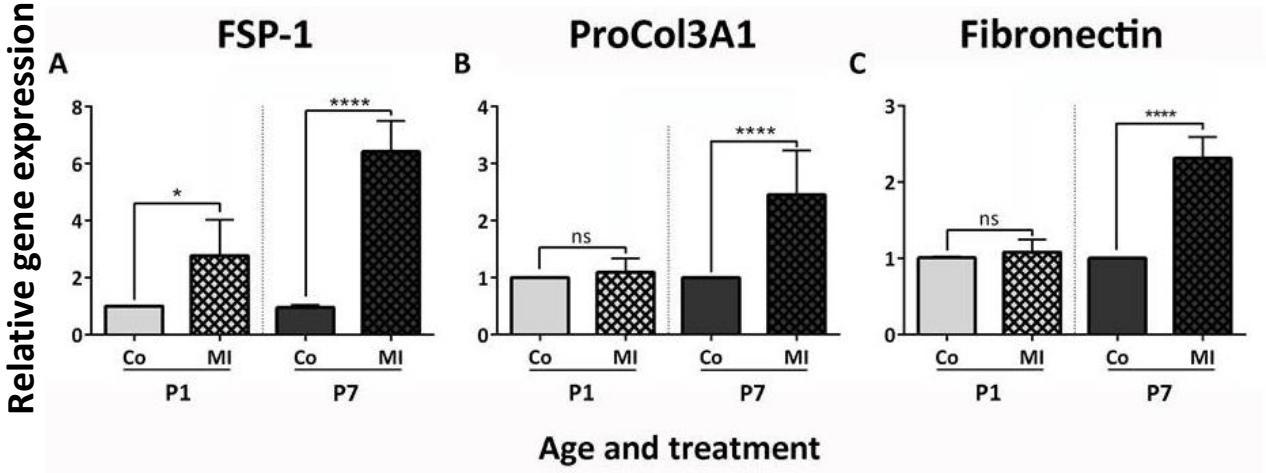


**Figure 5. 11. Increased expression of fibrosis genes in P7 hearts post-MI:**
Fibroblast-specific protein (*fsp-1),* pro-alpha-1 chains of type III collagen (procol3a1) and *fibronectin* expression levels were compared in hearts of neonatal mice following myocardial infarction (MI) injury sustained at P1 or P7 by qRT-PCR (n=6 hearts per group), relative to time-matched, intact control (Co) hearts (P5 and P11, n=4 hearts per group). Statistical analyses were performed to assess expression levels between control and injury groups (*p<0.05, *p<0.0001) using a student's un-paired t-test.

### 5.2.4. Retinoic acid signalling following MI in neonatal mice

To investigate RA signalling in P1 and P7 hearts four days post-MI; whole-mount X-gal staining was performed on injured hearts from RARE-LacZ mice compared to sham operated controls (Fig. 5.12). Sham procedure in these experiments involved thoracotomy without heart manipulation to permit simultaneous rearing of both treatment groups by the same dam, without inducing an epicardial response. In injured P1 hearts, X-gal$^{+}$ signal was detected in the infarct region proximal to the ligature and relatively diffusely in remote myocardial zones compared to P7 hearts, in which signal was localised almost exclusively within and proximal to the infarct core. Reporter expression in P7 hearts appeared to be more injury dependent, emphasised in one heart that sustained atrial damage and a substantial infarct due to erroneous suture placement (boxed heart, Fig.5.12).

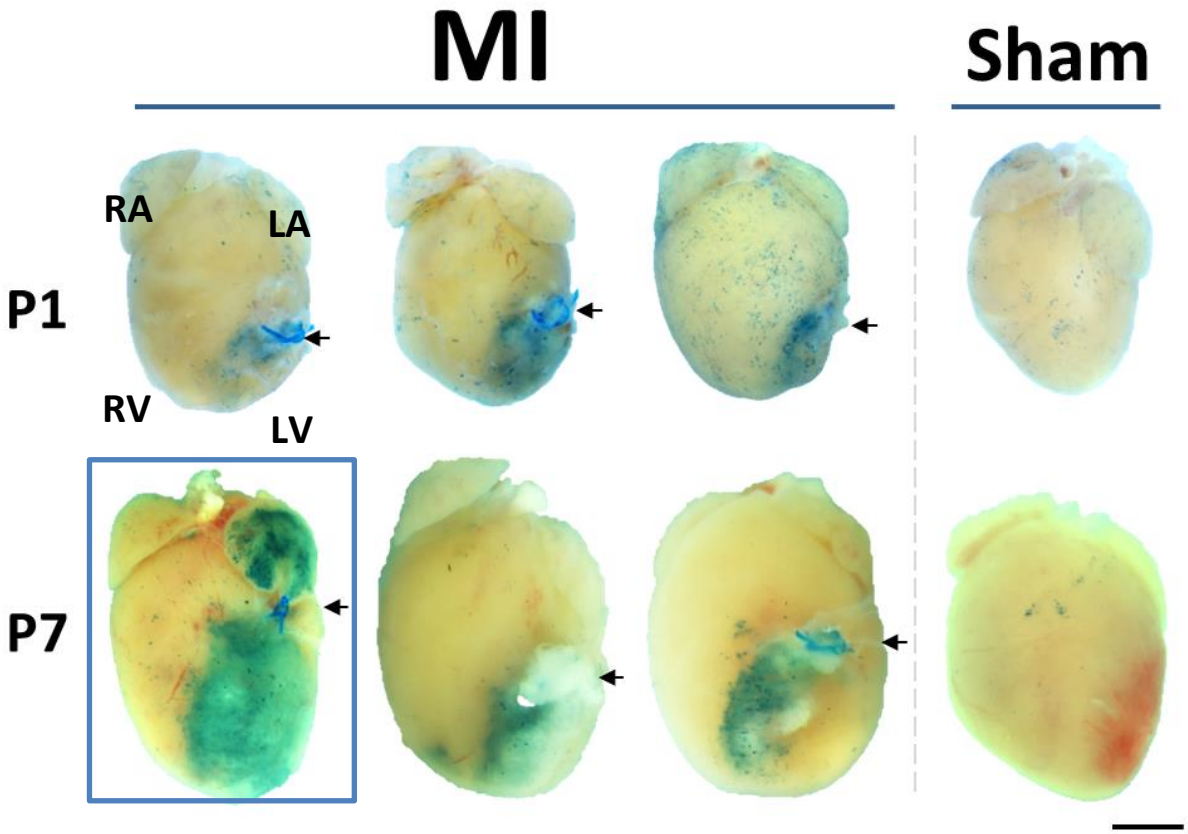


**Figure 5. 12. X-galactosidase activity in RARE-LacZ mice post-MI at P1 or P7:**
X-gal staining of hearts from RARE-LacZ mice that underwent LAD ligation or sham procedure at P1 or P7; 4 days post-MI. Boxed heart indicates an outlier that sustained atrial damage, demonstrating the injury-dependent RA response in P7 hearts. Arrowheads indicate suture placement. RA = right atria; RV = right ventricle; LA = left atria; LV = left ventricle. Hearts representative of n=8 P1, n=6 P7. Scale = 1 mm.

To further assess the distribution of LacZ reporter expression post-MI, β-gal expression and distribution was assessed in multiple sections from injured P1 and P7 hearts on D4 (Figure 5.13). To control for injury variability and relative reporter expression, hearts with similar portions of compromised left ventricular myocardium were compared. Injury zone size was estimated in P1 and P7 hearts by calculating the percentage volume of TnI negative (infarct) regions and adjacent epicardial and endocardial borders relative to total ventricular volume in 8-10 short axis ventricular sections per heart using Amira software. The injury zones in these hearts were estimated at 16% and 20% of the myocardium of hearts operated on at P1 and P7, respectively. β-gal expression and distribution were quantified in the same hearts by manual counting of nuclei in areas of β-gal$^{+}$ signal in intact and infarcted myocardial portions, demarcated by TnI$^{+/-}$ co-staining (Figure 5.13). The total percentage of β-gal$^{+}$ nuclei (relative to total nuclei) 4 days post-P1 injury was 2.7% with the average percentage of those cells within the infarct being 34%. The total percentage of β-gal$^{+}$ nuclei 4 days post-P7 injury was 3% with, on average, 83% of those cells localised to the infarct zone. Thus, the amount of reporter expression in these hearts was similar but the distribution was different, with reporter expression in P7 hearts being more localised to the infarct, suggesting that RA responsive cells may be different in the respective injury settings.

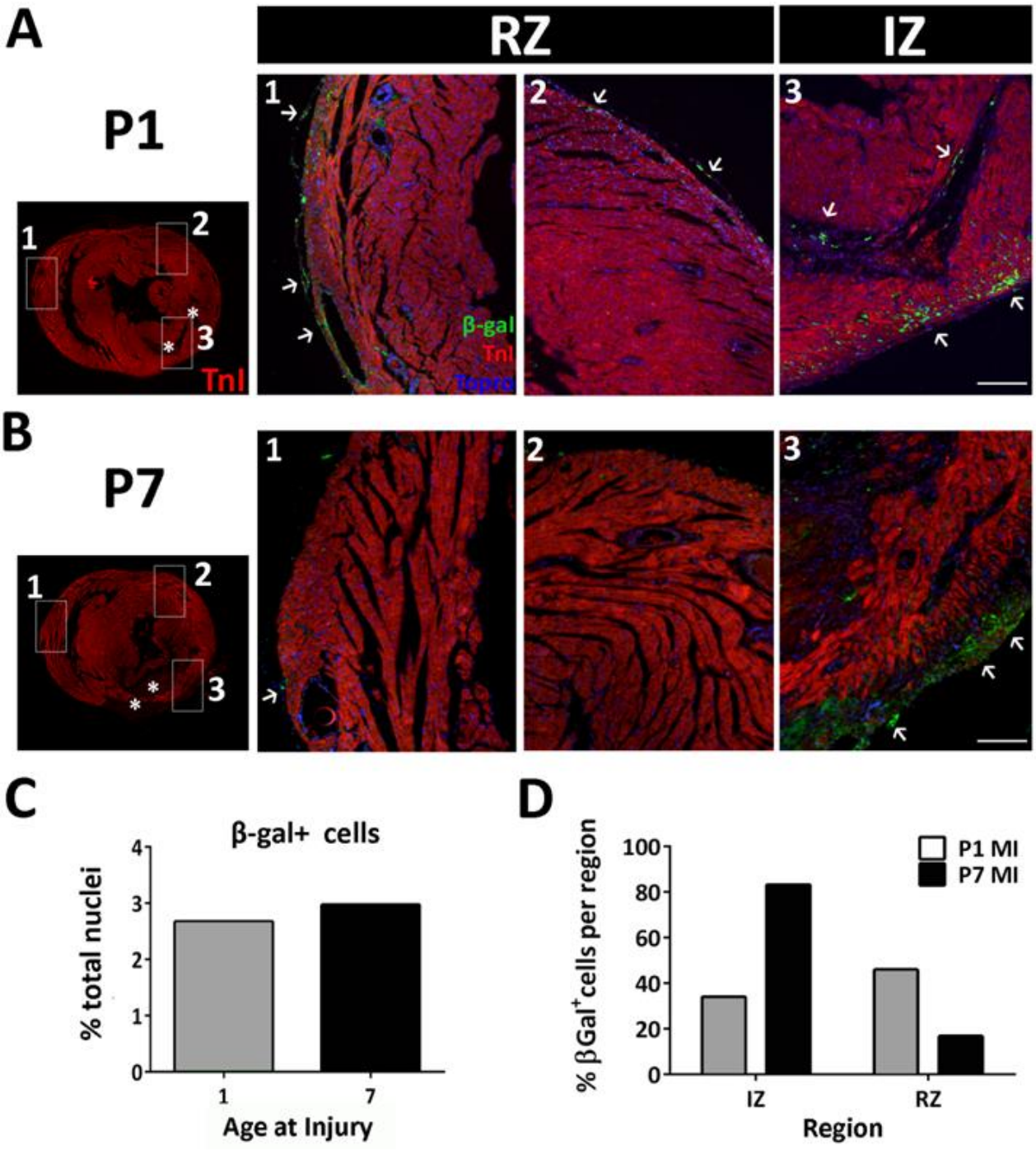


**Figure 5. 13. Distribution of retinoic acid responsive cells in P1 and P7 hearts post-MI:**
Immunodetection of β-gal$^+$ cells in a P1 (A) and P7 (B) RARE-LacZ$^+$ hearts with similar sized infarcts 4 days post-MI. (A) Low magnification image of a representative section (n=8-10 per time-point) of the P1 infarcted heart (asterix marks the infarct) with numbered boxes indicating zoomed in regions in remote zones (RZ) 1) right ventricle; 2) dorsal left ventricle and 3) injury zone (IZ). (B) As in A, except of a P7 infarcted heart. White arrows indicate regions of β-gal$^+$ signal. Viable muscle is labelled in red by troponin I (TnI) and nuclei are labelled with Topro nuclear stain (blue). (C) Histogram shows the percentage of β-gal$^+$ nuclei relative to the total nuclei calculated by counts of β-gal$^+$ cells over multiple sections from hearts shown in A and B. (D) Histogram shows the percentage of the total β-gal$^+$ cells within the infarct zone (IZ) or remote zones (RZ) in P1 and P7 hearts. Scale = 100µm.

To gain mechanistic insight into the modes of RA signalling in the respective injury settings, RA signalling components were assessed by qRT-PCR four days post-MI (Fig 5.14), as before (section 5.2.2 and 5.2.3). Expression levels of RA and retinoid X receptors α and β (*Rarα; Rarβ; Rxrα; Rxrβ)* were assessed, as were levels of the degrading enzyme *Cyp26b1* and the sequestering and/or nuclear transport protein, *Crabp2.* Surprisingly (given the robust LacZ reporter expression), relative to uninjured controls (intact P5 and P11 ventricles) the overall trend was decreased receptor expression post-MI at both P1 and P7 (Fig. 5.14A-D). *Rarα* expression was significantly reduced following MI at P1 (**p<0.01). In contrast, on D4 following P7 MI, there was no change in *Rarα* expression compared to control (P11) levels (Fig. 5.14A). *Rarβ* was significantly decreased following injury at both P1 (*p<0.05) and P7 (**p<0.01) compared to time-matched controls (Fig.5.14B). *Rxrα* and *rxrβ* levels followed the same pattern, with a significant reduction in *rxr*α on D4 post-P1 MI but not P7 MI (Fig.5.14C) and a significant reduction *Rxrβ* transcripts in both injury settings relative to controls in injured P1 (**p<0.01) and P7 (****p<0.0001) hearts (Fig. 5.14D). This overall decrease in receptor expression was surprising given the robust RA signalling observed in both injury groups by X-gal detection of RARE-LacZ reporter expression post-MI (Fig. 5. 11, 12) and increased Raldh2 protein detection within the infarct at this time-point (Fig. 5.8I). One explanation is that the levels of these widely expressed receptors were decreased due to the mass loss of myocardial cells that express them. *Cyp26b1* levels also demonstrated decreased expression in P1 hearts post-MI relative to controls (*p<0.05) with no change following injury at P7, or overall between P1 and P7 injury response (Fig 5.14E). *Crabp2* expression was almost five times control levels in P7 hearts post-MI (*p<0.05). It is possible that this reflects increased nuclear RA transport given the robust reporter expression in injured hearts of RARE-LacZ mice.

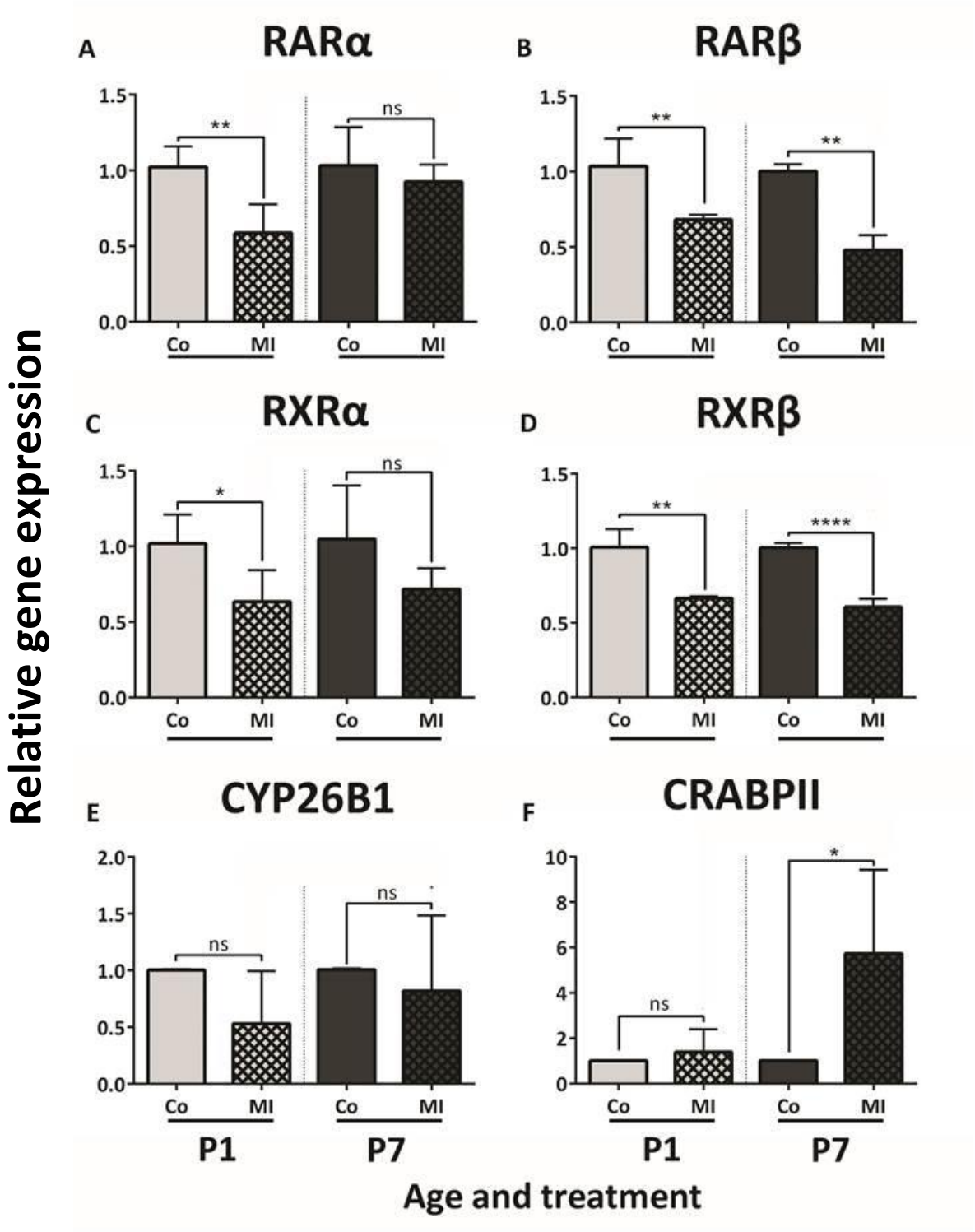


**Figure 5. 14. Expression of retinoic acid signalling pathway components post-MI at P1 or P7:** expression of retinoic acid (RA) receptor genes *rarα, rarβ;* retinoid X receptors *rxrα, rxrβ;* the RA metabolising gene, *cyp26b1 and* cellular retinoic acid binding protein II, *crabp2* were compared in hearts of neonatal mice following myocardial infarction (MI) injury sustained at postnatal day (P) 1 or P7 by qRT-PCR (n=6 hearts per group), relative to time-matched, intact control (Co) hearts (P5 and P11, n=4 hearts per group). Statistical analyses were performed to assess expression levels between control and injury groups (*p<0.05, **p<0.01, ****p<0.0001) using a student's un-paired t-test.

### 5.2.5. RA responsive cell-types in P1 and P7 hearts post-MI

To assess RA responsive cell types following injury in P1 and P7 hearts at the same time-point, immunodetection of the β-gal reporter was performed in long axis sections of RARE-LacZ hearts on D4 post-MI at P1 or P7; compared to time-matched 'sham' controls (intact hearts of P5 and P11 mice, respectively) (Fig. 5.15). Baseline β-gal expression in intact P5 and P11 hearts was detected in interstitial myocardial cells but only sparsely in the epicardium (Fig 5.15A). Following injury in P1 hearts, β-gal expression was expressed in α-SMA$^+$ vascular cells (Fig. 5.15B). Raldh2 expression was detected in serial sections (due to antibody incompatibility limiting co-localisation experiments) and was expressed within the infarct core, surrounding β-gal$^+$/αSMA$^+$ vascular cells, but not within vessels themselves. Raldh2 was also expressed in an interstitial pattern in sub-endocardial and sub-epicardial myocardium, as well as in the epicardium. Serial section staining of Wt1 also demonstrated epicardial expression in contiguous regions as β-gal and Raldh2. In P7 hearts four days post-MI, some β-gal expression was observed in αSMA$^+$ vascular cells within the infarct, but to a lesser extent than time-matched P1 infarcts (Fig.5.15C, D). Serial section staining of Raldh2 demonstrated a similar epicardial and sub-epicardial expression pattern with less pronounced Raldh2 expression in the TnI$^-$ infarct core, in the vicinity of β-gal$^+$/αSMA$^+$ vessels. Wt1 expression in serial sections was also detected in the epicardium (Fig. 5.15C). Of note, no reporter expression was detected in TnI$^+$ cardiomyocytes in the hearts assessed in these experiments.

To assess the total number of RA responsive αSMA$^+$ vessels in respective injury settings, αSMA$^+$ vessels, as clearly demarcated by vessel-like and lumen morphology, that contained β-gal$^+$ cells were counted over multiple short axis sections (n≥3) in hearts injured on P1 or P7 at D4 relative to total αSMA$^+$ vessel counts (Fig. 5.15). In hearts injured on P1, β-gal$^+$ cells were detected in 26% of αSMA$^+$ vessels; compared to 11% in hearts operated on at P7 ($p<0.05$, student's un-paired t-test).

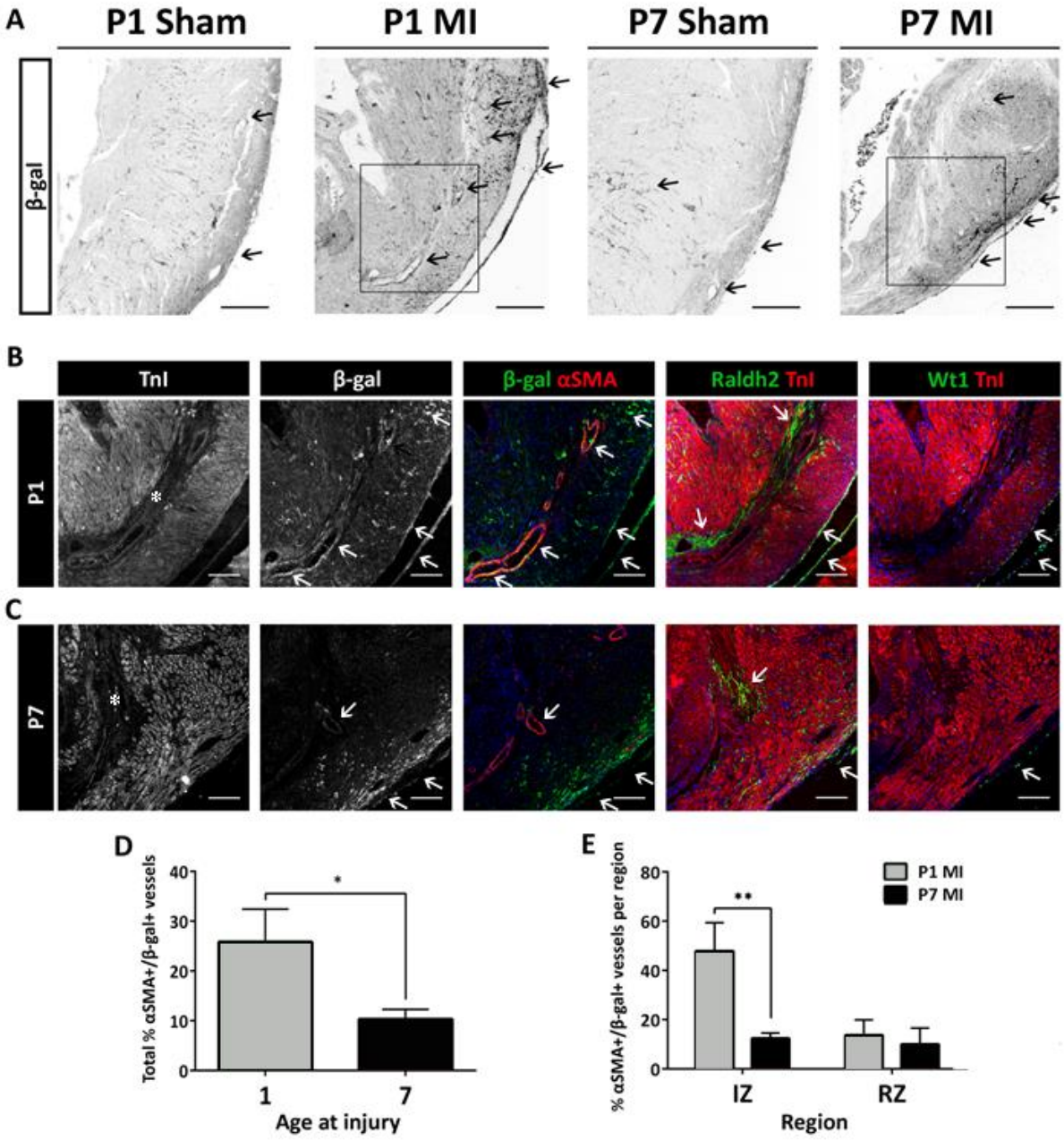


**Figure 5. 15. Retinoic acid responsive populations in P1 and P7 hearts:**
(A) Inverted grey-scale images of β-galactosidase (β-gal$^+$) staining (black arrows) in long axis sections of sham or myocardial infarction (MI) injured RARE-LacZ hearts 4 days post-injury at postnatal day (P) 1 or P7 Scale = 100µm. Boxes indicate zoomed regions in B and C. B) Serial section staining of P1 RARE-LacZ hearts and (C) P7 injured hearts with greyscale troponin I (TnI), β-gal, triple staining of β-gal + αSMA; Raldh2 + TnI; and Wt1 +TnI, all with Topro nuclear stain (blue). White arrows indicate colocalisation/similar regions of staining with β-gal$^+$ regions. Scale = 50µm. * indicates infarct core. Note β-gal$^+$ staining in αSMA$^+$ vessels in the infarcts of P1 injured mice coupled to robust Raldh2 expression within the infarct on serial sections; observed to a lesser extent in P7 hearts post-MI. Representative sections of n=3 hearts at P1, n=2 hearts at P7 (D) Histogram represents the percentage of αSMA$^+$ vessels in P1 and P7 hearts that also express β-gal calculated from short axis sections (not shown) (E) Histogram depicts the average percentage of the αSMA$^+$/ β-gal$^+$ vessels within the infarct zone (IZ) and remote zones (RZ) *p<0.05;**p<0.01, student's unpaired t-test.

Further, the percentage of β-gal$^+$/αSMA$^+$ vessels within the injury zone (i.e. TnI$^-$ myocardium and adjacent epicardial/endocardial borders) was significantly higher D4 post-P1 MI than P7 MI (48% compared to 13%: **p<0.01, student's unpaired t-test). These data imply heightened RA signalling in vascular cells in P1 hearts following MI. As RA signalling in VSMCs is associated with restriction of the mesenchymal lineage to permit late coronary remodelling, this may reflect heightened plasticity in the coronary vasculature of P1 hearts, which may influence their regenerative potential.

αSMA is also a marker of activated myofibroblasts (Roy et al., 2001) which were observed in and around the infarct (fig. 5.16). β-gal expression did not co-localise with non-vessel associated αSMA$^+$ signal in P1 or P7 hearts, although both aSMA and β-gal demonstrated a similar expression pattern to vimentin in serial sections. Vimentin is a commonly used marker of activated myofibroblasts and mesenchymal cells. This similar expression pattern is, therefore, suggestive of a mesenchymal profile in both populations. Fibronectin, which is an extracellular matrix (ECM) glycoprotein that binds integrins and collagen, and vimentin were also expressed in a similar pattern to β-gal within α-SMA$^+$ vessels (Fig. 5.17). Fibronectin and vimentin are associated with endothelial cell proliferation and angiogenesis under ischemic conditions (Glaser-Gabay et al., 2011). Further, RA signalling in VSMCs was shown to enhance fibronectin adhesion and facilitate coronary vessel remodelling *in vitro* and *in vivo* (Medhora, 2000) further supporting a role for RA signalling in enhancing angiogenesis post-MI.

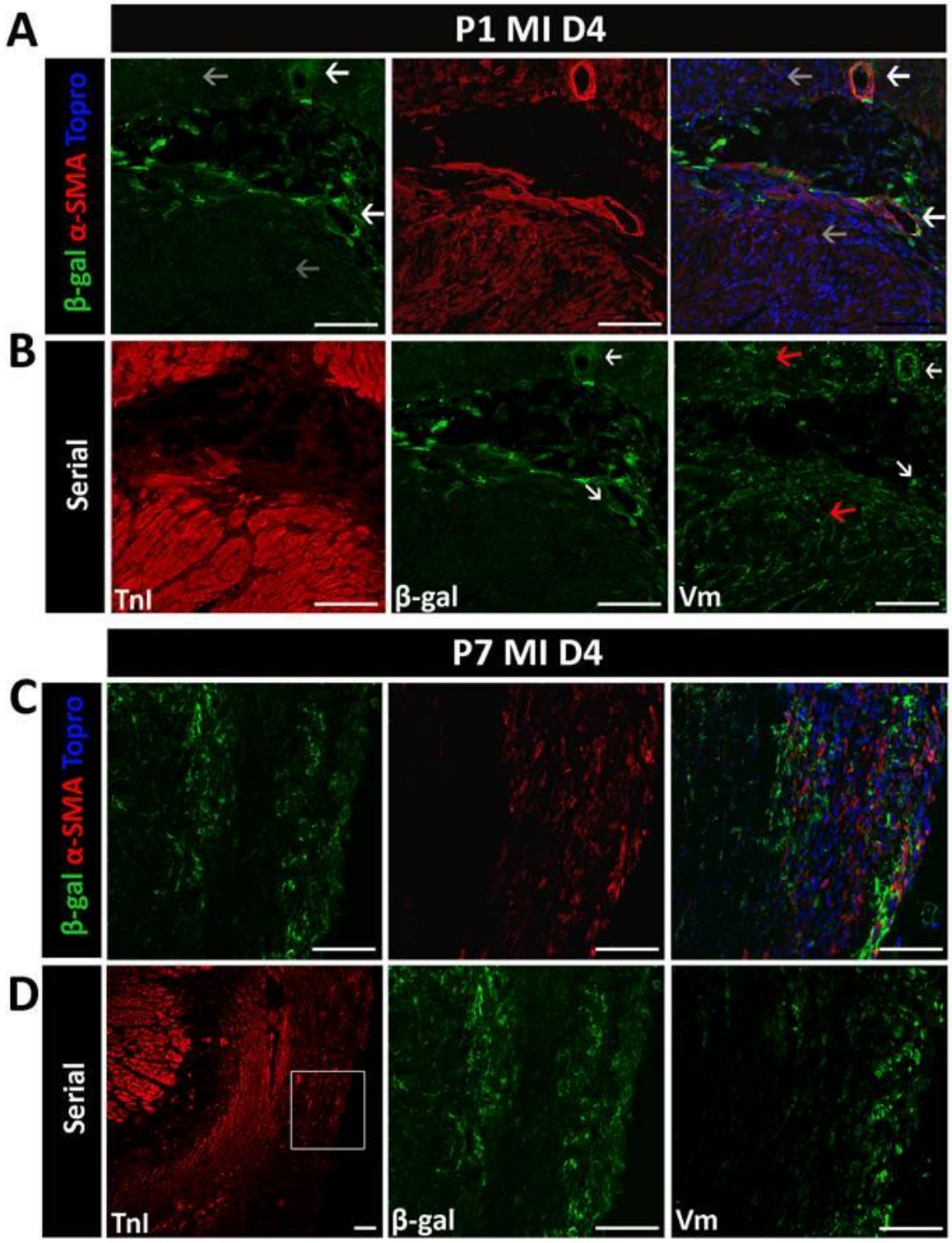


**Figure 5. 16. RARE-LacZ reporter does not co-localise with aSMA outside of vessels:** Immunoprofiling of β-gal$^{+}$ cells in P1 hearts 4 days post-MI (A and B) and in time-matched P7 infarcts (C and D) (sections representative of n=3 per group). (A) Co-staining of β-gal and α-SMA. White arrows indicate regions of co-expression (i.e. in vessel structures) and grey arrows indicate regions where colocalisation was not observed. (B) Serial section staining of β-gal and vimentin (Vm). White arrows indicate regions of overlap with β-gal and red arrows: α-SMA. Note extra-vessel expression of αSMA in P1 hearts also appears to be in the same regions as TnI in P1 hearts post-MI. (C) as in A for P7 injured heart (area indicated in boxed region in D). (D) As in B for P7 injured heart. Boxed region of TnI staining indicates zoomed in images of β-gal and vimentin in C and D. Scale = 50μm.

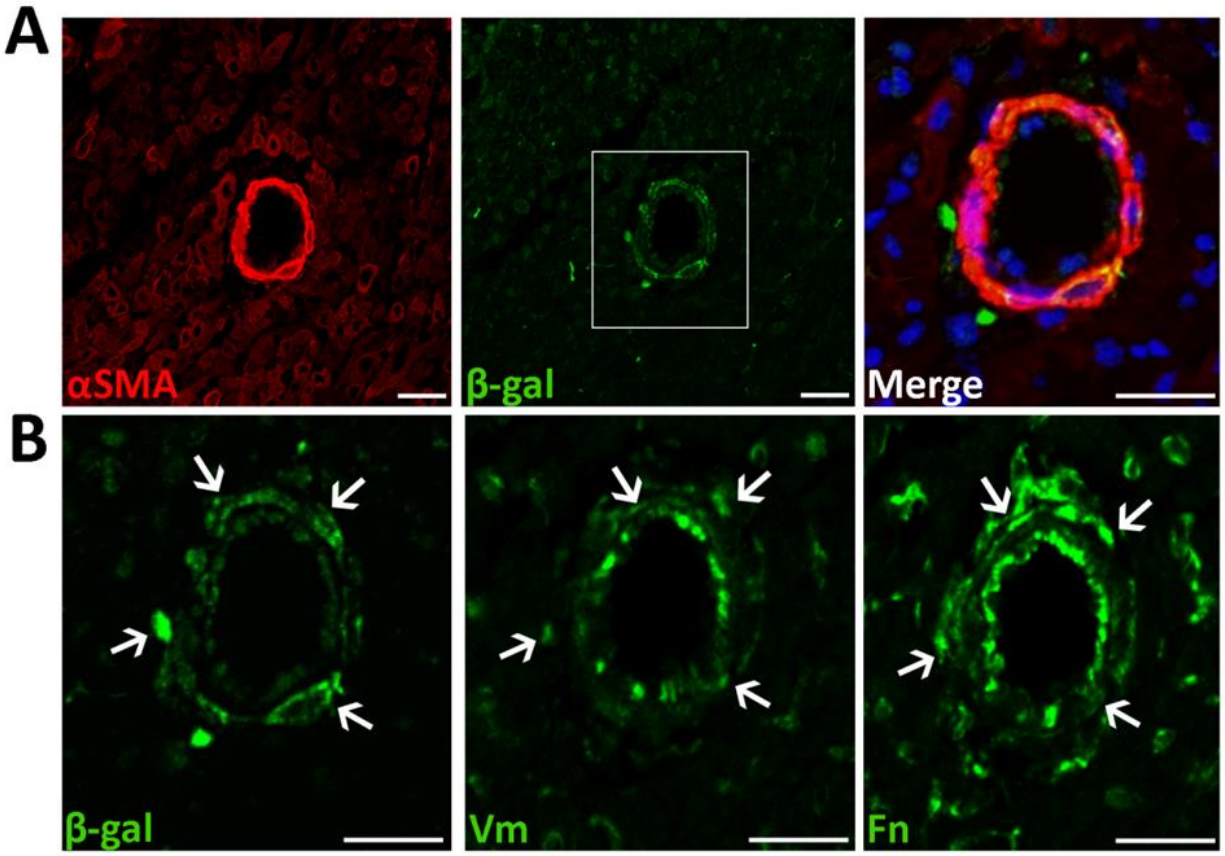


**Figure 5. 17. RARE-LacZ expression is associated with aSMA and ECM in coronary vessels following MI in P1 hearts:**

Representative image of an $\alpha SMA^{+}/\beta\text{-gal}^{+}$ vessel 4 days post-MI at P1 (n=3 hearts analysed). (A) colocalisation of β-gal with αSMA. Boxed region shows region of zoomed merged image on right with nuclear Topro staining. (B) Serial section staining of β-gal with vimentin (Vm) and fibronectin (Fn). Arrows indicate regions of potential overlap Scale = 25µm.

## 5.3. Discussion

This chapter set out to address the hypotheses: 1) epicardial potential is lost coincident with the loss of regenerative potential in neonatal mice, and 2) the loss of epicardial potential in neonatal hearts limits their capacity for regeneration.

### 5.3.1. Epicardial potential is lost coincident with the loss of regenerative potential

The expression of canonical epicardial genes were observed to decrease to adult levels by P7 (Fig 5.2), which correlated with a marked decrease in expression of the epicardial proteins Wt1 and Raldh2 (Fig.5.3). This was also associated with decreased epicardial RA signalling as detected by X-gal enzymatic staining of whole hearts of RARE-LacZ mice (Fig 5.4); which was further associated with decreased RA receptor expression and increased transcription of RA degrading and sequestering proteins (Fig 5.5). At P1, RA responsive cells, identified by immunodetection of β-gal in sections of RARE-LacZ$^{+}$ mice included epicardial cells, vascular cells and cardiomyocytes (Fig 5.6). In P7 hearts, β-gal expression was largely sub-epicardial and co-localised with αSMA$^{+}$ signal in VSMCs to a lesser extent, but not with TnI staining of myocytes (Fig 5.7). These experiments provide novel *in vivo* evidence of the epicardial transition from a progenitor source of cells and signals to a dormant epithelium in the first postnatal week in mice; coincident with their loss of regenerative potential.

### 5.3.2. Differential epicardial profiles in P1 and P7 hearts post-MI

Characterisation of the epicardial response to injury was compared when the 'regenerative window' was 'open' (in P1 hearts) and 'closed' (in P7 hearts) to investigate whether increased transcriptional activity and RA signalling in P1 hearts may contribute to their increased capacity for regeneration. In these experiments a differential epicardial profile was pronounced by immunohistochemistry four days post-MI (D4) (Fig. 5.8) at which point, injured P1 hearts demonstrated modest Wt1 expression; whilst injured P7 hearts demonstrated epicardial expansion with robust Wt1 expression. Conversely, serial section staining with

Raldh2 demonstrated robust expression within the underlying myocardium and infarct following MI at P1; whilst in P7 injured hearts, Raldh2 expression appeared more restricted to the epicardium and subepicardial regions. Serial section staining of Raldh2 and the fibroblast marker DDR2 demonstrated that Raldh2 expression in the infarct was similar to DDR2, which is a marker of fibroblasts (Fig. 5.9), which are the predominant RA responsive population in adult hearts post-MI (Bilbija et al., 2012). RA treatment of fibroblasts in culture prevented their proliferation (Bilbija et al., 2012), thus the robust expression of the Raldh2 in the infarcts of P1 mice may restrict fibrosis and scar formation.

qRT-PCR assessment of epicardial gene expression on D4 post-MI at P1 demonstrated a significantly different response to injury in P1 and P7 hearts, with reduced expression of *Wt1*, *Tbx18* and *tcf21* relative to intact P5 controls (Fig 5.10). In contrast, expression levels of these genes were upregulated in hearts that sustained MI on P7, similar to the response of adult hearts post-MI; in which the injury response is scarring and fibrosis. Contrary to the robust expression at the protein level 4 days post-P1 MI, *raldh2* expression also seemed to decrease relative to levels of intact time-matched controls ($p=0.053$). This was surprising given the robust expression of Raldh2 within the infarct at this time-point, but may reflect mRNA instability, delayed translation or a compensatory mechanism to restore RA to physiological levels: although a caveat of this explanation is that no increase in the RA metabolising gene *cyp26b1* was observed. *Crabp2* was differentially altered between injury groups and was upregulated D4 post-P7 MI (Fig 5.14F) and may reflect increased nuclear transport of RA to facilitate RA inducible gene expression, which was evident by assessment of reporter expression in RARE-LacZ mice. No alteration in *raldh2* expression was detected at the messenger level D4 post-P7 MI, which is equally surprising given epicardial Raldh2 expression by immunodetection. Investigation of RA signalling post-MI utilising the RARE-LacZ reporter, however, demonstrated the sensitivity of RA signalling to variable extents of injury (Fig 5.12), which may have confounded detection of appreciable alterations to *raldh2* expression.

Together, these experiments suggest that the epicardial profile in P1 hearts post-MI is atypical to the standard response of mammalian hearts to injury. P1 MI was not associated with upregulation of epicardial genes (Fig 5.10); which is typical of adult mouse hearts, and was observed in P7 hearts on D4 post-MI (Fig. 5.10). This may reflect higher baseline epicardial gene expression in P1 hearts compared to P7 hearts under physiological conditions, which may convey a heightened state of activation at baseline that translates to increased regenerative potential, and alleviates the need for further transcriptional epicardial activation following MI. Increased *Wt1* following P7 MI may still be sub-threshold to achieve any potential regenerative effect. However, *Wt1* levels in P1 infarcts were significantly decreased, relative to time-matched, uninjured controls, which suggest that higher basal *Wt1* levels are not necessarily permissive to regeneration.

Upregulation of epicardial genes in adult hearts post-MI is associated with fibrosis and scar formation (Ruiz-Villalba et al., 2015); which is also the repair route of P7 hearts (Section 4.7.2). This differential response to injury in P1 hearts may, therefore, be associated with reduced fibrosis and scar formation post-MI. Indeed, expression of *Fsp-1, Col3a1 and Fn1* were significantly upregulated D4 post-MI in P7 hearts, but not in time-matched P1 infarcts (Fig 5.11), suggesting that fibrosis was restricted in P1 hearts. A significant upregulation of *Fsp-1* was observed in P1 hearts relative to intact controls, however, which would be consistent with DDR2 expressing fibroblasts as a source of Raldh2 in the infarct; and may reflect a distinct fibroblast phenotype in P1 hearts, and one that is not fibrotic. Further work, including isolation and further molecular profiling of fibroblast populations from these respective settings will be necessary to assess this further.

Previous work in our lab also indicated that whilst $Wt1^{+}$ EPDCs activated in the adult heart post-injury may have similar expressional profiles to their embryonic counterparts, their phenotypes and functional roles may be different (Bollini et al., 2014). Given the loss of Wt1

expression within the first post-natal week, it is possible that the phenotypic change of $Wt1^+$ cells occurs in the same time-frame. However, these experiments assessed only one time-point post-MI and further expression analyses at other time-points will be necessary to assess whether or not reduced epicardial gene expression in infarcted P1 hearts at D4 has any appreciable effect on regeneration.

Differential RA signalling profiles were also detected in P1 and P7 hearts post-MI. In hearts of RARE-LacZ mice injured at P1, reporter expression was observed in the infarcted region and diffusely in remote myocardial regions (Fig 5 12, 13). Following P7 injury, X-gal reactivity was detected almost exclusively within the infarct zone, in an injury dependent manner. RARE-driven reporter activity was associated with fibrosis and remodelling in the adult heart, with the main RA responsive population identified as fibroblasts (Bilbija et al., 2012). X-gal reactive populations in P1 hearts may, therefore, reflect differential populations to those active in P7 and adult hearts post-injury and may be related to their heightened regenerative potential. Consequently, we aimed to isolate $LacZ^+$ cells from hearts infarcted at P1 or P7 by FACS-gal analysis in order to perform quantification and molecular profiling of respective cell types. Unfortunately attempts to establish this protocol were unsuccessful (Appendix III). Consequently, immunoprofiling of $\beta\text{-gal}^+$ cells was performed in P1 and P7 hearts at D4 post-MI. In my hands, β-gal immunostaining was only successful with one antibody, which was raised in rabbit and only on paraffin embedded, 4% PFA-fixed sections; with high-temperature, low-pH, citrate-based antigen retrieval and tyramide signal amplification. Consequently, colocalisation studies were confounded by most antibodies being raised in the same species and limited reactivity of certain markers in experiments optimised for β-gal detection. However, staining of serial sections demonstrated β-gal expression in the epicardium and in EPDCS, in a similar pattern to Raldh2 and Wt1 (Fig 5.15). B-gal was also found to co-localise with α-SMA expression in coronary vessels in hearts injured on both P1 and P7 on D4; with significantly more $\alpha SMA^+/\beta\text{-gal}^+$ cells detected in vessels of P1 hearts post-MI (Fig. 5.15). RA

signalling in VSMCs is implicated in maintaining plasticity of the coronary endothelial plexus to permit vascular remodelling (Azambuja et al., 2010). $\alpha SMA^{+}/\beta\text{-}gal^{+}$ vessels also expressed vimentin and fibronectin in a similar expression pattern to β-gal over serial sections (Fig 5.16); which are also both associated with endothelial cell proliferation and angiogenesis during vascular remodelling (Clark et al., 1982, Glaser-Gabay et al., 2011). Given the importance of revascularisation for the regenerative process, heightened coronary plasticity, possibly mediated by RA signalling may be a significant factor for the regenerative capacity of P1 hearts.

**5.4. Conclusions**

By employing a series of molecular and histological techniques to assess the epicardium and epicardial RA signalling in intact hearts, a consistent decrease in epicardial potential was reported by P7, coincident with the 'closing' of the 'regenerative window' in neonatal mice. This was taken to confirm our first hypothesis: that epicardial potential is lost coincident with the loss of regenerative potential in neonatal mice. Following injury, P1 hearts demonstrated subtle differences in epicardial response at the protein, messenger and RA signalling level, compared to non-regenerative P7 hearts. Reduced expression of epicardial genes in P1 hearts 4 days post-MI suggested that epicardial potential was sufficiently active at baseline in these hearts to be instructive towards regeneration, or that the reactive epicardium of the P1 heart is not instructive towards regeneration at all: although further experiments will be necessary to substantiate either assertion. Assessment of RA signalling in neonatal hearts identified a potential heightened RA response of coronary vessels following MI at P1, which may facilitate angiogenesis and vascular remodelling in these hearts. Again, more comprehensive temporal profiling and loss/gain of function studies will be necessary to validate this observation, but this could be a significant contributory factor for the regenerative capacity of neonatal mice. Also, this data suggests a distinct phenotype of fibroblast populations in P1 hearts that may

behave differently to those of P7 hearts, in which scarring and fibrosis is observed; although, again, further experiments will be required to investigate this, including isolation and profiling of respective fibroblast populations from respective injury settings. Thus, whilst we have not proven or disproven hypothesis 2; that the loss of epicardial potential in neonatal hearts limits their capacity for regeneration, interesting cellular profiles that may be significant for regeneration were described, which further our understanding of the mechanisms of mammalian heart regeneration.

# 6

# General discussion

This thesis set out to address four main aims:

1) Learn and establish the neonatal coronary artery ligation model in Oxford
2) Validate regeneration following coronary artery ligation in neonatal mice and characterise the regenerative process
3) Characterise the epicardium and RA signalling through the 'regenerative window'
4) Analyse the epicardium and RA signalling following injury at P1 and P7 in order to investigate the role(s) of the epicardium and RA in regenerative and reparative wound healing

These aims were established in order to address the hypothesis that epicardial potential and RA signalling may influence regeneration following MI in the neonatal mouse. The extent to which these aims were achieved and the implications of the work presented for both testing the initial hypothesis and its wider relevance and contributions to the field are now discussed.

**6.1. Refinement of neonatal coronary artery ligation surgery**

To address aim one and establish neonatal coronary artery ligation surgery in-house, significant changes were made to the original protocol developed by Sadek and colleagues (Mahmoud et al., 2014) according to UK requirements (as summarised in figure 6.1). Isoflurane and bupivacaine (Marcain, AstraZeneca, UK) anaesthetics, as well as aseptic methodologies were added into the established hypothermia anaesthetic protocol for inducing MI in neonatal mice, without extending the duration of the procedure; time taken for the animals to recover from the surgery, or procedural survival.

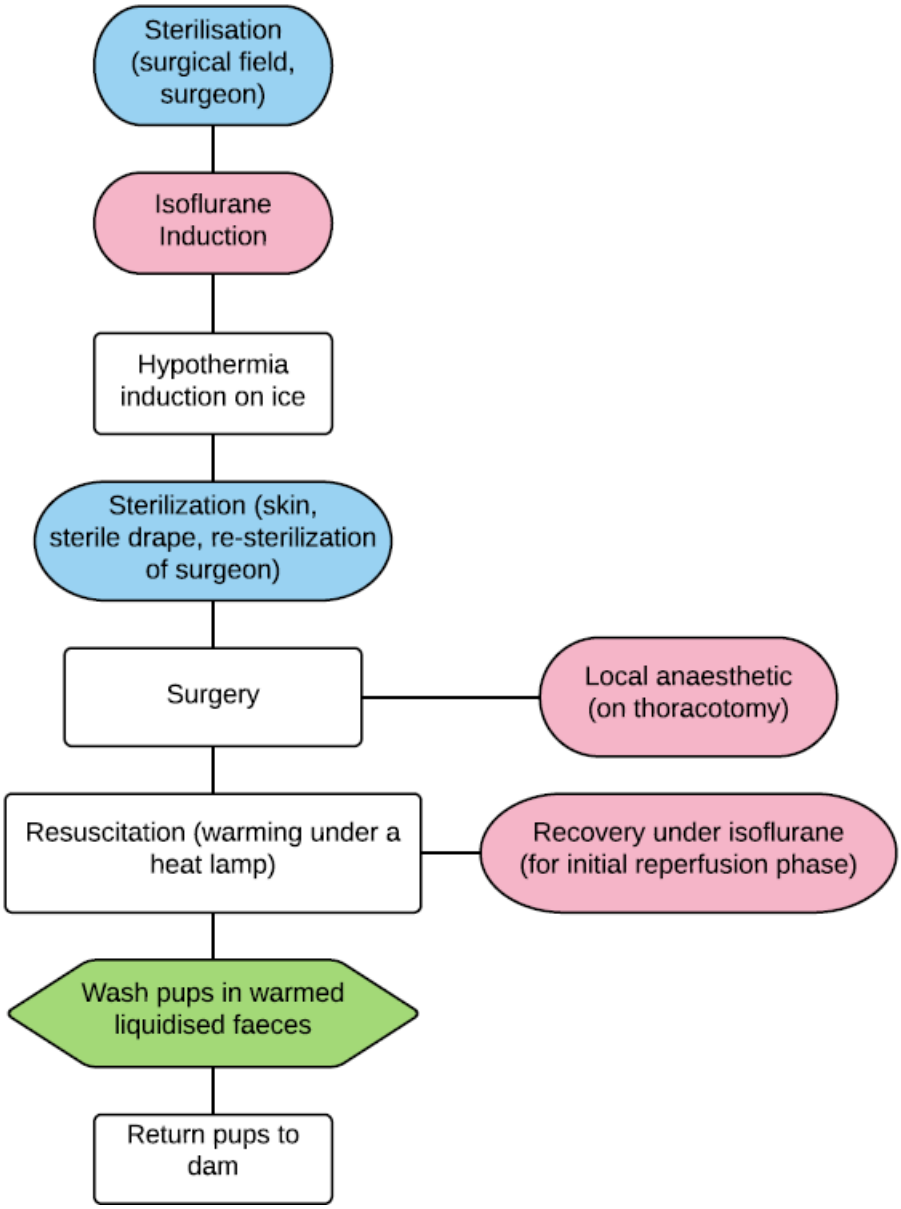


**Figure 6. 1. Schematic of refinements made to the surgical protocol:**
The steps of the surgical procedure for myocardial infarction surgery in neonatal mice are depicted by a flow chart. Original protocol steps are outlined in un-coloured boxes. Additional anaesthetic steps are indicated by rounded boxes with pink shading; additional aseptic steps are indicated in rounded boxes with blue shading. Other additional protocol steps are indicated by green hexagons.

These experiments and the resulting protocol amendments enabled the first implementation of neonatal coronary artery ligation surgery in the UK. This work was a pre-requisite for the progression of my project but, as an essential protocol refinement, may also serve as an example for future studies into the potential advantages of the combined use of hypothermia and anaesthetic agents in neonatal rodent procedures (Masters et al (*accepted pending revisions; Laboratory Animals*) and promote wider refinement of surgery in neonatal mice (Masters and Bergmann, *submitted to JAALAS*).

Although the incorporation of anaesthetics was required for licence amendment and our ability to implement the model in Oxford, we cannot rule out that the addition of multiple agents to the procedure altered the response of animals to injury. For instance, isoflurane has been shown to exert neuroprotective effects during hypoxia-ischemia and to cause neurodegeneration through prolonged exposure (Loepke et al., 2006) associated with DNA damage in multiple cell types (Kaymak et al., 2012). Isoflurane administration was also delivered in 100% oxygen, which may induce hypoxaemia, which was previously associated with reduced regenerative capacity in neonatal mice (Puente et al., 2014). One other group also described the incorporation of isoflurane induction prior to hypothermia in their surgical protocol. Following LAD ligation in P1 mice, however, this group did not observe regeneration (Konfino et al., 2015). This was suggested to be due to their use of isoflurane in oxygen (Sen and Sadek, 2015) which is in contrast to our findings: even following prolonged periods of isoflurane anaesthesia delivered in 100% oxygen to facilitate baseline heart measurements by MRI prior to induction of MI, we observed heightened myocardial regeneration with minimal anterior wall scarring by histology compared to time-matched infarcts of P7 mice (Fig. 4.11 and 4.12). License restrictions prevented the direct comparison of the original and amended protocol and potential effects on regeneration, although a comparative study to this end is warranted.

In addition, an important observation over the duration of the project was that, contrary to original protocol (Mahmoud et al., 2014) we did not observe specific targeting of maternal cannibalisation towards animals that underwent MI procedure compared to sham injured controls. Consequently, we were able to combine MI and sham treatments within litters to reduce both developmental variability and overall animal numbers used for experiments. Also, washing post-operative pups with liquidised warmed faeces prior to returning to the dam significantly reduced incidence of maternal cannibalisation/neglect. Previous attempts to ameliorate this involved handling of the dams and desensitisation with smells of the surgical procedure, as suggested by Sadek and colleagues (Mahmoud et al., 2014) which we found to be less effective and considerably more time-consuming.

### 6.2. Longitudinal assessment of heart injury and regeneration by MRI in neonatal mice

Given the reported differences of the extent of regeneration following various types of injury in neonatal mice, there was a clear need in the field for the improvement of methods to non-invasively assess cardiac anatomy and function through the course of the regenerative process. To this end, in collaboration with Prof. Schneider and colleagues, we established a protocol for MRI scanning of neonatal mice. In doing this, we were able to use MRI to non-invasively assess cardiac function in P1 mice for the first time. In addition, an optimised animal handling protocol was developed to scan individual neonatal mice repeatedly within the pre-weaning period. Further, we report the first successful combination of MRI with coronary artery ligation surgery in order to non-invasively characterise injury and regeneration in neonatal mice. Unfortunately, due to staff illness and absence, there have been significant delays in segmentation, reconstruction and analysis of the acquired MR data, which precluded the inclusion of this data in this thesis. Regardless, significant technical hurdles have been

overcome and the feasibility of using MRI to assess cardiac function in the 'regenerative window' was established.

Histological analysis showed that initial injuries were evident and reproducible following MI at P1 and P7. Following MI at P1, infarction injury was evident at D4 and D7 but by D21, myocardial thickness appeared restored with minimal collagen deposits were detected (Fig. 4.11 and 4.12). This was in contrast to hearts injured on P7, in which collagen deposition and significant remodelling were evident by D4 and at all time-points assessed thereafter (Fig. 4.14 and 4.15). During scans, localiser, or 'scout' images, that were acquired in order to orient scan angles, revealed abnormalities in MI hearts at D4, which were easily distinguishable from sham operated controls at this time-point (data unavailable). By D21, however, we were unable to distinguish injured and uninjured hearts from these images. Based on this and histological assessments, we concluded that P1 hearts have heightened regenerative capacity compared to P7 and adult hearts, and that evident regeneration (although incomplete), defined by relatively normal myocardial thickness in the region of infarction and the absence of significant anterior LV wall scarring, had occurred. The ongoing data analysis will provide conclusive evidence, either way, of the extent of initial injury and regeneration, both anatomically and functionally, in individual neonatal mice over time.

The application of MRI to assess cardiac regeneration in neonatal mice may assist other groups in reproducing the model. It will be critical for groups who are establishing this model to have robust and reliable methods of validation for initial injury and extent of regeneration over time in individual animals: particularly in the early phases of model establishment, and also during the assessment of experimental methods for extending the 'regenerative window'.

### 6.3. Epicardial potential in mammalian heart regeneration

Little is known about the epicardium in the postnatal mouse heart. Numerous changes to the biochemistry and cellular biology of the heart are described to occur within the first postnatal week, including: binucleation, polyploidy and terminal differentiation of cardiomyocytes (Soonpaa et al., 1996, Ikenishi et al., 2012); changes in the immunoprofile (Aurora et al., 2014); fibroblast density (Banerjee et al., 2007) and metabolism (Lopaschuk and Jaswal, 2010, Puente et al., 2014). The data presented in chapter 5.1 provides the first *in vivo* evidence of the epicardial transition from a progenitor source of cells and signals to a dormant epithelium between P1 and P7, identifying the epicardium as another cellular population that undergoes significant profile changes in the first postnatal week; coincident with the closing of the regenerative window. This lead to further experiments to investigate epicardial profiles post-MI at P1 or P7 to assess epicardial potential in mammalian heart regeneration, summarised in Table 6.1.

**Table 6. 1. Epicardial and retinoic acid signalling in intact and injured P1 and P7 hearts:**
+/- indicate more or less activation in respective settings. Arrows indicate where values differ from control (time-matched intact) levels. P, postnatal day; DPI, days -injury; RA, retinoic acid.

| | | | P1 | P7 | Possible explanations/implications: |
|---|---|---|---|---|---|
| **Intact** | Epicardium | mRNA | + | - | Heightened epicardial potential at P1 may enhance injury response? |
| | | Protein | + | - | |
| | RA signalling | mRNA (Receptors) | Relatively unchanged | | Heightened RA signalling at P1 (in the epicardium, cardiomyocytes and perivascular cells) related to higher expression of synthesising genes and low expression of metabolising and sequestering(?) genes; may enhance injury response? |
| | | (Sequestering) | - | + | |
| | | (Metabolising) | - | + | |
| | | LacZ reporter | + | - | |
| **4 DPI** | Epicardium | mRNA | ↓ | ↑ | Higher basal epicardial signalling at P1 may be sufficient for regeneration? Or epicardial signalling post-injury at P1 is not instructive towards regeneration? |
| | RA signalling | mRNA (Receptors) | ↓ | ↓ | Fewer receptors may reflect myocardial loss of ubiquitously expressed genes. Increased expression of genes associated with nuclear RA transport may enhance RA signalling post-MI at P7. |
| | | (Nuclear transport) | - | ↑ | |
| | | (Metabolising) | No change | | |
| | | Synthesizing enzyme | Different staining patterns | | RA signalling in different cell types/different responsive populations at P1 and P7 may alter the response to injury. Heightened RA signalling in perivascular cells at P1 may enhance vascular remodelling, the revascularisation process and thereby regeneration. |
| | | RARE-LacZ reporter | ↑ (Different staining patterns) | | |
| | | In vessels | + | - | |

### 6.3.1. Differential epicardial response in P1 and P7 hearts post-MI

#### 6.3.1.1. An atypical epicardial response to MI in P1 mouse hearts following injury

No previous studies have described the epicardial response to MI induced by LAD ligation in neonatal mice. Epicardial activation is the typical response of adult mouse hearts to injury, and is associated with scarring and fibrosis (Smart et al., 2011, Zhou and Pu, 2011, Zhou et al., 2011, Smart et al., 2012, Huang et al., 2012, van Wijk et al., 2012, Ruiz-Villalba et al., 2015). P7 hearts also adopt this default wound healing response. The regenerative outcome of P1 hearts, therefore, may be related to limited fibrosis. *FSP-1* was upregulated in both P1 and P7 hearts four days post-MI, suggesting activation of fibroblasts in hearts at both time-points, but upregulation of genes associated with collagen deposition (*ProCol3A1 and Fn1*) were upregulated exclusively in injured P7 hearts. Fibroblasts in injured P1 hearts may, therefore, be a distinct population, may have distinct roles, and non-fibrotic ones. Further, DDR2 labelled fibroblasts in the infarct of P1 hearts at D4 demonstrated a similar Raldh2 labelling pattern. RA treatment of fibroblasts *in vitro* inhibited their proliferation (Bilbija et al., 2012). As Raldh2 synthesises RA, it is possible that RA signalling in P1 infarcts *in vivo* also restricts fibrosis. Indeed, less Raldh2 immunoreactivity was detected in the infarct core of P7 hearts post-MI. During development, EPDCs are the main source of cardiac fibroblasts and their emergence during development coincides with cardiomyocyte proliferation and myocardial expansion (Ieda et al., 2009). Further, Ieda and colleagues observed a positive correlation between cardiomyocyte proliferation and fibroblast density in culture preparations; whilst adult cardiac fibroblast cultures stimulated myocyte hypertrophy but not proliferation (Ieda et al., 2009). This altered epicardial response at P1, therefore, may reflect a differential fibroblast profile which is more foetal-like and conducive to regeneration.

In adult hearts, epicardial derived signals were recently implicated in modulation of the immune response post-MI. Huang and colleagues analysed enhancer regions of epicardial genes activated both in development and in response to injury and identified exclusively

conserved CCAAT/enhancer binding protein (C/EBP) binding sites in Wt1 and Raldh2 promoter regions. Inhibition of epicardial C/EBP signalling resulted in significantly decreased fibrosis and improved contractile function after ischemia-reperfusion injury, associated with reduced neutrophil influx to the infarct zone (Huang et al., 2012). Thus injury-induced epicardial signalling, possibly via RA through expression of Raldh2, may act as a cue for immune cell infiltration and modulation of the immune/inflammatory response. Improved understanding of this potential interaction in regenerative and non-regenerative hearts could hold potential for modulating the balance between fibrotic and regenerative wound-healing in adult mammals post-MI.

#### 6.3.1.2. Enhanced angiogenesis in P1 hearts post-MI

Following LAD ligation, heightened RA signalling in αSMA positive vessels was observed in P1 hearts at D4 compared to time-matched infarcts of P7 hearts. This was particularly pronounced within the infarct region, in which robust Raldh2 expression was also detected. RA has been shown to restrict the mesenchymal lineage and inhibit muscularisation of developing vessels (Azambuja et al., 2010), thus increased RA signalling in vessels post-MI may aid in revascularising the compromised myocardium in these hearts. Neonatal heart regeneration was previously associated with a vascular response at D7 post LAD ligation (Porrello et al., 2013). Coronary corrosion casts demonstrated collateral vessel sprouting in lateral configurations distal to the occluded LAD, which did not anastomose with the ligated vessel until 21 days post-MI, suggestive of prolonged vascular remodelling post-MI.

Interestingly, the vascular response of P1 hearts following LAD ligation was perturbed in hearts depleted of macrophages (Aurora et al., 2014). Cardiomyocyte proliferation was not affected in these mice, but the regenerative response was impaired; highlighting that myocyte replenishment is one of a myriad of cellular events necessary for neonatal heart regeneration. At D7, macrophage gene expression profiles of infarcted P1 and P14 hearts were molecularly

distinct, with P1 macrophage transcriptomes demonstrating upregulation of pathways associated with angiogenesis, suggesting a differential immune response to MI at P1, which stimulated neovascularisation (Aurora et al., 2014). In line with this, injured neonatal mouse hearts were shown to contain a high number of embryonic-derived, tissue resident macrophages which, when cultured, secreted factors that stimulated endothelial cell tube formation *in vitro*; whereas culture medium from monocyte-derived infiltrating macrophages of injured adult hearts did not (Lavine et al., 2014). Also, abrogation of resident macrophages in neonates and monocyte-derived macrophages of adult hearts post-injury, impaired and ameliorated wound-healing in these respective settings. Interestingly, tissue resident macrophages of the mouse peritoneal cavity were recently shown to be recruited by RA which induced tissue-specific localisation and polarisation of macrophages via induction of GATA6 expression (Okabe and Medzhitov, 2014). It is possible, therefore, that RA within the infarct core of P1 hearts at D4 may recruit proangiogenic neonatal macrophages and impact regenerative wound healing. Thus, RA may have multiple pro-regenerative functions in the neonatal mouse heart. Further investigation of the interaction of RA and macrophages in neonatal heart regeneration is warranted.

### 6.4. Growth versus regeneration

When investigating factors which may influence the regenerative response of P1 hearts to MI, it is important to consider that the wound-healing in these hearts occurs on the substrate of physiological growth. Injury in this immature state, therefore, is closely related to the retained capacity for cell/tissue *generation,* which may become limited by P7 due to numerous cell, molecular and physiological changes that occur during the 'regenerative window', including the changes in epicardium and retinoic acid signalling described in this thesis. These factors undoubtedly play a combinatorial role in the restoration of lost tissue in injured P1 hearts, although perturbation to a single factor can shift the injury response towards adult-like scar

formation and fibrosis (Aurora et al., 2014, Mahmoud et al., 2013, Xin et al., 2013a). A key criticism of the model, therefore, is that, as the heart is still growing, injury resolution is not as much regeneration as an extension of physiological growth, and regeneration following injury in the setting of postnatal heart development, does not constitute 'true' regeneration. However, physiological growth continues postnatally long after the capacity to effectively restore lost myocardium is lost (by P7). Also, *de novo* myogenesis that occurs following ischemia and intra-myocardial collagen deposition, and the subsequent removal and/or resolution thereof, is not a part of normal development. Although heart growth and regeneration may share common characteristics, improved understanding of those that are specific to *de novo* myogenesis post-MI at P1; which are, furthermore, distinct from those of immature P7 hearts that undergo scarring and fibrosis after equivalent insults, provide a means of identifying aspects of mammalian myogenesis that are specific to regeneration. This is enhanced by demonstrations that application of factors that are important for regeneration in P1 hearts can extend regenerative capacity beyond the first week of life (Mahmoud et al., 2013, Porrello et al., 2013, Xin et al., 2013a). These studies demonstrated that manipulation of factors which influence cardiomyocyte cell-cycle arrest can be manipulated to improve myocardial regeneration following MI in adult mice; which reinforces the possibility that application of developmental myogenic cues, such as those from the epicardium, could also hold potential for improving heart regeneration in adult mammals, including humans.

## 6.5. Conclusions

To conclude, in relation to the initial project aims, this thesis describes:

1. Adaptation and refinement of neonatal coronary artery ligation surgery in-line with UK standards and legislation.

2. Histological evidence of appreciable heart regeneration in neonatal mice following LAD ligation at P1 and the establishment of a protocol to perform longitudinal MRI assessment of initial infarct and resolution over time.
3. Molecular profiling of the postnatal epicardium and epicardial RA signalling *in vivo* that implicates the loss of an embryonic epicardial profile with the 'closure' of the 'regenerative window'.
4. The description of a differential response of the epicardium and RA signalling following MI at P1 and P7, contributing a distinct profile of this dynamic cell population in regenerative wound healing in neonatal mice. In particular, a heightened RA responsive vascular phenotype was detected in P1 hearts post-MI, which may be related to increased plasticity of the coronary network and, thereby, regenerative capacity. Also, a differential fibroblast profile was indicated, which may limit the fibrotic response and promote regenerative mechanisms in P1 hearts post-MI.

### 6.6. Future work

Moving on from the studies presented in this thesis, there are a number of key areas for future work:

1) Validation of MRI as a means to detect and accurately quantify infarcts and cardiac function in neonatal mice and further characterisation of the model.
2) Further molecular profiling of the epicardium and RA responsive populations in P1 and P7 mice under physiological conditions and in response to MI; as well as their relation to immune signalling.
3) Test whether manipulation of RA in neonatal mice alters their regenerative response.
4) Investigate differential fibroblast populations in P1 and P7 hearts and their regenerative potential.

#### 6.6.1. Validation of MRI as a means to detect and quantify infarcts and cardiac function in neonatal mice

##### 6.6.1.1. The limits of neonatal heart regeneration

The ongoing analysis of longitudinal MRI scans in neonatal mice will provide invaluable contributions to the ongoing debate of whether or not neonatal mice regenerate their hearts post-MI. The histological analysis presented in chapter 4 provides evidence to support heightened regenerative capacity of P1 hearts compared to their P7 counterparts, but without confirmation of initial and equivalent injuries, limited conclusions can be drawn. This method should provide sufficient resolution to discern initial infarct size, which has been identified as a limiting factor for regeneration, and relate it to the extent and time-course of restoration of tissue and functional recovery. This sound evidence should be sufficient to settle this ongoing debate.

#### 6.6.1.2. Optimisation of infarct detection and quantification by MRI

As discussed, LGE MRI may be a more reliable way to measure infarction injury than wall motion measurements. Initial attempts to establish a protocol for LGE MRI in neonatal mice in this thesis were inconclusive but, by no means, extensive. Further attempts to optimise this protocol and compare it to infarct measurements by cine MRI are warranted. Optimum administration timings would need to be established, as was attempted, and the delivery system should be validated.

#### 6.6.1.2. Increased consistency of samples

Injury variability is a significant caveat of neonatal and adult LAD ligation models. The LAD is a forked vessel that is difficult to visualise in the myocardium and thus suture placement and injury size can vary considerably between samples. Consequently, the injury response can vary considerably between samples, as was evidenced in this thesis. MRI assessment of infarct size in treatment groups, for example, could be employed to non-invasively assess consistency of infarct size without requiring standard tissue destruction methods, which would considerably decrease the number of animals required for experiments.

#### 6.6.1.3. The regenerative window: narrow or wide?

This tool could also be employed to provide better characterisation of the 'regenerative window', which is poorly defined. Whether or not hearts injured at P3-P6, for instance, can regenerate is not known. Given the numerous changes that occur at the cellular, molecular and physiological levels in the hearts of mice in the middle of the first postnatal week, (including binucleation, polyploidy and terminal differentiation (Soonpaa et al., 1996, Ikenishi et al., 2012); changes in the immunoprofile (Aurora et al., 2014); fibroblast density (Banerjee et al., 2007), as well as the epicardial changes described herein), improved characterisation of the response of these hearts to injury could provide new clues for the key mechanisms of heart regeneration in neonatal mice.

### 6.6.2. Further molecular profiling of RA responsive populations in P1 and P7 mice under physiological conditions and in response to MI

#### 6.6.2.1. Expand post-MI time-course

In the present study, time-course analyses of P1 and P7 hearts post-MI by immunostaining of Wt1 and Raldh2 identified an intriguing differential epicardial response of P1 and P7 hearts to injury at D4. Consequently, initial gene expression and RA signalling analyses focussed on this time-point. Further temporal gene expressional profiling, and investigations of the RA signalling response to injury, would clarify whether or not the observed differences between P1 and P7 hearts at D4 is sustained and/or of functional consequence. Thus, a full time-course series of relative gene expression levels spanning key time-points (D1 D4, D7, D14, D21) through the process of regeneration (as tracked by MRI) would be performed; which would further form a basis for assessment of alterations to the epicardial/RA response in downstream loss/gain-of-function studies. Group sizes should be increased to n=6 per group to account for injury variability, which should also be minimised by determination of initial infarct size by MRI.

#### 6.6.2.2. Alternate isolation and quantification methods

A key issue confounding identification of β-gal$^{+}$ RA responsive cells in this project was that we were unable to optimise FACS-gal analysis and isolation. This would have enabled both quantification and molecular profiling of these populations, which would have enabled quantification and resolution of potentially distinct RA responsive profiles in respective injury settings; which may be relevant for regeneration vs fibrosis post-MI in these respective settings. Further, immunodetection and colocalisation studies were limited by antibodies being raised in the same species and variable reactivity in a staining protocol optimised for β-gal detection (IHC-P). FACS-gal isolation of LacZ$^{+}$ cells has been described as problematic, mainly due to variable and inefficient substrate uptake and retention, and has been phased-

out in many labs in favour of alternate, typically fluorescent, reporter systems. A fluorescent RARE reporter mouse-line is not, to the best of my knowledge, currently commercially available.

Although historically, the generation of genetic modifications in mice has been complex and time-consuming, the development of CRISPR (clustered regularly interspaced short palindromic repeat)- Cas (CRISPR-associated) protein technology offers an accelerated method for accurate and relatively cheap genome editing (Yang et al., 2013). CRISPR-Cas technology mimics mechanisms of the RNA-based adaptive immune system of bacteria and archaea, in which Cas9 proteins induce double stranded breaks in DNA at sites determined via simple base pair complementarity. By modifying the guide strand that directs Cas9 genome editing, it is possible to direct Cas9 mediated introduction of double-strand breaks into to any genomic locus in genomic DNA of any species. It is further possible to introduce templates into this locus which encode a reporter or mutation, in a single step process, with high efficiency. This technology has now been used for genome editing in numerous species for which embryonic stem cells are not available (Baltimore et al., 2015), and was used in mice to insert fluorescent reporter tags into numerous endogenous genes (Yang et al., 2013). This technology could be used to generate animals with the fluorescent tag in the place of the LacZ reporter downstream of RARE sequences and facilitate the experiments I was unable to perform.

### 6.6.3. Improved spatial resolution and validation of expressional analyses

Experiments in Chapter 5 identified variable distribution patterns of RA induced gene transcription in P1 and P7 hearts post-MI. Similarly, spatially distinct expression patterns are also reported in other cellular events in P1 hearts, including macrophage distribution (Aurora et al., 2014) and cardiomyocyte proliferation (Haubner et al., 2012, Porrello et al., 2013). Information about where a gene is upregulated or downregulated can provide valuable

insights into its function. A caveat of standard expressional analysis methods, such as qRT-PCR, RNA sequencing and FACS, is that they involve tissue destruction and thereby the loss of useful spatial information, which is then acquired in separate samples; usually by low-throughput, microscopy-based techniques such as *in situ* hybridisation. Expressional analyses that rely on tissue destruction also inevitably result in the loss of spatially restricted expression patterns that may be undetectable across a whole sample. Genome-wide Tomo-seq is a novel methodology by which 3D RNA sequencing can be performed to acquire expressional profiles across samples with high spatial resolution. This technique has been used to elegantly acquire a genome-wide 3D atlas of gene expression over multiple stages of zebrafish development (Junker et al., 2014). In order to obtain this spatially resolved information in regenerating P1 hearts, we have established collaboration with the pioneers of this methodology in Utrecht (of the Hubrecht Institute), who are currently performing Tomo-seq on hearts of mice that sustained MI on P1. Pilot data from this collaboration has identified three interesting gene clusters which may correspond to infarcted regions, border zones and remote myocardium; as well as multiple spatially dependent expression profiles of genes of interest, 7 days post-injury. Validation of this data by conventional *in situ* hybridisation is currently ongoing.

### 6.6.4. Manipulation of retinoic acid signalling in neonatal hearts post-MI

In chapter 5, we showed that Raldh2 expression was prominent within the infarct core of P1 hearts four days post-MI, and $\alpha SMA^+$ cells in vessels, particularly within the infarct region, appeared to have increased β-gal reactivity in RARE-$LacZ^+$ mice, indicative of increased responsiveness of this cell population to RA in these hearts. In P7 hearts post-MI, Raldh2 was detected mainly in the epicardium overlying the infarct, and fewer RA responsive VSMCs were detected in the infarcted and surrounding myocardium, possibly associated with reduced RA signalling in the infarct core. As described, RA signalling in VSMCs was previously shown to restrict VSMC differentiation, which was associated with enhanced plasticity of the coronary

endothelial plexus and enhanced vascular remodelling (Azambuja et al., 2010). High levels of RA within the infarct core and surrounding vessels may, therefore, facilitate revascularisation of P1 hearts post-MI. To investigate a permissive or instructive role of RA signalling in neonatal heart regeneration, RA levels could be manipulated in RARE-reporter (preferably fluorescent, see 6.2.2) neonatal mice by ectopic all-trans-RA (ATRA) administration or maternal supplementation of dietary vitamin A, to assess altered injury response in later stage (P7 neonates); possibly in combination with CYP45026B1 antagonists to prevent RA induced metabolism. To complement this, experiments to disrupt RA signalling *in vivo* could be employed in P1 neonates. This could be achieved by treatment with bischloroacetyldiamine (WIN,18446) which was recently shown to induce potent systemic acquired RA deficiency in mice by suppressing RA synthesis by Raldh2 (Paik et al., 2014). Appropriate administration routes as well as a dose response study would need to be established for both gain/loss of RA signalling studies in P1 mice. Subcutaneous and intra-peritoneal injections routes, as well as maternal supplementation via dietary administration at late stage gestation/postpartum, would be assessed. Under both conditions, altered baseline RA signalling would be assessed by quantitative FACS and *in situ* analyses of RA responsive populations. Further validation of decreased RA could be performed by ultra-performance liquid chromatography-tandem mass spectrometry (UHPLC-MS) to assess endogenous RA isomers and metabolites (Arnold et al., 2012). LAD ligation would then be performed on these animals and the regenerative responses assessed. Post-treatment, if viable, heart regeneration would be assessed by MRI and histology, compared to an appropriate vehicle treated control groups. Gross observations would be conducted in parallel to assess alterations to growth/physiology due to altered RA signalling. To assess a vascular effect of altered RA signalling on VSMCs and coronary remodelling, coronary casts would be performed in respective injury and treatment groups. Molecular profiling of immune cell types could be assessed in similar experiments by FACS and immunodetection to assess potential interactions between RA and the immune signalling.

### 6.6.5. Investigation of fibroblast profiles in P1 and P7 hearts post-MI

In hearts that sustained MI on P1 or P7, we observed significantly different gene expression profiles of canonical embryonic epicardial genes after four days, with apparent downregulation of genes post-MI at P1, compared to significant upregulation of epicardial genes post-MI at P7, relative to intact time-matched control levels. Higher baseline expression of epicardial genes at P1 may negate the need for upregulation following injury; although downregulation of these genes post-MI raised a question mark over whether enhanced epicardial response was instructive towards regeneration. In the same hearts, no upregulation of fibrosis-associated genes was observed, although upregulation of fibroblast-specific protein 1 (*fsp1)* was detected, suggestive of an activated fibroblast population in these hearts. Epicardial-derived cells (EPDCs) readily give rise to fibroblasts, which, during development, are associated with myocardial proliferation and compaction (Ieda et al., 2009), but in adulthood, are predominantly associated with ECM, collagen deposition and fibrosis (Ruiz-Villalba et al., 2015). To investigate a differential profile of fibroblast populations in P1 and P7 hearts post-MI, which may be instructive towards regeneration/fibrosis, isolation of the FSP-1 expressing population would be performed by FACS. RNA sequencing of respective fibroblast populations would provide an indication of their respective transcriptomes, and provide an indicator of function.

### 6.6.6. Application of epicardial signals to instruct heart regeneration in adult mammals

The data presented in chapter 5 describes subtle differences in epicardial profiles in P1 and P7 hearts post-MI; however, it is unclear based on this data, whether or not the epicardium has an instructive/permissive role in neonatal heart regeneration, and whether or not developmental epicardial signals could be applied to enhance regeneration in hearts beyond

the ‘regenerative window’. However, a recent study demonstrated that implantation of collagen patches that were soaked with conditioned media from epicardial mesothelial cell cultures (that were co-cultured with cardiomyocytes), over infarcts in adult mice, improved heart function by 2 weeks post-MI (Wei et al., 2015). This study showed that enhanced epicardial-myocardial signals can be applied to convey regenerative capacity in adult mammals. To investigate an instructive role of P1 epicardial cells following MI, similar experiments could be employed to generate conditioned media from P1 and P7 epicardial explants, which could be loaded into collagen patches and applied to adult hearts post-MI. The relative extents of remodelling/regeneration/functional recovery would provide an indication of whether or not the epicardium in P1 hearts is sufficient to convey heightened regenerative potential.

### 6.7. Final remarks

Mounting evidence in studies investigating the mechanisms of heart regeneration in newborn mice, including the data presented herein, highlights a distinct cellular, molecular and physiological profile of P1 hearts both at baseline and in response to injury. Thus, no pathway in isolation is likely to be sufficient for effective regeneration. The enhanced regeneration in adult mammals described by Wei and colleagues (2015) by application of epicardial signals, although significant, is still incomplete; likely due to the restricted ability of some cells of the adult heart, namely cardiomyocytes, to respond to myogenic cues in the injured adult heart. The prospect of extrapolating neonatal epicardial signals to exert regenerative effects in an adult mammals, therefore, will be multifaceted. Multiple systems and pathways would need to be targeted in combination, to simultaneously promote cardiomyocyte responsiveness, as well as to attenuate fibrosis and inflammation. The advent of gene therapy may make this feasible; although specific targeting of such treatments to prevent off-target carcinogenic effects would be a separate and significant challenge. The collagen matrix utilised by Wei and colleagues in mice and pre-clinical porcine models offers a starting point. In the meantime,

improved understanding of the necessary substrate for heart regeneration in mammals is essential, with the epicardium becoming an increasingly relevant cell population to translate developmental regenerative capacity to adult mammals, and ultimately humans (Vunjak-Novakovic, 2015). The unique setting of the neonatal mouse heart for investigating both the developmental and injury-responsive substrates necessary for mammalian myogenesis offers a powerful tool for improved investigation of these pathways, and the work presented in this thesis, as well as contributing an additional description of epicardial signalling in mammalian heart regeneration, will facilitate further and more refined research to this end.

**Appendix I**

Accepted pending revisions at *Laboratory Animals* 17/08/2015

Title: Isoflurane as an adjunct to hypothermia anaesthesia for thoracotomy in neonatal mice

Authors: M. Masters MSc[1] , P.R Riley PhD[1], Carver.R BVetMed MSc[2], K. Murphy BVetMed CVA[3]*

[1]Department of Physiology, Anatomy and Genetics, University of Oxford, United Kingdom

[2]Animals in Science Regulation Unit, Home Office, UK

[3]Department of Experimental Psychology, University of Oxford, United Kingdom

*Correspondence to: Kathy.murphy@bms.ox.ac.uk

Dr Kathy Murphy,

Department of Experimental Psychology,

University of Oxford,

United Kingdom

OX13UD

Fax: 01865618441 Telephone: 07xxxxxxxx

**Abstract:**

Hypothermia is a widely used anaesthetic method for cardiothoracic surgery in neonatal mice but may not be the most refined method due to the potential for pain and distress during induction and recovery. Here we describe the combinatorial use of volatile and local analgesic anaesthetics with hypothermia in a model of cardiac injury involving thoracotomy in neonatal mice. We observed no detriment to experiment duration or mortality. These adaptations may serve as an example of refinement for cardiothoracic/thoracotomy procedures involving neonatal mice.

**Key words:**

Refinement Neonatal Anaesthesia Hypothermia Isoflurane Thoracotomy

**Appendix II**

**Manuscript in preparation to submit to *JAALAS***

Title: A collaborative approach to achieving aseptic surgical technique in time-sensitive, high-throughput neonatal rodent surgery - a case study

Authors: M. Masters MSc[1] , C. Bergmann[2] *Drmedvet

[1]Department of Physiology, Anatomy and Genetics, University of Oxford, United Kingdom

[2] Department of Biomedical Services, University of Oxford, United Kingdom

*Correspondence to: caroline.bergmann@bms.ox.ac.uk

Dr Caroline Bergmann,

Address:

The Old Observatory, South Parks Road, OX13RQ Oxford, United Kingdom

Fax: Telephone: 01xxx xxxxxx

**Abstract:**
Aseptic technique is a mandate of all *in vivo* recovery procedures in the EU in order to maximise animal welfare and optimise research outcomes. General resources, such as the Home Office and LASA guidelines, provide comprehensive guidance on this topic. However, little exists in terms of guidance of aseptic practices for experimental procedures that pose specific technical or practical challenges; such as neonatal recovery surgery. These procedures are extremely time-sensitive and high-throughput. When preforming such procedures, researchers can be disinclined to adopt full aseptic technique as aseptic practices can increase experimental costs and duration: the latter of which can negatively impact animal welfare. In this case report, we discuss the collaborative approach to designing a time and cost effective aseptic protocol for cardiothoracic recovery surgeries in neonatal rodents. This protocol was designed to optimise animal welfare and experimental outcome without incurring additional procedural time or costs.

## Appendix III

**Fluorescence assisted cell sorting of LacZ positive cells:**

In order to quantify and molecularly profile retinoic acid (RA) responsive cells in hearts from neonatal mice under physiological and pathological conditions, we used fluorescence-assisted cell sorting (FACS) to detect galactosidase activity in mice harbouring the RARE-LacZ construct. Using the Invitrogen Detectagene™ LacZ Gene Expression Kit (D-2920; Thermofisher Scientific), the aim was to generate FITC-labelled cells based on β-galactosidase and fluorescein di-V-galactosidase (FDG) enzymatic activity, which could then be subjected to flow cytometry and sorted to molecularly profile specific cell types. Although previous reports suggest this method of labelling $LacZ^{+}$ cells is highly variable and noisy due to reagent efflux/leakage and uptake, the Detectagene™ Kit is reported to modify the FDG molecule to CMFDG (5-chloromethylfluorescein di-β-D-galactopyranoside) to minimise fluorescent product efflux, prevent endogenous cleavage of the CMFDG reagent (Chloroquine), and increase retention within cells (Verapamil); all which help to improve the cell staining and identification.

Given LacZ should be moderately expressed in a subset of cardiac cells in the postnatal mouse heart, we crossed the ubiquitous PGK-Cre mouse line (Jackson Laboratories) with the Rosa26-LacZ reporter line to generate $PGK^{Cre/R26R\text{-}LacZ}$ animals. These mice express high levels of LacZ globally, and were used to optimise and validate our protocol prior to experimental design. Using the Detectagene™ Kit, single cell suspensions from $PGK^{Cre/R26R\text{-}LacZ}$ and wild-type mice were stained under various conditions, including varying CMFDG concentrations, chloroquine and verapamil concentrations, and incubation times. Although changing these protocol parameters did not successfully distinguish a $FITC^{+}$ population of cells by flow cytometry, tissue samples from $PGK^{Cre+/R26R\text{-}LacZ+}$ incubated with X-gal readily generated blue precipitate, suggesting strong, ubiquitous LacZ expression. Graph A shows results from experimental parameters (indicated by an asterix in the table of conditions) in which we observed the most number of $FITC^{+}$ cells when compared to controls. It is suggested by others that this system is

notoriously problematic; and as such, most laboratories currently prefer the more reliable endogenously fluorescent reporter systems to identify their cells of interest.

**Single cell suspension protocol:**
**Reagents:**

1. Collagenase II
2. Ice cold PBS
3. Nylon 40 µm cell strainer
4. 2% FBS/PBS
5. Mouse BD block (BD Biosciences, #553141)
6. HBSS Medium

**Protocol:**

- For all experiments, hearts were harvested from $PGK^{Cre+/R26R\text{-}LacZ+}$ animals and wild-type littermates for controls, between P1 – P14.
- Tissue samples (lung and liver) were acquired from control and transgenic animals and were incubated in X-gal to confirm LacZ expression (or absence) alongside FACS-gal analysis.
- Tail biopsies were also processed for DNA profiling to confirm Cre and LacZ expression.

1) Digestion buffer (450 µg/ml collagenase II in warm HBSS) was pre-warmed at 37°C.
2) Hearts were harvested on ice in PBS
3) Hearts were finely chopped with a scalpel blade in PBS.
4) Myocardial tissue was transferred to a 15 ml falcon tube and incubated in 5 ml of pre-warmed digestion buffer for 90 minutes at 37°C agitating (orbital incubator) at 220RPM (in a 15 ml Falcon tube).
5) Tissue was aspirated with a pipette every 10-15 minutes to ensure proper digestion.
6) The digest solution was passed through a 40 µm cell strainer into a 50 ml Falcon tube.
7) The tube containing homogenate was centrifuged at 350 g for 10 minutes at 4°C
8) Supernatant was removed.
9) Red blood cells in the sample were lysed with 1X Red Cell Lysis Buffer and were incubated for 5 minutes at room temperature.
10) Samples were centrifuged at 350g for 10 minutes at 4°C and the supernatant was removed.
11) The cells from $PGK^{Cre+/R26R\text{-}LacZ+}$ / wild-type animals were then divided into control and experimental tubes (i.e. un-stained and stained) and were re-suspended in staining solutions of the compositions described in Table A (un-stained control samples were incubated without the CMFDG reagent) which were prepared in pre-warmed staining buffer (5%FCS/DMEM + 25 mM HEPES) and incubated at 37°C for 20 minutes.

**Table IA: conditions for FACS-gal experiments:**

| CMFDG | Verapamil | Chloroquine |
|---|---|---|
| ***50µM** | 200 µM | - |
| **100 µM** | 200 µM | - |
| **50 µM** | 200 µM | 30mM |
| **100 µM** | 200 µM | 30mM |

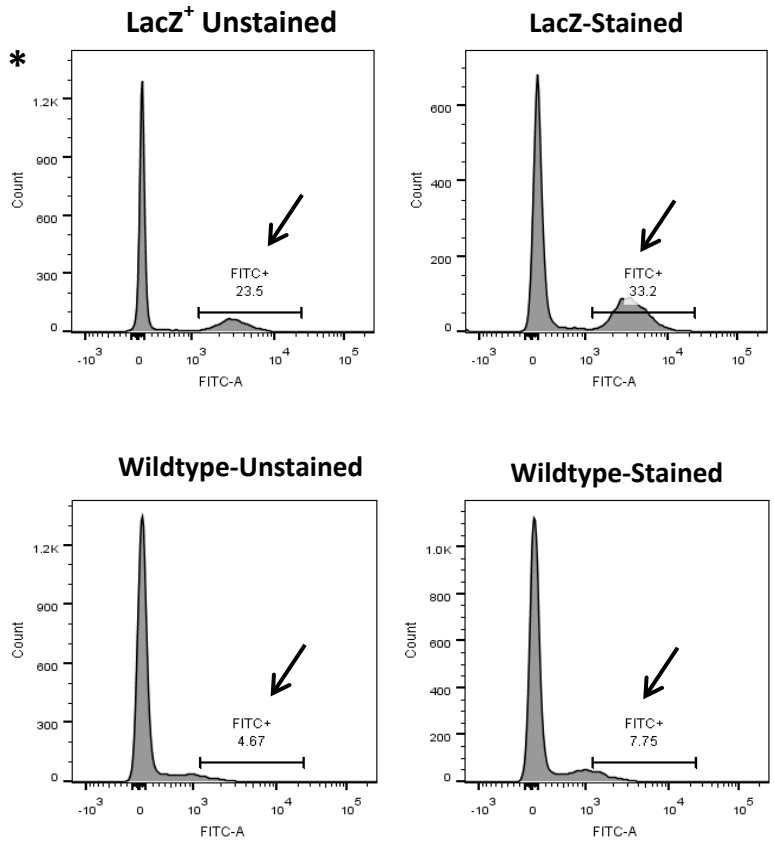


**Figure A. No distinct FITC signal was discriminated from noise BY FACS-gal:** No distinct fluorescein isothiocyanate (FITC) positive cell population (indicated by arrows) was discriminated from background noise or unstained controls in single cell suspensions from hearts of mice that ubiquitously expressed the LacZ construct from wild-type controls, by FACS-gal. Cells were incubated with 50 µM 5-chloromethylfluorescein di-β-D-galactopyranoside (CMFDG). Graphs show the largest observed FITC population across numerous experiments with numerous attempted conditions. * indicates staining conditions used in the table of conditions.

**Appendix IV**

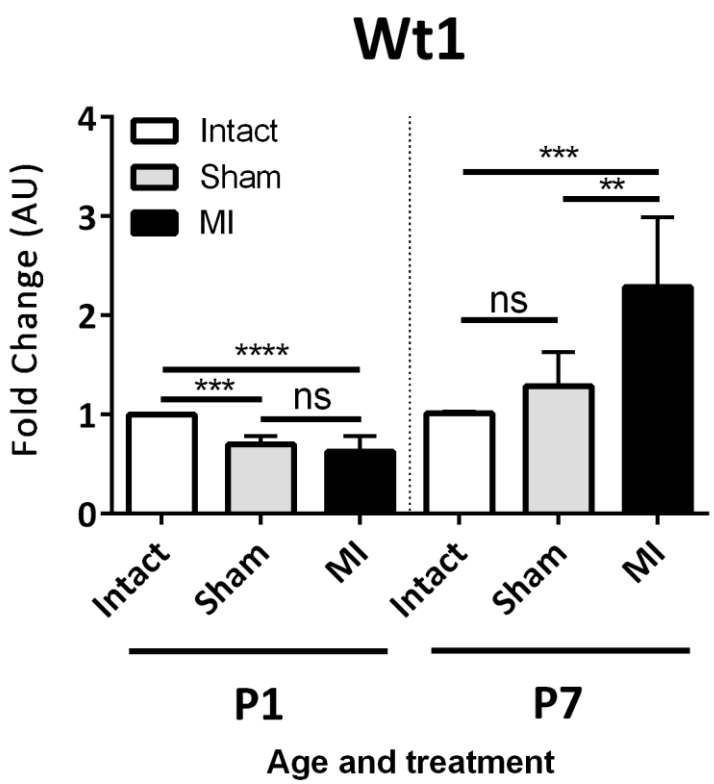


**Figure IV A: Selection of appropriate control for gene expression analysis by qRT-PCR:** to determine the most appropriate control for investigating changes in gene expression in P1 and P7 hearts post-MI, expression levels of Wt1 were compared between ventricular lysates from P1 and P7 hearts that where either uninjured; underwent needle placement without tying off of the ligature (sham); or MI (n=4-6 per group). Statistical analyses were performed using an ANOVA with Tukey's multiple group comparisons: (*p<0.05; **p<0.01; ***p<0.001; ****p<0.0001). Note that statistical significance was not detected between sham and MI groups following MI at P1, and statistical significance was weaker between sham and MI groups compared to between intact and MI groups following MI at P7. Intact controls were, therefore, deemed the most appropriate controls for further gene expression analyses in injured hearts.

**Appendix V**

**Manuscript submitted to Molecular Cell.**
**My contributions were performing adult LAD ligation surgeries and drug (Tβ4) treatment.**

## SWI-SNF-like foetal gene reprogramming dynamically regulates epicardial progenitor activity

Joaquim Miguel Vieira[1,2†], Sara Howard[2†], Sveva Bollini[1‡], Karina N. Dubé[2], Megan Masters[1], Damien N. Barnette[1], Daniel Metzger[3], Pierre Chambon[3], Benjamin Davies[4] and
Paul R. Riley[1,2*]
[1]Burdon Sanderson Cardiac Science Centre, Department of Physiology, Anatomy and Genetics, University of Oxford, Oxford, OX1 3PT, UK.
[2]Molecular Medicine Unit, UCL Institute of Child Health, London, WC1N 1EH, UK.
[3]Institut de Génétique et de Biologie Moléculaire et Cellulaire, INSERM U964/CNRS UMR
7104/Université de Strasbourg, 67404 IllKirch Cedex, France
[4]Wellcome Trust Centre for Human Genetics, University of Oxford, Oxford OX3 7BN, UK
[*]Correspondence to: paul.riley@dpag.ox.ac.uk
[†]Joint first author contribution
[‡]Current address: Regenerative Medicine Laboratory, University of Genoa, IRCCS AOU San
Martino-IST, Largo Rosanna Benzi, Genoa 16132, Italy

SUMMARY

Epicardium-derived cells (EPDCs) contribute cardiac cell types during development and have been proposed as a regenerative source in heart disease. The quiescent adult epicardium responds to Thymosin β4 (Tβ4) and myocardial infarction (MI) by reactivating a foetal gene program and mobilizing adult EPDCs to promote neovascularization and cardiomyogenesis. The mechanism for epicardial gene activation remains elusive. Here we reveal that SWI/SNF chromatin-remodelling complexes restored embryonic potential upon MI. BRG1, the essential ATPase subunit of SWI/SNF, physically interacted with Tβ4 and was recruited by CCAAT/enhancer-binding protein β (C/EBPβ) to discrete regulatory elements in the Wilm's tumour 1 (Wt1) locus; promoting transcription of Wt1 as the master regulator of embryonic EPDCs and Wt1as, an antisense lncRNA produced from within intron 1. Wt1as increased Wt1 mRNA stability through heteroduplex formation. These findings reveal novel essential functions for chromatin-remodelling and antisense RNA in the embryonic programming of EPDCs during cardiac development and repair.

**Appendix VI**

**My contributions were performing adult LAD ligation surgeries and drug (VEGF-C) treatment.**

ARTICLE

doi:10.1038/nature14483

# Cardiac lymphatics are heterogeneous in origin and respond to injury

Linda Klotz[1]*, Sophie Norman[2]*, Joaquim Miguel Vieira[2]*, Megan Masters[2], Mala Rohling[2], Karina N. Dubé[1], Sveva Bollini[3], Fumio Matsuzaki[4], Carolyn A. Carr[2] & Paul R. Riley[2]

**The lymphatic vasculature is a blind-ended network crucial for tissue-fluid homeostasis, immune surveillance and lipid absorption from the gut. Recent evidence has proposed an entirely venous-derived mammalian lymphatic system. By contrast, here we show that cardiac lymphatic vessels in mice have a heterogeneous cellular origin, whereby formation of at least part of the cardiac lymphatic network is independent of sprouting from veins. Multiple Cre–*lox*-based lineage tracing revealed a potential contribution from the putative haemogenic endothelium during development, and discrete lymphatic endothelial progenitor populations were confirmed by conditional knockout of *Prox1* in Tie2$^+$ and Vav1$^+$ compartments. In the adult heart, myocardial infarction promoted a significant lymphangiogenic response, which was augmented by treatment with VEGF-C, resulting in improved cardiac function. These data prompt the re-evaluation of a century-long debate on the origin of lymphatic vessels and suggest that lymphangiogenesis may represent a therapeutic target to promote cardiac repair following injury.**

In 1902, Florence Sabin proposed that the primary lymph sacs originate from the embryonic veins and then give rise to the entire lymphatic vasculature by sprouting and remodelling[1]. An alternative model of lymphatic development was proposed by Huntington and McClure in 1910, who suggested that lymph sacs arise in the mesenchyme, independently of veins, via distinct progenitor cells[2]. More recent evidence has supported Sabin's model, such that trans-differentiation of venous into lymphatic endothelial cells (LECs) is now widely accepted, with the veins regarded as the sole origin of the entire lymphatic vasculature in mammals[3–7]. To date, studies which support a venous origin have focused exclusively on the development of the systemic lymphatic vasculature. Organ-based lymphatics have received little attention and in the heart, while the presence of cardiac lymphatic vessels has been described[8], virtually nothing is known about their role during development or in the healthy or failing adult heart. We therefore sought to characterize the formation of the cardiac lymphatic vessels through developmental stages, to identify their embryonic origin and effect during organogenesis and to assess their response to pathological insult in the adult setting.

## Development of the cardiac lymphatic vasculature

Whole-mount staining of murine hearts for early LEC markers VEGFR-3 (ref. 9) and Prox1 (ref. 10), revealed the emergence of lymphatic vessels at embryonic day 12.5 (E12.5), sprouting from extra-cardiac regions proximal to the outflow tract, on the ventral side (Fig. 1a, increased magnification in Fig. 1b). At E14.5, lymphatic vessels were observed on the ventricular surface sprouting from the region of the sinus venosus, on the dorsal side (Fig. 1c, increased magnification in Fig. 1d and Extended Data Fig. 1a, increased magnification in Extended Data Fig. 1b). At E16.5 the major dorsal vessels spread inferiorly from the inflow region (Fig. 1e, increased magnification in Fig. 1f), while ventrally smaller vessels arose between the atria (Extended Data Fig. 1c, d). By E18.5, the vessels continued to expand and projected towards the apex of the heart on both dorsal and ventral surfaces (Fig. 1g, h and Extended Data Fig. 1e, f). From birth (postnatal day 0 (P0)), the vessels developed a more extensive branched network and expanded further over the ventral side of the neonatal heart (Fig. 1i, j). By P10, the cardiac lymphatics provided superficial coverage of the majority of the epicardial surface of the heart (Extended Data Fig. 1g, h) and appeared fully developed by P15 (Extended Data Fig. 1i, j). The lymphatic identity of the VEGFR-3- and Prox1-labelled cardiac vessels (Fig. 1a–j and Extended Data Fig. 1a–n) was further validated by co-immunostaining for the lymphatic vessel endothelial hyaluronan receptor 1 (Lyve-1), which also labels tissue macrophages[11]. Coronary LECs within the expanding plexus on both dorsal and ventral sides of the developing heart co-expressed VEGFR-3, Prox1 and Lyve-1 (Extended Data Fig. 1o–v). Cardiac lymphatic vessels aligned with the endomucin (Emcn)-positive coronary veins during late gestation (E15.5–18.5) (Fig. 1k–m) and established extensive inter-vessel connections analogous to blood vessel anastomosis (Fig. 1n–p). At birth (P0) lateral Lyve-1$^+$ sprouts beneath smooth-muscle-actin-positive coronary veins (Fig. 1q–s) were indicative of a close anatomical relationship between the coronary veins and developing lymphatic vasculature (Fig. 1t).

## A venous and non-venous contribution of LECs

Prox1$^+$ LECs did not appear to emerge or bud-off from Emcn-expressing coronary vessels between E12.5–14.5 (Extended Data Fig. 2a–i). Instead, extra-cardiac LECs migrated into the sinus venosus on the dorsal side, and outflow tract on the ventral side of the heart by E12.5 (Extended Data Fig. 2a, b, also Fig. 1a, b) and expanded to form a network proximal to Emcn$^+$ veins from E13.5 and E14.5 (Extended Data Fig. 2d–i) through to E17.5 (Extended Data Fig. 2j–o). Whole embryo staining at E10.5 and E12.5 (Extended Data Fig. 3a–f) revealed a Prox1/VEGFR-3-expressing LEC population emerging from the Emcn$^+$ common cardinal vein and migrating towards the neighbouring sinus venosus and outflow tract (Extended Data

[1]University College London, Institute of Child Health, Molecular Medicine Unit, 30 Guilford Street, London WC1N 1EH, UK. [2]University of Oxford, Department of Physiology, Anatomy and Genetics, South Parks Road, Oxford OX1 3PT, UK. [3]Regenerative Medicine Laboratory, University of Genoa & IRCCS AOU San Martino-IST, Largo Rosanna Benzi, 16132 Genoa, Italy. [4]Laboratory for Cell Asymmetry, RIKEN Center for Developmental Biology, 2-2-3, Minatojima-Minamimachi, Chuo-ku, Kobe 650-0047, Japan.
*These authors contributed equally to this work.

## Appendix VII

**Invited speaker at the International Conference on Tissue Engineering and Regenerative Medicine, Pretoria, SA, September 2014.**

Presenting author: Megan Masters

Institution: University of Oxford

Email: megan.masters@dpag.ox.ac.uk

Abstract title: Of Mice and Mending Broken Hearts

Abstract authors: Megan Masters and Paul R Riley

Category: Regeneration/tissue engineering

Abstract:

Coronary heart disease (CHD) remains a leading cause of death worldwide. When a coronary artery becomes blocked, the contingent heart muscle undergoes ischemic damage a non-contractile scar forms in its place. Consequently, the heart remodels and chronic heart failure ensues. Despite the rising incidence of CHD and heart failure, the only effective cure remains a heart transplant; for which the demand for donor organs far outweighs supply. The gold standard cure would be to non-invasively restore lost heart muscle (myocardium) and vasculature (coronaries), to regenerate the organ and recover full function. One approach to achieve this is to stimulate resident cell populations which are instructive towards myogenesis. The epicardium (the mesothelium which forms the outer layer of the heart) is one such cell population: it acts as a progenitor/stem cell pool for numerous cardiac cell types and provides trophic signals instructive to both myocardial development in mammals and heart regeneration in lower vertebrates.

While lower vertebrates are able to recover their hearts from substantial injury throughout life, it was long believed that heart regeneration was a capacity lost to mammals through evolution. However, recent technical leaps showed that newborn mice can regenerate heart muscle and function within weeks, but only if injured within the first few days of life (Porrello et al., 2011). If injured on or after postnatal day seven (P7), scarring and fibrosis are observed and adult like wound healing ensues. This brief time period after birth has been coined the "neonatal regenerative window". Through inducing ischemia in the neonatal mouse heart, we aim to understand the cell and molecular underpinnings of this 'switch' from regeneration to scarring and fibrosis in a mammalian setting; identify key mechanisms of the former; and extrapolate these findings to regenerating failing human hearts.

Given the roles of the epicardium in instructing developmental and regenerative myogenesis, we aimed to investigate the potential role(s) of this cell population and its derivative signals in mammalian heart regeneration. Previous studies showed that inhibiting one epicardial signal, retinoic acid (RA) signalling, blocked the myogenesis central to both mammalian heart development and zebrafish heart regeneration (Kikuchi et al., 2011, Chen et al., 2002). Here we implicate RA signalling in neonatal heart regeneration in mammals. We further implicate limited RA signalling in the insufficient regenerative response of the injured adult heart. We conclude that epicardial RA signalling may be important in modulating the regenerative versus fibrotic response in the mammalian heart; findings which may be significant in developing novel therapies to treat, or even cure heart failure.

## Bibliography:


ACHARYA, A., BAEK, S. T., HUANG, G., ESKIOCAK, B., GOETSCH, S., SUNG, C. Y., BANFI, S., SAUER, M. F., OLSEN, G. S., DUFFIELD, J. S., OLSON, E. N. & TALLQUIST, M. D. 2012. The bHLH transcription factor Tcf21 is required for lineage-specific EMT of cardiac fibroblast progenitors. *Development,* 139**,** 2139-49.

ANDERSEN, D. C., GANESALINGAM, S., JENSEN, C. H. & SHEIKH, S. P. 2014. Do neonatal mouse hearts regenerate following heart apex resection? *Stem Cell Reports,* 2**,** 406-13.

ANDERSEN, D. C., JENSEN, C. H. & SHEIKH, S. P. 2015. Comments to the article "A systematic analysis of neonatal mouse heart regeneration after apical resection". *J Mol Cell Cardiol,* 82**,** 59.

ANTOGNINI, J. F. 1993. Hypothermia eliminates isoflurane requirements at 20 degrees C. *Anesthesiology,* 78**,** 1152-6.

ARNOLD, S. L., AMORY, J. K., WALSH, T. J. & ISOHERRANEN, N. 2012. A sensitive and specific method for measurement of multiple retinoids in human serum with UHPLC-MS/MS. *J Lipid Res,* 53**,** 587-98.

AURORA, A. B., PORRELLO, E. R., TAN, W., MAHMOUD, A. I., HILL, J. A., BASSEL-DUBY, R., SADEK, H. A. & OLSON, E. N. 2014. Macrophages are required for neonatal heart regeneration. *J Clin Invest,* 124**,** 1382-92.

AUSONI, S. & SARTORE, S. 2009. From fish to amphibians to mammals: in search of novel strategies to optimize cardiac regeneration. *J Cell Biol,* 184**,** 357-64.

AZAMBUJA, A. P., PORTILLO-SANCHEZ, V., RODRIGUES, M. V., OMAE, S. V., SCHECHTMAN, D., STRAUSS, B. E., COSTANZI-STRAUSS, E., KRIEGER, J. E., PEREZ-POMARES, J. M. & XAVIER-NETO, J. 2010. Retinoic acid and VEGF delay smooth muscle relative to endothelial differentiation to coordinate inner and outer coronary vessel wall morphogenesis. *Circ Res,* 107**,** 204-16.

BALTIMORE, D., BERG, P., BOTCHAN, M., CARROLL, D., CHARO, R. A., CHURCH, G., CORN, J. E., DALEY, G. Q., DOUDNA, J. A., FENNER, M., GREELY, H. T., JINEK, M., MARTIN, G. S., PENHOET, E., PUCK, J., STERNBERG, S. H., WEISSMAN, J. S. & YAMAMOTO, K. R. 2015. Biotechnology. A prudent path forward for genomic engineering and germline gene modification. *Science,* 348**,** 36-8.

BANERJEE, I., FUSELER, J. W., PRICE, R. L., BORG, T. K. & BAUDINO, T. A. 2007. Determination of cell types and numbers during cardiac development in the neonatal and adult rat and mouse. *Am J Physiol Heart Circ Physiol,* 293**,** 1883-91.

BERGMANN, O., BHARDWAJ, R. D., BERNARD, S., ZDUNEK, S., BARNABE-HEIDER, F., WALSH, S., ZUPICICH, J., ALKASS, K., BUCHHOLZ, B. A., DRUID, H., JOVINGE, S. & FRISEN, J. 2009. Evidence for cardiomyocyte renewal in humans. *Science,* 324**,** 98-102.

BILBIJA, D., ELMABSOUT, A. A., SAGAVE, J., HAUGEN, F., BASTANI, N., DAHL, C. P., GULLESTAD, L., SIRSJO, A., BLOMHOFF, R. & VALEN, G. 2014. Expression of retinoic acid target genes in coronary artery disease. *Int J Mol Med,* 33**,** 677-86.

BILBIJA, D., HAUGEN, F., SAGAVE, J., BAYSA, A., BASTANI, N., LEVY, F. O., SIRSJO, A., BLOMHOFF, R. & VALEN, G. 2012. Retinoic acid signalling is activated in the post ischemic heart and may influence remodelling. *PLoS One,* 7**,** e44740.

BOHL, S., LYGATE, C. A., BARNES, H., MEDWAY, D., STORK, L. A., SCHULZ-MENGER, J., NEUBAUER, S. & SCHNEIDER, J. E. 2009. Advanced methods for quantification of infarct size in mice using three-dimensional high-field late gadolinium enhancement MRI. *Am J Physiol Heart Circ Physiol,* 296**,** H1200-8.

BOLLINI, S., VIEIRA, J. M., HOWARD, S., DUBE, K. N., BALMER, G. M., SMART, N. & RILEY, P. R. 2014. Re-activated adult epicardial progenitor cells are a heterogeneous population molecularly distinct from their embryonic counterparts. *Stem Cells Dev,* 23**,** 1719-30.

BRADE, T., KUMAR, S., CUNNINGHAM, T. J., CHATZI, C., ZHAO, X., CAVALLERO, S., LI, P., SUCOV, H. M., RUIZ-LOZANO, P. & DUESTER, G. 2011. Retinoic acid stimulates myocardial expansion by induction of hepatic erythropoietin which activates epicardial Igf2. *Development,* 138**,** 139-48.

BRAITSCH, C. M., COMBS, M. D., QUAGGIN, S. E. & YUTZEY, K. E. 2012. Pod1/Tcf21 is regulated by retinoic acid signalling and inhibits differentiation of epicardium-derived cells into smooth muscle in the developing heart. *Dev Biol,* 368**,** 345-57.

BRAITSCH, C. M., KANISICAK, O., VAN BERLO, J. H., MOLKENTIN, J. D. & YUTZEY, K. E. 2013. Differential expression of embryonic epicardial progenitor markers and localization of cardiac fibrosis in adult ischemic injury and hypertensive heart disease. *J Mol Cell Cardiol,* 65**,** 108-19.

BRYANT, D. M., O'MEARA, C. C., HO, N. N., GANNON, J., CAI, L. & LEE, R. T. 2015. A systematic analysis of neonatal mouse heart regeneration after apical resection. *J Mol Cell Cardiol,* 79**,** 315-8.

CAI, C. L., MARTIN, J. C., SUN, Y., CUI, L., WANG, L., OUYANG, K., YANG, L., BU, L., LIANG, X., ZHANG, X., STALLCUP, W. B., DENTON, C. P., MCCULLOCH, A., CHEN, J. & EVANS, S. M. 2008. A myocardial lineage derives from Tbx18 epicardial cells. *Nature,* 454**,** 104-8.

CAMELLITI, P., BORG, T. K. & KOHL, P. 2005. Structural and functional characterisation of cardiac fibroblasts. *Cardiovasc Res,* 65**,** 40-51.

CARMONA, R., GUADIX, J. A., CANO, E., RUIZ-VILLALBA, A., PORTILLO-SANCHEZ, V., PEREZ-POMARES, J. M. & MUNOZ-CHAPULI, R. 2010. The embryonic epicardium: an essential element of cardiac development. *J Cell Mol Med,* 14**,** 2066-72.

CHABLAIS, F., VEIT, J., RAINER, G. & JAZWINSKA, A. 2011. The zebrafish heart regenerates after cryoinjury-induced myocardial infarction. *BMC Dev Biol,* 11**,** 21.

CHEN, J., KUBALAK, S. W. & CHIEN, K. R. 1998. Ventricular muscle-restricted targeting of the RXRalpha gene reveals a non-cell-autonomous requirement in cardiac chamber morphogenesis. *Development,* 125**,** 1943-9.

CHEN, T., CHANG, T. C., KANG, J. O., CHOUDHARY, B., MAKITA, T., TRAN, C. M., BURCH, J. B., EID, H. & SUCOV, H. M. 2002. Epicardial induction of foetal cardiomyocyte proliferation via a retinoic acid-inducible trophic factor. *Dev Biol,* 250**,** 198-207.

CHIMENTI, S., CARLO, E., MASSON, S., BAI, A. & LATINI, R. 2004. Myocardial infarction: animal models. *Methods Mol Med,* 98**,** 217-26.

CHRISTOFFELS, V. M., GRIESKAMP, T., NORDEN, J., MOMMERSTEEG, M. T., RUDAT, C. & KISPERT, A. 2009. Tbx18 and the fate of epicardial progenitors. *Nature,* 458**,** 8-9.

CLARK, R. A., DELLAPELLE, P., MANSEAU, E., LANIGAN, J. M., DVORAK, H. F. & COLVIN, R. B. 1982. Blood vessel fibronectin increases in conjunction with endothelial cell proliferation and capillary ingrowth during wound healing. *J Invest Dermatol,* 79**,** 269-76.

D'ANIELLO, E., RYDEEN, A. B., ANDERSON, J. L., MANDAL, A. & WAXMAN, J. S. 2013. Depletion of retinoic acid receptors initiates a novel positive feedback mechanism that promotes teratogenic increases in retinoic acid. *PLoS Genet,* 9(8):e1003689.

DAREHZERESHKI, A., RUBIN, N., GAMBA, L., KIM, J., FRASER, J., HUANG, Y., BILLINGS, J., MOHAMMADZADEH, R., WOOD, J., WARBURTON, D., KAARTINEN, V. & LIEN, C. L. 2015. Differential regenerative capacity of neonatal mouse hearts after cryoinjury. *Dev Biol,* 399**,** 91-9.

DETTMAN, R. W., DENETCLAW, W., JR., ORDAHL, C. P. & BRISTOW, J. 1998. Common epicardial origin of coronary vascular smooth muscle, perivascular fibroblasts, and intermyocardial fibroblasts in the avian heart. *Dev Biol,* 193**,** 169-81.

DOLLE, P. 2009. Developmental expression of retinoic acid receptors (RARs). *Nucl Recept Signal,* 12;7:e006

ELDER, J. T., ASTROM, A., PETTERSSON, U., TAVAKKOL, A., GRIFFITHS, C. E., KRUST, A., KASTNER, P., CHAMBON, P. & VOORHEES, J. J. 1992. Differential regulation of retinoic acid receptors and binding proteins in human skin. *J Invest Dermatol,* 98**,** 673-9.

FISH, R., DANNEMAN, P., BROWN, M. & KARAS, J. 1997. Anaesthesia and Analgesia in Laboratory Animals. Elsevier *New York, USA*. Pg. 35 - 40

FITZGERALD, M. & BEGGS, S. 2001. The neurobiology of pain: developmental aspects. *Neuroscientist,* 7**,** 246-57.

GLASER-GABAY, L., RAITER, A., BATTLER, A. & HARDY, B. 2011. Endothelial cell surface vimentin binding peptide induces angiogenesis under hypoxic/ischemic conditions. *Microvasc Res,* 82**,** 221-6.

GONZALEZ-ROSA, J. M., MARTIN, V., PERALTA, M., TORRES, M. & MERCADER, N. 2011. Extensive scar formation and regression during heart regeneration after cryoinjury in zebrafish. *Development,* 138**,** 1663-74.

GONZALEZ-ROSA, J. M. & MERCADER, N. 2012. Cryoinjury as a myocardial infarction model for the study of cardiac regeneration in the zebrafish. *Nat Protoc,* 7**,** 782-8.

GONZALEZ-ROSA, J. M., PERALTA, M. & MERCADER, N. 2012. Pan-epicardial lineage tracing reveals that epicardium derived cells give rise to myofibroblasts and perivascular cells during zebrafish heart regeneration. *Dev Biol,* 370**,** 173-86.

GOURDIE, R. G., CHENG, G., THOMPSON, R. P. & MIKAWA, T. 2000. Retroviral cell lineage analysis in the developing chick heart. *Methods Mol Biol,* 135**,** 297-304.

GREENE, S. A. 2002. Veterinary Anaesthesia and pain management secrets, Hanley and Belfus. *Philedelphia, USA* Pg 111-115.

GUADIX, J. A., CARMONA, R., MUNOZ-CHAPULI, R. & PEREZ-POMARES, J. M. 2006. In vivo and in vitro analysis of the vasculogenic potential of avian proepicardial and epicardial cells. *Dev Dyn,* 235**,** 1014-26.

GUADIX, J. A., RUIZ-VILLALBA, A., LETTICE, L., VELECELA, V., MUNOZ-CHAPULI, R., HASTIE, N. D., PEREZ-POMARES, J. M. & MARTINEZ-ESTRADA, O. M. 2011. Wt1 controls retinoic acid signalling in embryonic epicardium through transcriptional activation of Raldh2. *Development,* 138**,** 1093-7.

HAUBNER, B. J., ADAMOWICZ-BRICE, M., KHADAYATE, S., TIEFENTHALER, V., METZLER, B., AITMAN, T. & PENNINGER, J. M. 2012. Complete cardiac regeneration in a mouse model of myocardial infarction. *Aging (Albany NY),* 4**,** 966-77.

HEIJMAN, E., DE GRAAF, W., NIESSEN, P., NAUERTH, A., VAN EYS, G., DE GRAAF, L., NICOLAY, K. & STRIJKERS, G. J. 2007. Comparison between prospective and retrospective triggering for mouse cardiac MRI. *NMR Biomed,* 20**,** 439-47.

HU, N., YOST, H. J. & CLARK, E. B. 2001. Cardiac morphology and blood pressure in the adult zebrafish. *Anat Rec,* 264**,** 1-12.

HUANG, G. N., THATCHER, J. E., MCANALLY, J., KONG, Y., QI, X., TAN, W., DIMAIO, J. M., AMATRUDA, J. F., GERARD, R. D., HILL, J. A., BASSEL-DUBY, R. & OLSON, E. N. 2012. C/EBP transcription factors mediate epicardial activation during heart development and injury. *Science,* 338**,** 1599-603.

IEDA, M., TSUCHIHASHI, T., IVEY, K. N., ROSS, R. S., HONG, T. T., SHAW, R. M. & SRIVASTAVA, D. 2009. Cardiac fibroblasts regulate myocardial proliferation through beta1 integrin signalling. *Dev Cell,* 16**,** 233-44.

IKENISHI, A., OKAYAMA, H., IWAMOTO, N., YOSHITOME, S., TANE, S., NAKAMURA, K., OBAYASHI, T., HAYASHI, T. & TAKEUCHI, T. 2012. Cell cycle regulation in mouse heart during embryonic and postnatal stages. *Dev Growth Differ,* 54**,** 731-8.

JESSUP, M. & BROZENA, S. 2003. Heart failure. *N Engl J Med,* 348**,** 2007-18.

JESTY, S. A., STEFFEY, M. A., LEE, F. K., BREITBACH, M., HESSE, M., REINING, S., LEE, J. C., DORAN, R. M., NIKITIN, A. Y., FLEISCHMANN, B. K. & KOTLIKOFF, M. I. 2012. c-kit+ precursors support post infarction myogenesis in the neonatal, but not adult, heart. *Proc Natl Acad Sci U S A,* 109**,** 13380-5.

JOPLING, C., SLEEP, E., RAYA, M., MARTI, M., RAYA, A. & IZPISUA BELMONTE, J. C. 2010. Zebrafish heart regeneration occurs by cardiomyocyte dedifferentiation and proliferation. *Nature,* 464**,** 606-9.

JUGDUTT, B. I. 2003. Ventricular remodelling after infarction and the extracellular collagen matrix: when is enough enough? *Circulation,* 108**,** 1395-403.

JUNKER, J. P., NOEL, E. S., GURYEV, V., PETERSON, K. A., SHAH, G., HUISKEN, J., MCMAHON, A. P., BEREZIKOV, E., BAKKERS, J. & VAN OUDENAARDEN, A. 2014. Genome-wide RNA Tomography in the zebrafish embryo. *Cell,* 159**,** 662-75.

KATZ, T. C., SINGH, M. K., DEGENHARDT, K., RIVERA-FELICIANO, J., JOHNSON, R. L., EPSTEIN, J. A. & TABIN, C. J. 2012. Distinct compartments of the proepicardial organ give rise to coronary vascular endothelial cells. *Dev Cell,* 22**,** 639-50.

KAYMAK, C., KADIOGLU, E., COSKUN, E., BASAR, H. & BASAR, M. 2012. Determination of DNA damage after exposure to inhalation anaesthetics in human peripheral lymphocytes and sperm cells in vitro by comet assay. *Hum Exp Toxicol,* 31**,** 1207-13.

KIKUCHI, K., HOLDWAY, J. E., MAJOR, R. J., BLUM, N., DAHN, R. D., BEGEMANN, G. & POSS, K. D. 2011. Retinoic acid production by endocardium and epicardium is an injury response essential for zebrafish heart regeneration. *Dev Cell,* 20**,** 397-404.

KIKUCHI, K., HOLDWAY, J. E., WERDICH, A. A., ANDERSON, R. M., FANG, Y., EGNACZYK, G. F., EVANS, T., MACRAE, C. A., STAINIER, D. Y. & POSS, K. D. 2010. Primary contribution to zebrafish heart regeneration by gata4(+) cardiomyocytes. *Nature,* 464**,** 601-5.

KIM, J., WU, Q., ZHANG, Y., WIENS, K. M., HUANG, Y., RUBIN, N., SHIMADA, H., HANDIN, R. I., CHAO, M. Y., TUAN, T. L., STARNES, V. A. & LIEN, C. L. 2010. PDGF signalling is required for epicardial function and blood vessel formation in regenerating zebrafish hearts. *Proc Natl Acad Sci USA,* 107**,** 17206-10.

KISPERT, A. 2012. No muscle for a damaged heart: thymosin beta 4 treatment after myocardial infarction does not induce myocardial differentiation of epicardial cells. *J Mol Cell Cardiol,* 52**,** 10-12.

KONFINO, T., LANDA, N., BEN-MORDECHAI, T. & LEOR, J. 2015. The type of injury dictates the mode of repair in neonatal and adult heart. *J Am Heart Assoc,* 4**,** e001320.

KRUITHOF, B. P., VAN WIJK, B., SOMI, S., KRUITHOF-DE JULIO, M., PEREZ POMARES, J. M., WEESIE, F., WESSELS, A., MOORMAN, A. F. & VAN DEN HOFF, M. J. 2006. BMP and FGF regulate the differentiation of multipotential pericardial mesoderm into the myocardial or epicardial lineage. *Dev Biol,* 295**,** 507-22.

LASA. 2010. Guiding Principles for Preparing for and Undertaking Aseptic Surgery. [ONLINE] Available at: http://www.lasa.co.uk/publications. [Accessed 09 October 15].

LAUGWITZ, K. L., MORETTI, A., CARON, L., NAKANO, A. & CHIEN, K. R. 2008. Islet1 cardiovascular progenitors: a single source for heart lineages? *Development,* 135**,** 193-205.

LAVINE, K. J., EPELMAN, S., UCHIDA, K., WEBER, K. J., NICHOLS, C. G., SCHILLING, J. D., ORNITZ, D. M., RANDOLPH, G. J. & MANN, D. L. 2014. Distinct macrophage lineages contribute to disparate patterns of cardiac recovery and remodelling in the neonatal and adult heart. *Proc Natl Acad Sci USA,* 111**,** 16029-34.

LEPILINA, A., COON, A. N., KIKUCHI, K., HOLDWAY, J. E., ROBERTS, R. W., BURNS, C. G. & POSS, K. D. 2006. A dynamic epicardial injury response supports progenitor cell activity during zebrafish heart regeneration. *Cell,* 127**,** 607-19.

LIMANA, F., BERTOLAMI, C., MANGONI, A., DI CARLO, A., AVITABILE, D., MOCINI, D., IANNELLI, P., DE MORI, R., MARCHETTI, C., POZZOLI, O., GENTILI, C., ZACHEO, A., GERMANI, A. & CAPOGROSSI, M. C. 2010. Myocardial infarction induces embryonic reprogramming of epicardial c-kit(+) cells: role of the pericardial fluid. *J Mol Cell Cardiol,* 48**,** 609-18.

LIN, E. P., MILES, L., HUGHES, E. A., MCCANN, J. C., VORHEES, C. V., MCAULIFFE, J. J. & LOEPKE, A. W. 2014. A combination of mild hypothermia and sevoflurane affords long-term protection in a modified neonatal mouse model of cerebral hypoxia-ischemia. *Anesth Analg,* 119**,** 1158-73.

LIVAK, K. J. & SCHMITTGEN, T. D. 2001. Analysis of relative gene expression data using real-time quantitative PCR and the 2(-Delta Delta C(T)) Method. *Methods,* 25**,** 402-8.

LOEPKE, A. W., MCCANN, J. C., KURTH, C. D. & MCAULIFFE, J. J. 2006. The physiologic effects of isoflurane anaesthesia in neonatal mice. *Anesth Analg,* 102**,** 75-80.

LOPASCHUK, G. D. & JASWAL, J. S. 2010. Energy metabolic phenotype of the cardiomyocyte during development, differentiation, and postnatal maturation. *J Cardiovasc Pharmacol,* 56**,** 130-40.

LUTTUN, A. & CARMELIET, P. 2003. De novo vasculogenesis in the heart. *Cardiovasc Res,* 58**,** 378-89.

MADEN, M. 2002. Retinoid signalling in the development of the central nervous system. *Nat Rev Neurosci,* 3**,** 843-53.

MAHMOUD, A. I., KOCABAS, F., MURALIDHAR, S. A., KIMURA, W., KOURA, A. S., THET, S., PORRELLO, E. R. & SADEK, H. A. 2013. Meis1 regulates postnatal cardiomyocyte cell cycle arrest. *Nature,* 497**,** 249-53.

MAHMOUD, A. I., PORRELLO, E. R., KIMURA, W., OLSON, E. N. & SADEK, H. A. 2014. Surgical models for cardiac regeneration in neonatal mice. *Nat Protoc,* 9**,** 305-11.

MANNER, J. 1993. Experimental study on the formation of the epicardium in chick embryos. *Anat Embryol (Berl),* 187**,** 281-9.

MANNER, J. 1999. Does the subepicardial mesenchyme contribute myocardioblasts to the myocardium of the chick embryo heart? A quail-chick chimera study tracing the fate of the epicardial primordium. *Anat Rec,* 255**,** 212-26.

MARCHANT, A. 2014. 'Do neonates feel pain?' A critical review. *Bioscience Horizons,* 7, 52-60.

MARQUES, I. J., LEITO, J. T., SPAINK, H. P., TESTERINK, J., JASPERS, R. T., WITTE, F., VAN DEN BERG, S. & BAGOWSKI, C. P. 2008. Transcriptome analysis of the response to chronic constant hypoxia in zebrafish hearts. *J Comp Physiol B,* 178**,** 77-92.

MARTINEZ-ESTRADA, O. M., LETTICE, L. A., ESSAFI, A., GUADIX, J. A., SLIGHT, J., VELECELA, V., HALL, E., REICHMANN, J., DEVENNEY, P. S., HOHENSTEIN, P., HOSEN, N., HILL, R. E., MUNOZ-CHAPULI, R. & HASTIE, N. D. 2010. Wt1 is required for cardiovascular progenitor cell formation through transcriptional control of Snail and E-cadherin. *Nat Genet,* 42**,** 89-93.

MASTERS, M. & RILEY, P. R. 2014. The epicardium signals the way towards heart regeneration. *Stem Cell Res,* 13**,** 683-92.

MEDHORA, M. M. 2000. Retinoic acid upregulates beta(1)-integrin in vascular smooth muscle cells and alters adhesion to fibronectin. *Am J Physiol Heart Circ Physiol,* 279**,** H382-7.

MERCER, S., ODELBERG, S. J. & SIMON, H. G. 2013. A dynamic spatiotemporal extracellular matrix facilitates epicardial-mediated vertebrate heart regeneration. *Dev Biol*. 382(2):457-69

MERKI, E., ZAMORA, M., RAYA, A., KAWAKAMI, Y., WANG, J., ZHANG, X., BURCH, J., KUBALAK, S. W., KALIMAN, P., IZPISUA BELMONTE, J. C., CHIEN, K. R. & RUIZ-LOZANO, P. 2005. Epicardial retinoid X receptor alpha is required for myocardial growth and coronary artery formation. *Proc Natl Acad Sci USA,* 102**,** 18455-60.

MICHIELON, G., DI CARLO, D., BRANCACCIO, G., GUCCIONE, P., MAZZERA, E., TOSCANO, A. & DI DONATO, R. M. 2003. Anomalous coronary artery origin from the pulmonary artery: correlation between surgical timing and left ventricular function recovery. *Ann Thorac Surg,* 76**,** 581-8.

MIKAWA, T. & FISCHMAN, D. A. 1992. Retroviral analysis of cardiac morphogenesis: discontinuous formation of coronary vessels. *Proc Natl Acad Sci USA,* 89**,** 9504-8.

MIKAWA, T. & GOURDIE, R. G. 1996. Pericardial mesoderm generates a population of coronary smooth muscle cells migrating into the heart along with ingrowth of the epicardial organ. *Dev Biol,* 174**,** 221-32.

MOLLOVA, M., BERSELL, K., WALSH, S., SAVLA, J., DAS, L. T., PARK, S. Y., SILBERSTEIN, L. E., DOS REMEDIOS, C. G., GRAHAM, D., COLAN, S. & KUHN, B. 2013. Cardiomyocyte proliferation contributes to heart growth in young humans. *Proc Natl Acad Sci USA,* 110**,** 1446-51.

MOORE, A. W., MCINNES, L., KREIDBERG, J., HASTIE, N. D. & SCHEDL, A. 1999. YAC complementation shows a requirement for Wt1 in the development of epicardium, adrenal gland and throughout nephrogenesis. *Development,* 126**,** 1845-57.

MURALIDHAR, S. A., MAHMOUD, A. I., CANSECO, D., XIAO, F. & SADEK, H. A. 2013. Harnessing the power of dividing cardiomyocytes. *Global Cardiology Science & Practise,* 2013 (3):212-2

NACHTRAB, G. & POSS, K. D. 2012. Toward a blueprint for regeneration. *Development,* 139**,** 2639-42.

NIEDERREITHER, K., MCCAFFERY, P., DRAGER, U. C., CHAMBON, P. & DOLLE, P. 1997. Restricted expression and retinoic acid-induced downregulation of the retinaldehyde dehydrogenase type 2 (RALDH-2) gene during mouse development. *Mech Dev,* 62**,** 67-78.

NIEDERREITHER, K., SUBBARAYAN, V., DOLLE, P. & CHAMBON, P. 1999. Embryonic retinoic acid synthesis is essential for early mouse post-implantation development. *Nat Genet,* 21**,** 444-8.

OKABE, Y. & MEDZHITOV, R. 2014. Tissue-specific signals control reversible program of localization and functional polarization of macrophages. *Cell,* 157**,** 832-44.

PAIK, J., HAENISCH, M., MULLER, C. H., GOLDSTEIN, A. S., ARNOLD, S., ISOHERRANEN, N., BRABB, T., TREUTING, P. M. & AMORY, J. K. 2014. Inhibition of retinoic acid biosynthesis by the bisdichloroacetyldiamine WIN 18,446 markedly suppresses spermatogenesis and alters retinoid metabolism in mice. *J Biol Chem,* 289**,** 15104-17.

PEREZ-POMARES, J. M. & DE LA POMPA, J. L. 2011. Signalling during epicardium and coronary vessel development. *Circ Res,* 109**,** 1429-42.

PIEVANI, A., AZARIO, I., ANTOLINI, L., SHIMADA, T., PATEL, P., REMOLI, C., RAMBALDI, B., VALSECCHI, M. G., RIMINUCCI, M., BIONDI, A., TOMATSU, S. & SERAFINI, M. 2015. Neonatal bone marrow transplantation prevents bone pathology in a mouse model of mucopolysaccharidosis type I. *Blood,* 125**,** 1662-71.

PORRELLO, E. R., MAHMOUD, A. I., SIMPSON, E., HILL, J. A., RICHARDSON, J. A., OLSON, E. N. & SADEK, H. A. 2011. Transient regenerative potential of the neonatal mouse heart. *Science,* 331**,** 1078-80.

PORRELLO, E. R., MAHMOUD, A. I., SIMPSON, E., JOHNSON, B. A., GRINSFELDER, D., CANSECO, D., MAMMEN, P. P., ROTHERMEL, B. A., OLSON, E. N. & SADEK, H. A. 2013. Regulation of neonatal and adult mammalian heart regeneration by the miR-15 family. *Proc Natl Acad Sci USA,* 110**,** 187-92.

POSS, K. D. 2007. Getting to the heart of regeneration in zebrafish. *Semin Cell Dev Biol,* 18**,** 36-45.

POSS, K. D., WILSON, L. G. & KEATING, M. T. 2002. Heart regeneration in zebrafish. *Science,* 298**,** 2188-90.

PUENTE, B. N., KIMURA, W., MURALIDHAR, S. A., MOON, J., AMATRUDA, J. F., PHELPS, K. L., GRINSFELDER, D., ROTHERMEL, B. A., CHEN, R., GARCIA, J. A., SANTOS, C. X., THET, S., MORI, E., KINTER, M. T., RINDLER, P. M., ZACCHIGNA, S., MUKHERJEE, S., CHEN, D. J., MAHMOUD, A. I., GIACCA, M., RABINOVITCH, P. S., AROUMOUGAME, A., SHAH, A. M.,

SZWEDA, L. I. & SADEK, H. A. 2014. The oxygen-rich postnatal environment induces cardiomyocyte cell-cycle arrest through DNA damage response. *Cell,* 157**,** 565-79.

RED-HORSE, K., UENO, H., WEISSMAN, I. L. & KRASNOW, M. A. 2010. Coronary arteries form by developmental reprogramming of venous cells. *Nature,* 464**,** 549-53.

ROSENTHAL, N. & HARVEY, R. P. 2010. *Heart Development and Regeneration,* London, Elsevier, Acad. Press. Pg. 135-235.

ROSSANT, J., ZIRNGIBL, R., CADO, D., SHAGO, M. & GIGUERE, V. 1991. Expression of a retinoic acid response element-hsplacZ transgene defines specific domains of transcriptional activity during mouse embryogenesis. *Genes Dev,* 5**,** 1333-44.

ROY, S. G., NOZAKI, Y. & PHAN, S. H. 2001. Regulation of alpha-smooth muscle actin gene expression in myofibroblast differentiation from rat lung fibroblasts. *Int J Biochem Cell Biol,* 33**,** 723-34.

RUDAT, C. & KISPERT, A. 2012. Wt1 and epicardial fate mapping. *Circ Res,* 111**,** 165-9.

RUI, L., YU, N., HONG, L., FENG, H., CHUNYONG, H., JIAN, M., ZHE, Z. & SHENGSHOU, H. 2014. Extending the time window of mammalian heart regeneration by thymosin beta 4. *J Cell Mol Med,* 18**,** 2417-24.

RUIZ-VILLALBA, A., SIMON, A. M., POGONTKE, C., CASTILLO, M. I., ABIZANDA, G., PELACHO, B., SANCHEZ-DOMINGUEZ, R., SEGOVIA, J. C., PROSPER, F. & PEREZ-POMARES, J. M. 2015. Interacting resident epicardium-derived fibroblasts and recruited bone marrow cells form myocardial infarction scar. *J Am Coll Cardiol,* 65**,** 2057-66.

SCHNABEL, K., WU, C. C., KURTH, T. & WEIDINGER, G. 2011. Regeneration of cryoinjury induced necrotic heart lesions in zebrafish is associated with epicardial activation and cardiomyocyte proliferation. *PLoS One,* 6**,** e18503.

SCHNEIDER, J. E., WIESMANN, F., LYGATE, C. A. & NEUBAUER, S. 2006. How to perform an accurate assessment of cardiac function in mice using high-resolution magnetic resonance imaging. *J Cardiovasc Magn Reson,* 8**,** 693-701.

SEN, S. & SADEK, H. A. 2015. Neonatal heart regeneration: mounting support and need for technical standards. *J Am Heart Assoc,* 4(1):e001727

SENYO, S. E., STEINHAUSER, M. L., PIZZIMENTI, C. L., YANG, V. K., CAI, L., WANG, M., WU, T. D., GUERQUIN-KERN, J. L., LECHENE, C. P. & LEE, R. T. 2013. Mammalian heart renewal by pre-existing cardiomyocytes. *Nature,* 493**,** 433-6.

SMART, N., BOLLINI, S., DUBE, K. N., VIEIRA, J. M., ZHOU, B., DAVIDSON, S., YELLON, D., RIEGLER, J., PRICE, A. N., LYTHGOE, M. F., PU, W. T. & RILEY, P. R. 2011. De novo cardiomyocytes from within the activated adult heart after injury. *Nature,* 474**,** 640-4.

SMART, N., DUBE, K. N. & RILEY, P. R. 2012. Epicardial progenitor cells in cardiac regeneration and neovascularisation. *Vascul Pharmacol*. 58(3):164-73

SMART, N., RISEBRO, C. A., CLARK, J. E., EHLER, E., MIQUEROL, L., ROSSDEUTSCH, A., MARBER, M. S. & RILEY, P. R. 2010. Thymosin beta4 facilitates epicardial neovascularization of the injured adult heart. *Ann N Y Acad Sci,* 1194**,** 97-104.

SMART, N., RISEBRO, C. A., MELVILLE, A. A., MOSES, K., SCHWARTZ, R. J., CHIEN, K. R. & RILEY, P. R. 2007a. Thymosin beta4 induces adult epicardial progenitor mobilization and neovascularization. *Nature,* 445**,** 177-82.

SMART, N., RISEBRO, C. A., MELVILLE, A. A., MOSES, K., SCHWARTZ, R. J., CHIEN, K. R. & RILEY, P. R. 2007b. Thymosin beta-4 is essential for coronary vessel development and promotes neovascularization via adult epicardium. *Ann N Y Acad Sci,* 1112**,** 171-88.

SOONPAA, M. H. & FIELD, L. J. 1997. Assessment of cardiomyocyte DNA synthesis in normal and injured adult mouse hearts. *Am J Physiol,* 272**,** H220-6.

SOONPAA, M. H., KIM, K. K., PAJAK, L., FRANKLIN, M. & FIELD, L. J. 1996. Cardiomyocyte DNA synthesis and binucleation during murine development. *Am J Physiol,* 271**,** H2183-9.

STUCKEY, D. J., CARR, C. A., TYLER, D. J. & CLARKE, K. 2008. Cine-MRI versus two-dimensional echocardiography to measure in vivo left ventricular function in rat heart. *NMR Biomed,* 21**,** 765-72.

STUCKMANN, I., EVANS, S. & LASSAR, A. B. 2003. Erythropoietin and retinoic acid, secreted from the epicardium, are required for cardiac myocyte proliferation. *Dev Biol,* 255**,** 334-49.

STURZU, A. C., RAJARAJAN, K., PASSER, D., PLONOWSKA, K., RILEY, A., TAN, T. C., SHARMA, A., XU, A. F., ENGELS, M. C., FEISTRITZER, R., LI, G., SELIG, M. K., GEISSLER, R., ROBERTSON, K. D., SCHERRER-CROSBIE, M., DOMIAN, I. J. & WU, S. M. 2015. Foetal Mammalian Heart Generates a Robust Compensatory Response to Cell Loss. *Circulation,* 132**,** 109-21.

SUCOV, H. M., DYSON, E., GUMERINGER, C. L., PRICE, J., CHIEN, K. R. & EVANS, R. M. 1994. RXR alpha mutant mice establish a genetic basis for vitamin A signaling in heart morphogenesis. *Genes Dev,* 8**,** 1007-18.

SUZUKI, Y., YEUNG, A. C. & IKENO, F. 2011. The representative porcine model for human cardiovascular disease. *J Biomed Biotechnol,* 2011**,** 195483.

TANG, S., HUANG, G., FAN, W., CHEN, Y., WARD, J. M., XU, X., XU, Q., KANG, A., MCBURNEY, M. W., FARGO, D. C., HU, G., BAUMGART-VOGT, E., ZHAO, Y. & LI, X. 2014. SIRT1-mediated deacetylation of CRABPII regulates cellular retinoic acid signalling and modulates embryonic stem cell differentiation. *Mol Cell,* 55**,** 843-55.

TIAN, X., HU, T., ZHANG, H., HE, L., HUANG, X., LIU, Q., YU, W., YANG, Z., ZHANG, Z., ZHONG, T. P., YANG, X., YAN, Y., BALDINI, A., SUN, Y., LU, J., SCHWARTZ, R. J., EVANS, S. M., GITTENBERGER-DE GROOT, A. C., RED-HORSE, K. & ZHOU, B. 2013. Subepicardial

endothelial cells invade the embryonic ventricle wall to form coronary arteries. *Cell Res,* 23**,** 1075-90.

TSUJI, M., OHSHIMA, M., TAGUCHI, A., KASAHARA, Y., IKEDA, T. & MATSUYAMA, T. 2013. A novel reproducible model of neonatal stroke in mice: comparison with a hypoxia-ischemia model. *Exp Neurol,* 247**,** 218-25.

VAN WIJK, B., GUNST, Q. D., MOORMAN, A. F. & VAN DEN HOFF, M. J. 2012. Cardiac regeneration from activated epicardium. *PLoS One,* 7**,** e44692.

VAN WIJK, B., VAN DEN BERG, G., ABU-ISSA, R., BARNETT, P., VAN DER VELDEN, S., SCHMIDT, M., RUIJTER, J. M., KIRBY, M. L., MOORMAN, A. F. & VAN DEN HOFF, M. J. 2009. Epicardium and myocardium separate from a common precursor pool by crosstalk between bone morphogenetic protein- and fibroblast growth factor-signalling pathways. *Circ Res,* 105**,** 431-41.

VON GISE, A., ZHOU, B., HONOR, L. B., MA, Q., PETRYK, A. & PU, W. T. 2011. WT1 regulates epicardial epithelial to mesenchymal transition through beta-catenin and retinoic acid signalling pathways. *Dev Biol,* 356**,** 421-31.

VUNJAK-NOVAKOVIC, G. 2015. Cardiac biology: A protein for healing infarcted hearts. *Nature,* 525**,** 461-2.

WANG, J., CAO, J., DICKSON, A. L. & POSS, K. D. 2015. Epicardial regeneration is guided by cardiac outflow tract and Hedgehog signalling. *Nature*. 522(7555):226-30

WANG, J., KARRA, R., DICKSON, A. L. & POSS, K. D. 2013. Fibronectin is deposited by injury-activated epicardial cells and is necessary for zebrafish heart regeneration. *Dev Biol*. 382(2):427-35

WANG, J., PANAKOVA, D., KIKUCHI, K., HOLDWAY, J. E., GEMBERLING, M., BURRIS, J. S., SINGH, S. P., DICKSON, A. L., LIN, Y. F., SABEH, M. K., WERDICH, A. A., YELON, D., MACRAE, C. A. & POSS, K. D. 2011. The regenerative capacity of zebrafish reverses cardiac failure caused by genetic cardiomyocyte depletion. *Development,* 138**,** 3421-30.

WECH, T., LEMKE, A., MEDWAY, D., STORK, L. A., LYGATE, C. A., NEUBAUER, S., KOSTLER, H. & SCHNEIDER, J. E. 2011. Accelerating cine-MR imaging in mouse hearts using compressed sensing. *J Magn Reson Imaging,* 34**,** 1072-9.

WEI, K., SERPOOSHAN, V., HURTADO, C., DIEZ-CUNADO, M., ZHAO, M., MARUYAMA, S., ZHU, W., FAJARDO, G., NOSEDA, M., NAKAMURA, K., TIAN, X., LIU, Q., WANG, A., MATSUURA, Y., BUSHWAY, P., CAI, W., SAVCHENKO, A., MAHMOUDI, M., SCHNEIDER, M. D., VAN DEN HOFF, M. J., BUTTE, M. J., YANG, P. C., WALSH, K., ZHOU, B., BERNSTEIN, D., MERCOLA, M. & RUIZ-LOZANO, P. 2015. Epicardial FSTL1 reconstitution regenerates the adult mammalian heart. *Nature,* 525**,** 479-85.

WIESMANN, F., RUFF, J., HILLER, K. H., ROMMEL, E., HAASE, A. & NEUBAUER, S. 2000. Developmental changes of cardiac function and mass assessed with MRI in neonatal, juvenile, and adult mice. *Am J Physiol Heart Circ Physiol,* 278**,** 652-7.

WILLS, A. A., HOLDWAY, J. E., MAJOR, R. J. & POSS, K. D. 2008. Regulated addition of new myocardial and epicardial cells fosters homeostatic cardiac growth and maintenance in adult zebrafish. *Development,* 135**,** 183-92.

WOLFENSOHN, S. & LLOYD, M. 2003. *Handbook of Laboratory Animal Management and Welfare*, Blackwell Publishing Ltd. London. Pg. 22-37.

WU, B., ZHANG, Z., LUI, W., CHEN, X., WANG, Y., CHAMBERLAIN, A. A., MORENO-RODRIGUEZ, R. A., MARKWALD, R. R., O'ROURKE, B. P., SHARP, D. J., ZHENG, D., LENZ, J., BALDWIN, H. S., CHANG, C. P. & ZHOU, B. 2012. Endocardial cells form the coronary arteries by angiogenesis through myocardial-endocardial VEGF signalling. *Cell,* 151**,** 1083-96.

WU, S. P., DONG, X. R., REGAN, J. N., SU, C. & MAJESKY, M. W. 2013. Tbx18 regulates development of the epicardium and coronary vessels. *Dev Biol,* 383**,** 307-20.

XAVIER-NETO, J., SOUSA COSTA, A. M., FIGUEIRA, A. C., CAIAFFA, C. D., AMARAL, F. N., PERES, L. M., DA SILVA, B. S., SANTOS, L. N., MOISE, A. R. & CASTILLO, H. A. 2015. Signalling through retinoic acid receptors in cardiac development: Doing the right things at the right times. *Biochim Biophys Acta,* 1849**,** 94-111.

XIN, M., KIM, Y., SUTHERLAND, L. B., MURAKAMI, M., QI, X., MCANALLY, J., PORRELLO, E. R., MAHMOUD, A. I., TAN, W., SHELTON, J. M., RICHARDSON, J. A., SADEK, H. A., BASSEL-DUBY, R. & OLSON, E. N. 2013a. Hippo pathway effector Yap promotes cardiac regeneration. *Proc Natl Acad Sci U S A,* 110**,** 13839-44.

XIN, M., OLSON, E. N. & BASSEL-DUBY, R. 2013b. Mending broken hearts: cardiac development as a basis for adult heart regeneration and repair. *Nat Rev Mol Cell Biol,* 14**,** 529-41.

YANG, H., WANG, H., SHIVALILA, C. S., CHENG, A. W., SHI, L. & JAENISCH, R. 2013. One-step generation of mice carrying reporter and conditional alleles by CRISPR/Cas-mediated genome engineering. *Cell,* 154**,** 1370-9.

YANG, Z., BERR, S. S., GILSON, W. D., TOUFEKTSIAN, M. C. & FRENCH, B. A. 2004. Simultaneous evaluation of infarct size and cardiac function in intact mice by contrast-enhanced cardiac magnetic resonance imaging reveals contractile dysfunction in non-infarcted regions early after myocardial infarction. *Circulation,* 109**,** 1161-7.

ZEISBERG, E. M. & KALLURI, R. 2010. Origins of cardiac fibroblasts. *Circ Res,* 107**,** 1304-12.

ZHOU, B., HONOR, L. B., HE, H., MA, Q., OH, J. H., BUTTERFIELD, C., LIN, R. Z., MELERO-MARTIN, J. M., DOLMATOVA, E., DUFFY, H. S., GISE, A., ZHOU, P., HU, Y. W., WANG, G., ZHANG, B., WANG, L., HALL, J. L., MOSES, M. A., MCGOWAN, F. X. & PU, W. T. 2011. Adult mouse epicardium modulates myocardial injury by secreting paracrine factors. *J Clin Invest,* 121**,** 1894-904.

ZHOU, B., HONOR, L. B., MA, Q., OH, J. H., LIN, R. Z., MELERO-MARTIN, J. M., VON GISE, A., ZHOU, P., HU, T., HE, L., WU, K. H., ZHANG, H., ZHANG, Y. & PU, W. T. 2012. Thymosin beta 4 treatment after myocardial infarction does not reprogram epicardial cells into cardiomyocytes. *J Mol Cell Cardiol,* 52**,** 43-7.

ZHOU, B., MA, Q., RAJAGOPAL, S., WU, S. M., DOMIAN, I., RIVERA-FELICIANO, J., JIANG, D., VON GISE, A., IKEDA, S., CHIEN, K. R. & PU, W. T. 2008. Epicardial progenitors contribute to the cardiomyocyte lineage in the developing heart. *Nature,* 454**,** 109-13.

ZHOU, B. & PU, W. T. 2011. Epicardial epithelial-to-mesenchymal transition in injured heart. *J Cell Mol Med,* 15**,** 2781-3.